The mRNA stability Regulator Khd4 determines infectious hyphae development in *Ustilago maydis*

Inaugural dissertation

for the attainment of the title of doctor

in the Faculty of Mathematics and Natural Sciences

at the Heinrich Heine University Düsseldorf

presented by

Srimeenakshi Sankaranarayanan

from Melur, Tamil Nadu, India

Heinrich Heine Universität Düsseldorf

Düsseldorf, October 2023

From the Institute of Microbiology

at the Heinrich Heine University Düsseldorf

Published with the permission of the
Faculty of Mathematics and Natural Sciences at
Heinrich Heine University Düsseldorf

Supervisor: Prof. Dr. Michael Feldbrügge

Co-Supervisor: Prof. Dr. Heiner Schaal

Date of the oral examination: 18.12.2023

The research detailed in this dissertation was conducted from August 2017 until June 2023 at the Institute of Microbiology, under the supervision of Prof. Dr. Michael Feldbrügge at Heinrich Heine University Düsseldorf.

Some sections of this dissertation have been published in scientific journals. The manuscript in Chapter 3.1 has been reproduced according to PNAS author rights. The manuscripts in Chapter 5, Appendix 1 have been reproduced according to Creative Commons Attribution 4.0 International license (CC BY). Images from other published articles have been cited and reproduced with permission under the terms and conditions of the CC BY license and Springer Nature. Published results and their interpretation remain unaltered. Parts of the work presented in this thesis have been published or accepted for publication:

Sankaranarayanan, S., Haag, C., Petzsch, P., Köhrer, K., Matuszyńska, A., Zarnack, K. and Feldbrügge, M., (2023a) The mRNA stability factor Khd4 defines a specific mRNA regulon for membrane trafficking in the pathogen *Ustilago maydis*. *Proc Natl Acad Sci USA* 120**:** e2301731120.

Sankaranarayanan, S.*, **Kwon, S.***, Heimel, K. and Feldbrügge, M., (2023b) The RNA world of fungal pathogens. *PLoS Pathog*. accepted

(*equal contribution)

City: Düsseldorf

Date: 18.12.2023 Srimeenakshi Sankaranarayanan

I hereby confirm that for each published or prepared manuscript incorporated in this thesis, the specific contributions of the doctoral researcher, Srimeenakshi Sankaranarayanan, and the other co-authors have been accurately documented.

City: Düsseldorf

Date: 18.12.2023 Prof. Dr. Michael Feldbrügge

Statutory declaration

This dissertation is the outcome of my research conducted in accordance with the "Principles for the Safeguarding and Good Scientific Practice" at the Heinrich Heine University Düsseldorf. It is affirmed that no other individual's work has been incorporated without proper acknowledgment. Experimental work presented in this thesis has been conducted at the Heinrich Heine University Düsseldorf. The literature cited in the text and listed in the reference section is the sole source used in this work. This dissertation has not been previously submitted or published in a similar form elsewhere. I have not previously failed a doctoral examination procedure.

City: Düsseldorf
Date: 18.12.2023

Srimeenakshi Sankaranarayanan
Matriculation number: 2687298

I dedicate this thesis to my parents, Sankaranarayanan and Ananthavalli.

நான் இந்த பணியை என் பெற்றோர் சங்கரநாராயணன் மற்றும் ஆனந்தவல்லிக்கு அற்பணிக்கிறேன்.

.

Summary

Fungal pathogens cause severe diseases, affecting public health, wildlife, and agriculture. A key for virulence in many fungal pathogens lies in their capacity for morphological plasticity, regulated through precise gene expression control. Understanding these infection strategies, particularly at the level of DNA and RNA, is vital to combat fungal diseases. However, our knowledge of the spatiotemporal regulation of gene expression at the RNA level in the fungal kingdom remains limited. In *Ustilago maydis*, the causative agent of corn smut, the morphological transition from yeast to hyphal growth is essential for infection. Previously, it was discovered that the multi-KH domain RNA-binding protein (RBP) Khd4 is important for morphogenesis and pathogenesis in *U. maydis.* Khd4 recognizes the AUACCC sequence via its KH domains 5 and 6. Failure to recognize the sequence by mutating these RNA-binding domains caused aberrant cell morphology, disturbed hyphae formation, and reduced virulence. However, the direct mRNA targets of Khd4 and its corresponding function remained unknown.

Presented in this thesis is the investigation into the regulatory role of Khd4 in determining infectious hyphae formation in *U. maydis.* To identify Khd4 mRNA targets, the RNA-proximity labeling hyperTRIBE approach was employed, which involves fusing the RNA-editing ADAR enzyme to the RBP to mark the target mRNA. Validation using Rrm4, a well-studied RBP in *U. maydis*, demonstrated the effectiveness of hyperTRIBE in identifying known Rrm4-mRNA interactions. This *in vivo* approach revealed that Khd4 selectively binds mRNAs encoding regulatory proteins involved in membrane trafficking via the AUACCC motif. Khd4 degrades these mRNAs by specifically interacting with its AUACCC element in the 3´ UTR. This precise mRNA decay process dictates the induction kinetics of these mRNAs, enabling faster attainment of new steady-state levels after transcriptional induction, and rapid clearance after transcriptional shut-off. Consequently, in the absence of Khd4, membrane trafficking is dysregulated, resulting in fragmented vacuoles, affecting polar growth. Hence, Khd4 unites target mRNAs encoding regulatory proteins into membrane trafficking mRNA regulon, orchestrating the dynamics of intracellular transport crucial for hyphal growth. Studying Khd4 localization revealed that the protein exhibits cortical localization under heat stress,

reminiscing that of the endoplasmic reticulum. Given the central role of ER in membrane trafficking, it is conceivable that Khd4 might regulate a subset of its target mRNAs in the vicinity of ER. In essence, the RBP Khd4 regulates infectious hyphae development by determining the exact levels of regulatory proteins crucial for this process.

Zusammenfassung

Pilzpathogene stellen eine erhebliche Bedrohung für die humane Gesundheit, die Tierwelt und die Landwirtschaft dar. Ein Schlüsselaspekt der Virulenz vieler Pilzpathogene liegt in ihrer Fähigkeit zur morphologischen Anpassung, die auf genetischer Ebene präzise reguliert wird. Das Verständnis dieser Infektionsstrategien, insbesondere auf der Ebene von DNA und RNA, ist entscheidend für die Bekämpfung von Pilzerkrankungen. Dennoch ist unser Wissen über die räumliche und zeitliche Regulation der Genexpression auf RNA-Ebene im Pilzreich gering. In *Ustilago maydis*, dem Erreger des Maisbrandes, ist der Übergang von Hefe- zu Hyphenwachstum entscheidend für die Infektion. Frühere Forschungen haben ergeben, dass das multi-KH-Domänen-RNA-Bindungsprotein (RBP) Khd4 eine zentrale Rolle in der Morphogenese und Pathogenese von *U. maydis* spielt. Khd4 erkennt die Sequenz AUACCC über seine KH-Domänen 5 und 6. Mutationen in diesen RNA-Bindungsdomänen und das damit einhergehende Ausbleiben der Bindung führte zu abweichender Zellmorphologie, gestörter Hyphenbildung und verminderter Virulenz. Die direkten mRNA-Ziele von Khd4 und deren zugehörige Funktionen blieben jedoch unbekannt.

In dieser Arbeit wurde die regulatorische Rolle von Khd4 bei der Entwicklung infektiöser Hyphen in *U. maydis* untersucht. Zur Identifizierung der von Khd4 gebundenen mRNAs wurde die HyperTRIBE-Methode zur RNA-Entfernungs-Markierung eingesetzt. Dieser Technik beinhaltet die Fusion des RNA-Editierungs-Enzyms ADAR mit dem zu untersuchenden RBP zur Markierung der Ziel-mRNA. Die Validierung unter Verwendung von Rrm4, einem gut erforschten RBP in *U. maydis*, bestätigte die Effektivität von HyperTRIBE bei der Identifizierung bekannter Rrm4-mRNA-Wechselwirkungen. Mithilfe dieses invivoAnsatzes konnte herausgefunden werden, dass Khd4 selektiv mRNAs über das Motiv AUACCC bindet, die für regulatorische Proteine kodieren und am Membrantransport beteiligt sind. Khd4 baut diese mRNAs gezielt ab, indem es spezifisch mit dem AUACCC-Element in der 3´-UTR interagiert. Dieser präzise Prozess des mRNA-Abbaus steuert die Induktionskinetik dieser mRNAs und ermöglicht ein schnelleres Erreichen neuer Steady-State-Werte nach der Transkriptionsinduktion sowie eine rasche Bereinigung nach dem Abschalten der Transkription. Infolgedessen ist in Abwesenheit von Khd4 der Membrantransport fehlreguliert, was zu fragmentierten Vakuolen führt und das hyphale Wachstum

beeinträchtigt. Khd4 vereint daher Ziel-mRNAs, die regulatorischen Proteine kodieren innerhalb eines mRNA-Regulon für den Membrantransport und orchestriert die Dynamik des intrazellulären Transports, der für das Hyphenwachstum entscheidend ist. Die Untersuchung der Lokalisierung von Khd4 ergab, dass das Protein unter Hitzestress eine kortikale Lokalisierung aufweist, die an die des endoplasmatischen Retikulums erinnert. Angesichts der zentralen Rolle des endoplasmatischen Retikulums beim Membrantransport ist es denkbar, dass Khd4 eine Teilmenge der Ziel-mRNAs in dessen Nähe reguliert.

Im Wesentlichen steuert Khd4 die Entwicklung infektiöser Hyphen, indem es die exakte Menge an regulatorischen Proteinen bestimmt, die für diesen Prozess entscheidend ist.

List of Abbreviations

ADAR	Adenosine deaminases acting on RNA	**µg**	Microgram
ARE	AU-rich element	**MAPK**	Mitogen-activated protein kinase
A-to-G	Adenosine-to-Guanosine	**MEN**	mitotic exit network
α	Anti	**ml**	Milliliter
BAM	Binary alignment map	**mRNA**	messenger RNA
bE/bW	Transcription factor bEast and bWest	**mRNP**	Messenger ribonucleotide particle
bp	Base pairs	**ng**	Nanogram
cDNA	complementary DNA	**NGS**	Next-generation sequencing
CDS	Coding sequence	**nm**	Nanometer
CELF1	CUGBP elav-like family member 1	**NM**	Nitrate medium
CFW	Calcofluor white	**nt**	Nucleotide
CLIP	Cross-linking and immunoprecipitation	**N-terminal**	Amino-terminal
CM	Complete medium	**OD**	Optical density
CMAC	7-amino-4-chloromethyl coumarin	**ORF**	Open reading frame
Ct	threshold cycles	**PCR**	Polymerase chain reaction
C-terminal	Carboxyl-terminal	**PDB**	Protein Data Bank
d.p.i.	Days post inoculation	**PPI**	Protein-protein interaction
DIC	Differential interference contrast	**PWM**	Position weight matrix
°C	Degree centigrade	**Q**	Glutamine
DNA	Deoxyribonucleic acid	**RBD**	RNA-binding domain
DNase	Deoxyribonuclease	**RBP**	RNA-binding protein
de novo	Beginning anew	**RIP**	RNA immunoprecipitation
E	Glutamate	**RNA**	Ribonucleic acid
ER	Endoplasmic Reticulum	**RNase**	Ribonuclease
et al.	And others	**RNA-seq**	RNA sequencing
g	Gram	**rpm**	Rounds per minute
g	Relative centrifugal force	**RRM**	RNA recognition motif
GAP	GTPase activating protein	**rRNA**	ribosomal RNA
gDNA	Genomic DNA	**RT-PCR**	Reverse transcription polymerase chain reaction
GEF	Guanine nucleotide exchange factor	**RT-qPCR**	Reverse transcription-quantitative polymerase chain reaction

GEM	Generic EnrichmentMap	**SDS - PAGE**	Sodium Dodecyl Sulfate - Polyacrylamide Gel Electrophoresis
GFF	Generic Feature Format	**s**	seconds
Gfp	Green fluorescence protein	**$t_{1/2}$**	Half-life
GO	Gene ontology	**TBS**	Tris-Buffered Saline
GTF	Gene transfer format	**TE**	Tris-EDTA
GTPase	Enzymes that hydrolyze the nucleotide GTP to GDP	**TF**	Transcription factor
h	Hours	**Tnos**	Terminator of the nopaline synthase gene of Agrobacterium tumefaciens
h.p.i	Hours post induction	**TPM**	Transcripts per million
iCLIP	Individual-nucleotide resolution UV crosslinking and immunoprecipitation	**TRIBE**	Targets of RBP Identification by Editing
in situ	Examination of a phenomenon exactly in the place where it occurs	**tRNA**	transfer RNA
in vivo	In a living organism	**TTP**	Tristetraprolin
in vitro	Outside the normal biological context	**U,A,G,C**	Uracil, Adenine, Guanine, Cytosine
Kat	mKate2 - a monomeric, basic red fluorescent protein	**UMI**	Unique molecular index
kb	Kilo base	**UPR**	Unfolded protein response
kDa	Kilodalton	**UTR**	Untranslated regions
k_{decay}	Decay rate constant	**UV**	Ultraviolet
KH	K homology	**$v_{degradation}$**	Rate of degradation
M	Molar	**$v_{synthesis}$**	Rate of synthesis
µl	Microliter	**3'**	Three prime ends
µm	Micrometer	**5'**	Five prime ends

Table of contents

1. Introduction

1.1 Fungal pathogens: A Threat to healthcare, agriculture, and Ecosystem

From being a source of sustenance and medical resources to playing a pivotal role in the decomposition of organic materials, the fungal kingdom emerges as a vital contributor that makes life on Earth habitable. About 450 million years ago, the partnership between fungi and plants allowed for the colonization of land, making it habitable for living organisms (PIROZYNSKI AND MALLOCH 1975, HUMPHREYS *et al.* 2010). However, over the past two centuries, fungi have emerged as critical pathogens, impacting the lives of humans, plants, and animals.

It is estimated that globally 1.6 million deaths occur every year due to invasive fungal infections. Approximately 1 billion individuals across the globe suffer from various fungal infections (ANONYMOUS 2017). To illustrate, with a mortality rate of up to 95%, invasive aspergillosis caused by *Aspergillus* species affects 300, 000 individuals annually (SUGUI *et al.* 2014). Similarly, *Candida albicans*, the main etiologic *Candida* species responsible for invasive candidaemia, is predicted to impact around 300, 000 individuals across the globe (BROWN *et al.* 2012a).

Recent times have witnessed a devastating upsurge of life-threatening secondary invasive fungal infections, such as aspergillosis, candidiasis, and mucormycosis, spurred by the Covid-19 pandemic (HOENIGL *et al.* 2022). Of significance, the Covid-19-associated mucormycosis, caused by filamentous fungi of the order Mucorales, became an epidemic in India, with a 36.5% mortality rate. This is likely attributed to the use of immunosuppressive drugs and systemic glucocorticoids to treat critically ill Covid-19 patients (PASQUIER 2023).

Fungal and fungal-like oomycete pathogens are also greater contributors to plant diseases compared to any other pests. The plant fungal epidemics have endangered the ecosystem and destroyed crop yield. Infections affecting crops like rice, wheat, maize, soybean, and potato endanger global food security. For example, the rice blast disease, caused by *Magnaporthe oryzae,* results in an annual loss of 30% in total rice production, and the infection of *Phakopsora pachyrhizi* leads to an 80% reduction in soybean yield (PENNISI 2010,DOEHLEMANN *et al.* 2017). Notably, the corn smut fungus *Ustilago maydis* can

impact up to 20% of corn production in certain regions (FISHER *et al.* 2012). It is estimated that if these fungal-related food losses had been mitigated, an estimated 600 million additional people could have been fed in 2011(FISHER *et al.* 2012).

The heightened risk of fungal infection extends beyond humans and plants to encompass diverse animal species. Recent examples include the mass mortality of bat species caused by the fungus *Pseudogymnoascus destructans* and of amphibian species caused by *Batrachochytrium destructans*. Predictions indicate a potential 70% decline in bat populations over the next year, with some species, such as the little brown bat*, Myotis lucifugus*, facing a greater than 99% risk of local extinction (FRICK *et al.* 2010). Furthermore, Chytridiomycosis, caused by *B. destructans*, has obliterated the biodiversity of several amphibian species such as frogs and salamanders. The Amphibians are the world's most endangered vertebrate class and Chytridiomycosis is a proximal driver of this event (FONES *et al.* 2017).

Climate change and the increase in human activities, such as global trading, have heightened the opportunity for the emergence of new fungal pathogens in recent years (GARCIA-SOLACHE AND CASADEVALL 2010). An in-depth understanding of pathogenic development in fungal pathogens is therefore urgently demanded to protect the environment, agriculture, and human health from deadly fungal diseases.

1.2 Hyphal morphogenesis and Gene expression control

Fungal pathogens exhibit remarkable morphological plasticity, a crucial trait for their virulence (GOW *et al.* 2002, MIN *et al.* 2020). In many fungal pathogens, the morphogenesis to hyphal form is a hallmark of infection (BRAND AND GOW 2009). Interestingly, the evolution of hyphal growth in fungi, believed to be driven by the necessity to infect larger organisms, marks their adaptation to land (NARANJO-ORTIZ AND GABALDÓN 2019). In line with this, hyphal cells have proven highly efficient for tissue penetration (BRAND 2012).

While *C. albicans* exhibits a range of morphologies, each with specific roles in infection, the invasive infection of host tissue and internal organs is mainly orchestrated by hyphal morphology (SUDBERY 2011, ERWIG AND GOW 2016, FERNANDES AND CARTER 2020). Similarly, the majority of fungal plant pathogens adopt filamentous, hyphal morphology as an efficient strategy to penetrate plant tissues and acquire essential nutrition for growth and survival (LO PRESTI *et al.* 2015).

The morphogenesis of fungal pathogens is a dynamic process, demanding constant optimization to respond to environmental cues. For instance, the formation of appressoria, an infection structure, in *U. maydis* is instigated by cues from plant surfaces, such as hydrophobicity (LANVER *et al.* 2010). This rapid adaptive response, in turn, relies on the precise orchestration of spatiotemporal gene expression control to navigate ever-shifting environmental conditions.

Since the emergence of the concept of genes as discrete heritable units from the experiments of Gregor Mendel, the inquiry of how the genotype of an organism manifests as its phenotype has held a profound fascination. While early investigation indicated that certain genes exert their influence on the phenotype only under specific conditions, the legendary work of Jacob and Monod underscored that the genes must be expressed before their corresponding phenotypes become evident (GANN 2010). From genome to proteome, gene expression is a complex process regulated at multiple levels.

Traditionally, transcriptional networks have been attributed as the primary driver of gene expression control during hyphal growth and pathogenicity. For example, the activation of transcription factors, including Efg1, Cph1, and Cph2, in *C. albicans* (KUMAMOTO AND VINCES 2005, GOW *et al.* 2012). and the heteromeric master regulator bE/bW in *U. maydis* (HEIMEL *et al.* 2010a HEIMEL *et al.* 2010a KUMAMOTO AND VINCES 2005) are known to induce gene regulatory cascades that are crucial for hyphal morphogenesis in these pathogens. However, it is imperative to recognize that transcriptional activity alone does not serve as a proxy for RNA abundance, and the complexity of gene expression regulation extends well beyond transcriptional control. In particular, understanding RNA metabolism (Fig. 1.1), and the precise regulation of mRNA and protein levels to meet cellular demands is essential. Yet, our current knowledge of posttranscriptional control in fungal morphogenesis and pathogenesis remains limited. Given the rise of antifungal-resistant strains (FISHER *et al.* 2016), investigating the post-transcriptional regulatory mechanism becomes paramount for developing novel antifungal treatment strategies.

1.3 Post-transcriptional regulation of gene expression

1.3.1 mRNA Maturation, Localization and Translation

Posttranscriptional regulation of gene expression begins immediately after RNA polymerase II binds to promoters and initiates mRNA synthesis. As transcription proceeds, a series of processing steps occur on nascent and pre-mRNAs (Fig. 1.1). These

steps include 5' end capping: involving the addition of a 7-methylguanosine cap to the first nucleotide (RAMANATHAN *et al.* 2016); splicing: removing non-coding intronic regions and joining the coding exonic region to create matured, spliced mRNAs (CHEN AND MOORE 2015); and 3′ end processing: involving cleavage and polyadenylation, ultimately forming mature mRNA (NEVE *et al.* 2017). Importantly, pre-mRNA can undergo alternative splicing and alternative 3′ end processing, diversifying the cellular transcriptome and proteome.

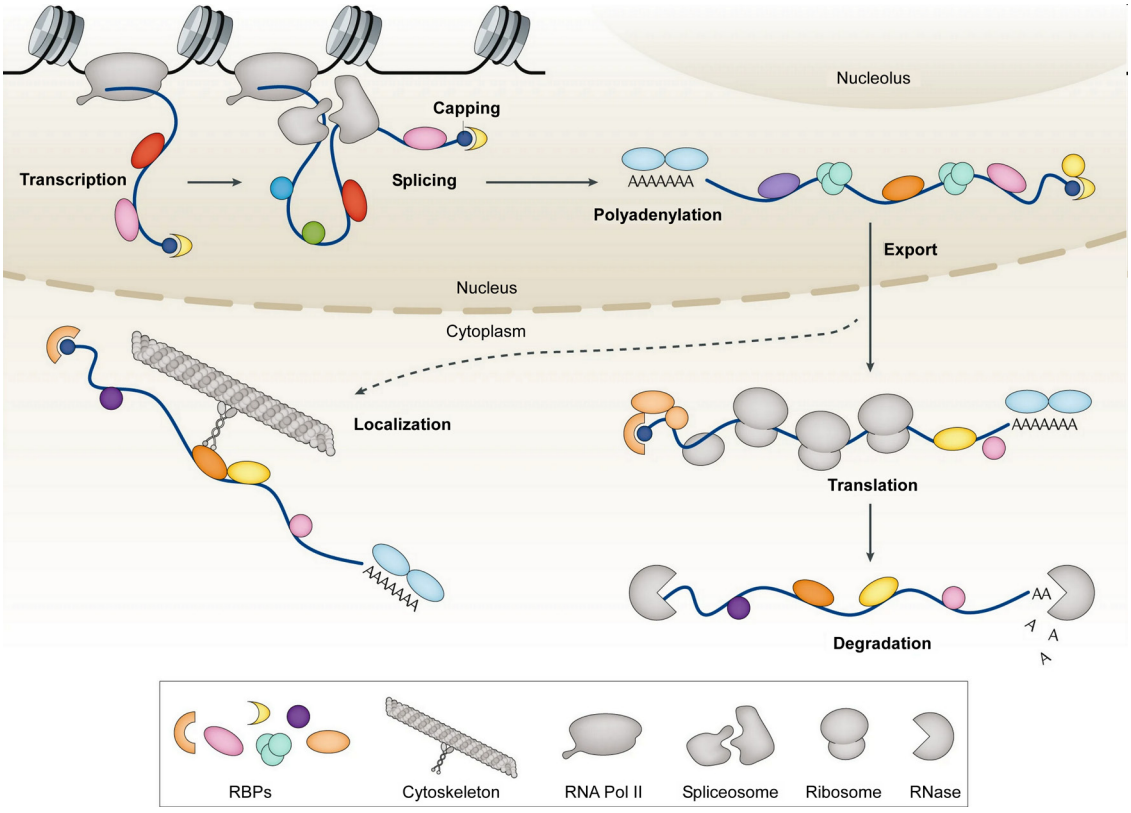

Fig. 1.1. Model depicting the posttranscriptional regulatory process that governs RNA life. Nuclear (transcription, splicing, capping, polyadenylation) and cytoplasmic (transport, localization, translation, degradation) steps of mRNA metabolism are depicted. In the nucleus, pre-mRNA undergoes co-transcriptional modification, including splicing, capping, and polyadenylation. Once matured, the mRNA exits the nucleus to cytoplasm either for direct translation or localization for immediate translation, or localized to a specific subcellular region for translation before eventual degradation. (Figure and legend adapted from GEBAUER *et al.* 2021 under the terms of Springer Nature license No. 5625890803643).

Following pre-mRNA processing, the resulting mature mRNA is exported to the cytoplasm, where its fate is closely linked to the precise timing and spatial context of translation (Fig. 1.1). Mainly, mRNA localization to specific subcellular regions is crucial for localized control over gene expression and the creation of translational hotspots. Transporting mRNAs to specific locations for translation proves to be more energy-efficient than ferrying individual proteins to these sites. Additionally, mRNA localization restricts protein concentration to specific subcellular regions, supporting *in*

situ protein translation, and preventing the deleterious effect of protein mislocalization (DAS *et al.* 2021).

In polar growing cells, mRNA localization to the growth site is essential for local translation in response to external stimuli. One prevalent mechanism for mRNA localization in many cell types is the active transport of mRNA on cytoskeletons by motor proteins such as myosin, kinesin, and dynein. For example, in *S. cerevisiae*, specific zipcodes within the *ash1* mRNA are recognized by the RNA-binding protein (RBP) She2. The She2-RNA complex then binds to the myosin motor protein, Myo4, via She3, facilitating the mRNP transport to the bud site along the actin cytoskeleton (NIESSING *et al.* 2018).

In contrast, in highly polarized cells like fungal hyphae and neurons, where the growth site is distant from the nucleus, long-distance mRNA transport is carried out along microtubule tracks, offering both speed and directionality (BOURKE *et al.* 2023). A well-characterized example is the transport of *β-actin* mRNA in dendrites and axons. Here, the RBP APC (adenomatous polyposis coli) binds to the mRNA and tethers it to the motor protein Kinesin-3 via the adapter protein KAP3, facilitating its movement along microtubule (BAUMANN *et al.* 2020).

A novel mode of long-distance mRNA transport was first observed in the filamentous pathogen *U. maydis.* In this process, mRNAs hitchhike on early endosomes along microtubules, coordinated by kinesin type 3 and dynein motor proteins, influencing hyphal polar growth (BAUMANN *et al.* 2014). Interestingly, these shuttling endosomes also carry ribosomes, indicating that the transported mRNAs are actively translated (MÜNTJES *et al.* 2021). As expected, this energy-efficient, organelle-based transport mode extends beyond *U. maydis* and is operational in various organisms including plants, humans, zebrafish, *Xenopus laevis* an African clawed frog (TIAN *et al.* 2020,LIAO *et al.* 2019,CIONI *et al.* 2019,SCHUHMACHER *et al.* 2023,POPOVIC *et al.* 2020). For instance, recent studies indicate that neuronal cells employ both early and late endosomes to distribute mRNAs to the distal site (CIONI *et al.* 2019, SCHUHMACHER *et al.* 2023). Importantly, in these systems, the mRNA transport is associated with membrane-coupled translation on the endosomal surface (CIONI *et al.* 2019, SCHUHMACHER *et al.* 2023).
Once precise localization is achieved (Fig. 1.1), mRNA confluences with ribosomes, initiating protein synthesis. The regulation of translation which occurs at every step of

protein synthesis is not only essential for a swift response during stress but is also critical for general cellular physiology. This regulation is mediated by *cis*-regulatory elements present in mRNAs and *trans*-acting factors such as translational machinery, and RNA-binding proteins (RBPs). For instance, during stress, phase-separated, membrane-less cytoplasmic granules form through interactions within and between RNAs and RBPs. These granules sequester translationally stalled mRNPs, ribosomes, and translation initiation factors, effectively reprogramming protein synthesis and promoting cell survival (PROTTER AND PARKER 2016).

Besides cytoplasm, the endoplasmic reticulum (ER) constitutes the primary site for ribosomes. Traditionally, it was believed that mRNAs encoding secretory proteins are translated on ER-bound ribosomes, aiding their import into the ER for post-translational modification required for secretion. However, recent evidence challenges this conservative view, suggesting that ER-bound ribosomes are also involved in the translation of a significant proportion of mRNAs encoding cytosolic proteins (REID AND NICCHITTA 2015). This indicates a broader role for the ER in shaping cellular transcriptome and proteome, thereby impacting cellular behavior.

1.3.2 mRNA stability control

Apart from mRNA synthesis, processing, and nuclear export, cytoplasmic mRNA abundance is strictly controlled through mRNA decay regulation (Fig. 1.1). By facilitating the degradation of specific mRNAs, this process fine-tunes cytoplasmic mRNA levels, ensuring precise protein-coding gene expression which in turn influences effective adaptation in response to changing developmental and environmental cues.

Although the model for mRNA decay was proposed as early as 1973 (APIRION 1973), the mRNA degradation process was initially regarded as a salvage pathway. However, it has become increasingly evident that mRNA stability control is far more critical than merely functioning as a waste-disposal system. One of the key factors, for example, influencing the steady-state level of an mRNA is its half-life (HARGROVE AND SCHMIDT 1989). Unstable mRNAs, characterized by increased synthesis and decay rates, achieve a new steady state level more rapidly than stable mRNAs after a transcriptional induction. Interestingly, while increasing the synthesis rate does not affect the response time, decreasing the mRNA half-life further enhances the response speed (PALUMBO *et al.* 2015).

This “increased mRNA synthesis and decreased half-life” strategy particularly applies to mRNAs encoding regulatory proteins that are rapidly produced in response to internal or external stimuli and tend to be unstable. For instance, immune response mediators like cytokines and chemokines are encoded by intrinsically unstable mRNAs, allowing for a quick response while restraining gene expression amplitude to prevent tissue damage (ANDERSON 2010). Similarly, the regulation of histone synthesis is determined at the level of mRNA stability, resulting in rapid increases in histone mRNA levels as cells enter S-phase and swift depletion at the end of the S-phase (KAYGUN AND MARZLUFF 2005).

mRNA degradation can be selectively utilized in a spatially restricted manner to increase the concentration of mRNAs in specific subcellular compartments. Examples include the *Drosophila* embryo, where mRNAs such as *nanos* and *hsp83*, are degraded throughout the cell via the RBP Smaug, except at the posterior pole, where their concentration is enriched. Similarly, in neurons, the microRNA, *let-7*, mediates mRNA decay in the soma, leading to a preferential enrichment of its target mRNAs in neurites (MENDONSA *et al.* 2023). Considering the importance of mRNA localization, accelerated decay might also prevent the adverse effect of mislocalized mRNAs (WALTERS AND PARKER 2014). Furthermore, by limiting the mRNA decay mechanism to distinct cellular locations, spatial regulation of mRNA decay can be achieved. For instance, Ire-1-mediated mRNA decay occurs exclusively in the ER to regulate mRNA degradation during ER stress (HOLLIEN AND WEISSMAN 2006).

The mechanism of mRNA decay is a multi-step process that involves different ribonucleolytic activities, including endonucleases that cleave RNA internally or exonucleases that degrade RNA from either the 5′ or 3′ ends. The specific ribonucleolytic activity utilized depends on the mRNA substrate and cellular conditions.

The canonical pathway of mRNA decay begins with deadenylation, where the poly(A) tail is shortened. This process is carried out by the Ccr4-Not complex or the poly(A)-specific ribonuclease, Pan2-Pan3 complex (PARKER 2012). In the mammalian fungal pathogen *C. neoformans,* deadenylation plays a critical role in host adaptation and invasion. Loss of Ccr4 leads to attenuated virulence and increased sensitivity to stress in this pathogen (BLOOM *et al.* 2019). Following deadenylation, the 5′-cap structure is removed by the Dcp1-Dcp2 decapping complex, and then mRNA is digested from the

5′-end by the 5′ to 3′ exonucleases, Xrn1. The mRNA can also be degraded in a 3′ to 5′ direction by the exosome complex before decapping, but this process is considered to be slower than the activity of the decapping complex (PARKER 2012).

The stability of mRNAs is determined by a combination of *cis*-acting elements within mRNAs and their corresponding *trans*-acting factors, which ultimately decide whether to recruit or exclude degradation machinery. One well-studied example is the AU-rich elements (AREs), commonly found in the 3′ UTR, which play a significant role in mediating mRNA decay (GARCÍA-MAURIÑO *et al.* 2017). The binding of RBPs like TTP, AUF1, and KRSP to ARE leads to the recruitment of deadenylation machinery for decay, while the RBP HuR binding stabilizes ARE-containing mRNAs. Similarly, GU-rich sequences (GREs) in the 3′ UTR promote mRNA decay by interacting with the RBP CELF1 (VLASOVA-ST LOUIS AND BOHJANEN 2011).

Cis-elements present in the 5′ UTR, such as upstream ORF, and upstream start codon can also influence mRNA stability by instigating mRNA decay pathways like non-sense mediated decay (PÉREZ-ORTÍN *et al.* 2013). A study using the RNA-based uORF system revealed that the presence of RNA G-quadraplex and A-rich elements in the 5′ UTR triggers mRNA decay in a translation-independent manner, respectively. The *cis*-elements in the coding regions can also shape the mRNA stability dynamic (JIA *et al.* 2020). For instance, coding region determinant (CRD), a *cis*-element present in the *c-myc* ORF modulates mRNA stability by inhibiting endonucleolytic specific cleavage (BERNSTEIN *et al.* 1992, TAFECH *et al.* 2007).

Many studies have revealed that the targets of mRNA decay pathways are not single mRNAs (KEENE 2007, KEENE AND TENENBAUM 2002). Instead, mRNAs encoding proteins with related functions are coordinately regulated by one or more specific RNA-binding proteins as mRNA regulons. Through this coordination, these RBPs control the fate of these mRNAs to determine their expression levels, thereby impacting their functional roles. For instance, the decay of ARE containing mRNAs encoding immune response proteins is co-regulated by the RBP TTP in mammals, by recruiting various decay factors (ANDERSON 2010). In *S. cerevisiae*, the RBP Cth2, the homolog of mammalian TTP, co-regulates the decay of mRNAs encoding iron-responsive elements by binding to the ARE elements in their 3′ UTR (PUIG *et al.* 2005). A more recent example is the co-regulation of mRNAs encoding cell cycle regulators by the RBP PTBP1 to control the cell cycle in pro-B cells (MONZÓN-CASANOVA *et al.* 2020).

Depending on the mRNP composition, a single mRNA can be a part of more than one regulon. Likewise, a single RBP can also be a member of more than one regulon (KEENE 2007). Besides mRNA decay, this coordinated regulation also occurs at levels of other regulatory processes such as pre-mRNA processing, nuclear export, RNA localization, and translation (PÉREZ-ORTÍN *et al.* 2013).

1.4 RNA binding proteins: A fundamental for RNA regulation

From the birth of an RNA molecule to its ultimate fate, RNA-binding proteins are central players in the posttranscriptional regulation process, orchestrating RNA synthesis, splicing, translation, localization, and degradation. Ranging from single-celled bacteria to the more complex eukaryotes, RBPs are found ubiquitously across different organisms.

Approximately 4,000 RNA-binding proteins (RBPs) have been identified in the human genome, of which around 1,500 RBPs are predicted to be involved in diseases, including neurological pathologies (GEBAUER *et al.* 2021). In fact, of all proteins in the human genome, a higher frequency of mutations observed in various Mendelian disorders are found to occur in RBPs, indicating their role in the maintenance of cellular homeostasis (GEBAUER *et al.* 2021). Examples include Fragile X syndrome, an inherited intellectual disorder, which arises from the expansion of CGG triplets within the 5′ UTR and/or mutations in the KH2 domain of the *fmr1* gene encoding the RBP FMRP essential for mRNA transport and translation in neurons. Mutations in the RBP RBM10 cause TARP syndrome, an X-linked pleiotropic developmental disorder that primarily affects males. RBPM10 serves as a splicing regulator and splicing alterations have been observed in lymphoblastoid cell lines derived from patients with the syndrome (GEBAUER *et al.* 2021).

1.4.1 Molecular basis of Protein-RNA interaction

RNA-binding proteins bind to mRNAs through molecular interactions between the chemical moieties present in protein residues and RNA nucleotides. The very same interactions that drive the formation of protein, and RNA tertiary structures also seal the RBP-RNA interaction, at a resolution where the boundaries between the RBP and RNA components begin to blend (CORLEY *et al.* 2020, MACKERETH AND SATTLER 2012). Specifically, sequence-specific RNA recognition occurs through various molecular interactions, including hydrogen bonding and electrostatic interactions with functional

groups, as well as hydrophobic and π-stacking interactions with nucleobases (MACKERETH AND SATTLER 2012). In contrast, non-sequence-specific contacts primarily rely on interactions with the sugar-phosphate backbone (MACKERETH AND SATTLER 2012, CORLEY *et al.* 2020).

The interactions between RBPs and RNA are highly dynamic. Upon binding, the site of RNA-RBP interactions tends to become rigid, while the neighboring regions in both RNA and proteins undergo a loosening effect to counteract the decrease in entropy. As a result, apart from the direct binding sites, adjacent residues, and nucleotides that are not directly involved in the interaction can still be instrumental in the overall binding processes (CORLEY *et al.* 2020). Importantly, unstructured regions in RNA and proteins are critical for such structural rearrangements during binding. For example, the intrinsically disordered region, the Arg-Gly-Gly motif, in the RBP, FMRP, co-folds with its target mRNA, enabling tight shape complementarity and base-specific recognition (HENTZE *et al.* 2018). Indeed, a substantial fraction of protein-RNA interaction occurs through unstructured regions that adopt structure after binding (CORLEY *et al.* 2020)

1.4.2 RNA binding domains (RBDs)

RNA-binding proteins are classified based on the presence of discrete domains that recognize specific sequences and structural elements within RNA. These domains, known as RNA-binding domains (RBDs), are typically short, with fewer than 100 amino acids, and recognize degenerate RNA sequences spanning 4-6 nucleotides (GERSTBERGER *et al.* 2014). Among the classic RNA-binding domains are the RNA-recognition motif (RRM), K-homology domain (KH domain), Zinc finger domains (Znf), and Pumilio homology domain (PUF), which are commonly associated with proteins binding to single-stranded RNA (ssRNA). Whereas, the double-stranded RNA Binding Domain (dsRBD), helicases domain, and pseudouridine synthase and archaeosine transglycosylase (PUA) domains recognize the double-stranded RNA (CORLEY *et al.* 2020).

For example, the RNA Recognition Motifs (RRM), one of the most abundant RNA-binding domains is composed of 90 amino acids and contains two conserved RNP motifs within its β_3 and β_1 sheets. These motifs expose three conserved aromatic residues on the β-sheet surface, creating a primary RNA-binding site (CORLEY *et al.* 2020, CLÉRY AND ALLAIN 2012).

Most RBPs contain multiple RBDs, often in multiple repeats. This modularity of RBD domains enables RBPs to efficiently bind to their target RNAs with high affinity and specificity (LUNDE *et al.* 2007). For example, the RBP hnRNPA1 relies on both of its RRM domains to achieve a high binding affinity and function in splicing repression (CORLEY *et al.* 2020). The linker regions connecting RBDs are also critical for facilitating protein-RNA interaction. The flexibility of these inter-domain contacts determines whether these multi-domain arrangements function cooperatively or independently. For instance, a rigid tandem configuration of RBDs can lead to RNA looping, either exposing or concealing access to specific regions of the RNA (MACKERETH AND SATTLER 2012).

1.4.3 K-Homology domain

Initially discovered in the RBP, hnRNPK, the K-Homology domains (KH) are relatively short, consisting of approximately 70 amino acids, and can bind both ssRNA and ssDNA (VALVERDE *et al.* 2008). The KH domains can be classified into two folds: Type I domains are predominantly found in eukaryotes, exhibiting a $\beta_1\alpha_1\alpha_2\beta_2\beta_3\alpha_3$ confirmation, forming a β-sheet composed of three antiparallel β-strands against three α-helices (Fig. 1.2A). In contrast, type II KH domains are commonly present in prokaryotes and feature an $\alpha_1\beta_1\beta_2\alpha_2\alpha_3\beta_3$ topology, wherein the β_2-strand and β_3-strand run parallel to each other with the β_1-strand being antiparallel to both (VALVERDE *et al.* 2008). Both types of KH domains contain a variable loop situated between the β_2-strand and β_3-strand in Type I KH domains, or between the β_1-strand and β_2-strand in Type II KH domains (Fig. 1.2A). The length of these variable loops varies, ranging from 3 amino acids to more than 60 amino acids. KH domain contains the conserved GXXG motif, which consists of the (I/L/V)-I-G-X-X-G-X-X-(I/L/V) sequence (I-Isoleucine, L-Leucine, V-Valine, G-Glycine), located between α_1 and α_2-helices. However, in some cases, the GXXG motif is either altered or interrupted, leading to diverged KH domains (CLÉRY AND ALLAIN 2012, VALVERDE *et al.* 2008).

The RNA binding surface of the KH domain comprises the GXXG motif on one side, and the β-sheet and the variable loop on the other side. Together, they form a binding

cleft that accommodates four nucleotides, with a preference for A/C-rich sequences (Fig. 1.2B; VALVERDE *et al.* 2008, NICASTRO *et al.* 2015). For example, the KH1 domain of the RBP PCBP2 recognizes the CCCU motif, whereas the KH3 domain of RBP Nova2 selectively binds the UCAC motif on target mRNA (DU *et al.* 2007, LEWIS *et al.* 2000, VALVERDE *et al.* 2008).

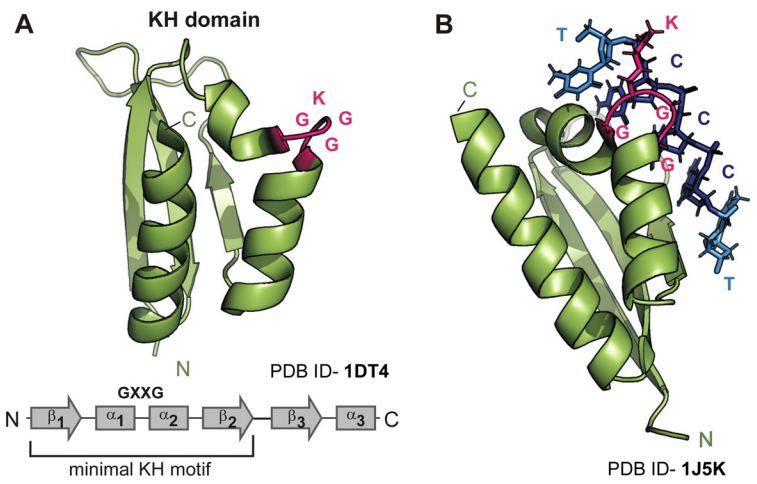

Fig. 1.2. Structure of the KH domain. **(A)** Crystal structure of NOVA KH3 domain. The GXXG loop (GKGG) is highlighted in magenta. Topology diagram of the KH fold is shown below. GXXG motif and minimal KH motif are labeled. **(B)** Solution structure of KH3 domain of hnRNPK interacting with a single-stranded DNA oligonucleotide. The GXXG loop (GKGG) is colored in magenta. KH3 domain specifically recognizes TCCC sequences (T- light blue; C- dark blue). (A-B) PDB ID- Identification code for the corresponding structure in the Protein Data Bank (PDB).

The two KH domains of ZBP1, KH3, and KH4 recognize the bipartite RNA sequences, C/A-CA-C/U and CGGAC, respectively. The center of the RNA binding cleft is hydrophobic and involves additional interactions such as hydrogen bonds which are coordinated by the GXXG motif to stabilize the protein-RNA interaction. However, stacking interactions between the KH domain and RNA are relatively scarce which also explains the lower binding affinity of this domain with single-stranded mRNAs (CORLEY *et al.* 2020). It is noteworthy that the third KH domain of the RBP, KSRP exhibits a binding preference for the G-rich sequences, highlighting the versatility of the KH domain in interacting with diverse nucleotide panels (NICASTRO *et al.* 2015; HOLLINGWORTH *et al.* 2012).

A recent finding has revealed that the small domain (SD) present in bacterial ribonucleases E/G belongs to the KH family, giving rise to the Type III KH characterized by αβααββ topology (PEREIRA AND LUPAS 2018).

The presence of augmented RBDs or multiple-KH domain repeats can help increase binding surface, affinity, and specificity either independently or synergistically. For instance, KH domains are often found to be augmented with the Quark domain and RNA

star domain for signal transduction and extension of binding surface to increase affinity, respectively (CORLEY *et al.* 2020).

RNA-binding proteins featuring KH domains are versatile in diverse RNA regulatory processes, including splicing, localization, translation, and stability. One prominently studied RBP, hnRNP K, with three KH domains, plays a pivotal role in regulating diverse biological processes and is implicated in various disease contexts. It engages in signal transduction and gene expression control by recognizing poly(C) stretches on RNA, influencing transcription, translation, and stability (WANG *et al.* 2018).

Another KH domain-containing RBP, KSRP, originally identified as part of a complex associated with intronic splicing enhancer elements (MIN *et al.* 1997), demonstrates a broad influence on RNA regulation. KSRP is linked to processes encompassing localization, mRNA decay, and translational repression. For instance, KSRP engages with RNA exosome complex for the degradation of mRNAs such as *fos*, *tnf,* and *il2* mRNA, thereby modulating the immune response in HeLa cells (GHERZI *et al.* 2004, BRIATA *et al.* 2005).

1.5 Methods for identifying *in vivo* binding of an RBP

To identify the RNA regulatory process, one must first characterize the RBP-RNA interactions involved. Approaches to study such interactions can be broadly categorized into protein-centric or RNA-centric. The protein-centric approaches comprise identifying the RNA repertoire bound by a specific RBP, while the RNA-centric involves exploring the RNA-bound proteome.

A common protein-centric strategy for identifying RBP targets involves immunoprecipitation of the specific RBP along with its associated RNAs. This method includes techniques such as RNA immunoprecipitation (RIP) or cross-linking and immunoprecipitation (CLIP) (HAFNER *et al.* 2021). In recent times, novel methods for identifying RBP targets through proximity RNA labeling have emerged. These methods involve fusing an RNA base editor with the RBP of interest which enables selective labeling of RNAs that are bound by the RBP (RAHMAN *et al.* 2018, BRANNAN *et al.* 2021).

1.5.1 CLIP

CLIP methods serve as the current gold standard for elucidating RBP target mRNAs. Among the diverse CLIP variants, such as high-throughput sequencing of RNA isolated by CLIP (HITS-CLIP), individual-nucleotide resolution CLIP (iCLIP), enhanced CLIP (eCLIP), infrared CLIP (irCLIP), and photoactivatable ribonucleoside-enhanced CLIP (PAR-CLIP) and proximity CLIP, these protocols share a fundamental core workflow (Ramanathan et al., 2019, Hafner et al., 2021).

To capture the *in vivo* RNA binding pattern of an RBP, all CLIP methods initiate with UV irradiation of living cells to irreversibly crosslink the RBP-RNA contact sites. Following crosslinking, the cells are lysed and subjected to careful RNase digestion to restrict the length of RNA fragments while simultaneously preventing excessive digestion that could compromise RBP binding sites. The cross-linked RNP of interest is then immunoprecipitated using RBP-specific antibodies, followed by proteinase K digestion to release crosslinked RNA fragments from the RBP. The resultant RNAs are converted into cDNA for high-throughput sequencing (Fig. 1.3A; BUSCH *et al.* 2020, HAFNER *et al.* 2021).

After sequencing, the reads are processed and mapped to the genome to identify the genomic positions of the nucleotides that crosslinked to the RBP. This information is then used to derive peaks, indicative of regions characterized by high density of RBP crosslinking. These peaks are subsequently used to identify binding features such as RNA-binding motifs or structures that drive the dynamic RBP-RNA interactions. Because these peaks are derived from RNA sequences bound by the immunoprecipitated RBP, the CLIP techniques offer identification of the RBP binding site at nucleotide resolution (BUSCH *et al.* 2020, HAFNER *et al.* 2021).

1.5.2 HyperTRIBE

Although the CLIP methods offer high-resolution RBP binding site information, they suffer from notable drawbacks: 1. The requirement of large amounts of input material, 2. Biases are introduced by biochemical steps such as immunoprecipitation, RNase digestion, ligation, and target mRNA expression, 3. Influence of nucleotides (e.g., Uracil) in UV crosslinking, affecting the detected targets (RAMANATHAN *et al.* 2016). The low efficiency of UV crosslinking during host-microbe interaction and the scarcity

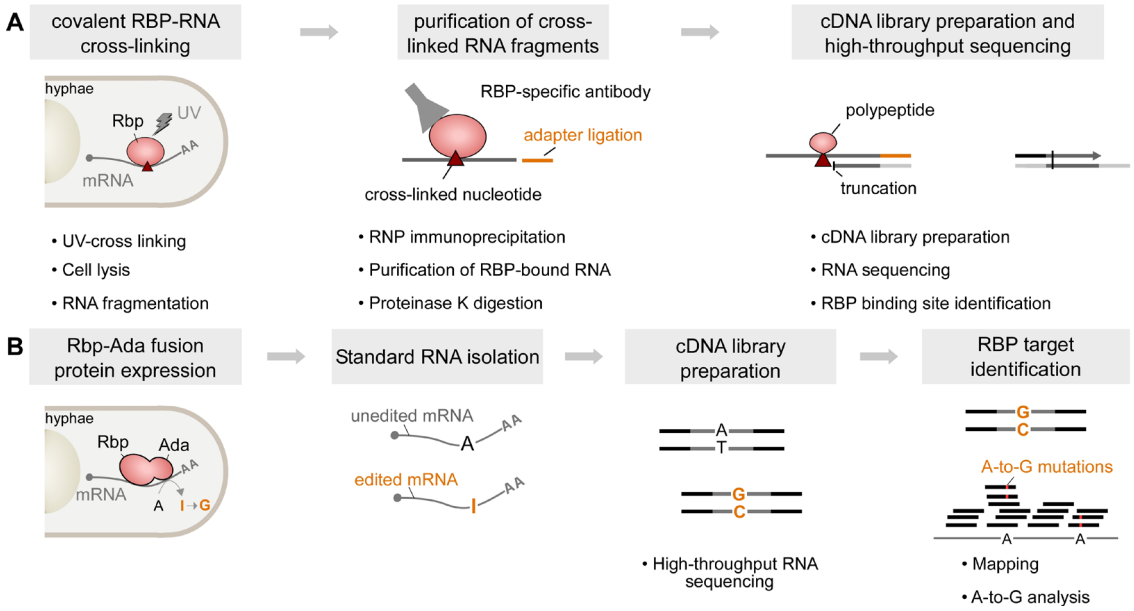

Fig. 1.3. Schematic overview depicting the CLIP and hyperTRIBE methods. **(A)** Schematics representing the key steps involved in the CLIP protocol. The process initiates with UV irradiation (indicated by the red triangle) to covalently crosslink RBPs with their bound RNA molecules. Following cell lysis, RNAs are fragmented, resulting in the formation of RBP-bound RNA fragments. In the subsequent step, the RBP (Rbp) of interest is immunoprecipitated and the adapter is ligated to bound RNA. The immunoprecipitated RBP-RNA complex is then purified using SDS-PAGE. The RBP is digested using proteinase K to release the bound RNA fragments, leaving a short peptide at the cross-linking site. The RNA fragments are subjected to reverse transcription to generate cDNA libraries for RNA-seq and RBP binding site identification. **(B)** In the hyperTRIBE method, the Rbp of interest is fused with the catalytic domain of ADAR (Ada). When the fusion protein (Rbp-Ada; red) binds its target mRNA (grey; grey circle- 5′ cap; AA- poly(A) tail), the Ada domain catalyzes the conversion of nearby adenosine (A) into inosine (I; orange), which is recognized as guanine (G; orange) by cellular enzymes. Total RNAs are subsequently isolated and used to generate cDNA libraries for RNA-seq analysis. "I" indicates the position of deaminated adenosine in the edited mRNA. This editing process leads to the conversion of A-T base pairs to G-C base pairs. Sequencing reads are aligned to the reference genome to identify RBP targets containing the editing sites.

of fungal biomass within the host tissues further complicate the application of this laborious method in fungal pathogens.

Recently, an RNA proximity labeling technique called hyperTRIBE was developed as an alternative to identify mRNA targets of RBPs in *Drosophila melanogaster* (McMahon *et al.* 2016, Rahman *et al.* 2018). HyperTRIBE utilizes the fusion of the catalytic domain of ADAR (Adenosine deaminase acting on RNA) with the RBP of interest. The endogenous *Drosophila* ADAR contains a dsRBD domain for RNA recognition and a catalytic domain that deaminates nearby adenosine to inosine. In hyperTRIBE, the ADAR catalytic domain carrying the hyperactive E488Q mutation is used for improved editing (Rahman *et al.* 2018 Rahman *et al.* 2018). When the hyperTRIBE fusion protein interacts with mRNAs through the RNA-binding domain of

the RBP, the linked catalytic domain irreversibly deaminates nearby adenosine to inosine on the mRNA, which is recognized as guanosine both *in vivo* and *in vitro.* The transcriptome is then sequenced to identify RBP-bound target mRNAs with novel "A-to-G" footprints (Fig. 1.3B).

The crystal structure of the human ADAR2 catalytic domain revealed a zinc ion positioned at the catalytic center directs the water molecule to displace ammonia during the nucleophilic hydrolytic deamination of adenosine. The coordination of the zinc ion is mediated by a histidine residue (H394), and two cysteine residues (C451, and C516). Furthermore, the glutamate residue (E396) engages in hydrogen bonding with a water molecule to contribute to this coordination (MACBETH *et al.* 2005). This catalytic zinc center is surrounded by the positive electrostatic potential, serving as a binding site for the dsRNA target (MACBETH *et al.* 2005). Since the site of nucleophilic attack for deamination lies in the major groove of the dsRNA, the ADAR catalytic domain employs base-flipping mechanisms to access the reactive base, a necessary step for the reaction (MATTHEWS *et al.* 2016). Interestingly, the heightened editing after replacing the negatively charged glutamate (E488) residue with the neutral glutamine (Q) caused protonation-independent hydrogen binding with N3 of the orphan cytidine in the dsRNA, resulting in efficient base flipping, and so increased catalytic rate (KUTTAN AND BASS 2012, DOHERTY *et al.* 2021).

In contrast to techniques such as iCLIP, hyperTRIBE offers a simple experimental procedure to determine the RBP targets. Especially, the absence of RBP immunoprecipitation and cross-linking, combined with the requirement of less input material, make hyperTRIBE an ideal tool for the identification of RBP targets during fungal pathogenesis. In addition to fruit flies, the hyperTRIBE approach has also been successfully established in mammalian, as well as plant systems for RBP target detection (NGUYEN *et al.* 2020,JIN *et al.* 2020,ARRIBAS-HERNÁNDEZ *et al.* 2021,CHENG *et al.* 2021). Interestingly, even though the plants lack ADAR orthologues akin to fungi, the functional viability of the hyperTRIBE technique remains intact in plants. In line with this, it is worth noting that the expression of human ADAR2 in *S. cerevisiae* leads to the deamination of yeast transcripts, suggesting the potential applicability of this potent technique in *U. maydis* (EIFLER *et al.* 2013).

1.6 *Ustilago maydis*: A dimorphic fungal pathogen

Ustilago maydis is a basidiomycete fungal pathogen, a causative agent of smut disease in maize plants (Fig. 1.4A). The pathogen exclusively infects the maize (*Zea mays*) and its ancestor, teosinte (*Z. mays* subsp. *mexicana*), and affects all aerial organs of the plant. Infection of *U. maydis* is characterized by the induction of anthocyanin production and the formation of large tumors where fungal spores develop (DE LANGE *et al.* 2014, LANVER *et al.* 2017). Consequently, the smut disease leads to diminished plant growth, lower crop yield, and subsequent economic losses (MARTÍNEZ-ESPINOZA *et al.* 2002).

U. maydis exists in two morphologies: a saprophytic yeast-like form and a pathogenic hyphal form. The life cycle of *U. maydis* initiates with the germination of diploid spores which undergo meiosis to create a promycelium wherein haploid nuclei migrate (Fig. 1.4B). The haploid cells bud off from the promycelium following mitosis to enter the vegetative life cycle. These haploid yeast-like cells proliferate via budding (Fig. 1.4C). The vegetative life cycle culminates when two non-pathogenic haploid cells of compatible mating type are recognized on the leaf surface (Fig. 1.4D; VOLLMEISTER *et al.* 2012, LANVER *et al.* 2017, LANVER *et al.* 2018). This recognition is mediated by a pheromone response system involving seven transmembrane domain receptors and the ligand, small lipopeptide pheromones, encoded at the biallelic *a*-mating type locus. Pheromone binding initiates the MAPK signaling pathway that orchestrates gene expression to induce conjugation tubes and cell cycle arrest (VOLLMEISTER *et al.* 2012). The developed conjugation tubes orient towards the pheromone gradient of the mating partner for fusion. Central to this regulation is the transcription factor Prf1, which not only contributes to conjugation tube formation but is also essential for the expression of *b* mating-type genes *bE* and *bW* (VOLLMEISTER *et al.* 2012).

The fusion results in the formation of dikaryotic hyphae, a hallmark infectious structure that grows polarly by elongating at the tip and inserting retraction septa at the basal end (Fig. 1.4E). This morphological shift from yeast to hyphae is facilitated by the bE and bW proteins, which by forming a heterodimeric complex orchestrates a hierarchical, multilayered transcriptional network controlling more than 340 genes (HEIMEL *et al.* 2010b). These genes encode proteins that play vital roles in the transition from budding to polarized growth and cell cycle arrest sustainment (HEIMEL *et al.* 2010b). Notably, the bE/bW heterodimeric complex commences only when derived from the different alleles of the multiallelic *b* locus. The bE/bW transcription factor does not directly regulate

numerous b-responsive genes; rather, their activation requires the participation of a secondary central regulator, Rbf1, induced by bE/bW (HEIMEL *et al.* 2010b).

Upon perceiving plant signals, dikaryotic filaments develop appressoria, specialized infection structures that facilitate the penetration of plant cells by degrading the cell wall (Fig. 1.4F-G; SCHIRAWSKI *et al.* 2005,LANVER *et al.* 2014). Inside the plant, the resumption of cell cycle arrest, results in cell division. During this phase, a clamp-like structure is developed for proper nucleus distribution (SCHERER *et al.* 2006). A key for this process is the Clp1 protein, which interacts with bW proteins and Rbf1 (HEIMEL *et al.* 2010a). This leads to the inactivation of the bE/bW complex and the subsequent downregulation of the pheromone-response pathway via Rbf1 (SCHERER *et al.* 2006, HEIMEL *et al.* 2010a).

After entering the plant, hyphae initially grow intracellularly, enclosed by plant plasma membrane to establish a tight interaction zone for colonization. Later, they proliferate intercellularly, resulting in massive proliferation and hyphal fragmentation (Fig. 1.4H). Together with the irregular division of host cells, these events give rise to the development of large tumors at all aerial parts of the plants. Within these tumors, the black teliospores are formed through karyogamy. Mature spores are then released and dispersed by the wind (Fig. 1.4I-K; VOLLMEISTER *et al.* 2012, LANVER *et al.* 2017, LANVER *et al.* 2018).

U. maydis is a biotrophic fungal pathogen, sustain by feeding off the host cell without killing them. During infection, the pathogenic fungi secrete an arsenal of effector proteins, to suppress plant defense and reprogram the host metabolism (LANVER *et al.* 2017). Effectors like Pep1 and Pit2 hinder the plant defense system by inhibiting the host peroxidase Pox12 and cysteine proteases, respectively (DOEHLEMANN *et al.* 2009, MUELLER *et al.* 2013). The abundant expression of these critical proteins during the biotrophic phase imposes enormous stress on ER, necessitating the unfolded protein response (UPR) pathway to preserve ER homeostasis and secretion (LANVER *et al.* 2018).

In *U. maydis*, the UPR is tightly linked to the establishment of biotrophic development and altered specifically after plant entry (HEIMEL *et al.* 2010a,HEIMEL *et al.* 2013,PINTER *et al.* 2019). Mainly, this interaction renders *U. maydis* resistant to ER stress, increasing its secretion capacity before host colonization and promoting long-term UPR activity

(HEIMEL *et al.* 2010a,HEIMEL *et al.* 2013,PINTER *et al.* 2019,HARTING AND HEIMEL 2020).

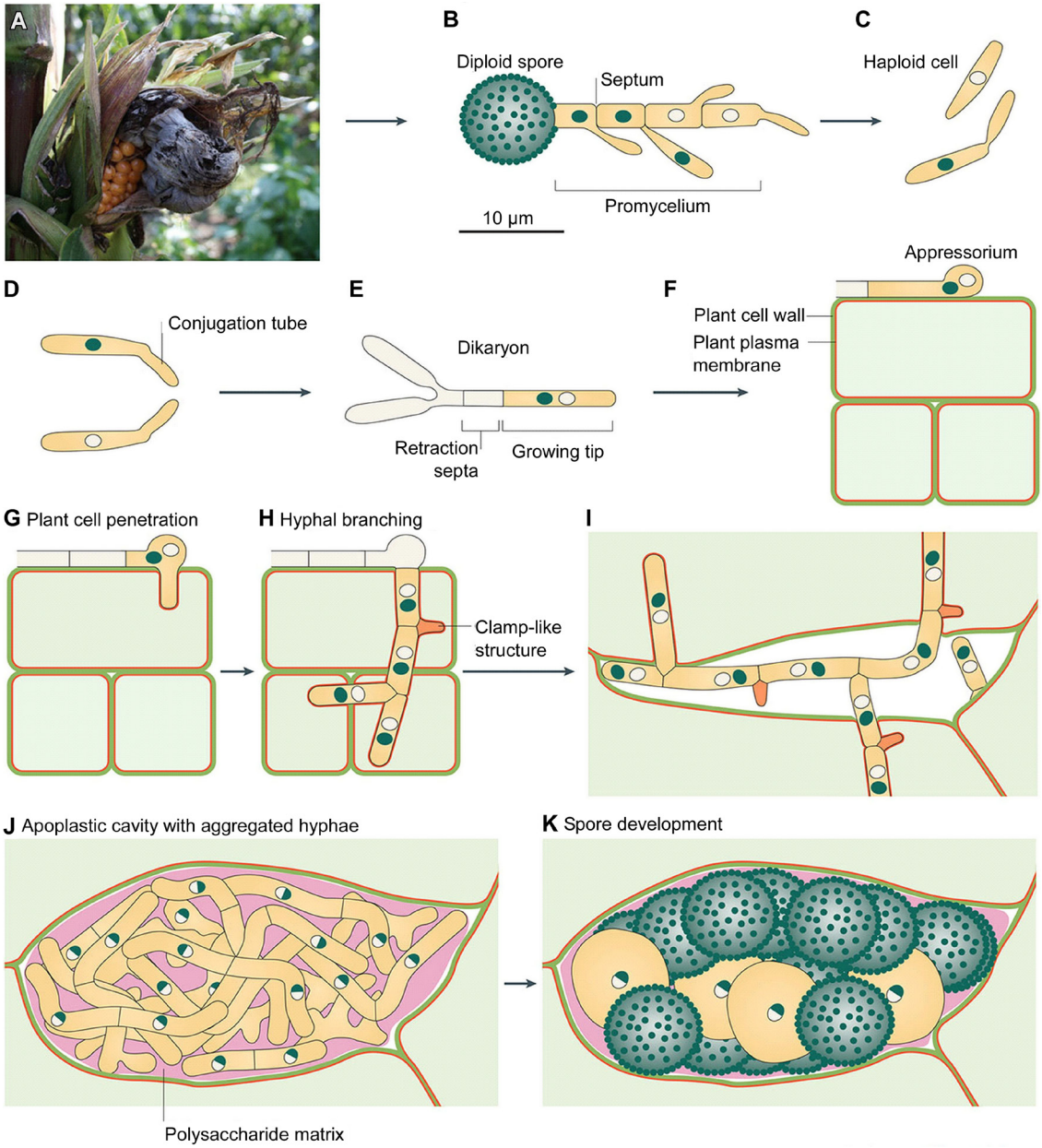

Fig. 1.4. The life cycle of the dimorphic fungal pathogen *Ustilago maydis*. **(A)** Symptoms of a cob infection by *U. maydis* in a maize field. The infection is locally confined and characterized by the induction of anthocyanin biosynthesis and the formation of large tumors in which fungal spores develop. **(B)** Diploid spores are released when tumors break open. They are dark colored owing to their high melanin content and have a characteristic round shape and surface ornamentation. Meiosis takes place in germinating spores; the four resulting haploid nuclei migrate into a promycelium, in which they become delineated by septa. **(C)** Following mitotic divisions, haploid cells bud off from these compartments. **(D)** After detection of a compatible mate, the budding program ceases and cells develop conjugation tubes that are directed towards each other. **(E)** After cell fusion, a filamentous cell cycle-arrested dikaryon is produced. Only the growing tip of this filament is filled with cytoplasm (yellow), whereas older parts are vacuolated (grey) and become sealed off by regularly spaced septa. These retraction septa enable filament elongation and the formation of an infective structure (appressorium) in extended infectious hyphae. **(F)-(G)** Hyphal tip cells develop appressoria in specific locations on the leaf surface and then penetrate plant cells. **(H)** During early

stages of infection, the cell cycle arrest is released, hyphae begin to branch and clamp-like structures (orange) assure correct segregation of the two nuclei. During these intracellular stages, hyphae are completely encased by the host plasma membrane (red). **(I)** With the onset of plant tumor formation, fungal hyphae are mainly detected intercellularly. **(J)** Subsequently, the two nuclei of the dikaryon fuse, followed by the substantial proliferation of diploid cells that form huge aggregates in apoplastic cavities. Aggregated hyphae become embedded in a gelatinous polysaccharide matrix (pink). **(K)** Hyphae then fragment and undergo spore development. In all panels, white and dark grey nuclei indicate that they are haploid and have different mating-type genes. Nuclei that are half white and half dark grey indicate diploid nuclei that are generated through the fusion of white and dark grey nuclei. Image in part a courtesy of R. Rösser, Max Planck Institute for Terrestrial Microbiology, Marburg, Germany. (Figure and legend adapted from LANVER *et al.* 2017 under the terms of Springer Nature license No. 5617680925598).

In spite of decades of extensive research, a comprehensive understanding of the posttranscriptional regulatory network underlying the pathogenesis of *U. maydis* remains poorly understood. Nevertheless, the existence of a well-established molecular toolbox positions *U. maydis* as the suitable model system for studying RNA biology during fungal virulence (BRACHMANN *et al.* 2001, STEINBERG AND PEREZ-MARTIN 2008, TERFRÜCHTE *et al.* 2014, MÜNTJES *et al.* 2020, LANVER *et al.* 2017). For example, a recent time-resolved transcriptional profiling via RNA sequencing offers valuable insights into the gene expression modules across various fungal developmental stages (LANVER *et al.* 2018). Haploid laboratory strains like AB33 and SG200 have streamlined fungal research. In AB33, the bE/bW transcription factor is expressed under the control of the nitrate-inducible P_{nar1} promoter. This enables the synchronous induction of hyphal polar growth through a mere change in the nitrogen source (BRACHMANN *et al.* 2001). Whereas, the solo pathogenic strain SG200, expressing compatible mating genes in a single genetic background, facilitates infection experiments without the requirement for an appropriate mating partner (BÖLKER *et al.* 1995).

Moreover, the conservation of biological processes such as mitosis, and long-distance transport between *U. maydis* and metazoan (VOLLMEISTER *et al.* 2012, STEINBERG AND PEREZ-MARTIN 2008), extends the potential of the pathogenic fungi to probe complex biological questions beyond pathogenesis, providing insights into cellular biology at a broader scale. Studying *U. maydis* as a model pathogen also revealed a significant interplay between RNA biology and membrane trafficking. For a more detailed discussion on this topic, please refer to Appendix 1 (Chapter 5), which contains a review published in PLOS Pathogens (SANKARANARAYANAN *et al.* 2023b).

1.7 Khd4: A key RBP for morpho- and pathogenesis in *U. maydis*

In *U. maydis*, the investigation into 27 RBPs, consisting of well-recognized RNA-binding domains, via reverse genetic approaches, unveiled three candidates- Khd4, Rrm4, and Khd1- associated with aberrant phenotypes upon their deletion (BECHT *et al.* 2005). Among these, Khd4, characterized by its multi-KH domain, emerged as a crucial component for the proper morphology and pathogenicity of *U. maydis*. Deletion of *khd4* causes pleiotropic phenotype, resulting in cytokinesis defective yeast cells, aberrant hyphal cells characterized by shortened and thickened morphology, and reduced virulence (VOLLMEISTER *et al.* 2009; Fig. 1.5C-E).

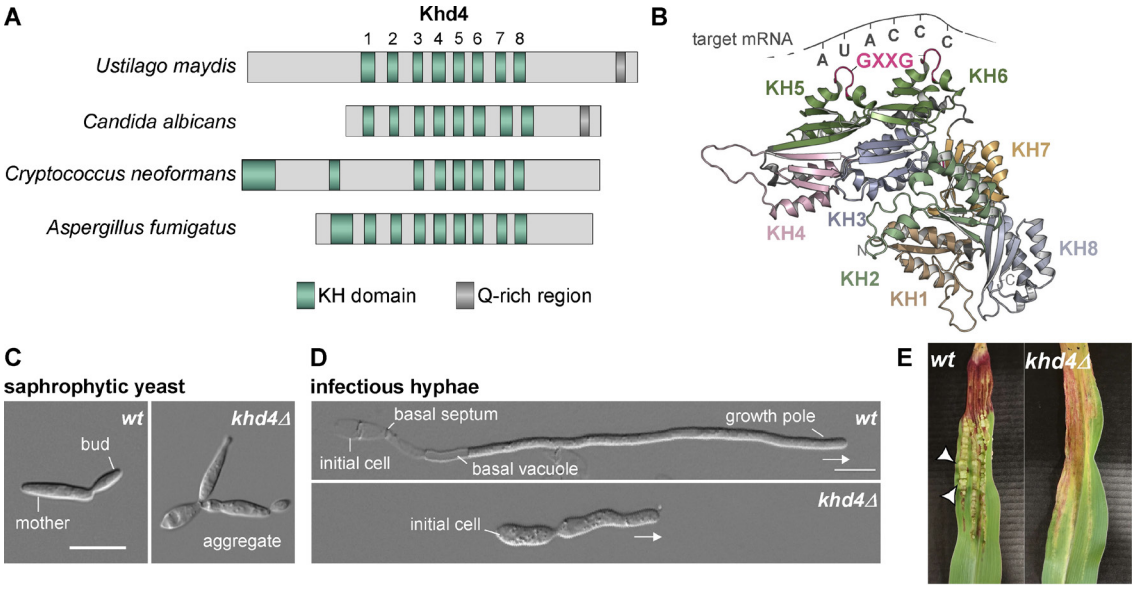

Fig. 1.5. The multi-KH RBP Khd4 is indispensable for the morphology and pathogenicity of *U. maydis*. **(A)** Conservation of the multi-KH domains (green) in Khd4 and homologs from pathogenic fungi. **(B)** Structure model of Khd4 predicted by Alphafold2. Khd4 contains 8 central KH domains. KH5-6 is necessary and sufficient for AUACCC binding (grey). GXXG motif is shown in magenta color. **(C)** AB33-derived *wt* (left) and *khd4Δ* (right) yeast cells. Scale bar: 10 µm. **(D)** AB33-derived *wt* (top) and *khd4Δ* (bottom) hyphal cells. Arrow mark indicates the growth direction. Scale bar: 10µm **(E)** Typical symptoms of maize seedling infection experiments. While the wildtype induces the formation of characteristic tumours (white arrowheads), *khd4Δ* strains only elicit anthocyanin formation and chlorosis.

Additionally, the absence of Khd4 leads to diminished pheromone production and conjugation hyphae formation. Remarkably, although the *khd4Δ* cells can form infectious hyphae capable of penetrating the plant cells, the elicitation of the plant defense system substantially inhibits further fungal growth (VOLLMEISTER 2009; Personal communication with Lea Geißl).

Khd4 is a large protein, about ~151 kDa in molecular weight, formed by 1416 amino acids. Initially reported to contain six KH domains, recent structural predictions using

AlphaFold 2 have revealed that Khd4, in fact, comprises eight KH domains, including 3 classic domains having GXXG loop (KH2, 5, and 6), and 5 divergent domains. In line with the structural predictions, the domains KH5 and 6 (formerly known as KH3 and KH4, respectively), containing the conserved KH domain topology, are crucial for RNA binding (Fig. 1.5A-B). By employing yeast three-hybrid analysis, it was previously revealed that KH5 and 6 bind mRNAs by recognizing the AUACCC motif, an RNA binding element that is necessary and sufficient for Khd4 binding. Mutations in the GXXG domains of KH5 and KH6 domains abolished the RNA binding property of Khd4 and caused a phenotype akin to *khd4* deletion. This strongly implies that the RNA-binding property of Khd4 is essential for its function, indicating the necessity of the systematic identification of Khd4 RNA targets (VOLLMEISTER 2009).

Furthermore, homologs of Khd4 with a comparable number of KH domains, are also present in mammalian fungal pathogens like *C. albicans*, *C. neoformans*, and *A. fumigatus.* This underscores the strong conservation of Khd4 function in fungal pathogenic programs and emphasizes the significance of characterizing this protein to combat fungal diseases (Fig. 1.5A).

Beyond its KH domains, the N- and C- terminus of Khd4 are predicted to be highly disordered. It has been known that such intrinsically disordered regions can interact with protein and RNA, forming higher-order assemblies such as membrane-less compartments (DECKER AND PARKER 2012). Notably, the C-terminal region features a region with a high prevalence of glutamine (Fig. 1.5A; Q-rich regions), commonly associated with prion-like domains (PrLDs). The combination of RNA-binding domains and PrLDs in proteins often points to a heightened tendency for phase separation (WIEDNER AND GIUDICE 2021). Indeed, in line with this, Khd4 demonstrates the ability to undergo phase separation, forming membrane-less cytoplasmic stress granules under heat stress (VOLLMEISTER 2009). This behavior persists despite its predominant cytoplasmic distribution under normal conditions.

Under laboratory conditions, Khd4 is a cytoplasmic protein with relatively low expression levels. Deletion of *khd4* renders the cells a slow growth rate (doubling time ~4h) accompanied by defects in cell wall composition (VOLLMEISTER 2009). Given its significance, attempts to genetically modify the *khd4* gene for functional manipulation are challenging attributed to its critical role.

1.8 Aim of this study

Despite its paramount importance, the significance of Khd4 in shaping the morphology and pathogenicity remained unknown. This study aimed to investigate the role of Khd4 in orchestrating infectious hyphae development in the pathogen *U. maydis*.

To understand RBPs, an essential first step was identifying their direct binding to mRNA targets. Previous endeavors to uncover Khd4 targets using conventional biochemical approaches, such as the CLIP method, proved unsuccessful due to its high molecular weight and low expression levels. Therefore, the primary objective of this thesis was to establish a novel method called hyperTRIBE in *U. maydis,* the first of its kind in a fungal system. To validate the feasibility of hyperTRIBE in fungal systems, we initially applied this method to the well-studied RNA-binding protein, Rrm4. Following successful validation, we utilized hyperTRIBE to unveil *in vivo* mRNA targets of Khd4, with the Khd4 binding site AUACCC serving as a stringent criterion for identifying high-confidence target mRNAs.

The second objective was to decode the regulatory potential of Khd4 in RNA regulation by employing Khd4 binding sites on high-confidence target mRNAs. Additionally, this study sought to explore how Khd4 mediates cellular processes that influence the polar growth of infectious hyphae.

In summary, this thesis combined transcriptome-wide *in vivo* binding studies with computational techniques, fungal genetics, and cell biology to elucidate the role of Khd4 in *U. maydis* pathogenic development. Studying Khd4 sets a foundation for understanding the significance of RNA regulation in fungal pathogenesis, potentially paving the way for innovative anti-fungal therapies. Significantly, the successful application of hyperTRIBE to identify *in vivo* target mRNAs establishes a robust precedent for future studies on RNA-binding proteins in fungi.

2 Results

The following chapters provide the study towards understanding the role of the multi-KH domain RBP Khd4 in the pathogenic development of *U. maydis*. The complete study is organized into three distinct parts.

- The first part (Chapter 2.1) presents a comprehensive study elucidating the novel role of Khd4 in the spatiotemporal gene expression control during infectious hyphae development in *U. maydis*. Additionally, it details the application of the RNA-editing-based hyperTRIBE technique. This study has already been published in PNAS 2023 under the title “The mRNA stability factor Khd4 defines a specific mRNA regulon for membrane trafficking in the pathogen *Ustilago maydis*”. Hence, it is adapted with minor changes without affecting the scientific content. In accordance with standard scientific protocol, the utilization of the personal pronoun "we" in this chapters refers to the reader and the writer, as well as my scientific collaborators and myself.
    - The detailed information about the pilot study, which serves as a proof-of-principle for validating the hyperTRIBE technique using the well-studied RBP Rrm4, is described in Chapter 5, Appendix 2.

- The second part (Chapter 2.2) describes the subcellular localization study of Khd4, providing insights into its potential role in the endoplasmic reticulum.

- The third part (Chapter 2.3) predicts the potential mRNA regulons controlled by Khd4 during the infection of *U. maydis* in plant hosts.

2.1 The mRNA stability factor Khd4 defines a specific mRNA regulon for membrane trafficking in the pathogen *Ustilago maydis*

Srimeenakshi Sankaranarayanan[a], Carl Haag[a], Patrick Petzsch[b], Karl Köhrer[b], Anna Matuszyńska[c], Kathi Zarnack[d,e,1], and Michael Feldbrügge[a,1]

a Heinrich Heine University Düsseldorf, Institute for Microbiology, Cluster of Excellence on Plant Sciences, 40204 Düsseldorf, Germany.

b Biologisch-Medizinisches Forschungszentrum (BMFZ), Heinrich Heine University Düsseldorf, Universitätsstr. 1, 40204 Düsseldorf, Germany.

c Computational Life Science, Department of Biology, RWTH Aachen University, Worringerweg 1, 52074 Aachen, Germany.

d Buchmann Institute for Molecular Life Sciences (BMLS), Goethe University Frankfurt, 60438 Frankfurt a.M., Germany.

e Institute of Molecular Biosciences, Goethe University Frankfurt, 60438 Frankfurt a.M., Germany.

[1] Shared corresponding authorship

This research article was published in PNAS in 2023 and is available at https://doi.org/10.1073/pnas.2301731120

Significance

Fungal pathogens cause severe diseases in humans, animals, and plants. To develop new defense strategies, we need to understand how infection is precisely regulated at the DNA and RNA levels. However, knowledge on RNA regulation in fungal pathogens is currently scarce. Here, we adopt a powerful *in vivo* RNA labeling technique for fungi. Thereby, we uncover how a key RNA-binding protein (RBP) orchestrates the polar growth of infectious hyphae by determining the exact stability of mRNAs encoding regulators of membrane trafficking. Thus, we disclose a different regulatory concept for infection: a single RBP determines the precise timing of expression for numerous regulatory proteins at the level of mRNA stability. This opens up the opportunity to use RBPs as novel fungicide targets

Abstract

Fungal pathogens depend on sophisticated gene expression programs for successful infection. A crucial component is RNA regulation mediated by RNA-binding proteins (RBPs). However, little is known about the spatiotemporal RNA control mechanisms

during fungal pathogenicity. Here, we discover that the RBP Khd4 defines a distinct mRNA regulon to orchestrate membrane trafficking during pathogenic development of *Ustilago maydis*. By establishing hyperTRIBE for fungal RBPs, we generated a comprehensive transcriptome-wide map of Khd4 interactions *in vivo*. We identify a defined set of target mRNAs enriched for regulatory proteins involved, e.g., in GTPase signaling. Khd4 controls the stability of target mRNAs via its cognate regulatory element AUACCC present in their 3′ untranslated regions. Studying individual examples reveals a unique link between Khd4 and vacuole maturation. Thus, we uncover a distinct role for an RNA stability factor defining a specific mRNA regulon for membrane trafficking during pathogenicity.

2.1.1 Introduction

Fungal pathogens are ubiquitous and pose a serious threat to public health, agriculture, and wildlife. Fungal infections are estimated to cause more than 1.5 million deaths per year (BROWN *et al.* 2012b) and account for a 30% reduction in crop yield worldwide (FISHER *et al.* 2020). A widespread virulence strategy of these pathogens is their capacity for morphological plasticity, i.e., the alternation between yeast and hyphal growth forms (GOW *et al.* 2002,MIN *et al.* 2020). In particular, hyphae formation is a criterion for successful host invasion in many pathogenic fungi (BRAND AND GOW 2009). For example, the human pathogen *Candida albicans* requires the morphological transition from yeast-like to hyphal growth to invade host tissue and selectively escape the host immune system (SUDBERY 2011,ERWIG AND GOW 2016). In the plant pathogen *Ustilago maydis,* the switch from yeast to hyphal form is tightly linked to mating and is essential for plant entry and infection (LANVER *et al.* 2017).

The polarized growth of fungal hyphae is intimately associated with intracellular membrane trafficking. Vesicle transport, for example, mediates the delivery of new plasma membranes and cell wall material to growth poles and therefore determines the shape and growth direction of hyphal cells (RIQUELME *et al.* 2018). Equally important is the recycling of excess plasma membrane components via endocytosis. Furthermore, the balance between endocytosis and exocytosis forms the basis for dynamic hyphal growth (COMMER AND SHAW 2020). The transport of cargo between different cellular compartments is robustly controlled by distinct regulatory proteins. In particular, small GTPases such as Rab, Rho, Arf, and Arl, and their interaction partners serve as master regulators of vesicle trafficking (DAUTT-CASTRO *et al.* 2021).

The link between membrane trafficking and infectious hyphal growth is well-studied in the plant pathogen *U. maydis* causing corn smut disease (MÜNTJES *et al.* 2021). To maintain its morphology and pathogenicity, this phytopathogen inordinately depends on endocytosis mediated by the bidirectional shuttling of early endosomes (WEDLICH-SÖLDNER *et al.* 2000). Besides their role in endocytosis, the shuttling early endosomes also offer a transportation platform for organelles such as peroxisomes as well as mRNAs and associated polysomes throughout the hyphal cells (STEINBERG 2014, MÜNTJES *et al.* 2021). For such a complex process to be coordinated, robust spatiotemporal control of the associated proteins is essential. At the post-transcriptional level, it was found that the RNA-binding protein (RBP) Rrm4 transports mRNAs of morphological regulators, such as all four septin-encoding mRNAs, along fungal hyphae, determining the local translation and the spatial distribution of the translation products (KÖNIG *et al.* 2009,BAUMANN *et al.* 2014).

Previously, we discovered that a second RBP, Khd4, is crucial for morphogenesis and pathogenesis in *U. maydis*. The loss of Khd4 resulted in cytokinesis defects in yeast-like cells, aberrant morphology of hyphae, and impaired virulence (Fig. 2.1A; Chapter 5, Appendix 2, Fig. 5.2A; VOLLMEISTER *et al.* 2009). Khd4 is a multi-KH domain-containing RBP, with KH domains 3 and 4 being crucial for RNA binding. Based on binding studies in the heterologous yeast three-hybrid assay, Khd4 recognizes the RNA motif AUACCC, and its KH domains 3 and 4 are necessary and sufficient for binding. Mutations in KH domains 3 and 4 severely impact the morphology and virulence of *U. maydis,* suggesting that the RNA binding potential of Khd4 is responsible for its function (VOLLMEISTER *et al.* 2009). However, it is currently unclear how Khd4 tunes the morphological transition and pathogenic development. Here, we perform a transcriptome-wide identification of *in vivo* target mRNAs in infectious hyphae. We demonstrate that Khd4 regulates the expression of a distinct set of regulatory proteins involved in membrane trafficking and reveal a new link to post-transcriptional control of vacuole biogenesis.

2.1.2 Results

Loss of Khd4 causes defects in polar growth of infectious hyphae

To study the role of Khd4 during pathogenic development, we focused on the formation of infectious hyphae. For this, we conducted a time-course analysis to determine the appropriate induction time needed for hyphae establishment. As the genetic background,

we used the laboratory strain AB33, which expresses the heteromeric master transcription factor (bE/bW) for hyphal formation under the control of the nitrate-inducible P_{nar1} promoter. By switching the nitrogen source, hyphal growth can be induced synchronously in a highly reproducible manner

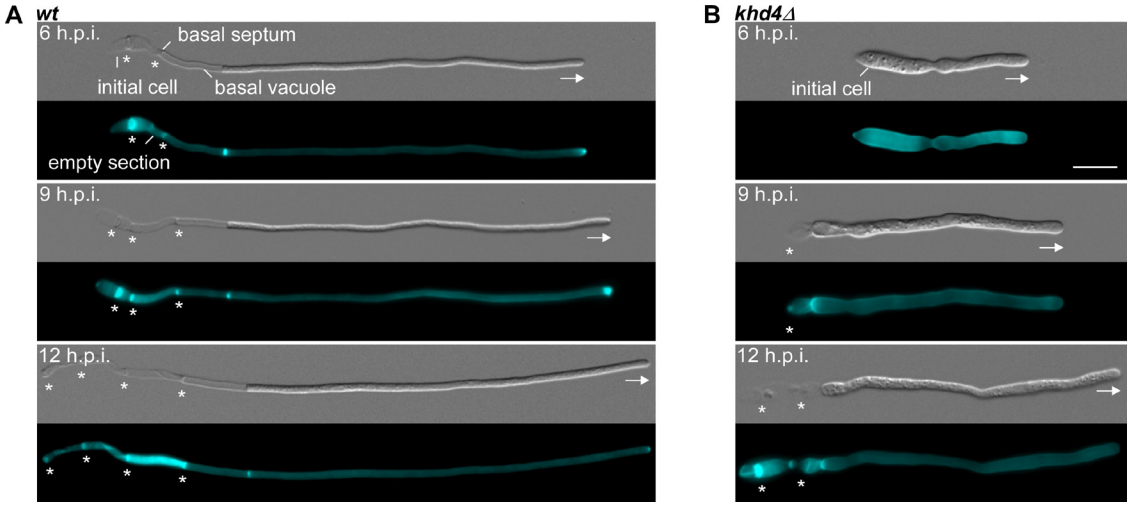

Fig. 2.1. Khd4 is important for hyphal growth. Differential interference contrast (DIC, Top panels) and Calcofluor white staining (Bottom panels; CFW, 18) of **(A)** wild-type (*wt*) and **(B)** *khd4Δ* hypha grown for 6, 9, and 12 hours post induction (h.p.i.). All strains are derivatives of AB33. Basal septa and growth directions are marked by asterisks and arrows, respectively (scale bar: 10 µm.).

(Fig. 2.1A; BRACHMANN *et al.* 2001). The resulting hyphae grow unipolarly by tip expansion up to a defined length of about 100 µm. This maximal length is maintained over time by the insertion of regularly spaced septa, generating characteristic cytoplasm-free sections consisting of cell wall remnants at the basal pole (Fig. 2.1A; FREITAG *et al.* 2011,BAUMANN *et al.* 2014). Observations of wildtype hyphae with basal septa were already evident at six hours post induction (6 h.p.i.; Fig. 2.1A). In contrast, the deletion of *khd4* resulted in delayed hyphal development (Fig. 2.1A-B; Chapter 5, Appendix 2, Fig. 5.2B-E). Compared to wildtype hyphae, the *khd4Δ* hyphae were shorter, thicker, and aggregated at 6 h.p.i. (Fig. 2.1A-B; Chapter 5, Appendix 2, Fig. 5.2A, F). However, prolonging the induction time caused a gradual recovery of hyphal length, reduced the diameter, and increased the basal septa insertion in *khd4Δ* cells (Fig. 2.1B; Chapter 5, Appendix 2, Fig. 5.2B-E). A longer period of hyphal induction also diminished hyphal aggregation (Chapter 5, Appendix 2, Fig. 5.2F). Although *khd4*Δ hyphae can attain comparable lengths to wildtype, it is known that the virulence of *khd4*Δ strains is severely reduced, highlighting the critical role of Khd4-mediated RNA regulation also during later stages of pathogenic development (VOLLMEISTER *et al.* 2009). In essence, the loss of RNA-binding protein Khd4 disturbs the morphological dynamics during the formation

of infectious hyphae. Based on these results, we determine 9 h.p.i. as the optimal time point for further analysis.

Establishing hyperTRIBE for fungal RNA-binding proteins

Mutations in the RNA-binding domains mimic the loss-of-function phenotype of *khd4* deletion (VOLLMEISTER *et al.* 2009). Identifying mRNA targets of Khd4 is therefore crucial to dissect its function. Hence, we adapted hyperTRIBE, a technique well-suited for the investigation of proteins with high molecular weight or low expression that are difficult to purify (MCMAHON *et al.* 2016,RAHMAN *et al.* 2018,XU *et al.* 2018). HyperTRIBE exploits the RNA editing activity of the catalytic domain of ADAR (Adenosine Deaminase Acting on RNA) from *Drosophila melanogaster* carrying the mutation E488Q to increase editing (KUTTAN AND BASS 2012; designated Ada). We fused the codon-optimized catalytic Ada domain with the green fluorescent protein (enhanced version, designated Gfp, Clontech) to the C terminus of the RBP of interest (Fig. 2.2A-B). Expression of the fusion protein is controlled by the arabinose-inducible P_{crg1} promoter that is repressed by glucose (Fig. 2.2A-B; BOTTIN *et al.* 1996,BRACHMANN *et al.* 2001). The resulting construct was inserted ectopically at the *ip*^{s} locus (LOUBRADOU *et al.* 2001) in the deletion mutant of the RBP of interest. To assess RBP-Ada-Gfp functionality, we compared it to a control strain expressing RBP-Gfp (Fig. 2.2B).

For a proof-of-principle study, we chose Rrm4, as its cognate mRNA targets have been extensively investigated at the transcriptome-wide level using iCLIP (individual-nucleotide resolution Cross-Linking and ImmunoPrecipitation; OLGEISER *et al.* 2019). A detailed description of the experimental setup is given in the Chapter 5, Appendix 2 (subsection 5.2.1, Supporting Information Text; Fig. 5.3-5.5). In brief, the expression of the Rrm4-Ada-Gfp protein by arabinose induction rescued the *rrm4*Δ phenotype (Chapter 5, Appendix 2, Fig. 5.3A-F), indicating that the fusion protein is functional. As a control for background editing, we used the strain expressing Ada-Gfp protein with N-terminal mKate2 fusion (a monomeric form of the red fluorescent protein, designated Kat; MÜNTJES *et al.* 2020) in the wildtype background (control-Ada; Fig. 2.2B). Control-Ada was expressed at higher levels than Rrm4-Ada-Gfp, localized uniformly throughout hyphae, and did not interfere with hyphal growth (Chapter 5, Appendix 2, Fig. 5.3D, Fig.

5.4A-C). To avoid potential artifacts caused by overexpression of RBPs, we did not attempt to express the RBP-Ada-Gfp levels similar to control-Ada.

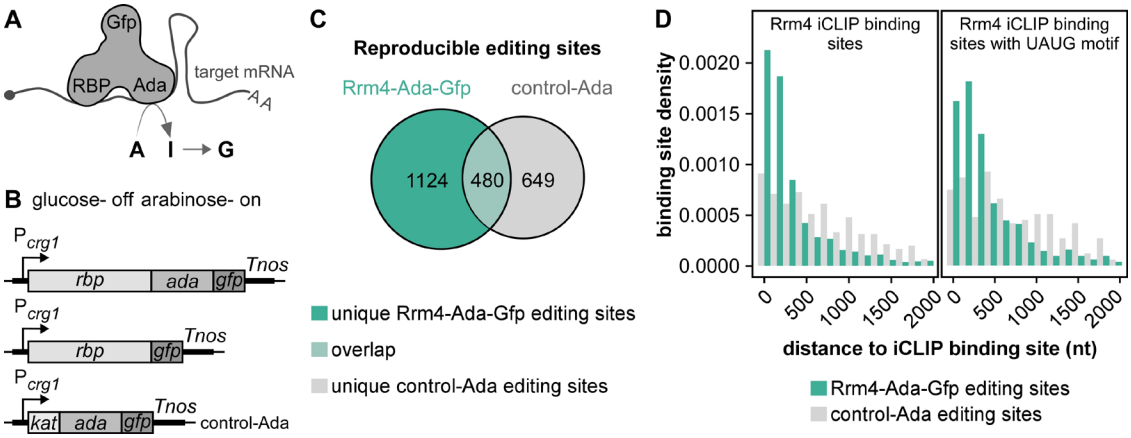

Fig. 2.2. HyperTRIBE identifies bona fide targets of Rrm4. **(A)** Schematics of the hyperTRIBE technique. The binding of the RBP–Ada–Gfp fusion protein to target mRNA results in the editing of adjacent adenosine (A) to inosine (I) which is converted to guanine (G) (Ada—hyperactive version of *Drosophila* ADAR catalytic domain; Gfp—green fluorescent protein; AA—poly(A) tail, 5′ cap structure is depicted by a gray circle). **(B)** HyperTRIBE constructs with arabinose inducible P_{crg1} promoter (on), which is repressed by glucose (off). Fusion proteins of RBP, Ada, Gfp, and/or Kat (Kat—mKate2, red fluorescent protein; *Tnos*—transcription terminator). **(C)** Overlap of reproducible editing events from Rrm4–Ada–Gfp (sea green) and control–Ada (gray). The number of reproducible editing events within each category is stated inside. **(D)** Histogram displaying the distance of editing events to the nearest Rrm4 iCLIP binding sites (Left) or the nearest UAUG-containing Rrm4 iCLIP binding sites (Right) in edited transcripts specific to Rrm4–Ada–Gfp (sea green) compared to control–Ada (gray).

We sequenced mRNAs of hyphae expressing the hyperTRIBE constructs that were induced under promoter-on conditions (arabinose) for 6 hours. The A-to-G editing events in the sequencing data were detected using the published hyperTRIBE pipeline (RAHMAN *et al.* 2018). Editing events were deemed reproducible when detected in two independent experimental replicates (Chapter 5, Appendix 2, Fig. 5.5A). Notably, Rrm4-Ada-Gfp expression led to twice as many reproducible editing sites as control-Ada (Fig. 2.2C; Chapter 5, Appendix 2, Fig. 5.5A-). In our system, the control-Ada construct harboring only the catalytic domain of ADAR shows substantial background activity. This is different from the initial reports on mammalian and *Drosophila* hyperTRIBE systems but fits with observations for the more recently established plant hyperTRIBE system (31,25). Importantly, the increased background activity of control-Ada can be clearly separated from the editing events for the RBP of interest (see below).

Comparing the hyperTRIBE data with Rrm4-bound transcripts from iCLIP data showed significant overlap, whereby, ~84% of the transcripts with unique Rrm4-Ada-Gfp editing

sites had also been detected as Rrm4-bound in the published iCLIP data, demonstrating a higher enrichment compared to the control-Ada (Chapter 5, Appendix 2, Fig. 5.5E-G).

Interestingly, compared to control-Ada editing sites, the majority of editing sites on mRNAs unique to Rrm4-Ada-Gfp were predominantly located near the actual Rrm4 binding sites (Fig. 2.2D; median distance=159 nucleotides (nt)). Additionally, only the Rrm4-Ada-Gfp editing sites demonstrated enrichment in proximity to the UAUG-containing binding sites, a motif recognized by the third RRM domain of Rrm4 (Fig. 2.2D; median distance=252 nt). In summary, we conclude that the specificity of Ada in hyperTRIBE is largely determined by the attached RBP. Our pilot study has thus laid the foundation for using hyperTRIBE for *in vivo* detection of Khd4 target mRNAs.

Khd4 interacts with mRNAs enriched for its binding motif AUACCC

Following the same experimental strategy (Fig. 2.2B; Chapter 5, Appendix 2, Fig. 5.6A-B), we first verified that Khd4-Ada-Gfp rescued the mutant *khd4*Δ phenotype with respect to hyphal morphology, length, and thickness (Chapter 5, Appendix 2, Fig. 5.6C-E). In line with Rrm4-Ada-Gfp, the levels of Khd4-Ada-Gfp were also lower compared to control-Ada (Chapter 5, Appendix 2, Fig. 5.6F-G). To assess the specificity of Khd4-Ada-Gfp editing, we designed a reporter mRNA, containing six tandem copies of the previously identified Khd4 binding motif AUACCC (VOLLMEISTER *et al.* 2009) in the 3′ untranslated region (UTR) of the Kat coding sequence. This synthetic mRNA was constitutively expressed using the P_{tef} promoter (Chapter 5, Appendix 2, Fig. 5.6H). We harvested hyphae (6 h.p.i.) grown in the promoter-on condition and sequenced *kat_(auaccc)*$_6$ mRNA using transcript-specific primers (see Chapter 5, Appendix 2, Materials and methods). Strikingly, we observed two reproducible A-to-G editing events in the reporter mRNA only after the expression of Khd4-Ada-Gfp (Chapter 5, Appendix 2, Fig. 5.6H). Thus, the Khd4-Ada-Gfp fusion protein is fully functional, and the Ada domain can edit Khd4 mRNA targets with high specificity. Notably, this experiment also demonstrated for the first time that the AUACCC motif indeed serves as an *in vivo* Khd4 binding motif in *U. maydis*.

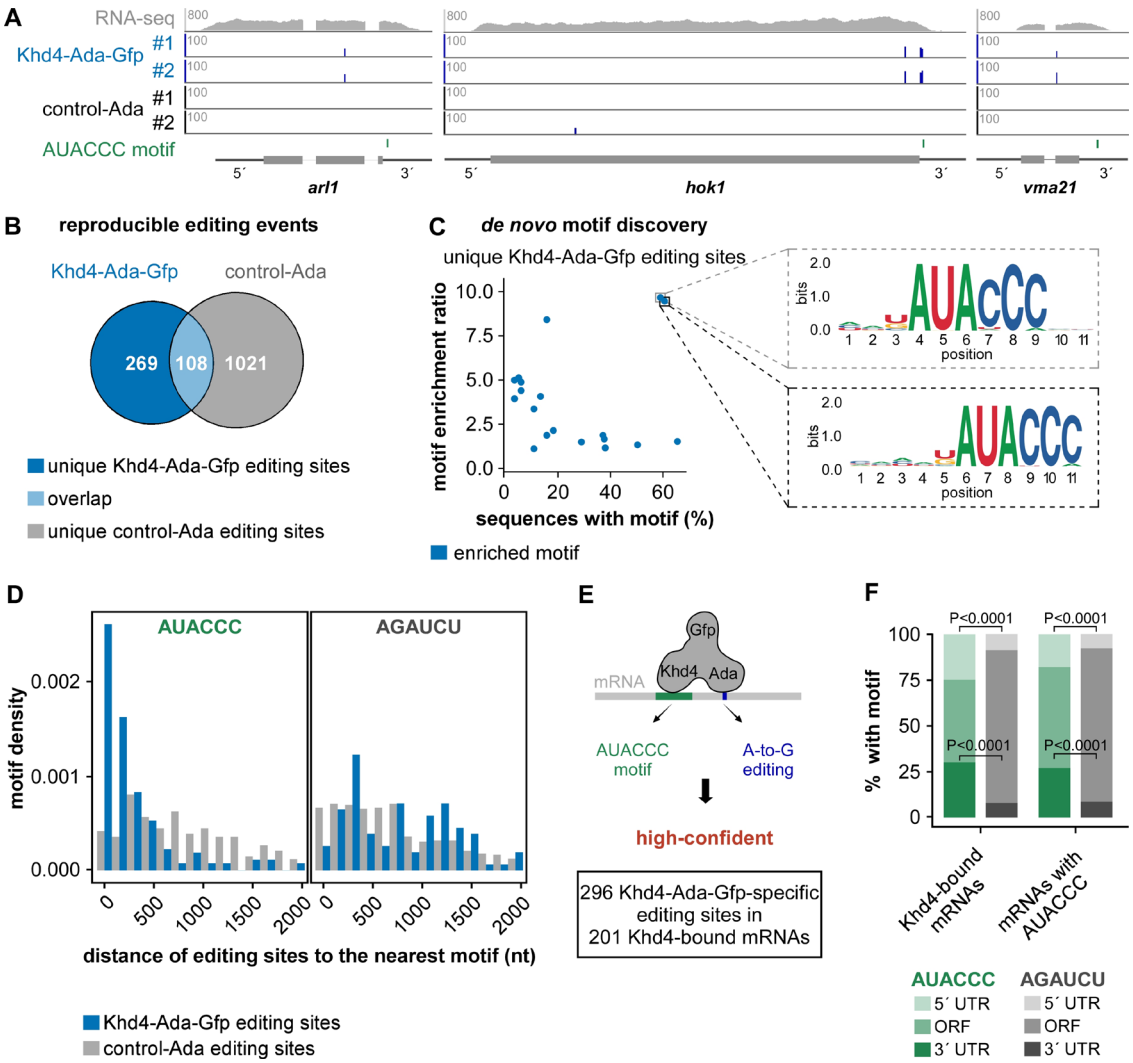

Fig. 2.3. HyperTRIBE identifies highly specific targets of Khd4. **(A)** HyperTRIBE data of Khd4 on selected target transcripts (*arl1*, UMAG_10313; *hok1*, UMAG_11790; *vma21*, UMAG_11418). Tracks showing RNA-seq read coverage (Top) followed by editing tracks of Khd4–Ada–Gfp and control–Ada (#1-replicate 1, #2-replicate 2). The bottom track displays the position of the AUACCC motif. The gene model with the exon/intron structure below was extended by 300 nt on either side to include 5′ and 3′ UTRs (5′ and 3′, respectively). **(B)** Overlap of reproducible editing sites from the Khd4–Ada–Gfp (blue) and control–Ada (gray). The overlapping region is depicted in light blue color. The numbers of reproducible editing sites in each category are indicated. **(C)** *De novo* motif discovery analysis on sequences carrying unique Khd4–Ada–Gfp editing sites. Scatter plot compares the relative enrichment ratio of enriched motifs (blue; relative to the background control) with the percentage of each motif in the tested sequences. The enlarged region (indicated by dotted box) presents the sequence logo of motifs exhibiting both high enrichment and overrepresentation in Khd4–Ada–Gfp-edited sequences. For motif enrichment, a 501-nt window centered on Khd4–Ada–Gfp editing sites was used. **(D)** Histogram showing the distribution of editing sites from the nearest AUACCC (Left) or AGAUCU (Right; a point mutated version of AUACCC) motifs in transcripts specific to Khd4–Ada–Gfp (blue) compared to control–Ada (gray). **(E)**. Schematic depiction of high-confident, Khd4-bound mRNA selection using hyperTRIBE. High-confident target mRNAs are those that contain Khd4–Ada–Gfp-specific editing sites (blue; A-to-G editing) and at least one AUACCC motif (green). **(F)** Stacked bar graph describing the percentage of AUACCC (green) or AGAUCU (gray) motifs per transcripts region (5′ UTR, ORF and 3′ UTR) for Khd4-bound mRNAs and all AUACCC-containing mRNAs. Statistical analysis was carried out using Fisher's exact test.

To detect Khd4 targets, reproducible editing events were identified from two replicate experiments for Khd4-Ada-Gfp (Fig. 2.3A; Chapter 5, Appendix 2, Fig. 5.7A-B). In contrast to Rrm4-Ada-Gfp, editing events for Khd4-Ada-Gfp were substantially lower, however, the reproducibility was higher than for those obtained with Rrm4-Ada-Gfp or control-Ada (Chapter 5, Appendix 2, Fig. 5.5C-D, Fig. 5.7B-D). Comparing reproducible editing events from Khd4-Ada-Gfp and control-Ada showed that the majority of editing sites were unique to either Khd4-Ada-Gfp (n=269) or the control-Ada (n=1021), with 108 editing sites overlapping between both sets (n=108; Fig. 2.3B). Importantly, *de novo* motif enrichment analysis using

XSTREME identified only the motif AUACCC near Khd4-Ada-Gfp editing sites as highly enriched (Fig. 2.3C). About 81% of the transcripts with unique Khd4-Ada-Gfp editing events contained the AUACCC motif (Chapter 5, Appendix 2, Fig. 5.8A). In contrast, the control motifs, including the AGAUCU motif, a point-mutated version of AUACCC that demonstrated no binding by Khd4 in the yeast three-hybrid assay (VOLLMEISTER *et al.* 2009), the antisense motif GGGUAU and the scrambled sequence ACACUA were not significantly enriched compared to the entire transcriptome (Chapter 5, Appendix 2, Fig. 5.8A). Moreover, neither of these motifs showed specific enrichment in transcripts unique to the control-Ada (Chapter 5, Appendix 2, Fig. 5.7E, Fig. 5.8A). Thus, Khd4-Ada-Gfp recognizes mRNAs via the AUACCC motif at the transcriptome-wide level *in vivo.*

Similar to Rrm4-Ada-Gfp, most of the Khd4-Ada-Gfp-specific editing sites were found within 500 nt from the nearest AUACCC motif (median distance=120 nt) and progressively declined with increasing distance (Fig. 2.3D). In contrast, the background editing sites from control-Ada were not enriched towards the closest AUACCC motif (median distance=863 nt) nor did the control motifs (AGAUCU, GGGUAU, ACACUC) show any spatial enrichment towards either type of editing sites (Fig 3D; Chapter 5, Appendix 2, Fig. 5.8B-D).

The transcripts overlapping between Khd4-Ada-Gfp and control-Ada were nonetheless significantly enriched for the AUACCC motif (n=60 mRNAs with 66 editing sites), indicating Khd4-dependent editing, and were hence included as Khd4-Ada-Gfp targets in order to avoid false negatives (Fig. 2.3E; Chapter 5, Appendix 2, Fig. 5.8A). Based on these results, we defined a high-confident set of 201 Khd4-bound mRNA targets that

harbored Khd4-Ada-Gfp editing sites (n=296) and contained at least one AUACCC motif (Fig. 2.3E). Transcripts carrying Khd4-Ada-Gfp specific editing sites but lacking the AUACCC motif (n=74 mRNAs with 81 editing sites) did not show enrichment for other motifs and were not investigated further (Chapter 5, Appendix 2, Fig 5.9A-C).

Examining the positional distribution of the AUACCC motifs in Khd4-bound mRNAs and other AUACCC-containing transcripts revealed a predominant occurrence in the 5′ and 3′ UTRs (Fig. 2.3F). The strong enrichment of AUACCC motifs in these regions was even more apparent when compared to the control motif AGAUCU, which was almost exclusively found in the open reading frames (ORFs), reflecting that ORFs are generally much longer than UTRs in *U. maydis* (Fig. 2.3F). Within the 3′ UTR, the AUACCC motifs preferentially occurred towards the beginning (Chapter 5, Appendix 2, Fig. 5.9D). Hence, our data suggest that AUACCC motifs present in the 3′ UTR constitute the major binding sites for Khd4 in the identified target mRNAs.

To evaluate the biological roles of Khd4-bound mRNAs, we performed gene ontology (GO) enrichment analysis using the R package gProfiler2 (Ensembl annotation; RAUDVERE *et al.* 2019). We observed a significant overrepresentation of processes related to small GTPase-mediated signal transduction processes, such as Ras and Rho protein signaling and GTPase regulator activity (Chapter 5, Appendix 2, Fig. 5.9E, Fig. 5.10A). The Khd4-bound mRNAs associated with these GO terms encode well-studied membrane trafficking regulators such as the small GTPase Arl1 that participate in the trans-Golgi network and secretion, the Ras GTPase activating protein (GAP) Sar1, and the Rho guanine nucleotide exchange factor (GEF) Rom2 that function in actin cytoskeleton regulation (Chapter 5, Appendix 2, Fig. 5.10A; MANNING *et al.* 1997,BEREPIKI *et al.* 2011,GÖHRE *et al.* 2012,JUST AND PERÄNEN 2016,LABBAOUI *et al.* 2017). In addition, by manually analyzing the Khd4-bound mRNAs for encoded functions and subcellular localization, we found that a distinct subset of target mRNAs was involved in the endomembrane system such as endoplasmic reticulum, Golgi apparatus, and vacuoles, with the most carrying the AUACCC motif in their 3′ UTR (Chapter 5, Appendix 2, Fig. 5.10B). Hence, Khd4 might be involved in the post-transcriptional control of membrane trafficking regulators. Khd4 appears to coordinate the regulation of these functionally related mRNAs into an mRNA regulon, which enables robust and dynamic control over membrane trafficking. In summary, we find that Khd4-Ada-Gfp interacts specifically with a distinct set of target mRNAs *in vivo* via the

AUACCC binding motif, preferentially in the 3´ UTR. Intriguingly, the identified target mRNAs frequently encode regulatory proteins involved in membrane trafficking.

Loss of Khd4 increases the abundance of mRNAs with AUACCC motif in their 3´ UTR

Our previous microarray analysis in yeast cells showed that the AUACCC motif was enriched in the 3´ UTR of the transcripts that exhibited an increase in mRNA abundance in the absence of Khd4 (VOLLMEISTER *et al.* 2009). This suggests an impact on mRNA stability. Since our hyperTRIBE data showed that Khd4 binds only a subset of AUACCC-containing mRNAs in hyphae, we tested for a differential mRNA abundance between wildtype and *khd4*Δ hyphae using RNA sequencing (RNA-seq; *khd4Δ* hyphae vs. *wt* hyphae; 9 h.p.i. see Fig. 2.1A-B; Chapter 5, Appendix 2, Fig. 5.2B-F).

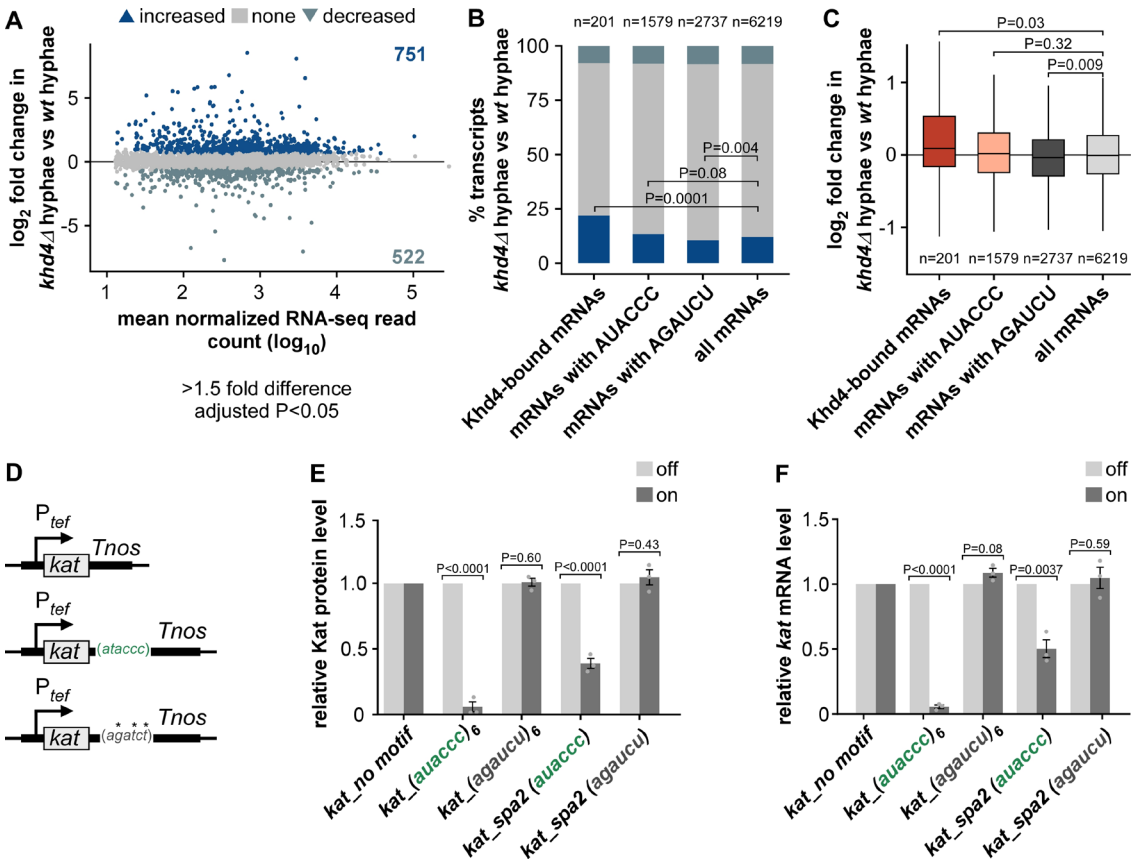

Fig. 2.4. *khd4* deletion increases the abundance of transcripts with 3′ UTR AUACCC. **(A)** Difference in mRNA abundance (*khd4Δ* hyphae vs. *wt* hyphae; *wt*-wildtype) in hyphal cells following khd4 deletion. Shown is the $\log_2$-transformed fold change plotted against the $\log_{10}$-transformed mean normalized RNA-seq read counts. Blue dots represent values of transcripts with a significant change in their mRNA abundance (>1.5-fold change, $P < 0.05$, Benjamini–Hochberg correction, >10 average normalized reads), and gray dots represent remaining transcripts. Numbers inside the plots indicate genes with significantly increased or decreased mRNA abundance. **(B)** Stacked bar graph of the percentage of genes with differential mRNA abundance in hyphal cells after *khd4* deletion for Khd4-bound mRNAs, all mRNAs

with AUACCC motif, all mRNAs with AGAUCU motif, and all expressed mRNAs in hyphae (>10 average normalized reads). The dark and light blue bars represent the percentage of transcripts that are significantly increased and decreased in their mRNA abundance, respectively (>1.5-fold change, $P < 0.05$, Benjamini–Hochberg correction). The percentage of remaining transcripts is depicted by a gray bar. Statistical analysis of the percentage of transcripts with increased expression levels was performed using Fischer's exact test. The number of transcripts in each set is represented at the Top. **(C)** Box plot of changes in mRNA expression (log2-transformed fold change, *khd4Δ* hyphae vs. *wt* hyphae) for Khd4-bound mRNAs (red), all mRNAs with AUACCC motif (salmon), mRNAs with AGAUCU motifs (dark gray), and all expressed mRNAs (light gray) in hyphal cells. Statistical significance between the mean mRNA expression level (log2-transformed fold change) was calculated using the Student's *t* test. The number of transcripts in each set is given at the bottom. **(D)** Schematics of reporter constructs for testing the binding effect of Khd4 on the 3′ UTR AUACCC. The constitutively active P_{tef} promoter mediates the expression of the Kat fluorescent reporter in the genetic background of arabinose-inducible Khd4–Gfp. Reporter constructs carrying no binding motif (Top), the AUACCC binding motif (center), or the AGAUCU binding motif (Bottom) in their 3′ UTR are depicted chronologically. *Tnos*—transcription terminator. *—mutated nucleotides. **(E)** Shown are the relative fluorescence level of Kat proteins in on (dark gray; Khd4-induced) compared to off (light gray; Khd4-repressed) conditions in strains expressing kat mRNA tethered to different 3′ UTR regions (n = 3 independent experiments; error bars: SEM; $auaccc_6$ or $agaucu_6$—3′ UTR consisting of six repeats of the respective motifs; *kat_spa2 (auaccc)*—36 nt-long endogenous 3′ UTR sequence of spa2 gene that contains a single AUACCC motif; *kat_spa2 (agaucu)*—36 nt-long endogenous 3′ UTR sequence of spa2 gene with mutated AUACCC motif). **(F)** The relative *kat* transcript level in on conditions (dark gray) compared to the transcript levels under off conditions (light gray), measured via RT-qPCR. Statistical significance between on and off conditions in E and F was calculated using multiple unpaired Student's *t* tests. (n = 3 independent experiments; error bars: SEM).

Differential expression analysis revealed that about one-fifth of all transcripts showed significant changes in mRNA abundance following *khd4* deletion (1273 out of 6765 protein-coding genes; >1.5 fold change; P<0.05; Benjamini-Hochberg correction, >10 average normalized reads), most of which had increased mRNA levels (Fig. 2.4A). Loss of *khd4* caused a significant increase in the expression levels of Khd4-bound mRNA targets compared to all transcripts, confirming that the hyperTRIBE-identified targets are indeed regulated by Khd4. Of note, this trend could not be observed when analyzing all AUACCC-containing mRNAs (Fig. 2.4B-C), underlining that the knowledge of binding motifs alone is not sufficient to dissect the regulatory function of Khd4.

Interestingly, for the Khd4-bound mRNA targets as well as for all AUACCC-containing mRNAs with increased mRNA levels in *khd4*Δ hyphae, the AUACCC motif was primarily enriched in their 3′ UTR. (Chapter 5, Appendix 2, Fig. 5.11A). This indicates that AUACCC located in the 3′ UTR affects mRNA stability. Essentially, these results strengthen our hypothesis that the interaction of Khd4 with the 3′ UTR AUACCC determines mRNA stability.

AUACCC in the 3′ UTR functions as a Khd4-dependent mRNA stability element

To test whether Khd4 binding causes increased mRNA turnover, we applied our Kat reporter system to quantify the regulatory potential of AUACCC motifs in the 3′ UTR. We inserted either six tandem repeats of AUACCC or an endogenous sequence of equal length carrying a single AUACCC motif from the 3′ UTR of *spa2* mRNA (UMAG_04468), encoding a polarisome protein, into the 3′ UTR of the *kat* ORF (Materials and methods; CARBÓ AND PÉREZ-MARTÍN 2008,ZHENG *et al.* 2020). The *spa2* 3′ UTR with mutated binding motif, AGAUCU, and the Kat construct without any motifs served as controls (Fig. 2.4D). All constructs were generated in the strain expressing arabinose-inducible Khd4-Gfp as mentioned before. The expression of the reporter constructs was controlled by the constitutively active P_{tef} promoter to exclude differences in mRNA amounts due to transcriptional regulation.

Measuring the fluorescence intensity of Kat under the promoter-on condition revealed that the presence of a single AUACCC binding motif in the 3′ UTR was sufficient to significantly reduce the amount of *kat* reporter mRNA. Concurrently, turning off the Khd4 expression rescued the Kat fluorescence level (Fig. 2.4E; Chapter 5, Appendix 2, Fig. 5.11B-C), validating that the regulatory potential of the AUACCC motif is dependent on Khd4. Indeed, quantifying the reporter transcript level manifested the same expression pattern, implying that the decrease in Kat fluorescence is caused at the mRNA level by Khd4 binding to the 3′ UTR (Fig. 2.4F). At both protein and mRNA levels, the presence of six AUACCC repeats in the 3′ UTR caused a stronger reduction, indicating a dose-dependent response. This effect was lost when mutating the binding site (Fig. 2.4E-F; Chapter 5, Appendix 2, Fig. 5.11B-C). Thus, the AUACCC in the 3′ UTR functions as a *cis*-regulatory mRNA instability element in a Khd4-dependent manner.

Khd4 tightly regulates the expression of distinct targets involved in membrane trafficking

In addition to rapid clearance, intrinsically unstable mRNAs reach steady-state levels faster than stable mRNAs after transcriptional induction. Therefore, regulatory proteins are often encoded by such unstable mRNAs permitting faster response time (see below, HARGROVE AND SCHMIDT 1989). Since Khd4 targets encode regulatory proteins involved in membrane trafficking, we wondered whether the Khd4-mediated mRNA instability controls the amount of protein produced during hyphal morphogenesis. Such mRNA

targets should be expressed upon hyphal induction and carry the regulatory element AUACCC in their 3´ UTR for increased turnover.

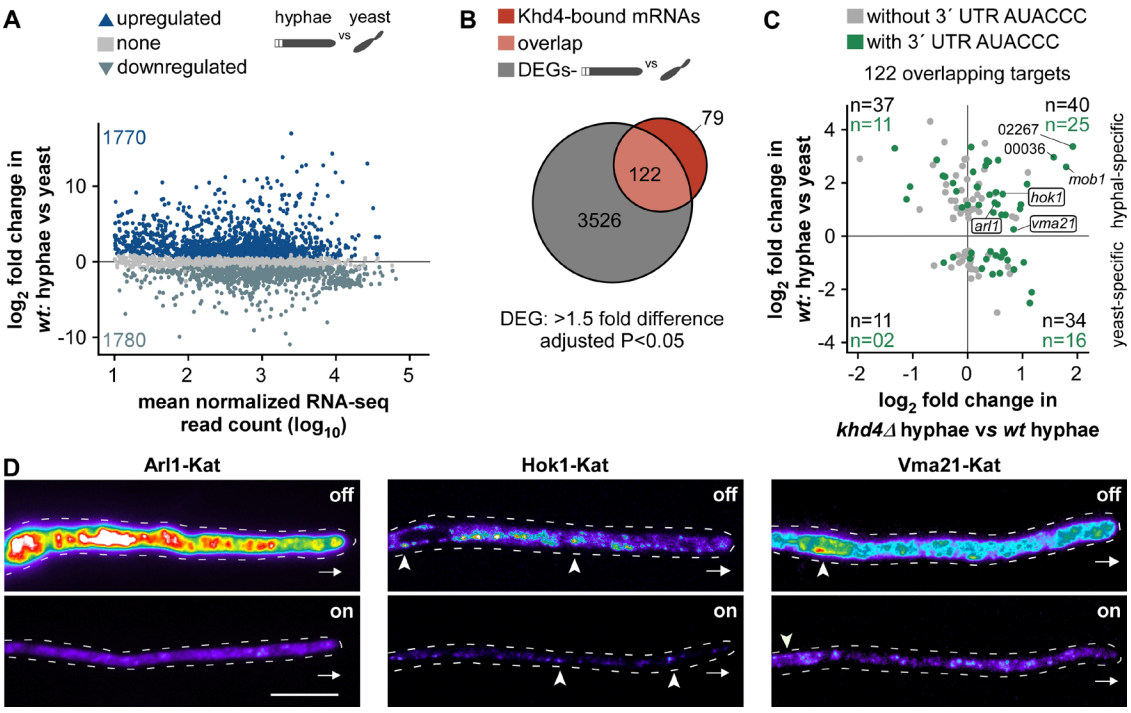

Fig. 2.5. Khd4 regulates subcellular protein levels of membrane-trafficking regulators. **(A)** MA plot showing the differential mRNA abundance in *wt* cells upon hyphal induction (*wt*: hyphae vs. yeast). Shown is the log2-transformed fold change plotted against the log10-transformed mean normalized read counts. Blue dots represent values of transcripts with a significant change in their mRNA abundance (>1.5-fold change, $P < 0.05$, Benjamini–Hochberg correction, >10 average normalized reads), and gray dots represent remaining transcripts. Numbers inside the plot indicate upregulated and downregulated genes. Silhouette images of elongated hyphae and dividing yeast are shown. **(B)** Overlap (light red) between the differentially expressed genes (DEGs) in wildtype cells (gray) following the switch from yeast to hyphae (*wt*: hyphae vs. yeast; >1.5-fold difference, $P < 0.05$, Benjamini–Hochberg correction, >10 average normalized reads; gray) and Khd4-bound mRNAs (red). **(C)** Scatterplot comparing mRNA expression levels (log_2-transformed fold change) of the overlapping high-confident Khd4-bound mRNAs from B in wildtype cells (*wt*: hyphae vs. yeast), and hyphal cells following *khd4* deletion (*khd4Δ*: hyphae vs. wt hyphae). Transcripts with a 3′ UTR AUACCC motif are indicated by green dots. The numbers in black and green within each quadrant indicate the total number of target transcripts and the count of targets with 3′ UTR AUACCC, respectively. We manually included *vma21* in our analysis since it showed a significant increase in mRNA abundance when *khd4* is absent, despite a marginal increase in expression during hyphal growth. In addition, 02267,00036 are shortened IDs representing UMAG_02267 and UMAG_00036, respectively. **(D)** Fluorescent micrographs in false color (black/blue—low intensity, red/white—high intensity) of hyphae (6 h.p.i.) constitutively expressing target genes (arl1—left, hok1—center, vma21—right) under Khd4-repressed off (Top) and Khd4-induced on (Bottom) conditions. Arrowheads and arrow marks indicate the corresponding target protein's location (Hok1 on early endosomes; Vma21 in the perinuclear region) and the growth direction, respectively (scale bar: 10 µm.).

To identify hyphal-specific genes, we sequenced mRNAs from yeast cells and compared them with our hyphal transcriptome (9 h.p.i.). This analysis detected more than 3500 genes with differential mRNA abundance as a response to hyphae formation (Fig. 2.5A).

Studying the Khd4-bound mRNAs identified by hyperTRIBE revealed that 61% of them showed a significant differential mRNA abundance during morphogenesis (122 out of 201 transcripts), with most exhibiting increased mRNA amounts in hyphae compared to yeast cells, suggesting a hyphal-specific transcriptional induction (77 out of 122 transcripts, 63%; Fig. 2.5B-C). Interestingly, 52% of these hyphal-specific targets also showed increased mRNA abundance in the absence of *khd4* (40 out of 77 transcripts), with half containing the AUACCC motif in their 3′ UTR (25 out of 40 transcripts, 63%). In contrast, the minor fraction of hyphal-specific targets with decreased levels after *khd4* deletion showed enrichment of the motif in the 5′ UTR (17 out of 37 transcripts, 46%), suggesting a role of Khd4 in translation (Chapter 5, Appendix 2, Fig. 5.12A). Nevertheless, we noted that most of the Khd4-bound mRNA targets responded to *khd4* deletion with increased mRNA levels and harbored the AUACCC motif in their 3′ UTR (Fig. 2.5C).

To validate whether Khd4 determines the steady-state levels of encoded proteins of its target mRNAs *in vivo*, we selected the target transcripts, namely *arl1*, *hok1*, and *vma21*, encoding proteins function in small GTPase signaling, early endosome transport, and vacuolar biogenesis, respectively (UMAG_10313 and UMAG_11418 exhibit high sequence identity with the respective Arl1 and Vma21 orthologs of other fungi; Chapter 5, Appendix 2, Fig. 5.12B-C). In pathogenic fungi, the highly conserved Arf GTPase Arl1 participates in hyphal growth and virulence by regulating the endosomal trans-Golgi network and secretion (LABBAOUI *et al.* 2017,PATIÑO-MEDINA *et al.* 2019,YU AND LEE 2017). Hok1 regulates the bidirectional movement of early endosomes by recruiting motor proteins Kin3 and split dynein Dyn1/2 during long-distance transport (BIELSKA *et al.* 2014). Vma21 is required for the precise assembly of the multi-subunit V-ATPase complex in the vacuole of the budding yeast *Saccharomyces cerevisiae* (FINNIGAN *et al.* 2011). The three mRNAs encoding Arl1, Hok1, and Vma21 harbored 3′ UTR AUACCC motifs and showed increased expression levels during hyphal growth. Interestingly, loss of Khd4 enhanced this increase even further (Fig. 2.5C; Chapter 5, Appendix 2, Fig. 5.12D).

We ectopically expressed the target transcripts using the constitutively active P_{tef} promoter in the background of the arabinose-inducible Khd4-Gfp strain. To detect the abundance of the encoded proteins and their subcellular localization, the ORFs of the target transcripts were tagged with Kat, followed by the insertion of the corresponding

endogenous 3′ UTR (Chapter 5, Appendix 2, Fig. 5.12E). Indeed, as seen in our RNA-seq analysis, the absence of Khd4 resulted in an increased amount of encoded protein in all three cases (Fig. 2.5D, Chapter 5, Appendix 2, Fig. 5.12F-G). These results reinforce that Khd4 regulates the expression of these target mRNAs at the level of mRNA stability. Despite the same constitutively active promoter and insertion at the same ectopic locus, each target mRNA exhibited a different protein expression level under promoter-on and -off conditions (Fig. 2.5D; Chapter 5, Appendix 2, Fig. 5.12G), suggesting the presence of an additional layer of regulation at the post-transcriptional or post-translational level.

Based on these results, we hypothesize that Khd4 destabilizes mRNAs encoding regulatory proteins and thereby functions as a key variable for achieving faster steady-state levels of these transcripts during hyphal development (Fig. 2.5C). Using a single-compartment model, we simulated the impact of mRNA stability on gene expression (HARGROVE AND SCHMIDT 1989,WHITE *et al.* 2013). Our analysis confirmed that unstable mRNAs attain faster steady-state levels, enabling quick response times. Thus, intrinsically unstable mRNA is indispensable for rapid on-off kinetics for faster cellular responses (Chapter 5, Appendix 2, Fig. 5.13A).

Building upon these findings, we used the mathematical model to investigate the dynamics of *mob1* mRNA, a Khd4 target encoding a kinase regulator in the presence and absence of Khd4. Using the measured *mob1* expression levels (Chapter 5, Appendix 2, Fig. 5.13B) and an estimated mRNA half-life ($t_{1/2}$) of 8 min (as determined in *S. cerevisiae*; MILLER *et al.* 2011), we simulated *mob1* induction kinetics during hyphal induction (Chapter 5, Appendix 2, Fig. 5.13C). Accordingly, the loss of Khd4 resulted in the stabilization of *mob1* mRNA to a half-life of $t_{1/2}$=22 min, which was sufficient to explain the elevated initial and new steady-state levels, without changing the synthesis rate. Furthermore, this stabilization caused a significant delay in *mob1* induction kinetics, reaching the new steady state only after 2 hours of morphogenesis. While termination of *mob1* synthesis rapidly cleared the mRNA in wildtype cells, stabilized *mob1* took considerably longer to return to its original steady-state levels (Chapter 5, Appendix 2, Fig. 5.13C).

Thus, our model showcases that the absence of Khd4 causes the stabilization of *mob1* mRNA, resulting in delayed induction kinetics and an overshooting of absolute expression levels. These aspects will likely have adverse effects since regulatory proteins

should not accumulate excessively in the cell. We, therefore, propose that the continuous availability of Khd4 during hyphal morphogenesis (confirmed at the mRNA, protein, or subcellular localization level; Chapter 5, Appendix 2, Fig. 5.13D-H) is crucial to ensure the rapid response kinetics of its target mRNAs.

Loss of Khd4 causes dysregulation of membrane trafficking genes in *khd4*Δ cells

As Khd4 plays a vital role in controlling the precise expression levels of membrane trafficking regulators, we wondered if loss of Khd4 would cause compensatory effects through altered gene expression. Akin to the wildtype cells, we determined the hyphal-specific transcripts in *khd4*Δ cells by evaluating our RNA-seq data of *khd4*Δ hyphae and yeast cells (9 h.p.i.; *khd4*Δ: hyphae vs yeast; see Materials and methods) and detected ~3500 genes with differential mRNA abundance in response to hyphae formation in the *khd4*Δ cells (Fig. 2.6A; >1.5-fold change, P<0.05, Benjamini-Hochberg correction, >10 average normalized reads). Comparing genes with differential mRNA abundance revealed that the majority were regulated similarly in both wildtype and *khd4Δ* cells, suggesting that the hyphal growth program itself is not abolished in the absence of Khd4 (Pearson correlation coefficient R=0.86, P<2.26e-16; Fig. 2.6B; Chapter 5, Appendix 2, Fig. 5.14A). However, we identified about 2000 genes exhibiting exclusive regulation in either wildtype or *khd4Δ* cells (Fig. 2.6B; 818 or 927 genes specifically regulated in the wildtype or *khd4Δ* cells, respectively).

To distinguish the effect of *khd4* deletion in hyphal cells, we performed a GO term analysis on upregulated genes that are specific either to wildtype *or khd4Δ* cells (n=349, upregulated exclusively in wildtype cells; n=437, upregulated exclusively in *khd4Δ* cells; Fig. 2.6B-C; Chapter 5, Appendix 2, Fig. 5.14B). Interestingly, in contrast to the wildtype cells, the genes upregulated exclusively in *khd4*Δ cells were mainly enriched for functional categories associated with the endomembrane system such as endoplasmic reticulum, Golgi vesicle transport, cytoplasmic vesicles, and cellular macromolecule localization. We also found enriched terms related to ER-Golgi metabolisms such as glycosylation, carbohydrate, and phospholipid metabolic processes (HEBERT *et al.* 2005; Fig. 2.6C; Chapter 5, Appendix 2, Fig. 5.14B), indicating that in comparison to wildtype

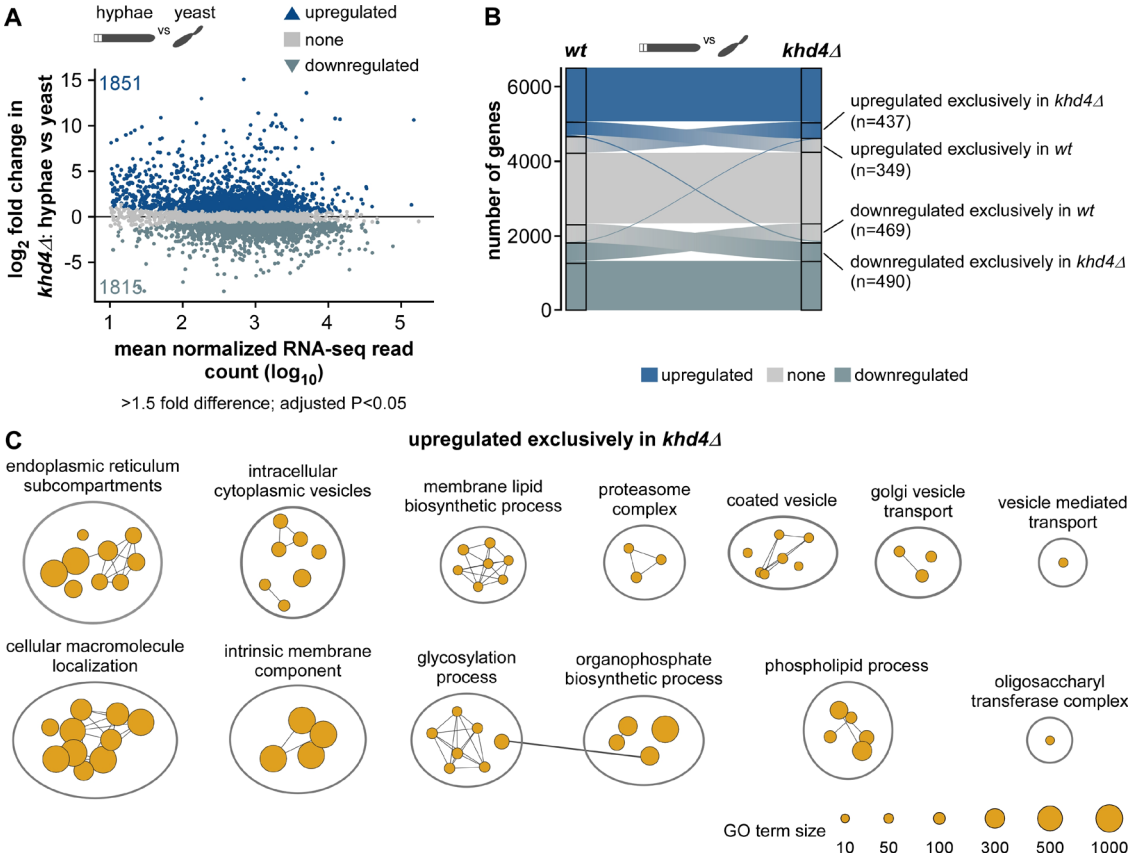

Fig. 2.6. Loss of Khd4 causes dysregulation of membrane trafficking. **(A)** MA plot showing the differential mRNA abundance in *khd4Δ* cells (*khd4Δ*: hyphae vs. yeast) following hyphae formation. Log_2-transformed fold change values of genes are plotted against the log_{10}-transformed mean normalized read counts. Blue dots represent transcripts with a significant change in their mRNA abundance (>1.5-fold change, $P < 0.05$, Benjamini-Hochberg correction, >10 average normalized reads), and gray dots represent remaining transcripts. Numbers inside the plots indicate the upregulated and downregulated genes. Silhouette images of elongated hyphae and dividing yeast cells are shown on Top. **(B)**. Alluvial plot showing the distribution of upregulated (up; dark blue), downregulated (down; light blue), and nonregulated (none; gray) genes in *wt* and *khd4Δ* cells following the switch from yeast to hyphae. The labeled regions represent genes that are exclusively upregulated (n = 349 in *wt*, n = 437 in *khd4Δ*) or downregulated (n = 469 in wt, n = 490 in khd4Δ) in either *wt* or *khd4Δ* cells. Importantly, these genes were regulated exclusively in *wt* or *khd4Δ* cells but not in the corresponding regions of the other set. Two slender blue lines depict differentially expressed genes exhibiting opposite regulation between *wt* and *khd4Δ* cells. The central flow in the middle of the alluvial plot depicts the gene transition between different categories. The width of the flow accurately represents the number of genes undergoing this transition. **(C)** GO terms that are significantly ($P < 0.05$, multiple-testing correction with g: SCS algorithm) overrepresented in genes upregulated exclusively in *khd4Δ* cells after hyphal induction (orange; >1.5-fold change, $P < 0.05$, Benjamini–Hochberg corrections, >10 average normalized reads). The reference GO term sizes are given below.

cells, the genes encoding membrane trafficking components are dysregulated during hyphal growth in the *khd4Δ* cells. Thus, loss of Khd4 causes specific alterations in the amounts of mRNAs encoding membrane trafficking components, supporting the notion that Khd4 is an important regulatory protein to orchestrate membrane trafficking during hyphal growth.

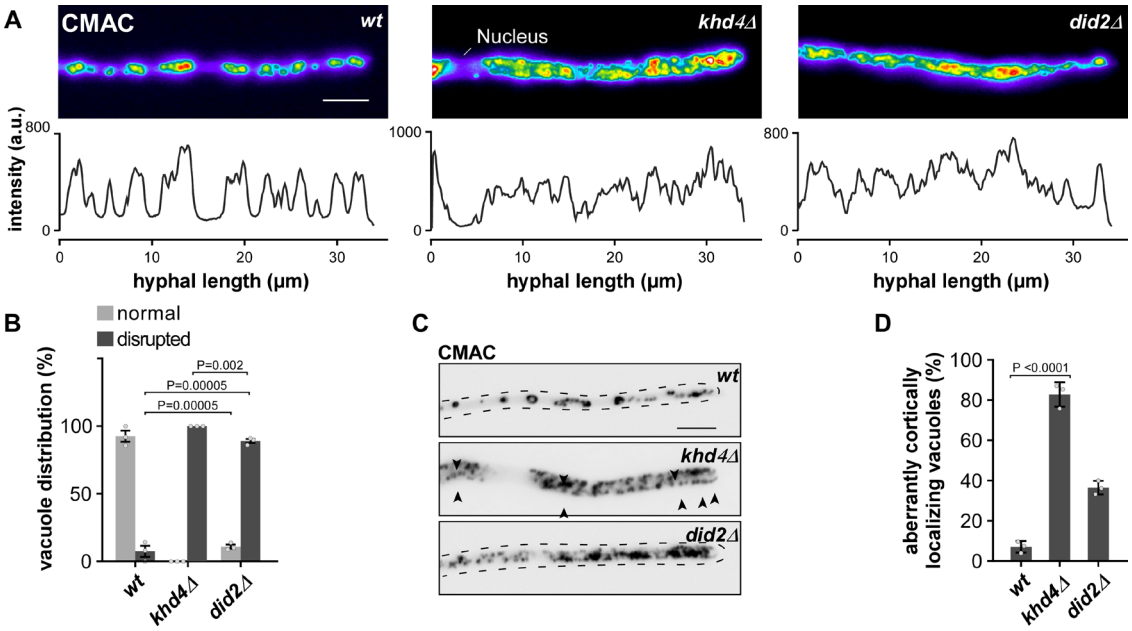

Fig. 2.7. Loss of Khd4 severely affects vacuole formation and localization. **(A)** False colored maximum projections of z-stacks acquired from hyphal cells (AB33 derivatives; 10 h.p.i.) stained with the vacuolar stain CMAC (Top). The line graphs below depict the fluorescent intensity profile of the respective hyphal cells. a.u.—arbitrary units (scale bar: 10 µm.). **(B)** Bar graph depicting the percentage of vacuole distribution (normal—light gray, disrupted—dark gray) in hyphal cells from AB33 derivatives (>25 hyphal cells per strain; n = 3, gray dots represent the mean value of independent experiments; error bars: SEM; unpaired Student's *t* test). **(C)** Inverted micrographs of hyphal cells (10 h.p.i.) stained with CMAC dye to visualize the vacuole. (Scale bar: 5 µm.) **(D)** Percentage of hyphal cells containing aberrant cortical localizing vacuoles. The mean values from n = 3 independent experiments are shown as gray dots (>25 hyphal cells were analyzed; error bar: SEM; unpaired Student's t test). Quantification in B and D involved manual assessment through visual inspection.

Loss of Khd4 causes defects in vacuole formation and localization

To evaluate the impact of *khd4* deletion on membrane trafficking in more detail, we examined the endocytic pathway leading to vacuole biogenesis in hyphal cells. As a control for defective membrane trafficking, we used cells lacking Did2, an ESCRT-III regulator involved in endosome maturation and identity (endosomal sorting complex required for transport; HAAG *et al.* 2017). Studying the endocytic pathway with FM4-64 uptake assays revealed that loss of Khd4 heavily delayed endocytosis. In time-resolved microscopy of wildtype hyphae, FM4-64 first stained the plasma membrane followed by bidirectionally shuttling endosomes and finally the vacuoles. After 25 min of staining, most of the FM4-64 signals in the wildtype hyphal cells were static (49%), while about 13% of the signals were found on processively moving early endosomes (Chapter 5, Appendix 2, Fig. 5.14C-D). By contrast, the loss of Khd4 caused a reduction in both static (36%) and processive signals (4%), and a significant increase (60%) in diffusively moving signals (Chapter 5, Appendix 2, Fig. 5.14C-D). A similar defect was observed

for cells lacking Did2, leading to a deficiency in vacuolar protein sorting. Also, both *khd4Δ* and *did2Δ* cells showed a strong reduction in the intensity and distance between static signals throughout the hyphae (Chapter 5, Appendix 2, Fig. 5.14C-D).

To analyze vacuole morphology more closely, we stained vacuoles with CMAC (7-amino-4-chloromethylcoumarin; HAUGLAND 1995). In general, vacuoles were evenly distributed in wildtype hyphae (Fig. 2.7A-B). However, in *khd4Δ* and *did2Δ* hyphae, the vacuoles were smaller, less defined, and found scattered throughout the hyphal cells (Fig. 2.7A-B). Interestingly, in about 80% of *khd4Δ* hyphae, the vacuoles were positioned aberrantly towards the cell cortex, neatly outlining the hyphal cells (Fig. 2.7C-D), whereas less than 10% of the wildtype cells and ~40% of the *did2Δ* cells contained cortically positioned vacuoles (Fig. 2.7C-D).

In summary, loss of Khd4 results in defective vacuole formation that correlates with aberrant polar growth of infectious hyphae and discloses a novel link between RNA biology and vacuole formation.

2.1.3 Discussion

The morphogenesis of fungal pathogens is intensively regulated at the level of transcription. Key transcription factors, for example, the heteromeric master regulator bE/bW in *U. maydis* and Efg1 in *C. albicans*, control the dimorphic switch from yeast to hyphae as part of the underlying pathogenic program (KUMAMOTO AND VINCES 2005,HEIMEL *et al.* 2010b). The precise expression output is, however, determined at the level of RNA regulation. Yet, little is known about how transcriptional and post-transcriptional mechanisms cooperate during pathogenic development. Here, we report that in *U. maydis*, the RNA-binding protein Khd4 is a vital regulator of the polar growth of infectious hyphae. Mapping the RNA binding of Khd4 uncovers a distinct set of target mRNAs encoding regulatory proteins involved in membrane trafficking. We find that Khd4 is required to maintain the accurate levels of these target mRNAs by regulating their mRNA stability, thereby functioning at the core of the hyphal gene expression program.

A key technical advance of our study is the successful application of the RNA editing-based hyperTRIBE method (RAHMAN *et al.* 2018) to identify direct mRNA targets of RBPs in infectious hyphae of *U. maydis*. To this end, we conduct a pilot study with the well-known RBP Rrm4 and a detailed analysis of Khd4. In both cases, unique target

transcripts are identified, with editing sites consistently enriched near the RBP binding sites. This feature serves as a critical quality criterion for the obtained data set, enabling the discovery of unknown binding motifs for other RBPs in the future. In case of Khd4, *de novo* motif discovery analysis successfully recovers the AUACCC binding motif as a top candidate, which is found in over 80% of the edited transcripts. This implies that, despite the increased background editing observed in our control experiments, specific hyperTRIBE editing is guided by the tested RBP in the fungal system. Importantly, using this *in vivo* binding information rather than relying only on motif content enables the identification of Khd4-regulated RNA networks (see below).

RBPs determine RNA regulation such as localization, translation, and stability by interaction with their cognate *cis*-regulatory elements. We discover that Khd4 functions at the level of mRNA stability by controlling the abundance of target mRNAs when the regulatory motif AUACCC is present in their 3′ UTR. Khd4 thereby regulates the spatiotemporal gene expression in hyphal cells by mediating mRNA turnover. In other systems, several RBPs are thought to mediate mRNA decay by directly recruiting the Ccr4-Not deadenylation complex. For instance, in *D. melanogaster,* the RBP Bicaudal-C interacts with the NOT3/5 subunit of the Ccr4-Not complex, via its KH domain (CHICOINE *et al.* 2007,MINEGISHI *et al.* 2021). We hypothesize that Khd4 recruits the evolutionarily conserved Ccr4-Not complex for mRNA-specific poly(A) tail shortening (MILLER AND REESE 2012,COLLART *et al.* 2013). Studies on the roles of such *cis* and *trans*-acting factors in fungal pathogens are currently scarce. However, similar functions are known from the mammalian RBPs TTP and CELF1, which cause rapid mRNA turnover by binding to the AU-rich and GU-rich mRNA decay elements in the 3′ UTR of mRNAs, respectively (BARREAU *et al.* 2005,VLASOVA-ST LOUIS AND BOHJANEN 2011).

Interestingly, we observe that targets of the mRNA stability factor Khd4 encode numerous regulatory proteins such as GTPases. Consistently, regulatory proteins such as cytokines and transcriptional factors are commonly encoded by unstable mRNAs in other systems (ANDERSON 2010,THOMPSON *et al.* 2023). This permits the transient expression of these proteins, which otherwise would cause undesirable side effects from prolonged exposure. Furthermore, unstable mRNAs facilitate the rapid attainment of steady-state levels following transcriptional induction (Chapter 5, Appendix 2, Fig. 5.13A; HARGROVE AND SCHMIDT 1989, BRUCE AND WILKINSON 2006,WHITE *et al.* 2013,MOORE

et al. 2014). Consistently, we observe that Khd4-bound mRNAs are transcriptionally induced during the transition from yeast to hyphal cells, suggesting that mRNA destabilization is crucial for the precise expression of regulatory proteins during hyphal morphogenesis. Consequently, the loss of Khd4 changes the underlying regulatory dynamics, reflected in hyphae with a delayed polar growth program (Chapter 5, Appendix 2, Fig. 5.13A-C).

Our findings implicate Khd4 as a regulator of membrane trafficking. By binding to AUACCC motifs in the 3′ UTR, Khd4 destabilizes a distinct subset of mRNAs encoding membrane trafficking regulators, dictating their exact subcellular protein levels. This coordinated regulation is consistent with the concept that RBPs co-regulate functionally related mRNAs, also referred to as mRNA regulons (KEENE 2007). Thus, we hypothesize that Khd4 defines a specific mRNA regulon for the coordinated regulation of membrane trafficking. Consistently, in the absence of *khd4,* the dynamic control of membrane trafficking is disturbed, as evidenced by aberrant vacuole biogenesis in fungal hyphae. It is already known that fungal RBPs such as Ssd1 (BAYNE *et al.* 2022, THAMMAHONG *et al.* 2019, GANK *et al.* 2008), Puf4 (KALEM *et al.* 2021), She3 (ELSON *et al.* 2009b) and Rrm4 (BAUMANN *et al.* 2014,MÜNTJES *et al.* 2021) play vital roles in the morphology and virulence of fungal pathogens. However, the concept of a defined RNA regulon for coordinating a specific biological process is predominantly described in higher eukaryotes. For example, by recognizing 3′ UTR AU-rich elements and stem-loop structures, RBPs such as TTP and Roquin promote the degradation of mRNA regulons that encode inflammatory regulators, such as cytokines, modulating immune responses (ANDERSON 2010,DIAZ-MUÑOZ AND OSMA-GARCIA 2022).

Our study unveils a novel link between RNA regulation and vacuole maturation. Correct vacuole biogenesis plays an instrumental role in the virulence of fungal pathogens (PALMER *et al.* 2005,LIU *et al.* 2006,LI *et al.* 2017,HU *et al.* 2021) Notably, appressoria-like infection structures in phytopathogens are strongly related to the development of vacuole-dependent basal septa (FREITAG *et al.* 2011), a process that is severely disturbed in *khd4Δ* hyphae. Therefore, Khd4-mediated control of the membrane trafficking mRNA regulon might also impact early infection processes such as plant entry.

Strikingly, the Khd4-bound mRNAs are enriched for regulatory proteins involved in small GTPase signaling. Small GTPases participate in a wide range of biological

processes (ROJAS *et al.* 2012,ARKOWITZ AND BASSILANA 2015,DAUTT-CASTRO *et al.* 2021). For example, Arl1, an Arf-like small GTPase, regulates secretion in *C. albicans* (LABBAOUI *et al.* 2017). The small GTPases Rac1 and Cdc42 control the morphology and pathogenicity of *U. maydis* (MAHLERT *et al.* 2006). Our findings reveal that Khd4 is essential for the exact levels of Arl1 in hyphal cells. While most studies on small GTPase regulation focus on the GTP hydrolysis cycle and post-translational modifications (BOS *et al.* 2007,AHEARN *et al.* 2011), our study discloses a regulation at the level of the mRNA amounts. Khd4 also determines the precise subcellular levels of mRNAs encoding other endomembrane regulators, such as Hok1 and Vma21, which act in endosomal motor function (BIELSKA *et al.* 2014) and V-ATPase assembly in the vacuole, respectively (MALKUS *et al.* 2004). Thus, RNA regulation appears to play a major role in the membrane trafficking pathway during infectious hyphal growth.

In essence, we find that the RBP Khd4 functions as a key mRNA stability factor orchestrating membrane trafficking during pathogenic development. Identifying direct target mRNAs has been highly rewarding in resolving the underlying RNA regulation and disclosing new links to cell biological processes such as vacuole maturation. Our study thereby demonstrates the importance of RBPs during fungal pathogenicity and will serve as a blueprint to study the role of RBPs in other fungal/host pathosystems. Noteworthy, hyperTRIBE is very well suited to identify target mRNAs when the pathogen is in intimate contact with the host. This will be central to developing our understanding of the role of RNA biology in fungal virulence and creating new avenues of research into antifungal therapeutic strategies.

Materials and methods

All strains and plasmids were generated following standard methods and incubation procedures (BRACHMANN *et al.* 2004). The mRNA targets of RBPs were identified using HyperTRIBE. *De novo* motif discovery analysis was conducted using the XSTREME tool from the MEME suite. Differential gene expression analysis comparing RNA-seq data was performed using DESeq2. The GO term enrichment analysis was carried out using the R package gProfiler2 and visualized with the Cytoscape plugin, EnrichmentMap (KOLBERG *et al.* 2020, MERICO *et al.* 2010). Relative fluorescence levels were measured using the Infinite M200 plate reader (Tecan Group Ltd., Männedorf, Switzerland). RT-qPCR analysis was performed using the $\exp(-\Delta C_t)$ method in Stratagene Mx3000P (Agilent Technologies). Western blotting analysis, microscopy,

and image processing were performed as described previously (DEVAN *et al.* 2022). For detailed methods, Chapter 5, Appendix 2, Materials and Methods.

Data, Materials and Software Availability

All sequencing data are available in the NCBI Gene Expression Omnibus (GEO) under the SuperSeries accession number GSE224487. The collection contains RNA-seq data from *khd4Δ* and wildtype hyphae and yeast cells (GSE224486), as well as hyperTRIBE data from strains expressing Rrm4-Ada-Gfp, Khd4-Ada-Gfp and control-Ada in *U. maydis* hyphae (GSE224485).

Acknowledgments

We would like to sincerely thank Dr. Andreas Brachmann, Dr. Kerstin Schipper, Dr. Seomun Kwon for valuable scientific inputs; Melanie Honstein for generating the reporter strains. Thorsten Wachtmeister for NGS support; U. Gengenbacher and S. Esch provided tremendous technical assistance; Melina Klostermann, Nina Kim Stoffel for the support with bioinformatics and biochemical analyses, respectively. The work was funded by grants from the Deutsche Forschungsgemeinschaft (German Research Foundation; https://www.dfg.de/) to MF (Germany's Excellence Strategy EXC-2048/1 - Project ID 39068111; CRC1535/1-A03 – Project ID 458090666, FOR2333-TP03 FE 448/12-1), KZ (FOR2333-TP02 ZA 881/3-1), and AM (CRC1535/1-B02 – Project ID 458090666) as well as by the graduate school Molecules of Infection-III to MF and SS. The funders had no role in study design, data collection and analysis, decision to publish, or preparation of the manuscript.

2.2 Khd4 condensates at the sites of polar growth under heat stress

Stress granules are dynamic biomolecular condensates implicated in mRNA translation, storage, stabilization, and localization of mRNAs. This membrane-less compartment forms exclusively in response to stress, and is primarily composed of RBPs, poly(A) mRNAs, stalled translation-associated factors, including the 40s ribosomal subunit, and translation initiation factors (MARCELO *et al.* 2021,DECKER AND PARKER 2012).

RNA-binding proteins are key constituents of stress granules, attributed to the multivalency capacity of their RNA-binding domains, and intrinsically disordered regions (MARCELO *et al.* 2021,DECKER AND PARKER 2012). The formation of stress granules involves the phase separation of RNA and protein molecules, driven by the combination of protein-protein, protein-RNA, and RNA-RNA interactions (VAN TREECK AND PARKER 2018). Although only a limited number of RBPs are essential for the core stress granule formation, others play auxiliary roles by facilitating the inclusion of their target mRNAs (WOLOZIN AND IVANOV 2019). By sequestering these mRNP complexes, stress granules effectively stall mRNA translation, allowing cells to cope with cellular stress by prioritizing the translation of cytoprotective proteins (DECKER AND PARKER 2012).

Previous research discovered that Khd4 forms cytoplasmic stress granules in yeast cells during heat stress (VOLLMEISTER 2009). This chapter extends this finding, underscoring that Khd4-positive granules resemble the site of polar growth in yeast and infectious hyphal cells. Due to the importance of the stress response network in fungal pathogens, studying the RNP granules under different stress conditions might also reveal novel effects of posttranscriptional control mechanisms in fungal virulence.

2.2.1 Localization of Khd4 during heat stress

As a marker for stress granule assembly, the DEAD-Box RNA helicase Dhh1 (UMAG_10655), well-known for its role in the RNP granule assembly (DECKER AND PARKER 2012), was employed. To study stress-induced localization, both Khd4 and Dhh1 were C-terminally tagged with Gfp and Kat, respectively, and co-expressed from their endogenous loci. A strain constitutively expressing Gfp served as a negative control. Heat stress was induced by incubating the cells at 40 °C for 20 minutes (Fig. 2.8A; Materials and methods).

Under normal conditions, Khd4-Gfp and Dhh1-Kat were predominantly found in the cytoplasm (Fig. 2.8B-C). Even without heat stress, a significant portion of the Dhh1-Kat signal consistently appeared in the cytoplasmic granular bodies, highlighting the recognized role of Dhh1 in P-bodies, cytoplasmic membrane-less organelles involved in mRNA degradation (Fig. 2.8B-C; DECKER AND PARKER 2012).

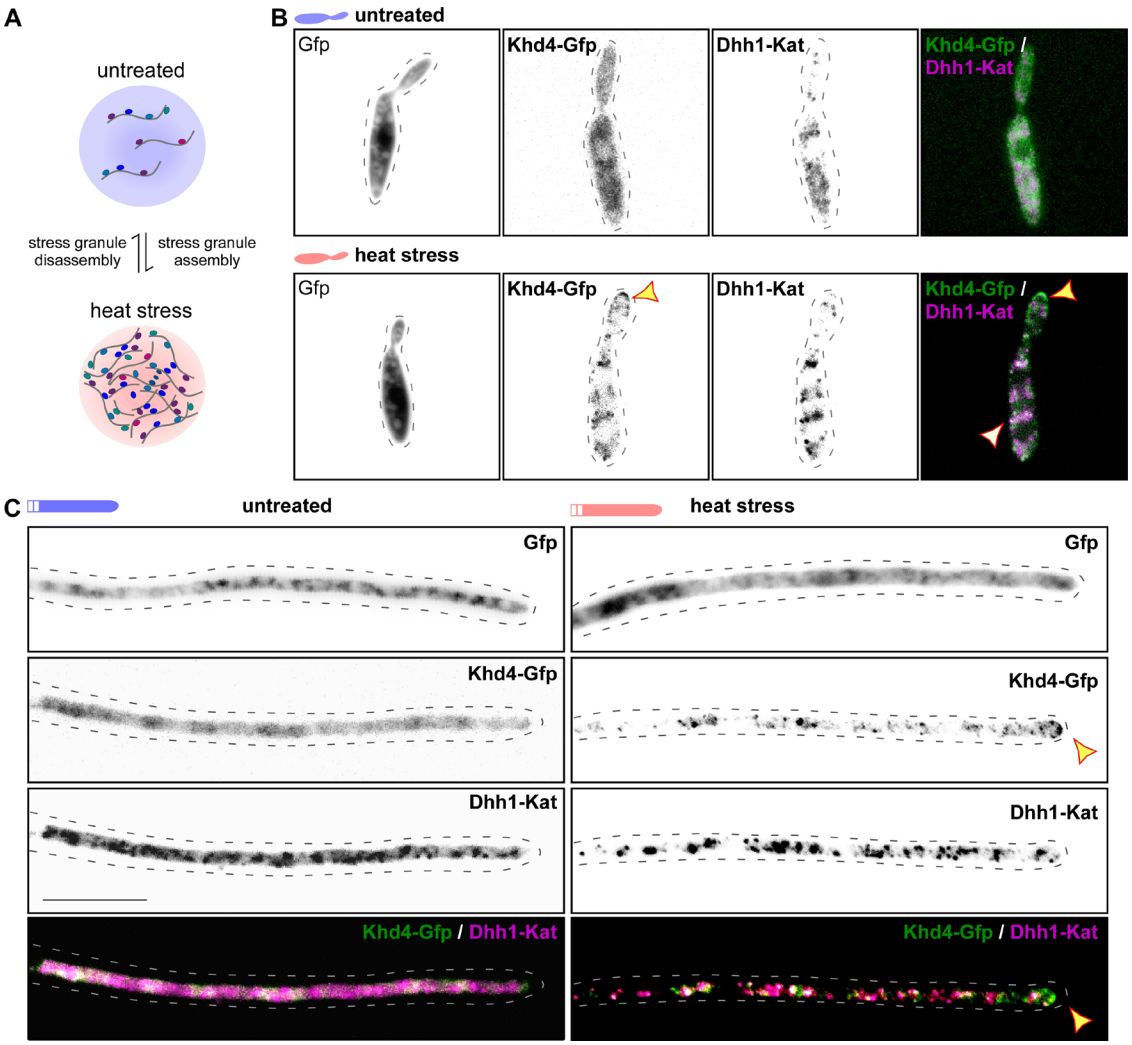

Fig. 2.8. Khd4 accumulates at the cortex of the growth pole under heat stress. **(A)**. Schematic illustration of stress granule induction by heat shock. The onset of heat stress causes phase separation of RNP granules into cytoplasmic condensates (Red), which are disassembled (Blue) after the stress has abated. (RNAs- grey; RBPs- colored elliptical structures). **(B)**. Inverted fluorescent micrographs of yeast cells under normal (top; 28 °C) and heat shock (bottom; 40 °C for 15 minutes) conditions. Fluorescent proteins are labeled accordingly Scale bar: 10 µm. Silhouette images of yeast cells are indicated at the top (blue- untreated cells; red- heat-stressed cells; maximum projections images of z-stacks). **(C)**. Inverted fluorescent micrographs of AB33-derived hyphal cells under normal (Left; 28 °C) and heat shock (Right; 40 °C for 15 minutes) conditions. Scale bar: 10 µm. Silhouette images of the hyphal cells are shown in the top (blue- untreated cells; red- heat-stressed cells; maximum projections images of z-stacks) Yellow arrowheads in B and D indicate the accumulation of Khd4-Gfp signal at the growth apex

Upon heat stress induction, both RBPs promptly accumulate into granular bodies with prominent co-localization between Khd4-Gfp and Dhh1-Kat, consistent with previous

results (VOLLMEISTER 2009). Interestingly, in contrast to Dhh1-positive stress granules, Khd4-positive granules primarily congregated at the cell periphery, especially at the growth pole of yeast and hyphae, despite its lower expression levels compared to Dhh1 (Fig. 2.8B-C). Cytoplasmic foci formation was not observed in the Gfp control, affirming the specificity of the assembled biomolecular condensate to RNA-binding proteins (Fig. 2.8B-C).

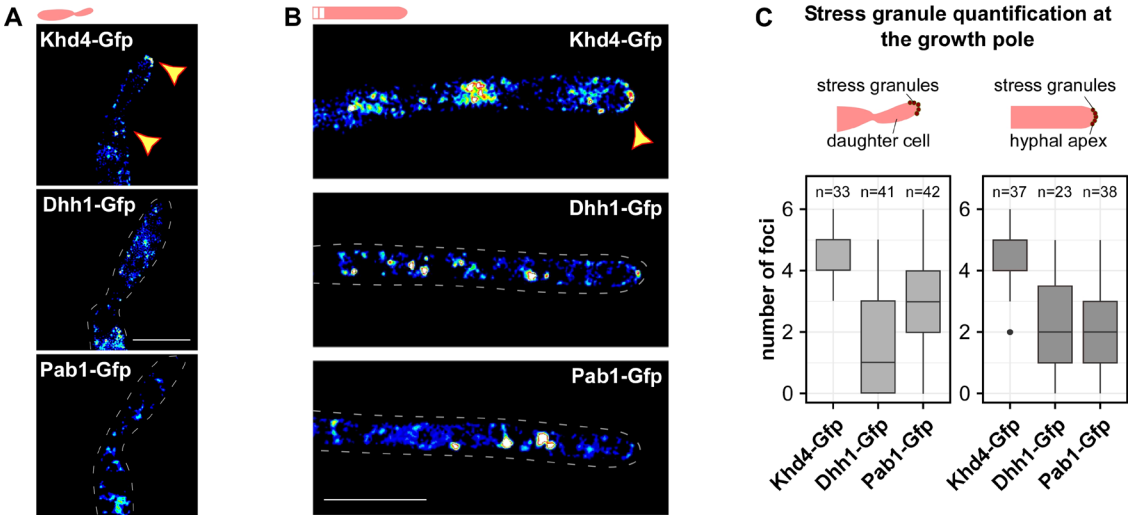

Fig. 2.9. Distribution of Khd4 under heat stress visualized by SR-SIM. False colored maximum projection images of z-stacks acquired from yeast **(A)** and hyphal cells **(B)** after heat stress, visualized by the super-resolution Structured Illumination Microscopy (SR-SIM). The arrowhead (yellow) indicates the predominant localization of Khd4 signals at the growth pole, a pattern that is less pronounced in the case of the RNA-helicase Dhh1 and the poly (A) binding protein Pab1. In (A), the arrow head also indicates cortical accumulations for Khd4 signals (Heat shock- 40 °C for 15 minutes). **(C)** Boxplot showing the number of stress granules at the growth tip in yeast (left) and hyphal (right) cells after elicitation of stress granule formation by heat stress, visualized by the super-resolution SIM. The data represent a single experimental run (n=1), and the number of cells quantified is provided inside. The schematics at the top indicate the specific region of interest considered for this quantification.

To gain clear insights into the subcellular localization pattern, super-resolution structured illumination microscopy (SR-SIM) was utilized to visualize Khd4 under heat stress (Fig. 2.9A-C). Besides Dhh1, the study also included the multi-functional, poly(A) binding protein Pab1 (UMAG_03494) as an RBP control. Like Khd4, both RBPs were C-terminally tagged with Gfp and expressed endogenously.

SR-SIM analysis unequivocally demonstrated a distinct subcellular localization pattern for Khd4 under heat stress: Khd4-positive granular bodies exhibited a prominent accumulation at the growth pole, forming a characteristic crescent-shaped configuration in nearly all quantified cells (Fig. 2.9A-C). This specific localization pattern was not observed for Pab1- and Dhh1-positive granules. Furthermore, the Khd4-positive granules

were observed to accumulate cell cortex in both yeast and hyphal cells (Fig. 2.9A-B). This suggests a unique functional role for Khd4 in this subcellular region.

The dispensability of Khd4 for stress granule formation in *U. maydis* (VOLLMEISTER 2009) suggests that its condensation at polar growth sites may be a result of elevated RBP concentration in these subcellular locations under normal conditions, rather than being a specific response to stress-induces cytoplasm to cortical movement. This stress-induced localization of Khd4 bears a resemblance to endoplasmic reticulum localization in *U. maydis* (WEDLICH-SÖLDNER *et al.* 2002,SCHIRAWSKI *et al.* 2005), indicating a potential link between the post-transcriptional regulatory function of Khd4 and the ER.

In essence, the subcellular-localization patterns of Khd4 during heat stress mirror the localization of the ER in the cell cortex. This observation suggests a potential regulatory role for Khd4 in this specific subcellular region.

2.3 Prediction of potential Khd4-regulated mRNA regulon in plantae

In addition to polar growth, membrane trafficking regulation also determines the success of fungal pathogens during infection. This includes the precise secretion of effectors proteins for manipulating host metabolism and acquiring nutrients from the host for energy. Recently, it has been observed that the transcriptional upregulation of genes responsible for regulating membrane trafficking is closely associated with the process of plant penetration and the establishment of early biotrophic interactions in U. maydis (LANVER et al. 2018).

To this end, this study has demonstrated that Khd4 might be involved in the coordinated regulation of mRNA encoding proteins engaged in membrane trafficking into an mRNA regulon. This chapter aims to predict Khd4-mediated mRNA regulons involved in pathways related to membrane trafficking and other virulence-related processes during infection. AUACCC-containing mRNAs served as a proxy to predict potential Khd4 mRNA regulons involved in the infection process. Besides the position of AUACCC, their co-expression pattern in planta is also considered, which provides insights into which mRNA molecules are simultaneously active.

In order to identify transcripts involved in the pathogenic program, a systematic approach was adopted. Specifically, AUACCC-containing mRNAs exhibiting increased expression profiles within the host plant were selected. This relied on pre-established co-expression modules in *U. maydis* derived from an extensive infectious time-course study (LANVER et al. 2018). Within these modules, genes exhibiting similar expression patterns were organized into distinct color-coded clusters (LANVER et al. 2018). For instance, the red module consists of genes that were expressed exclusively on the plant surface (0.5-1 days post inoculation). The light-green module was expressed during the plant penetration stage (1-2 d.p.i.), whereas the magenta module was induced at 0.5-2 d.p.i. and persisted until 12 d.p.i. The cyan module also known as the tumor module was induced after biotrophy establishment (2-4 d.p.i.), commencing tumor formation (LANVER et al. 2018).

In the first step, the AUACCC-containing mRNAs within the virulence-related modules, specifically those categorized as red, light-green, magenta, and cyan were singled out. Due to the crucial roles in ER-related processes such as protein catabolism, autophagy, and cell cycle regulation, the genes present in the light-cyan and yellow modules were

also integrated into the regulon analysis (LANVER et al. 2018). It is worth noting that the expression profiles of genes within these two modules remained the same irrespective of the bioinformatics tools used, indicating the robust functional relationships between these genes (LANVER et al. 2018).

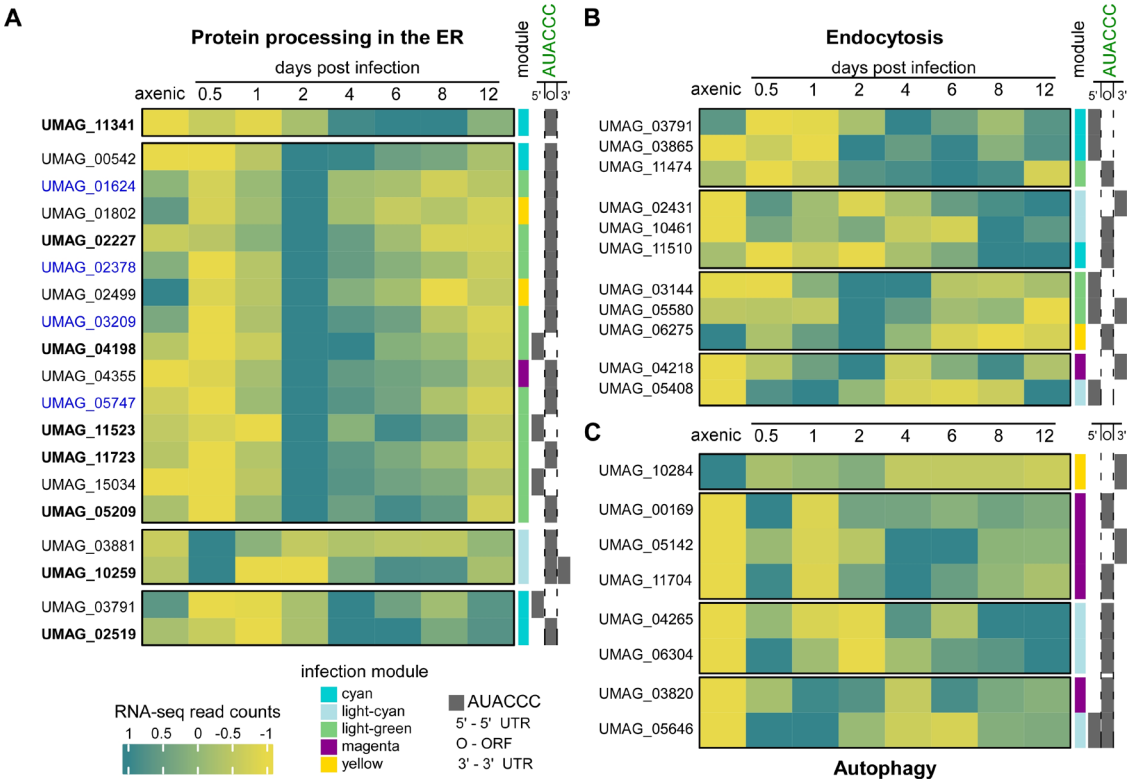

Fig. 2.10. Expression levels of AUACCC-containing mRNAs involved in pathways associated with membrane trafficking process during infection. **(A)** Heatmap showing the distribution of expression levels for AUACCC-containing mRNAs associated with protein processing in the ER. Columns indicate the eight developmental stages of *U. maydis* (axenic (yeast stage), 0.5, 1, 2, 4, 6, 8, 12 dpi). The left annotation indicates the co-expression module to which the transcript belongs following LANVER *et al.* 2018: cyan, magenta, light-green, yellow, and light-cyan. The position of the AUACCC motif (green) in 5′ UTR (5′), ORF (O), and 3′ UTR (3′) is also indicated (grey box). Transcripts in bold encode proteins function in N-glycosylation while those in blue represent SEC proteins involved in COP II vesicle formation. Due to functional redundancy, transcripts associated with the N-glycosylation pathway are grouped with those linked to protein processing in the ER. **(B)** Heatmap displaying the expression level distribution of mRNAs containing the AUACCC motif associated with endocytosis and **(C)** autophagy.

This systematic selection process yielded a total of 1043 AUACCC-containing mRNAs distributed across six distinct infection-related expression modules. Subsequently, these transcripts were subjected to KEGG Mapper analysis to identify mRNA regulons encoding functionally related proteins participating in analogous metabolic or signaling pathways. Only pathways with at least 5 genes were selected for further analysis (Table 5; KANEHISA AND SATO 2020,KANEHISA *et al.* 2022; https://www.genome.jp/kegg/mapper/).

2.3.1 Membrane trafficking regulon

The comprehensive analysis resulted in 41 pathways, among which 26 exhibited a slight yet discernible increase in enrichment for AUACCC-containing mRNAs when contrasted with all KEGG annotated genes from *U. maydis* (Table 5). These pathways encompass crucial cellular processes such as endocytosis, N-glycan biosynthesis, and autophagy, intricately linked to membrane trafficking mechanisms. This finding corroborates the previous results in infectious hyphae, further underscoring the potential involvement of Khd4 in the regulation of membrane trafficking during plant infection. Although not enriched in comparison to reference, the protein processing in the ER pathway was also included in the analysis due to its pivotal role in governing the membrane logistics and the observed redundancy with genes associated with N-glycosylation, which are shared between these sets (Fig. 2.10A).

In agreement with the importance of secretion, examining gene expression levels in transcripts related to protein processing in the endoplasmic reticulum (ER) pathway, including eight transcripts involved in the N-glycosylation process, revealed a significant surge precisely at the 2 d.p.i., a stage for establishing biotrophy (Fig. 2.10A). Similarly, transcripts containing the AUACCC motif associated with endocytosis and autophagy displayed induction at 1-2 days post inoculation (d.p.i.), persisting throughout late infection stages (Fig. 2.10B-C), underscoring the significance of cellular recycling mediated by autophagy during the early as well as late biotrophy establishment phase.

Endocytosis plays a fundamental role in nutrient uptake, intercellular communication, and cell signaling by internalizing plasma membrane components destined for either vacuole degradation or plasma membrane recycling when the pathogen is in close contact with the host. Recent findings indicate that autophagy also involves receptor recycling and signaling (BIRGISDOTTIR AND JOHANSEN 2020). These interdependencies between endocytosis and autophagy are further illustrated by their prominent role in ensuring vacuole biogenesis and quality control (BIRGISDOTTIR AND JOHANSEN 2020).

Notably, most of the AUACCC-containing transcripts associated with autophagy exhibit a sharp increase at 0.5 d.p.i, a crucial stage for plant penetration (Fig. 2.10C). In the rice blast fungi *M. oryzae*, autophagy is known to be essential for the formation of appressorium required for plant penetration (ZHU et al. 2019). A key step in

autophagosome formation involves the conjugation of ubiquitin-like ATG-8 proteins to the phosphatidylethanolamine on the autophagic membrane (ZHOU et al. 2022). Interestingly, three ATG8-interacting proteins, namely ATG3 (UMAG_00169), ATG4 (UMAG_05142), and ATG5 (UMAG_11704), involved in ubiquitin-like conjugation machinery, the PI3K complex protein ATG6 (UMAG_04265), involved in lipid kinase complex, are encoded by transcripts containing the AUACCC motif. ATG5, however, carries the motif in its 3′ UTR, while the rest contains the binding site in the ORF region (Fig. 2.10C). This suggests that Khd4 may coordinately regulate these transcripts into an mRNA regulon thereby dynamically regulating autophagy.

The protein processing in the ER pathway also includes genes responsible for COPII vesicle formation. Of all the COPII-regulating proteins– Sar1, Sec13, Sec31, Sec23, and Sec24, the transcripts encoding three of them, namely, Sec23 (UMAG_01624), Sec24 (UMAG_03209) (inclusive of its paralog, Sec24C (UMAG_02378)), and Sec31(UMAG_05747), not only share the same expression pattern when the fungus is inside the host but also carry the AUACCC motif within their ORF region (Fig. 2.10A; FROMME et al. 2008). Also, many transcripts involved in ER protein processing, endocytosis, and autophagy carry the AUACCC motif within their ORF region.

These observations strongly suggest that Khd4 may coordinate these transcripts into an mRNA regulon, thereby dynamically regulating N-glycosylation, COPII vesicle formation, endocytosis, and ATG-8 assembly posttranscriptionally. This coordination is likely to exert a significant influence on secretion and cellular recycling during pathogen-host communication (Fig. 2.10A-C).

2.3.2 Cell cycle regulon

In addition to pathways related to membrane trafficking, the KEGG mapper analysis suggests that the posttranscriptional regulatory potential of Khd4 extends to various processes during infection, including cell cycle regulation, MAPK pathway, spliceosome, ribosome biogenesis, mRNA surveillance pathway, RNA degradation, DNA replication and repair, secondary metabolites biosynthesis, steroid biosynthesis and phosphatidylinositol signaling pathway (Table 5).

Precise control of the cell cycle is a vital determinant for successful plant infection in *U. maydis*. Studying the expression of the AUACCC-containing transcripts functioning in the cell cycle revealed heightened expression in axenic culture, reflecting the dividing

yeast cell stage, followed by a secondary induction at 2 d.p.i., signifying the release of the cell cycle arrest after plant penetration and early biotrophic growth (Fig. 2.11A; LANVER *et al.* 2018). Notably, many of these transcripts contain AUACCC in their 3´ UTR, highlighting the pivotal role of Khd4 in rapidly modulating their steady-state levels following transcriptional induction during cell cycle regulation (Fig. 2.11A). Markedly, the deletion of *khd4* resulted in cell-cycle-defective yeast cells (Fig. 5.2A), and the mutant did not display hyphal proliferation in planta.

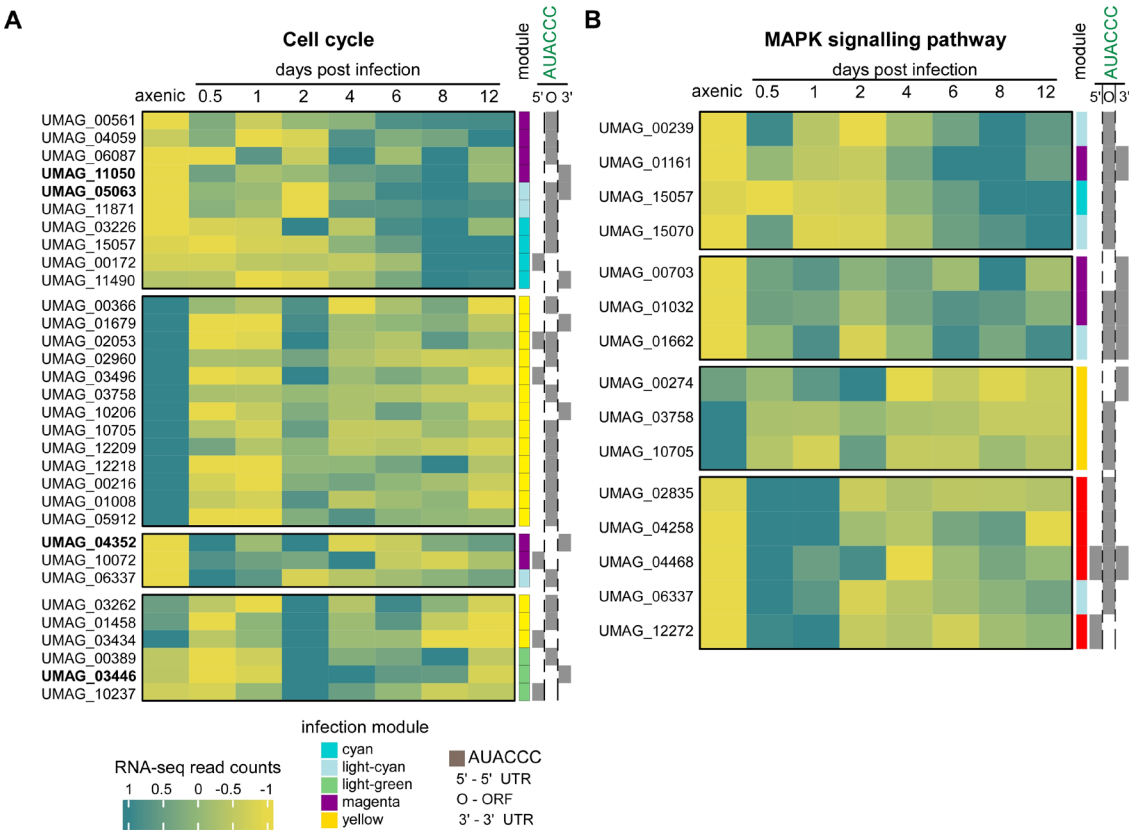

Fig. 2.11. Expression levels of AUACCC-containing mRNAs encoding proteins involved in cell cycle and MAPK signaling process. **(A)** Heatmap showing the distribution of expression levels for AUACCC-containing mRNAs associated with cell cycle regulation. Columns indicate the eight developmental stages of *U. maydis* (axenic (yeast stage), 0.5, 1, 2, 4, 6, 8, 12 dpi). The left annotation indicates the co-expression module to which the transcript belongs following LANVER *et al.* 2018: cyan, magenta, light-green, red, yellow, and light-cyan. The position of the AUACCC motif (green) in 5´ UTR (5´), ORF (O), and 3´ UTR (3´) is also indicated (grey box). Transcripts in bold encode proteins function in the Mitotic Exit Network (MEN) pathway. Due to functional redundancy, transcripts associated with meiosis, and DNA replication are grouped with those linked to cell cycle regulation. **(B)** Heatmap displaying the expression level distribution of mRNAs containing the AUACCC motif associated MAP-Kinase signaling pathway.

One key observation is that several members of the evolutionarily conserved GTPase module of the mitotic exit network (MEN) contain AUACCC sequences in the 3´ UTR of the encoding mRNAs (Fig. 2.11A). Furthermore, their expression is increased *in planta* after penetration, suggesting a cell cycle regulon. This includes the small GTPase

Tem1 (UMAG_11050), its guanine-nucleotide exchange factor Lte1 (UMAG_05063), the protein kinase Dbf2 (UMAG_03446), and the Dbf2-associated protein Mob1 (UMAG_04352).

Although the cognate GTPase activating protein Bfa1 (UMAG_02890) involved in the MEN pathway is not annotated in KEGG, it is noteworthy that Bfa1 also features the AUACCC motif in its 3′ UTR and exhibits expression in planta (cyan; LANVER *et al.* 2018). Recently, it was shown that mitotic exit regulation is essential for pathogenicity in *Fusarium graminearum* (MIAO *et al.* 2023). Numerous AUACCC-containing transcripts encode proteins participating in the MAPK module, a conserved signaling pathway governing morphological and pathogenic development (Fig. 2.11B; VOLLMEISTER *et al.* 2012).

Overall, this systematic analysis identifies a potential Khd4-mediated mRNA regulon that orchestrates membrane trafficking and cell cycle during *U. maydis* infection in plants, thus underscoring the potential function of Khd4 during infection.

3 Discussion and Perspectives

From synthesis to decay, RNA-binding proteins (RBPs) guide every aspect of RNA life. While mRNA synthesis initiates with transcription factors (TFs), it is worth noting that RBPs account for a substantial 20% of the expressed protein-coding transcriptome in human cells (GERSTBERGER *et al.* 2014). In contrast, TFs, although encoded by a similar number of genes, represent only a modest 3% of the total transcript abundance within the cell (GERSTBERGER *et al.* 2014). This contrast underscores the paramount importance of posttranscriptional regulatory mechanisms in orchestrating gene expression control.

Despite the central role of RNA regulation in gene expression control, its impact on fungal virulence remains largely unexplored. Previous studies have indicated that Khd4, a multi-KH domain containing RBP, is a prerequisite for the proper morphology and pathogenicity of *U. maydis*. Efforts to decipher its RNA-binding potential, including the use of a heterogenous yeast three-hybrid system, unveiled the AUACCC sequence as a pivotal and sufficient motif for RNA interaction. However, the precise role of Khd4, especially its direct binding RNA targets involved in *U. maydis* virulence, proved elusive (VOLLMEISTER *et al.* 2009).

Hence, this thesis aimed to uncover the Khd4-RNA interaction networks involved in the formation of the infectious hyphae in the pathogenic fungi *U. maydis*. The establishment of hyperTRIBE in this investigation, an RNA proximity labeling technique, allowed the detection of Khd4 targets and related Khd4-binding to Khd4-dependent changes in mRNA abundance, offering a transcriptome-wide view of the regulation of Khd4-bound mRNAs. The findings disclosed that Khd4 binds mRNAs encoding regulatory proteins involved in membrane trafficking and regulates their mRNA stability. Furthermore, it was demonstrated that by rendering mRNAs instable, Khd4 efficiently regulates their steady-state levels following hyphal morphogenic cues. In essence, this thesis underscores that gene expression control at the RNA level is indispensable for infectious hyphae development. It revealed a novel role for an RNA-binding protein in the regulation of membrane trafficking. Additionally, this study provides preliminary insights into the potential function of Khd4 in proximity to the endoplasmic reticulum, paving the way for new research directions.

3.1 Successful establishment of hyperTRIBE to detect targets of fungal RBPs

In this study, the successful adaptation of the hyperTRIBE technique, originally developed in *D. melanogaster*, enabled the identification of RBP targets for fungi. This method has proven effective in identifying RBP targets in various systems, including mammalian cells, and plants, such as *Arabidopsis thaliana*, *Physcomitrium patens* as well as malarial parasites (McMahon *et al.* 2016,Liu *et al.* 2017,Rahman *et al.* 2018,Liu *et al.* 2019,Jin *et al.* 2020,Nguyen *et al.* 2020,Arribas-Hernández *et al.* 2021,Biswas *et al.* 2021,Cheng *et al.* 2021,Zhou *et al.* 2021).

HyperTRIBE is particularly attractive to fungal pathogens for three main reasons. Firstly, this method capitalizes on the proximity labeling technique, relying on the expression of Ada fusion proteins for target RNA detection. Secondly, hyperTRIBE streamlines target identification by requiring less starting material (Ramanathan *et al.* 2019,McMahon *et al.* 2016). On the other hand, standard CLIP-based methods demand large input requirements, complicating the RNA detection from discrete, small-cell populations such as fungal biomass inside the host tissues (Ramanathan *et al.* 2019). Furthermore, the CLIP-based methods may fail to work for high-molecular-weight and low-abundant RBPs such as Khd4, and or RBPs with limited interactome (Ramanathan *et al.* 2019,McMahon *et al.* 2016). Thirdly, the hyperTRIBE approach facilitates the potential to detect stage-specific mRNA targets by controlling the expression of RBP-Ada fusion proteins. In addition to chemical or light-inducible promoters, such as the TetON system (Ingole *et al.* 2022), this can also be achieved by endogenous conditionally active promoters such as UMAG_03597 which can be used to identify mRNA targets of RBP-ADA fusion protein during the biotrophic establishment phase of *U. maydis* (Schmitz *et al.* 2020). HyperTRIBE can also function as a straightforward *in vivo* RBP-RNA binding assay, enabling the assessment of RBP interactions with specific mRNA molecules using Sanger sequencing. To ensure efficient deamination of adenosine, the catalytic activity of Ada requires approximately 24 seconds, underscoring the necessity for persistent contact between the RBP-Ada fusion protein and RNA (Kuttan and Bass 2012). This capability holds promise for future investigations into the strength of RBP-RNA binding.

3.2 HyperTRIBE editing reflects the precise binding properties of RBPs

To assess the applicability of hyperTRIBE in fungal systems, as a proof-of-principle study, a pilot experiment was conducted using the well-studied RBP Rrm4. The comparative analysis between Rrm4-Ada-Gfp and Khd4-Ada-Gfp confirmed that the

fusion proteins were catalytically active, and efficiently edited mRNAs in a reproducible manner. However, notable differences emerged in their editing patterns strongly indicating that RBPs are the main drivers of Ada editing specificity:

Rrm4-Ada-Gfp, consistent with previous iCLIP findings indicating that Rrm4 binds to over 50% of the *U. maydis* transcriptome (OLGEISER *et al.* 2019), exhibited a threefold increase in editing sites compared to Khd4-Ada-Gfp. This suggests that Ada editing is influenced by the RNA-binding capacity of the associated RBP. In contrast, Khd4-Ada-Gfp exhibited highly consistent editing efficiencies across replicates, underscoring the enhanced affinity and specificity of Khd4 for its target mRNAs. For instance, Khd4 showed stronger binding to the AUACCC-containing sequence compared to the interaction of Rrm4 with its known target RNA sequence (KÖNIG *et al.* 2007,VOLLMEISTER 2009). Furthermore, *de novo* motif discovery analysis emphasized the prominence of the Khd4-binding sequence, AUACCC, in sequences edited by Khd4-Ada-Gfp, highlighting the sequence-specific RNA recognition of Khd4. Conversely, such motifs were not found in Rrm4-Ada-Gfp edited sequences.

Rrm4 contains 3 RNA Recognition Motifs (RRM3) and it is known from the previous iCLIP experiments that the third RRM domain binds the UAUG motif specifically, which constitutes only about one-third of all Rrm4 binding sites (OLGEISER *et al.* 2019). The absence of UAUG motifs in the *de novo* motif analysis for Rrm4-Ada-Gfp edited sequences could be due to the high prevalence of short UAUG motifs throughout the genome, making it difficult to distinguish them from background sequences. Alternatively, this might suggest that RNA recognition by RRM1 and 2 predominates in Rrm4-Ada-Gfp targets.

The findings presented in this study demonstrate that independent of the RBP characteristics, the RBP-Ada editing results in highly specific target transcripts and binding sites in the hyperTRIBE system. For instance, over 80% overlap was observed between Rrm4-Ada-Gfp edited transcripts and the iCLIP-derived target mRNA repertoire of Rrm4. Similarly, more than 80% of the transcripts edited specifically by Khd4-Ada-Gfp contained at least one AUACCC motif in their transcript regions. Furthermore, the editing sites for both RBPs were found near their respective binding sites, affirming that hyperTRIBE editing effectively captures *in vivo* RBP binding in fungal cells.

3.3 Low editing efficiency of *Drosophila* Ada in fungal cells

In comparison to the global Rrm4 binding profile from iCLIP (OLGEISER *et al.* 2019), Rrm4-Ada-Gfp expression identified significantly fewer target mRNAs. Despite the binding by Rrm4-Ada-Gfp, numerous functionally relevant Rrm4 targets, including *cts1* and *septin*, remained undetected in the hyperTRIBE system due to sub-threshold editing (<5%) observed in these mRNAs (Appendix 3, Fig. 5.15A). The binding of Rrm4 with *cts1* mRNA is crucial for proper secretion of the endochitinase, while its binding to *septin* mRNAs like *cdc3*, *cdc10*, *cdc11*, and *cdc12* ensures the formation of septin filament at the growth tip (KOEPKE *et al.* 2011,BAUMANN *et al.* 2014,ZANDER *et al.* 2016).

Similar low editing efficiency for *Drosophila* Ada was also observed in the plant hyperTRIBE systems (ARRIBAS-HERNÁNDEZ *et al.* 2021,CHENG *et al.* 2021). Given that fungi and plants lack ADAR orthologs (JIN *et al.* 2009), their cellular conditions may be less conducive to Ada activity than those in *Drosophila* and mammalian systems (XU *et al.* 2018,NGUYEN *et al.* 2020). Strikingly, the *Drosophila* Ada also showed lower editing efficiency in the human prostate cancer line than its human ortholog (JIN *et al.* 2020). While the cytidine deaminase, APOBEC-1, catalyzing C-to-T edits, functioned efficiently in mammalian cells, no substantial editing was found in the fruit fly system (ABRUZZI *et al.* 2023). These studies emphasize the variation in editing efficiency among different RNA base editors across different systems. Therefore, in future, attempts must be made to select the appropriate RNA base editor to further improve the efficacy of the hyperTRIBE method in fungal systems. Recent developments in the hyperTRIBE system in *S. cerevisiae* have indicated that human ADAR2 exhibits higher activity and increased signal-to-noise ratio in baker's yeast than the *Drosophila* Ada (PIAO *et al.* 2023).

It is noted that in *U. maydis,* and plant hyperTRIBE systems, *Drosophila* Ada displays substantial background editing in the absence of the RBP fusion (ARRIBAS-HERNÁNDEZ *et al.* 2021,CHENG *et al.* 2021). This aberrant activity can be partially attributed to the increased expression levels of control-Ada in comparison to RBP-Ada fusions in the current hyperTRIBE system (Fig. 5.4A-B). Nonetheless, it is crucial to acknowledge that control-Ada editing tends to lack specificity in target selection when compared to RBP-Ada fusion proteins. To address the issue of control-Ada-induced false negatives in future experiments, maintaining consistent expression levels across hyperTRIBE constructs is paramount. Furthermore, normalizing ADAR expression levels to the editing proportion can also mitigate the impact of inconsistent expression levels on target

mRNA detection (ARRIBAS-HERNÁNDEZ *et al.* 2021). It is also recommended to incorporate deep sequencing and use cDNA library kits with unique molecular indices (UMIs) to enhance the resolution of target detection (KIVIOJA *et al.* 2011).

The synthetic derivative of human ADAR2, RESCUE, has the potential to replace *Drosophila* Ada in fungal hyperTRIBE. RESCUE offers high editing efficiency with increased specificity and the unique capability of concurrent A-to-G and C-to-U editing, significantly expanding the editable window (ABUDAYYEH *et al.* 2019,BURGESS 2019). Recently, PIE-seq, an RBP target detection method that combines dual RNA base editors, Apobec1 and ADAR2, with the target RBP, has shown promise for future applications. It enhances RBP target discovery by mitigating nucleotide biases associated with different RNA base editors (RUAN *et al.* 2023).

3.4 AUACCC within the 3′ UTR causes mRNA instability

RBPs typically control RNA regulation by recognizing the regulatory *cis*-elements present in target mRNAs. Studying the distribution of Khd4 binding sites revealed that the RBP binds mRNAs preferentially through the UTR regions, mainly via 3′ UTRs. Interestingly, the deletion of *khd4* in hyphal cells increased the expression of transcripts carrying the 3′ UTR AUACCC motif. Subsequent analysis confirmed that the AUACCC motif in the 3′ UTR functions as a destabilizing element upon binding by Khd4. This suggests that Khd4 mediates spatiotemporal gene expression in hyphal cells by governing mRNA turnover.

While studies on the roles of such *cis* and *trans*-acting factors in fungal pathogens are currently scarce, comparable functions are known for mammalian RBPs. For instance, RBPs, tristetraprolin (TTP), and CELF1 cause rapid mRNA turnover by binding to the AU-rich and GU-rich mRNA decay elements in the 3′ UTR of mRNAs, respectively (BARREAU *et al.* 2005,VLASOVA-ST LOUIS AND BOHJANEN 2011).

RBPs facilitate mRNA degradation by specifically recruiting and activating the mRNA decay machinery to target mRNAs. For instance, the RBP TTP induces mRNA destabilization by directly interacting with the CNOT1 subunit of the CCR4-NOT deadenylation complex via its C-terminal domain (FABIAN *et al.* 2013). Mutations in the TTP- CNOT1 interface have been found to impair TTP-mediated mRNA degradation (FABIAN *et al.* 2013). Some RNA-binding domains are capable of mediating protein-protein interaction, in concert with RNA binding (CORLEY *et al.* 2020). For example, in

D. melanogaster, the RBP Bicaudal-C interacts with the NOT3/5 subunit of the Ccr4-Not complex, via its KH domain (CHICOINE *et al.* 2007,MINEGISHI *et al.* 2021). The hypothesis put forward is that Khd4 recruits the evolutionarily conserved Ccr4-Not complex for mRNA-specific poly(A) tail shortening (MILLER AND REESE 2012,COLLART *et al.* 2013). Furthermore, the co-localization of Khd4 with the decapping activator Dhh1 suggests a potential connection between Khd4-mediated mRNA deadenylation and the subsequent decapping process (FISCHER AND WEIS 2002,VIJJAMARRI *et al.* 2023). Consistently, the RBP Roquin-mediated mRNA decay, besides deadenylation, also involves mRNA decapping (ESSIG *et al.* 2018). However, it is important to note that further investigation is necessary to fully elucidate the mechanistic details underlying the processes.

Significantly, the KH5 and 6 domains of Khd4 exhibit high conservation across mammalian fungal pathogens. Furthermore, the KH domains display a general preference for C-rich sequences in target RNA (VALVERDE *et al.* 2008,NICASTRO *et al.* 2015). This robustly supports the idea that the Khd4-AUACCC regulatory mechanism remains conserved among these pathogenic fungi.

3.5 mRNA destabilization governs gene expression during hyphae formation

The virulence of many fungal pathogens is tightly associated with their ability to shift to hyphal morphology, a process involving significant transcriptional rewiring. In *U. maydis*, this shift is driven by the master transcriptional factors bE and bW, triggering a multi-layered transcriptional network of over 300 genes (HEIMEL *et al.* 2010b). However, it is unclear how the posttranscriptional program is altered during infection and how these two complex gene regulatory networks are coordinated at these different levels of regulation. Investigation into Khd4-bound mRNAs revealed that many of these transcripts were not only transcriptionally induced during the yeast-to-hyphae transition but also counterintuitively contained the AUACCC motif in their 3′ UTR for mRNA instability. This underscores the multifaceted role of Khd4-mediated mRNA decay beyond mere repression of target gene expression.

The target analysis revealed that the mRNA stability factor, Khd4, primarily targets mRNAs encoding regulatory proteins such as GTPases. A similar trend was observed in other systems where regulatory proteins like cytokines, kinases, and TFs are encoded by unstable mRNAs (ANDERSON 2010,THOMPSON *et al.* 2023). Utilizing a single-

compartment mathematic model (HARGROVE AND SCHMIDT 1989), this study demonstrated that Khd4-mediated mRNA decay governs the precise induction kinetics of its target mRNAs after transcription. This promotes rapid production of these regulatory proteins upon hyphal induction, followed by faster clearance after transcription ceases. Consistently, deletion of *khd4* alters the underlying regulatory dynamics, resulting in hyphal cells with a delayed polar growth program. Thus, during infectious hyphae morphogenesis, the tight coupling of transcriptional activation with mRNA instability, regulated by trans-acting factors like RBP Khd4, precisely fine-tunes the induction dynamics of the respective mRNAs involved in hyphal morphogenesis.

mRNA degradation plays a crucial role in coordinating transcription and translation. In *S. cerevisiae*, the global decrease in mRNA synthesis is counterbalanced by decreased degradation to maintain gene expression homeostasis (SUN *et al.* 2013). Notably, decay factors like the Ccr4-Not complex and the 5′-3′ exonuclease Xrn1 can translocate from the cytoplasm to the nucleus, directly influencing transcription activation, highlighting the interplay between mRNA synthesis and decay (CHÁVEZ *et al.* 2016,HECK AND WILUSZ 2018). Recently, a single-molecule imaging study uncovered a positive correlation between increased decay and active translation (DAVE *et al.* 2023). This discovery aligns with earlier observations suggesting that decay factors operate in concert with ribosomes during translation (TUCK *et al.* 2020,DAVE *et al.* 2023). In the future, understanding the intricate relationship between mRNA synthesis, translation, and decay is crucial for deciphering the regulatory network during infectious hyphae development.

3.6 Khd4 promotes mRNA stabilization by 5′ UTR AUACCC binding

Many RBPs exhibit multifunctionality, participating in various aspects of gene expression. For instance, the RBP NOVA plays regulatory roles in alternative splicing as well as in poly (A) site usage in neurons (VAN NOSTRAND *et al.* 2020). When analyzing the distribution of the AUACCC motif in Khd4-bound mRNAs, a notable pattern emerges: targets exhibiting reduced abundance in the absence of Khd4 showed significant enrichment of this binding site within their 5′ untranslated regions (UTR). Examples include *don1* (UMAG_10152) encoding an FYVE domain-containing guanine nucleotide exchange factor (FREITAG *et al.* 2011,GÖHRE *et al.* 2012) and *kin3* (UMAG_06251) encoding Kinesin-3 motor protein, involved polar hyphal growth and membrane trafficking (SCHUCHARDT *et al.* 2005,BAUMANN *et al.* 2012). This suggests that in a binding position-dependent manner Khd4-mediated posttranscriptional

regulation stabilizes its mRNA targets, potentially unveiling a novel link between RNA-binding position and stabilization regulation.

The 5′ UTRs, positioned upstream of the start codon, are actively involved in directing translation (HINNEBUSCH *et al.* 2016). Although many conundrums still exist regarding translation and mRNA stability (see above), efficient translation is also known to protect mRNA from degradation (PARKER 2012,HINNEBUSCH *et al.* 2016,THEIL *et al.* 2018). For example, the poly(A) leader in 5′ UTR enables cap-independent mRNA translation by recruiting PABP1, enhancing mRNA stability, but causing mRNA destabilization during translation inactivity (JIA *et al.* 2020). Based on this context, it is conceivable that the increased stability resulting from Khd4 binding to the 5′ UTR could facilitate the recruitment of translation machinery, promoting translation. Further reinforcing the notion, the interaction of the RBP SF3B4 with the 5′ UTR *cis*-element AG-(X)3-ACA/G/C increases the translation of mRNAs encoding secretory proteins at the ER by associating with the ribosome receptor, p180 (UENO *et al.* 2019). Additionally, in human cells, the RBP eIF3 stimulates translation by directly recruiting of 43S preinitiation complex upon recognizing the m_6A sites in the 5′ UTR, enabling cap-independent translation (MEYER *et al.* 2015).

Alternatively, the 5′ UTR AUACCC binding by Khd4 may keep the mRNA in a translationally inactive state until specific signals warrant its translation. This mechanism is exemplified in other systems such as in *C. neoformans*, where Puf4 binds to the 5′ UTR of mRNAs like *fks1*, involved in cell wall biogenesis, resulting in translational repression, thereby mRNA stabilization (KALEM *et al.* 2021). Loss of Puf4 releases translation repression but decreases mRNA stability which is negatively influenced by the increased translation rate (KALEM *et al.* 2021,ROY AND JACOBSON 2013). This ultimately provides echinocandin resistance to the pathogen (KALEM *et al.* 2021). Similarly, in *D. melanogaster,* the female-specific RBP sex-lethal (SXL) inhibits translation of the limiting component of the dosage compensation complex, male-specific lethal-2 (*msl-2*) mRNA, through its interaction with the 5′ UTR of the mRNA, hindering ribosomal scanning (BECKMANN *et al.* 2005).

In *U. maydis*, maintaining proper Clp1 levels is crucial for fungal proliferation, and UPR-mediated gene expression during ER stress in planta. While the *clp1* transcript levels are detectable upon *b* induction, the protein only becomes evident during hyphal penetration

of the plant (Chapter 1.5; HEIMEL *et al.* 2010a). Notably, *clp1* mRNA features an AUACCC motif in its 5′ UTR. Furthermore, it is also edited by Khd4-Ada-Gfp, albeit with low efficiency (Appendix 3, Fig. 5.15B). The interaction between Khd4 and the 5′ UTR AUACCC motif may maintain the *clp1* mRNA in a translationally inactive state until penetration, ensuring a timely Clp1 protein level (Appendix 3, Fig. 5.15B). Of note, *clp1* mRNA also carries an AUACCC motif in its 3′ UTR. After plant penetration, Khd4 might differentially bind to the 3′ UTR AUACCC, contributing significantly to the maintenance of steady-state Clp1 protein levels.

Khd4 also binds mRNAs by interacting with the AUACCC binding motif in their coding sequences (CDS), a binding interface also known to impact the translation efficiency of an mRNA (GRZYBOWSKA AND WAKULA 2021). In future, investigating the significance of the AUACCC motif in the 5′ UTR and CDS will offer insights into other roles of Khd4, particularly its role in translation regulation. The *spa2* mRNA, which encodes a polarisome component involved in fungal polar growth (CARBÓ AND PÉREZ-MARTÍN 2008,ZHENG *et al.* 2020), contains three AUACCC motifs distributed in the 5′ UTR, ORF, and 3′ UTR regions. The 3′ UTR AUACCC of *spa2* mRNA functions as a destabilizing element (Fig. 2.4E). Ultimately, exploring the significance of these binding sites and whether the regulatory potential of Khd4 in these distinct binding sites operates co-operatively or alternatively, would be intriguing. Nonetheless, it is worth noting that the majority of the mRNA targets display increased levels in the absence of Khd4 with significant enrichment for 3′ UTR AUACCC. This indicates that mRNA destabilization constitutes the major role of Khd4.

3.7 Posttranscriptional regulation of membrane trafficking

In *khd4Δ* cells, delayed polar growth coincides with wider hyphal cells, reminiscent of defects in intracellular membrane trafficking. Similar phenotypes have been observed in fungi with aberrant membrane trafficking. In *A. nidulans*, *myoE* deletion, essential for actin-dependent vesicle trafficking, results in thicker cells and slower hyphal growth (TAHERI-TALESH *et al.* 2012), whereas in *C. albicans*, deletion of the formin encoding *bni1* disrupts Spitzenkörper formation, leading to wider, slow growing hyphae (PUERNER *et al.* 2021).

Studying Khd4-bound mRNAs demonstrates Khd4 as a regulator of membrane trafficking. By interacting with 3′ UTR AUACCC, Khd4 destabilizes a subset of mRNAs

encoding regulatory proteins involved in membrane trafficking, controlling their subcellular protein levels. This coordinated regulation is in line with the concept of mRNA regulon, where RBPs co-regulate functionally related mRNAs (KEENE 2007). Consequently, the absence of Khd4 disrupts membrane trafficking, leading to the misregulation of process-associated genes and the formation of aberrant vacuoles (Fig. 3.1). Similar regulatory networks are well-established in higher eukaryotes; for instance, in immune cells, RBPs like TTP and Roquin target mRNA regulons containing inflammatory regulators, such as cytokines, to effectively modulate immune responses (ANDERSON 2010,DIAZ-MUÑOZ AND OSMA-GARCIA 2022).

This study discloses a distinct link between RNA regulation and vacuole maturation. Proper vacuole biogenesis is instrumental for fungal pathogens' virulence (PALMER *et al.* 2005,LIU *et al.* 2006,LI *et al.* 2017,HU *et al.* 2021). Loss of Khd4 severely impairs the formation of vacuole-dependent empty sections in hyphae, a process closely related to appressoria-like infection structure formation in phytopathogens (FREITAG *et al.* 2011). Therefore, Khd4-mediated control of the membrane trafficking mRNA regulon may also impact early infection processes such as plant entry. Of note, autophagy, a catabolic process involved in vacuole biogenesis, is vital for appressoria formation in the rice blast fungus *M. oryzae* (ZHOU *et al.* 2022). Persistently, the expression of autophagy genes coincides with the plant penetration stage in *U. maydis,* with four ATG proteins (ATG3-6) involved in autophagosome membrane formation harboring the AUACCC motif.

Asymmetric intracellular vesicle trafficking is a highly dynamic process, adapting to varying cellular demands. This is of particular importance to polarized cells like fungal hyphae and neurons, where membrane trafficking is essential for maintaining cell shape and promoting growth (STEINBERG *et al.* 2017,RIQUELME *et al.* 2018). In addition to conventional posttranslational modification, regulating the abundance of trafficking components is also crucial for modulating the transport process. For instance, in mammalian cells, endocytosis of the plasma membrane depends on the concentration of the vesicle coat protein Clathrin (MOSKOWITZ *et al.* 2005).

This study underscores the significance of Khd4-mediated mRNA decay in maintaining the exact levels of endomembrane regulators. Notable examples include the small GTPase Arl1–involved in secretion (LABBAOUI *et al.* 2017), Hok1–critical for endosomal motor function (BIELSKA *et al.* 2014), and Vma21–necessary for V-ATPase assembly in

the vacuole (MALKUS *et al.* 2004). Khd4-bound mRNAs also exhibit enrichment for regulatory proteins associated with small GTPases signal transduction, which is pivotal for cytoskeletal remodeling and membrane trafficking (DAUTT-CASTRO *et al.* 2021, OLAYIOYE *et al.* 2019). In addition to the GTP hydrolysis cycle and post-translational modifications (BOS *et al.* 2007,AHEARN *et al.* 2011), these findings indicate that the small GTPase regulation also occurs at the level of mRNA stability, implying an additional layer of regulation.

Similar insights are emerging in other systems. Alternative splicing, governed by RBPs such as CELF1, RBFOX, and Nova, has been shown to govern membrane trafficking dynamics in muscles, epithelial, and neuronal cells, respectively (BLUE *et al.* 2018). Additionally, miRNAs have been implicated in modulating the expression levels of components like Sar1A, and Sec23A of COPII machinery, required for vesicle formation (BISNETT *et al.* 2021). It is worth noting that *U. maydis* Sec proteins (Sec23, Sec24, Sec24C, and Sec31), feature the AUACCC motif in their coding sequences. In essence, these findings highlight that the dynamics of membrane trafficking during hyphal polar growth are decided at the level of RNA and in *U. maydis*, it relies on the presence of Khd4.

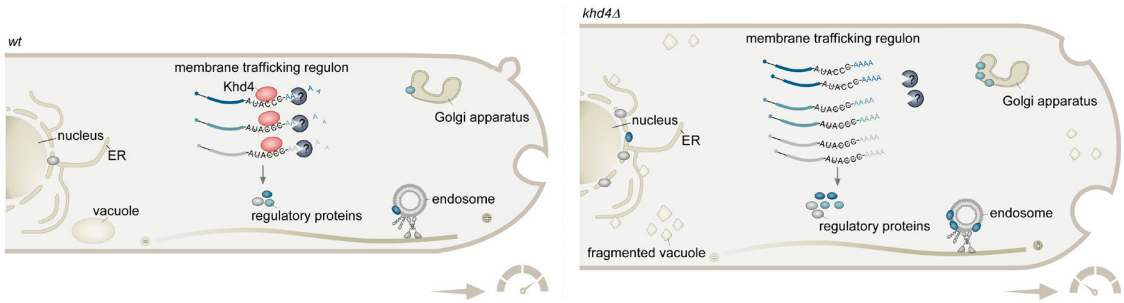

Fig. 3.1. Khd4-mediated mRNA destabilization governs subcellular levels of membrane trafficking regulators. Schematic representation of wildtype (left; wt;) and *khd4Δ* (right; thicker) hyphae. **Left:** Khd4 (red) recognizes the 3′ UTR AUACCC motif and orchestrates the destabilization of mRNAs encoding membrane trafficking regulators into an mRNA regulon, potentially recruiting mRNA decay factors (mRNAs, encoding their corresponding regulatory proteins, are illustrated in dark green, light green, and grey; AAA-poly(A) tail). This action regulates the induction kinetics of these mRNAs, fine-tuning their steady-state levels post-transcriptionally. This process orchestrates the membrane trafficking dynamics, ensuring the proper morphology and polar growth of infectious hyphae. **Right:** In the absence of Khd4, these mRNAs are stabilized, resulting in delayed responses and excessive regulatory protein levels. This leads to dysregulated membrane trafficking, evident in fragmented vacuoles, thicker hyphal cells, and delayed polar growth. Bluish-grey pacmans represent mRNA decay factors, and speedometers denote polar growth rates. The arrow indicates the growth direction. Endomembrane compartments such as ER, Golgi apparatus, vacuoles, and endosomes are labeled accordingly.

3.8 Khd4-mediated RNA regulation might be involved in ER stress response

Analysing Khd4 localization revealed that the protein is consistently found to be cytoplasmic throughout hyphae development, with no specific subcellular accumulation. However, when exposed to heat stress, Khd4 relocated to stress granules. Interestingly, these Khd4-positive granular bodies concentrated at specific subcellular regions, including the cell cortex, nuclear periphery, and specifically, the growth tip. This pattern is reminiscent of the endoplasmic reticulum (ER) network seen in *U. maydis* and plant cells (WEDLICH-SÖLDNER *et al.* 2002,GRIFFING *et al.* 2017). In particular, the concentration of these granules at the growth tip coincides with the presence of a prominent ER cap in the hyphal apex (WEDLICH-SÖLDNER *et al.* 2002). Emerging evidence suggests that the ER membrane surface can trigger the formation of cellular condensates (SNEAD AND GLADFELTER 2019), suggesting that the Khd4-positive granule localization might indeed be proximal to the cortical ER.

Remarkably, truncating the C-terminal region of Khd4 (Khd4$^{\Delta 865\text{-}1416}$), which includes the KH7-8 domains, and Q-rich regions, consistently led to its cortical localization. This implies that Khd4 can reside at the cell cortex under normal conditions, possibly regulated by RNA-binding capacity, protein-protein interaction, and posttranslational modifications in these regions. In *S. cerevisiae,* the cytoplasmic RBP Puf2 transiently associates with the plasma membrane depending on the Ypk1-mediated phosphorylation status (GALEZ *et al.* 2021). Additionally, posttranslational modification of nuclear RBPs like Fus and TDP-43 leads to their cytoplasmic localization, which is associated with disease development (STERNBURG *et al.* 2022).

The ER plays a central role in the membrane trafficking pathway by directly interacting with endomembrane compartments (WENZEL *et al.* 2022). ER-associated UBE2J1 protein positions endosomes to the perinuclear region for selective cargo delivery for degradation (CREMER *et al.* 2021,WENZEL *et al.* 2022).

Loss of Khd4 results in defects indicative of disrupted ER homeostasis. This is evidenced by vacuole fragmentation, a known TORC1-mediated ER-stress response in *S. cerevisiae* (STAUFFER AND POWERS 2015). Vacuoles are also involved in the selective degradation of damaged ER, a process referred to as micro-ER-phagy (FERRO-NOVICK *et al.* 2021). Additionally, the absence of Khd4 also makes cells sensitive to ER stress inducers like

tunicamycin (Appendix 3, Fig. 5.15C) and results in secretion defects (M. Sc. Lea Geißl. Data not shown).

During the *U. maydis* pathogenic program, the UPR regulates the ER-dependent secretory pathway to resolve ER homeostasis (SCHMITZ *et al.* 2018). Based on the findings, it is plausible to speculate that Khd4 regulates a subset of mRNAs, such as those encoding membrane trafficking proteins, at the vicinity of the ER, a localization-specific interactome. In humans, the RBP TIS11B mediates the formation of TIS-granule at the ER, where it enriches membrane proteins mRNAs containing ARE-elements in their 3´ UTR (MA AND MAYR 2018). Translation in this specialized subcellular compartment, TIGER, facilitates the assembly of encoded proteins into specific protein complexes, which are critical for the trafficking of plasma membrane proteins (MA AND MAYR 2018).

Recently, a novel pathway known as ERAS (ER-associated RNA silencing) was discovered in *C. elegans.* In this pathway, the general RNA silencing machinery, including Argonaute protein AGO2, actively degrades mRNAs encoding secretory proteins during ER stress at the cytoplasmic surface of the ER. This unconventional mechanism functions to further impede the influx of additional proteins into the ER during periods of "traffic jam" caused by misfolded proteins (EFSTATHIOU *et al.* 2022).

Furthermore, beyond its established role in translating mRNAs encoding secretory proteins, there is a growing body of evidence suggesting that the ER also participates in the translation of mRNAs encoding cytosolic proteins (REID AND NICCHITTA 2015). It is conceivable that Khd4 binds to a subset of target mRNAs encoding proteins associated with ER-dependent processes, thereby regulating their stability. In the absence of Khd4, this regulatory dynamic is disrupted causing ER stress. Thus, hypothesizing that Khd4-mediated mRNA regulation may play a novel role in ER quality control in *U. maydis*.

In conclusion, the findings in this thesis demonstrate the pivotal role of RNA regulation in governing spatiotemporal gene expression control in fungal pathogens. The results have unveiled a regulatory concept for fungal infection, where the multi-KH RBP Khd4 orchestrates infectious hyphae polar growth by modulating the stability of mRNA regulons, which consist of regulatory proteins encoding mRNAs with the AUACCC motif, thereby regulating membrane trafficking (Fig. 3.1). These insights are expected to catalyze further comparative studies exploring the roles of RNA regulation in the infection of related fungal pathogens, thus laying a foundation for advancing the

understanding of fungal pathogenesis and fostering the development of novel anti-fungal therapies.

3.9 Future perspectives

This study, using functional transcriptomics and loss-of-function analyses, has advanced the understanding of Khd4 as an mRNA stability regulator and its role in orchestrating membrane trafficking during pathogenic development. It has opened up new avenues for exploring the precise mechanism of Khd4, elaborately addressing when, where, how, and the context in which the RBP operates.

The current hypothesis postulates that Khd4 may also influence ER homeostasis. To initiate this investigation, confirming whether the cortical accumulations of Khd4-positive granules under heat stress are indeed at the ER is crucial. This can be addressed by expressing an existing ER-marker, where the Kat reporter is fused with the signal peptide of ER calreticulin and the ER-retention HDEL sequence at its N- and C-terminus, in strains expressing Khd4-Gfp for co-localization studies.

For an in-depth understanding of the role of Khd4 in ER homeostasis, spatial proteomics, and transcriptomics, including biochemical fractionation followed by mass spectrometry can be employed. This approach enables the analysis of changes in ER fractions under various conditions, including *khd4* deletion. Additionally, the "localized RNA recording" technique (MEDINA-MUNOZ *et al.* 2020), involving the fusion of an ER-membrane resident protein, such as Sec61, with the RRM domain of Pab1 and an RNA-base editor like Ada, can be employed. This fusion allows for the editing of ER-localized RNA after interaction with the RRM of Sec61, thereby enabling the quantification of mRNA abundance in the vicinity of ER during stress conditions by RNA-seq. Utilizing these methods in conjunction can help investigate the impact of Khd4 on ER homeostasis through loss-of-function analysis at the levels of RNA and protein.

As previously noted, the C-terminal truncated version of Khd4 (Khd4$^{\Delta 865\text{-}1416}$), encompassing KH domain 7 and 8 along with unstructured regions, consistently localizes to the cortical regions. The prior study also demonstrates that deleting the N-terminal regions containing KH domains 1 and 2 results in an aberrant phenotype. Therefore, it is essential to map the domains of Khd4 by truncations. Firstly, this aims to pinpoint domains critical for potential ER association, and secondly, it seeks to identify other functionally important regions in a broader context such as proper morphology, and

pathogenicity. Leveraging the AlphaFold-predicted structure, a systematic analysis of N- and C-terminal regions can uncover functionally critical domains. Subsequently, these critical domains can be assessed for their impact on loss-of-function phenotype, mRNA stability regulation, and subcellular localization. Once the functionally important domain is elucidated, single-point mutations can be carried out to decode minimal functional regions.

The regulatory potential of any RBP relies on its interactions with other proteins and protein complexes, playing a pivotal role in RNA processing. Gaining insights into the mechanism of Khd4's action requires the identification of its protein interaction partners. This can be achieved through techniques like Khd4 co-immunoprecipitation and *in vivo* proximity-dependent protein labeling approach such as turbo biotin ligase tag (TurboID), which can reveal the protein interactome of Khd4 (SHI *et al.* 2023). Combining these two approaches enhances the precision of identifying true Khd4-interaction partners.

To deepen knowledge, conducting a differential protein binding analysis by comparing functionally critical truncated Khd4 versions, particularly those involved in cortical localization, with the full-length protein is essential. Subsequently, the functional relevance of the identified protein partners can be validated through knockout and overexpression experiments to confirm their roles in the Khd4-mediated processes. This can help identify the dynamics of these interactions with Khd4, including whether they occur exclusively under specific conditions or developmental stages.

Combined with mathematical modeling, this study described the mechanistic insights into the Khd4-mediated gene expression regulation during hyphal morphology development. It has unveiled the role of Khd4 in mRNA destabilization by binding to the 3′ UTR AUACCC sequence, fine-tuning their steady-state levels for a rapid response. However, the exact quantitative changes in the steady-state levels of Khd4-bound mRNAs remain undisclosed. To understand the dynamic behavior of Khd4 targets, quantifying their mRNA turnover rates is imperative. In future, adopting metabolic RNA labeling techniques, such as SLAM seq (HERZOG *et al.* 2017), is recommended to uncover global shifts in mRNA half-lives in the presence and absence of Khd4 in *U. maydis*. Such mRNA half-life analysis can also reveal other mRNAs with highly stable or rapidly degraded profiles, thereby unveiling broader gene regulatory networks in *U. maydis*.

Studying Khd4 targets revealed that binding the AUACCC motif in the 5′ UTR stabilizes mRNA, potentially impacting translation regulation. Further analysis has shown that AUACCC-containing targets involved in membrane trafficking regulation during *U. maydis* infection often feature these cis-elements in their 5′ UTR or ORF region. To investigate the positional effect of Khd4 binding in these regions, the established Kat reporter assay can be adapted. This involves introducing hexameric repeats of the AUACCC motif or the endogenous 5′ UTR sequence of Khd4 targets into the 5′ UTR of the Kat reporter. Incidentally, the "AUA" sequence of the binding site AUACCC can function as a cryptic start codon, recruiting the initiator tRNA, Met-tRNA$_i^{Met}$, and facilitating the synthesis of full-length proteins (KEARSE AND WILUSZ 2017). To confirm cryptic translation, the epitope tags, such as HA-tag, can be placed in the 5′ UTR under examination. In addition to fluorescent assays, it is essential to conduct ribosome profiling assays to assess the impact of 5′ UTR AUACCC binding on ribosome association and translation efficiency. This multifaceted approach promises to shed light on the intricate relationship between Khd4 binding, mRNA stability, and translation regulation, unraveling the molecular intricacies governing these processes.

Khd4 is crucial for the proper virulence of *U. maydis*. Loss of Khd4 causes reduced virulence, with mutant hyphae unable to proliferate in plants. Additionally, the lack of Khd4 disrupts the secretion process, vital for delivering effectors during plant colonization. Although infectious hyphae form, the deletion of *khd4* arrests mutant hyphae development following plant penetration. To understand the role of Khd4 in virulence, it is critical to determine the developmental stages it regulates. The use of conditional promoters, active during specific *U. maydis* infection stages (SCHMITZ *et al.* 2020), can help assess the significance of Khd4 in these phases.

Recent research has unveiled how *U. maydis* adapts transcriptionally during infection (LANVER *et al.* 2018). However, a significant knowledge gap exists regarding the analogous posttranscriptional regulatory networks involved in this process. In the future, it is crucial to identify stage-specific Khd4-bound mRNAs to bridge this gap and reveal the plasticity of mRNA regulons during infection.

HyperTRIBE emerges as the preferred method for identifying RBP target mRNAs when the pathogen intimately interacts with the host. Establishing hyperTRIBE to uncover Khd4 targets in plantae will yield valuable insights into the adaptability of the Khd4-

mediated mRNA regulon across various infection stages and within the host environment. Addressing the low editing efficiency observed with Drosophila Ada is essential for more effective target mRNA identification in plants. Consideration should be given to employing more efficient RNA-base editors like RESCUE (ABUDAYYEH *et al.* 2019). Additionally, the low percentage of fungal-origin sequencing reads at two days post-infection underscores the need for deep sequencing to comprehensively capture Khd4-bound mRNAs. To optimize cost-efficiency in sequencing, one approach is to constitutively express the RNA base editor alone as a control, ensuring the capture of all potential editing sites controlled by Ada.

4 Materials and methods

All methods pertaining to Chapter 2.1 are elaborated in Chapter 5 (Appendix 2, subsection 5.2.2), which provides comprehensive detail. It is important to note that these methods are part of the published dataset.

4.1 Heat stress analysis and microscopy

For heat stress analysis, yeast cells were grown in 20 ml of complete medium (CM; supplemented with glucose) at 28 ° C until the OD600 of 0.5. Hyphal growth was induced by shifting 20 ml of yeast culture in CM-medium to NM medium (NM-nitrate minimal medium) and grown for 6. h.p.i. at 28 °C on a rotary shaker at 200 rpm. Microscopic analyses were performed using laser-based epifluorescence microscopy, Zeiss Axio Observer Z1 (Oberkochen, Germany) as described before (BAUMANN *et al.* 2012). Image processing was carried out using the MetaMorph software package (version 7.7.0.0, Molecular Devices, Seattle, IL, USA). SR-SIM was conducted using the Zeiss Elyra PS at the Center for Advanced Imaging (CAI) at Heinrich Heine University Düsseldorf. To induce heat stress, 1 ml of the cell culture was transferred into 2 ml centrifuge tubes and placed on the preheated thermo-block of temperature 40 °C for 20 min, with agitation at 200 rpm. Subsequently, 1 µl of heat-stressed cell culture was placed on the agarose cushion (2%) and promptly visualized under microscopy. Since the stress granules are transient structures, the visualization must be carried out as quickly as possible.

4.2 Identification of potential Khd4-mediated mRNA regulons in infection

To identify transcripts involved in the pathogenic program, AUACCC-containing mRNAs showed increased expression in the virulence-associated modules, including red, light-green, magenta, and cyan, sourced from a published infection time-course dataset (LANVER *et al.* 2018). Moreover, the AUACCC-containing transcripts from the light-cyan and yellow modules were also integrated into the analysis. The rationale for including these modules in the analysis is given in the corresponding results section (chapter 3.3). The resulting transcripts were used for KEGG mapper analysis to detect mRNAs encoding functionally related proteins engage in analogous metabolic and signaling pathways (Table 5; KANEHISA AND SATO 2020,KANEHISA *et al.* 2022; https://www.genome.jp/kegg/mapper/). Only pathways with a minimum of 5 genes were considered for further analysis.

5 Appendix

The Appendix is divided into three distinct parts.

- The first part (Appendix 1) presents the published review of "The RNA world of fungal pathogens" in PLOS Pathogens 2023, and it is adapted with minor changes without affecting the content.

- The second part (Appendix 2) presents the supplemental information pertaining to Chapter 2.1. This is a part of the published results in PNAS 2023 and therefore included with minor changes.
- The third part (Appendix 3) contains additional results concerning Chapter 3 but not included in Chapter 2.

5.1 Appendix 1

The RNA world of fungal pathogens

Srimeenakshi Sankaranarayanan[1,$], Seomun Kwon[1,$], Kai Heimel[2], and Michael Feldbrügge[1, *]

1 Heinrich-Heine University Düsseldorf, Institute for Microbiology, Cluster of Excellence on Plant Sciences, Universitätsstr. 1, 40225 Düsseldorf, Germany

2 Georg-August University Göttingen, Institute for Microbiology and Genetics, Göttingen Center for Molecular Biosciences (GZMB), Grisebachstr. 8, 37077, Göttingen, Germany

* feldbrue@hhu.de

$ Authors contributed equally

This pearls review is accepted for publication in PlosPathogens.

Fungal pathogens execute well-defined infection programs that are intensively regulated at the posttranscriptional level. RNA biology determines the precise timing and subcellular expression of the encoded proteins. This temporal coordination is especially vital for membrane trafficking in order to synchronize the intracellular organelle network. This includes vacuole maturation, intra- and extracellular vesicle transport, protein entry into mitochondria, peroxisomes, and the ER. Here, we explore the intimate link between membrane trafficking, organelle function, and the RNA world during fungal plant pathogenesis, with a specific emphasis on the corn smut *Ustilago maydis*.

Endosomal mRNA transport generates and prevents intracellular gradients in infectious hyphae

Many fungal pathogens require regulation of hyphal morphology for host invasion. These highly polarised hyphae rely on active transport along the cytoskeleton to deliver proteins to distinct subcellular regions. A fundamental mechanism is the transport of mRNAs, providing precise spatial and temporal control of protein synthesis. RNA-binding proteins (RBPs) play central roles in dictating the fate of mRNA from synthesis to degradation. Key RNA-binding proteins, for example, She3 and Rrm4, mediate actin- and microtubule-dependent mRNA transport in *Candida albicans* and *U. maydis*, respectively (ELSON *et al.* 2009a,BÉTHUNE *et al.* 2019). Importantly, studying Rrm4 has uncovered a novel transportation mechanism: mRNAs hitchhike on the cytoplasmic surface of endosomes, linking mRNA and membrane trafficking (BÉTHUNE *et al.* 2019).

Rrm4 harbors three N-terminal RRM domains for RNA-binding, with notable cargo mRNAs including all four *septins*: Cdc3, Cdc10, Cdc11 and Cdc12 (OLGEISER *et al.* 2019). During transport, endosome-coupled translation ensures the formation and assembly of heterooctameric septin complexes on endosomes. These complexes are ultimately delivered to the growth pole, resulting in the formation of septin filaments with a defined gradient emanating from the hyphal tip (Fig. 5.1A).

A transcriptome-wide iCLIP analysis revealed that Rrm4 interacts with hundreds of mRNAs, primarily through their 3´ UTR (OLGEISER *et al.* 2019). This finding highlights the critical role of endosomal mRNA transport in efficiently distributing bulk mRNAs and associated ribosomes throughout hyphae, thereby preventing concentration gradients around the nucleus (BAUMANN *et al.* 2014,MÜNTJES *et al.* 2021). Interestingly, a substantial number of mRNAs encoding mitochondrial proteins contain the Rrm4 binding site within their 3´ UTR. Thus, Rrm4-mediated mRNA transport and endosome-coupled translation might facilitate mitochondrial protein entry, similar to processes observed in polar growing neurons (CIONI *et al.* 2019).

An outstanding question is how mRNAs are linked to transport endosomes. In plants, endosomal transport RBPs directly interact with the small GTPase Rab5, while in animal cells, the FERRY complex and annexin have been implicated in this process (MÜNTJES *et al.* 2021). In *U. maydis,* the scaffold protein Upa2 interacts with the poly(A)-binding protein, Pab1, to stabilize endosomal mRNA transport complexes (JANKOWSKI *et al.* 2019). Furthermore, the C-terminus of Rrm4 contains a novel binding platform comprising three MLLE domains that operate in a strict hierarchy: while MLLE1 and MLLE2 serve accessory functions, MLLE3 is essential for the endosomal attachment of Rrm4 (DEVAN *et al.* 2022). Specifically, MLLE3 recognizes two PAM2-like sequences in the endosomal adaptor protein Upa1, which, through its FYVE zinc finger domain, anchors the mRNP complex to the endosome by recognizing phosphatidylinositol 3-phosphate, the characteristic lipid of early endosomes (Fig. 5.1A). Recently, the first evidence of endosomal mRNA transport was also discovered in hyphae of *Sordaria macrospora* (MÜNTJES *et al.* 2021) suggesting that related fungal pathogens, such as *Aspergillus fumigatus,* may also utilize this mRNA transport process for hyphal development.

Regulation of mRNA stability determines membrane trafficking dynamics

Human pathogens such as *Cryptococcus neoformans* and *C. albicans* as well as plant pathogens such as *U. maydis* regulate RBP-mediated mRNA stability to control their virulence (HALL AND WALLACE 2022,SANKARANARAYANAN *et al.* 2023a). In *U. maydis*, the multi-KH domain RBP Khd4 is crucial for morphology and pathogenicity (VOLLMEISTER *et al.* 2009). A transcriptome-wide target mRNA detection analysis was performed using hyperTRIBE (Targets of RBP Identification By Editing). In this method, Khd4 was fused with the hyperactive version of the heterologous RNA-editing enzyme ADAR (Adenosine Deaminase Acting on RNA), enabling the marking of target mRNAs through adenosine editing, which were subsequently identified using high-throughput sequencing. This *in vivo* approach, revealed that Khd4 binds mRNAs encoding regulatory proteins involved in membrane trafficking and specifically interacts with AUACCC regulatory elements in their 3′ untranslated region (UTR) triggering degradation (SANKARANARAYANAN *et al.* 2023a). Without this regulation, target mRNAs are stabilized, leading to a delayed response time during hyphal induction and pathological overshooting of their expression levels (Fig. 5.1B). As a consequence, membrane trafficking dynamics are disrupted, causing aberrant vacuole biogenesis, and temporally altered hyphal polar growth. Hence, Khd4 unites target mRNAs encoding regulatory proteins into a defined membrane trafficking RNA regulon to ensure coordinated control of intracellular trafficking during hyphal growth (SANKARANARAYANAN *et al.* 2023a). Given the significance of proper vacuole biogenesis in the development of appressoria-like infection structures in phytopathogens, the regulatory potential of Khd4 expands the influence of RBPs in affecting pathogen entry into plant hosts.

Cytoplasmic mRNA splicing coordinates UPR and ER trafficking during infection

Another tight link between RNA biology, protein, and membrane trafficking is the regulation of the unfolded protein response (UPR) mediating ER homeostasis during secretion. Unconventional splicing of *cib1* mRNA occurs on the cytoplasmic surface of ER membranes and is mediated by the transmembrane kinase/RNase Ire1 in response to ER stress (Fig. 5.1C). The mature mRNA encodes the key bZIP transcription factor eliciting UPR. Importantly, human- and plant-pathogenic fungi rely on a functional UPR for virulence, as it plays a central role in thermotolerance, antifungal drug resistance, and proper protein secretion (HEIMEL 2015). In *U. maydis*, the UPR is adapted to the

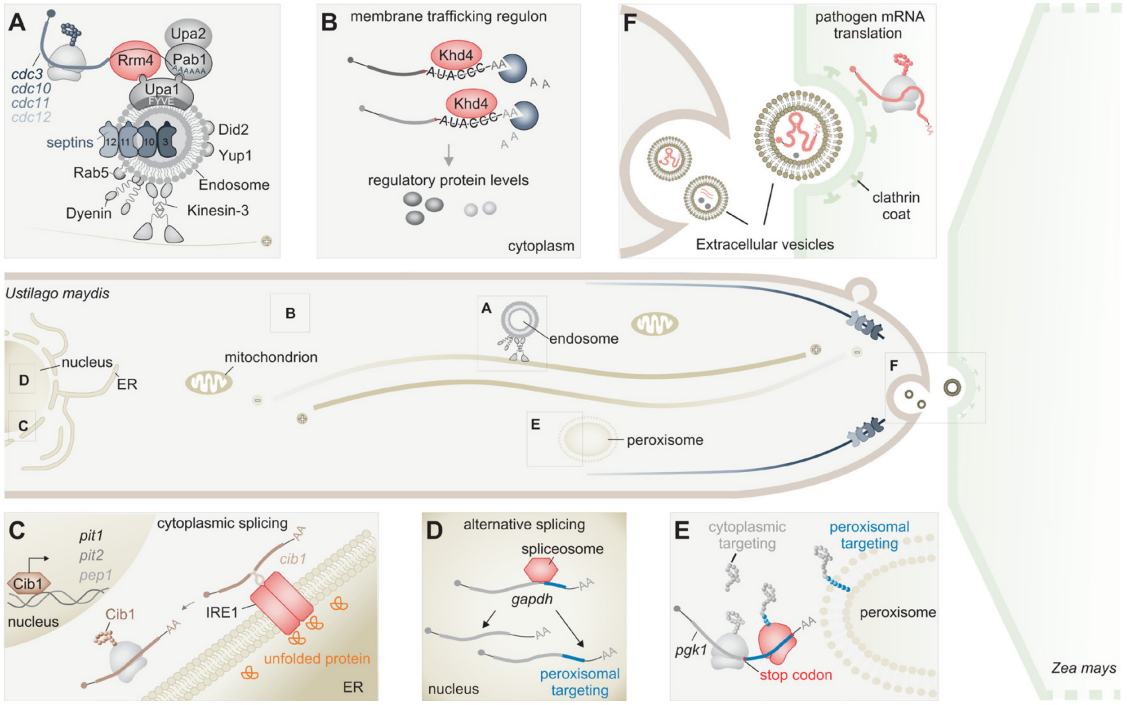

Fig. 5.1. In fungal hyphae, mRNA-dependent processes drive membrane trafficking. Schematic depiction of *U. maydis* hyphae (left) interacting with its plant host, *Zea mays* (right). Distinct cellular processes within the hyphae have been marked and magnified. **(A)** Early endosomes act as a platform for the transport of mRNAs. Rrm4 (red) facilitates the mRNA transport by hitchhiking onto Rab5-positive early endosomes. Interactions between Rrm4, the poly(A)-binding protein, Pab1, and the FYVE domain-containing adapter protein Upa1 enable the attachment of mRNAs to early endosomes. The scaffold protein Upa2 stabilizes the transport complex. This bidirectional movement relies on motor proteins, kinesin, and dynein, traveling along anti-parallel microtubules. The local translation of the cargo mRNAs like *septin* (blueish grey) on early endosomes is essential to generate higher-order septin filaments extending from the hyphal tip. **(B)** Khd4 (red) orchestrates membrane trafficking by regulating the subcellular levels of regulatory proteins crucial for this process. The RBP coordinates the destabilization of mRNAs encoding membrane trafficking regulators (grey) into an mRNA regulon through the recognition of the AUACCC motif present in their 3' UTRs. This mRNA decay process determines the induction kinetics of these mRNAs, fine-tuning their steady-state levels following transcriptional induction. Pacmans in bluish-grey depict mRNA decay factors. **(C)** Unconventional splicing of *cib1* mRNA in the cytoplasm elicits the unfolded protein response (UPR), required to preserve ER homeostasis during infection. Upon ER stress, the ER membrane-localized Ire1 kinase/RNase (red) is activated through its direct interaction with unfolded or misfolded proteins (orange) or by reduced Ire1-Bip1 interaction. This activation prompts the splicing of an intron from the *cib1* mRNA (brown) in the cytoplasm. The resulting spliced *cib1* mRNA is translationally active, leading to the production of the Cib1 protein (brown) -a bZIP transcription factor, which in turn, induces the expression of UPR genes to restore ER homeostasis and secretion. These include genes such as *pit1, pit2,* and *pep1*, encoding effector proteins vital for fungal infection. **(D)-(E)** Posttranscriptional regulation determines the dual targeting of peroxisomal proteins. **(D)** Alternative splicing of *gapdh* mRNA leads to the expression of an isoform containing peroxisomal targeting sequence (blue), which facilitates peroxisomal targeting after translation. The spliceosome complex is represented in red (*gapdh*-glyceraldehyde-3-phosphate dehydrogenase). **(E)** Ribosomal readthrough past stop codon (red box) of *pgk1* mRNA integrates cryptic peroxisomal targeting sequence (blue) at the C-terminus, facilitating peroxisomal entry. The ribosome executing the stop-codon readthrough is depicted in red (*pgk1*- 3-phosphoglycerate kinase). **(F)** Fungal mRNAs (red) encoding effector proteins are packaged within extracellular vesicles (EVs) as a means to transport into the host plant. The internalization of these fungal EVs into the plant host (light green) might be aided by clathrin-mediated endocytosis. Following their entry into plant cells, the delivered fungal mRNAs are subsequently translated using the plant's own

translation machinery, thus outsourcing the production of fungal effector proteins within the plant for pathogenic development. In addition to RNAs, the cargoes of fungal EVs encompass proteins, and secondary metabolites, both depicted in grey.

biotrophic lifestyle of the fungus and exerts additional virulence-related functions that connect cellular physiology with the development and even transcriptional regulation of host-manipulating effectors.

During the pathogenic program, the UPR is specifically activated after plant invasion. This correlates with increased expression of more than 200 effectors many of which follow the classical ER-dependent secretory pathway (SCHMITZ *et al.* 2018). During infection, the interaction between

Cib1 and the regulatory protein Clp1 promotes mutual stabilization and accumulation of both proteins (HEIMEL *et al.* 2013,PINTER *et al.* 2019). As Clp1 levels are decisive for initiating fungal proliferation (SCHERER *et al.* 2006,HEIMEL *et al.* 2010a), this interaction ensures elevated secretory capacities of fungal cells prior to host colonization. In parallel, the Cib1/Clp1 complex promotes modulated UPR gene expression, enabling long-term UPR activity (HEIMEL *et al.* 2013). Transcriptome-wide analysis revealed comprehensive upregulation of genes involved in membrane transport and protein processing in the ER (PINTER *et al.* 2019), consistent with the increased demand for membrane traffic and effector delivery throughout infection.

Excessive ER stress is suppressed by the negative feedback of the UPR on the signaling network, which controls the expression of the vast majority of effector genes (SCHMITZ *et al.* 2018). Importantly, some effector genes are a direct target of the UPR regulator Cib1 (HAMPEL *et al.* 2016) and thus may escape this global repression, arguing for an important contribution of these effectors in virulence. Indeed, 3 of the 4 directly regulated effector-related genes encode essential virulence factors (Fig. 5.1C; *pit1, pit2, pep1*) (SCHMITZ *et al.* 2018). Interestingly, another mode of fine-tuning UPR kinetics is found in *C. neoformans*. Here, binding of the pumilio-type RNA-binding Puf4 to the mRNA encoding the Cib1-like protein Hxl1 supports unconventional splicing during UPR activation and mRNA degradation during recovery from ER stress (GLAZIER *et al.* 2015). In essence, RNA regulation at the level of unconventional splicing is upstream of a defined transcriptional response regulating correct ER-dependent membrane trafficking.

Diverse RNA regulation determines peroxisomal protein entry

Peroxisomes are essential organelles involved in myriad cellular processes including lipid homeostasis, reactive oxygen metabolism, and secondary metabolite production. In *U. maydis*, several glycolytic enzymes such as glyceraldehyde-3-phosphate dehydrogenase (GAPDH) and 3-phosphoglycerate kinase (PGK-1) are targeted to peroxisomes through alternative splicing and translational readthrough, respectively. In both cases, the C-terminus gains a functional peroxisomal targeting sequence (Fig. 5.1D-E) (FREITAG *et al.* 2012). As peroxisomal membranes are impervious to NAD^+/NADH, the cryptic peroxisomal localization of these enzymes coordinates redox cycling between cytoplasm and peroxisomes. Significantly, stop-codon readthrough stands out as the predominant mechanism employed by both fungi and mammals to generate cryptic peroxisomal targeting sequences, whereby ribosomes continue translating past a termination codon to produce peroxisomal isoforms. This low rate of stop-codon readthrough rates enables the release of small but steady amounts of these enzymes to support peroxisome metabolism (SCHUEREN *et al.* 2014,BITTNER *et al.* 2022). For translational readthrough, both *U. maydis* and human cells require a specific sequence context involving the UGA stop codon followed by the dinucleotide CU (STIEBLER *et al.* 2014). A recent discovery revealed another mechanism involving translation initiation with non-AUG start codons that target 6-phosphogluconate dehydrogenases of the pentose phosphate pathway to peroxisome (KREMP *et al.* 2020). Notably, removing the peroxisomal targeting sequence from these bona fide cytosolic enzymes reduces the virulence of *U. maydis*, underscoring the significance of RNA regulation-dependent peroxisomal protein targeting in pathogenic development.

Extracellular vesicle-mediated transport of RNAs determines host communication

Intracellular membrane and RNA trafficking processes can influence the extracellular milieu via secretion. Pathogenic fungi secrete molecular weapons, termed effectors, to manipulate the host during infection. Extracellular RNAs (exRNAs) are emerging as a novel class of effectors that can modulate host gene expression. The phenomenon of bidirectional cross-kingdom RNAi (ckRNAi) has been particularly well documented in plant-pathogen interactions, whereby both partners secrete small RNAs (sRNAs) that silence genes in one another (CHENG *et al.* 2023). The first sRNA effectors were discovered in *Botrytis cinerea,* which is loaded into AGO1-RISC of the host *Arabidopsis thaliana* to downregulate plant defense-related genes (WEIBERG *et al.* 2013). ckRNAi is

a widespread phenomenon; sRNA effectors have been found in various other fungal, oomycetes, and even in bacterial pathogens and symbionts (CHENG *et al.* 2023).

The routes of secretion and uptake of RNA during host-pathogen interaction are contentious, due to several possible mechanisms and a large variability between the systems. Extracellular vesicles (EVs) are one of the ubiquitous means of RNA secretion. In plant-pathogen interactions, *A. thaliana* sRNAs targeting *B. cinerea* transcripts were found associated with EVs, and DEAD-box RNA helicases and annexins have been implicated in their secretion (HE *et al.* 2021). As for the uptake of exRNAs, clathrin-mediated endocytosis of fungal EVs is a likely route of fungal sRNA effector delivery, but it remains to be elucidated how these sRNAs escape endosomes and are loaded into host AGOs (CHENG *et al.* 2023).

Besides canonical sRNAs and mRNAs, tRNAs and tRNA fragments, circular RNAs, and even rRNAs can be secreted (CHENG *et al.* 2023). As EVs can carry much larger RNAs, there is an intriguing possibility of fungal mRNA delivery and translation into functional effector proteins in host cells (Fig. 5.1F). EV-associated mRNAs of *Paracoccidiodes brasiliensis* are translation-competent, yielding protein products *in vitro*. A comprehensive analysis of mRNAs associated with EVs from *U. maydis* cultures, designed to mimic infectious hyphae, has identified several candidate mRNA effectors that meet the following criteria: relatively enriched in EVs compared to the cells and up-regulated during infection (KWON *et al.* 2021). As expected for a pathway parallel to conventionally secreted effectors, ER-targeted mRNAs and those encoding proteins with signal peptides were underrepresented in EVs. Notable among mRNA effector candidates are those encoding metabolic enzymes, which may reflect the capacity of *U. maydis* to reprogram the host metabolism (KWON *et al.* 2021). The biological relevance of these diverse RNA species from pathogens remains to be discovered, whether they serve as virulence factors or elicitors of host immunity during interaction with the host, or alternatively as mediators of intraspecies communication between fungal cells.

Conclusions and future directions

Studying *U. maydis* as a model pathogen reveals an intricate interplay between RNA biology and membrane trafficking. The regulation of RNA processes like splicing, localization, translation, and stability, precisely governs the exact translation levels of virulence factors. This investigation unveils a novel connection involving small GTPase

regulation, septins, UPR, peroxisomal function, and the pathogen RNA trafficking to host cells.

Understanding RNA biology is essential for studying the fundamental biology of fungal pathogens. A recent demonstration showcased that in *Magnoporthe oryzae* tRNA modification and codon usage regulate unconventional secretion of protein effectors (LI *et al.* 2023). Advances in techniques like iCLIP and HyperTRIBE have propelled the investigation of RBPs in fungal pathogens, enabling detailed mapping of RBP-binding across the transcriptome. HyperTRIBE, in particular, offers a unique avenue to delve into the host-pathogen interaction interface at the RNA level. These methods promise discoveries that advance fungal pathogenesis understanding, fostering novel anti-fungal therapies.

Acknowledgments

We are grateful to lab members for the valuable discussion and critical reading of the manuscript. Research was financed by grants from the Deutsche Forschungsgemeinschaft (Germany's Excellence Strategy EXC-2048/1 – Project ID 39068111 to MF; CRC1535/1-A03 – Project ID 458090666 to MF; CRC1208/2-A09 project ID 267205415 to MF; FOR2333-TP03 FE448/12-1 to MF; RU5116 to MF; GRK 2466 NEXTplant project ID 391465903 to MF; FOR2333-TP03 FE 448/12-1 to MF; Heisenberg grant HE6977/3-1 to KH; HE6977/5-1 project ID 458329234 to KH; the International GRK2172 PRoTECT – project number 273134146 to KH) as well as the Jürgen Manchot Trust (iGRAD-MOI to MF, SS).

5.2 Appendix 2

5.2.1 Supporting Information Text

Rrm4 is a key RBP for endosome-dependent RNA transport in *U. maydis*

In highly polarized cells such as fungal hyphae, the active trafficking of mRNA determines the spatial and temporal regulation of subcellular protein expression levels. A well-studied translocation mechanism is the endosome-dependent long-distance transport of mRNAs along microtubules in the dimorphic plant pathogen *Ustilago maydis*. The key transport unit of this machinery is Rrm4, one of the best-characterized RNA-binding proteins in fungal pathogens (MÜNTJES *et al.* 2021). Rrm4 contains three N-terminal RRM domains for RNA binding and three C-terminal MLLE domains for protein-protein interaction. Loss of Rrm4 abolishes mRNA transport, causing defective hyphae, with increased bipolar growth and reduced insertion of basal septa (Fig. 5.3C-D). A recent *in vivo* iCLIP study revealed that Rrm4 binds to a diverse set of mRNAs, accounting for over 60% of protein-coding genes in *U. maydis.* The binding study also revealed that the third RRM domain specifically recognizes the UAUG motif present in the mRNA targets (iCLIP- individual-nucleotide resolution cross-linking and immunoprecipitation; Fig. 5.5E; OLGEISER *et al.* 2019). This comprehensive knowledge of Rrm4 in terms of its RNA binding property provides an excellent model to validate the target identification capacity of hyperTRIBE in fungi.

Fusion of Ada preserves the function of Rrm4

To develop Rrm4-hyperTRIBE, we fused Ada-Gfp to the C-terminus of Rrm4 and expressed the fusion protein using the arabinose-inducible P_{crg1} promoter in the ip^s locus of a strain carrying *rrm4* deletion (Fig. 5.3A-B). Inhibiting P_{crg1} expression in this strain produces a typical *rrm4* deletion phenotype, characterized by bipolar hyphal growth with reduced insertion of basal septa. The strain expressing Rrm4-Gfp without Ada served as a control (Fig. 5.3A-D). As expected, Rrm4-Gfp expression fully rescued the *rrm4Δ* phenotype, leading to unipolar growing hyphae akin to wildtype cells (Fig. 5.3C-D). While a similar effect was observed for Rrm4-Ada-Gfp expression, we also detected a significant number of bipolar hyphae, possibly due to its lower expression levels as a result of Ada fusion (Fig. 5.3C-D; Fig. 5.4B) Nevertheless, the fluorescence microscopy analysis revealed that the Rrm4-Ada-Gfp fusion proteins mainly localized to bidirectionally shuttling endosomes at a velocity similar to the Rrm4-Gfp control, suggesting that the Rrm4-Ada-Gfp fusion protein is functional (Fig. 5.3E-F). Expression

of the control-Ada did not affect the phenotype of hyphal cells (Fig. 5.3D; Fig. 5.4A-C). We confirmed the expression of full-length fusion proteins upon arabinose induction, and noticed higher expression levels for Rrm4-Gfp control, explaining the intense signal in transport endosomes (Fig. 5.3E; Fig. 5.4A-B). In summary, the full-length Rrm4-Ada-Gfp fusion protein was successfully expressed in *U. maydis,* and the Ada fusion protein complements the function of wildtype Rrm4.

Rrm4-Ada-Gfp identifies bona fide Rrm4 targets

Despite being expressed at lower levels than control-Ada, Rrm4-Ada-Gfp expression yielded approximately 4000 editing sites per replicate, which is twice as many as control-Ada editing events (Fig. 2.2C; Fig. 5.5A). This finding aligns with the broad target repertoire of Rrm4, suggesting that the magnitude of Ada editing is proportional to the binding landscape of the attached RBP. In addition to Ada editing frequency, the reproducibility of Ada editing was similar between Rrm4-Ada-Gfp and control-Ada, most likely due to the promiscuous and broad RNA binding tendencies of Rrm4 (Fig. 5.5B-D).

Comparing reproducible editing events from Rrm4-Ada-Gfp and control-Ada revealed 1124 and 649 unique editing events, respectively, with 480 editing sites shared between the two sets (Fig. 2.2C). Notably, 84% of mRNAs with unique Rrm4-Ada-Gfp editing events were bona fide Rrm4 iCLIP targets, while the enrichment of Rrm4 iCLIP targets in mRNAs with editing sites unique to control-Ada was lower (Fig. 5.5E-F; 73% of transcripts). Transcripts specific to overlapping editing events showed higher enrichment for Rrm4 iCLIP targets than control-Ada, suggesting Rrm4-Ada-Gfp specific editing (Fig. 5.5F; ~83% of transcripts).

Analyzing the spatial distribution of editing events relative to Rrm4 binding sites revealed that editing sites on mRNAs unique to Rrm4-Ada-Gfp were predominantly located in proximity to the actual Rrm4 binding site, with the number of editing events decreasing as the distance increased. (Fig. 2.2D, left panel; median distance=159 nt). Although there was significant enrichment for Rrm4 iCLIP targets, the editing sites in mRNAs specific to control-Ada were not enriched towards Rrm4 iCLIP binding sites (Fig. 2.2D, left panel; median distance=628 bp). Rrm4 contains three RNA Recognition Motifs (RRM3), and previous iCLIP experiments have shown that about one-third of Rrm4 binding sites encompass the UAUG motif that is bound by the third RRM domain

(OLGEISER *et al.* 2019). Notably, the editing sites on mRNAs specific to Rrm4-Ada-Gfp were also enriched in proximity to the UAUG-containing binding sites (Fig. 2.2D, right panel; median distance to nearest iCLIP site with UAUG motif: Rrm4-Ada-Gfp=252 nt, control-Ada=695 nt). These findings indicate that Ada editing is highly specific towards the true binding sites of the attached RBPs and distinct from background Ada editing. For instance, in target mRNA *ubi1,* encoding a natural fusion protein of ubiquitin and ribosomal 60S subunit protein L40 fusion protein, the editing site is found closer to the UAUG-containing binding site (KÖNIG *et al.* 2009; Fig. 5.5G). Nonetheless, a *de novo* motif prediction around the Rrm4-Ada-Gfp editing sites using XSTREME did not yield a conclusive motif, possibly because the UAUG binding motif is only bound by the third RRM domain of Rrm4 and no other motif for the other two RRM domains could be identified to date (OLGEISER *et al.* 2019). In summary, these results confirm that Ada editing events are guided by the attached RBP and hyperTRIBE can identify true RBP targets in fungal pathogens.

Mathematical modeling to study dynamic mRNA concentration changes

To test the effect of mRNA stability we have employed a well-established, single-compartment mathematical model of mRNA, as presented in the original work by Hargrove and Schmidt (HARGROVE AND SCHMIDT 1989) and White, Brewer and Wilson (WHITE *et al.* 2013). mRNA concentrations can be modified by altering the rates of synthesis ($v_{\text{synthesis}}$) and/or degradation ($v_{\text{degradation}}$):

$$\frac{d[\text{mRNA}]}{dt} = v_{\text{synthesis}} - v_{\text{degradation}}$$

where mRNA synthesis is modeled with zero-order rate kinetics and rate of degradation with first-order kinetics.

$$v_{\text{synthesis}} = k_{\text{synthesis}}$$

$$v_{\text{degradation}} = k_{\text{decay}} \cdot (\text{mRNA})$$

We assume that the rate of mRNA decay is inversely related to the mRNA half-life ($t_{1/2}$):

$$t_{1/2} = \frac{ln2}{k_{\text{decay}}}$$

hence the longer half-time translates to a slower rate of mRNA decay

$$k_{\text{decay}} = \frac{ln2}{t_{1/2}}$$

For numerical integration, we implemented the model in Python and performed a set of experiments *in silico* to test the effect of perturbing either of the rates. The code is openly available under https://github.com/AnnaMatuszynska/mRNAturnoverkinetics.

Change in *mob1* steady-state levels during hyphal morphogenesis

In this simulation, we have solved the initial value problem for *mob1* in wildtype and *khd4Δ* cells during the morphological transition from yeast to hyphae. The steady-state mRNA levels of *mob1* were quantified in Transcripts per million (TPM) using RNA-seq data from the yeast and hyphal transcriptome of both wildtype and *khd4*Δ cells. In our RNA-seq data, we observed ~10-fold induction in *mob1* expression during hyphal morphogenesis (Fig. 5.13B). In *khd4*Δ cells, the 10-fold increase persisted, but the expression levels were elevated in both yeast and hyphal stage (Fig. 5.13B). Based on these results, for the wildtype, the starting condition is set to 30 TPM corresponds to the steady-state level of mRNA in yeast. In the hyphal stage, the steady-state level reaches 300 TPM (Fig. 5.13B). To obtain mRNA half-lives, we have utilized the estimated half-life from *S. cerevisiae* (MILLER *et al.* 2011). Assuming that the half-life of *mob1* is 8 minutes, we have fitted the rate constant for the synthesis to reach the 300 TPM in a steady state

$$\frac{d[\text{mRNA}]}{dt} = v_{\text{synthesis}} - v_{\text{degradation}} = 0$$

$$v_{\text{synthesis}} = v_{\text{degradation}}$$

$$v_{\text{synthesis}} = \frac{ln2}{t_{1/2}}(mRNA_{steady}) = \frac{ln2}{8}(300)$$

and simulated the change in mRNA over time. In wildtype cells, the onset of hyphal morphogenesis led to a 10-fold increase in *mob1* level, quickly reaching a new steady state within 57 min of induction. The rate of synthesis has been set to zero after 3 hours of induction (180 min) and we observed exponential mRNA decay leading to the original steady-state level within 80 min (Fig. 5.13C). Similarly, a change in mRNA concentration in the *khd4*Δ mutant has been simulated, using 80 TPM as a steady-state

level in the yeast stage, and 800 TPM as a steady-state level in the hyphal stage (Fig. 5.13B). Notably, stabilizing the *mob1* mRNA to a half-life of $t_{1/2}$=22 min is sufficient to reach the increased steady-state levels without changing the rate of synthesis (Fig. 5.13C). Moreover, the stabilized *mob1* in *khd4Δ* cells takes longer than 6 hours to reach its original steady-state level after the termination of mRNA synthesis (Fig. 5.13C).

We also utilized the simple model to study the impact of mRNA stability kinetics on the response time required for mRNAs to reach the steady-state level (Fig. 5.13A). The model has been parametrized to achieve a 10-fold increase for each mRNA type (Fig. 5.13A; unstable, moderately stable, and stable mRNAs), starting from an initial concentration of 1. The rate of synthesis was calibrated as earlier to reach a steady-state level that was 10-fold higher than the initial concentration. The half-lives of mRNAs were estimated from *S. cerevisiae* (MILLER *et al.* 2011).

Our model revealed that the response times of mRNAs are based on their stability characteristics. Unstable mRNAs, characterized by a faster synthesis rate (0.87 transcript/min) and faster decay ($t_{1/2}$=8 min), exhibited a rapid response, reaching the steady state approximately in 1 hour after induction (Fig. 5.13A). In contrast, stable mRNA, with a slower synthesis rate (moderately stable mRNA=0.3 transcripts/min; stable mRNA=0.12 transcript/min) and slower decay (moderately stable mRNA, $t_{1/2}$=22 min; stable mRNA, $t_{1/2}$=60 min), required a longer time to reach the steady-state, indicating a delayed response (Fig. 5.13A). These findings highlight the importance of intrinsically unstable mRNA in achieving rapid on-off kinetics and facilitating faster cellular response.

Overall, our mathematical models emphasize the significant role of mRNA turnover kinetics in precisely controlling gene expression levels following transcriptional induction.

5.2.2 Materials and methods

Plasmids, strains, and growth conditions

For molecular cloning of plasmids, the *E. coli* K-12 derivative Top10 (Life Technologies, Carlsbad, CA, USA) was used. All *U. maydis* strains used in this study are derivatives of AB33 and generated by transforming the cells with linearized plasmids (BRACHMANN *et al.* 2001,BRACHMANN *et al.* 2004,TERFRÜCHTE *et al.* 2017). For ectopic integration of hyperTRIBE constructs (Fig. 2.2B), the plasmids were linearized with AgeI (New England Biolabs) and integrated into the *ip*^{s} locus (LOUBRADOU *et al.* 2001). For ectopic integration into the *upp3* locus, the plasmids were linearized using SwaI (NEB) restriction enzyme (SARKARI *et al.* 2014). Genomic DNA of wildtype strain UM521 (*a1b1*) was used as a template for PCR amplification. For RNA-editing, the amino acid sequence of the ADAR catalytic domain from *D. melanogaster* (Accession number: AHN59262.1; starting from M271 till E669) carrying the hyperactive E488Q mutation (KUTTAN AND BASS 2012) was used (MCMAHON *et al.* 2016,XU *et al.* 2018). The DNA sequence corresponding to the ADAR catalytic domain was codon-optimized for *U. maydis* before fusing to the RNA-binding protein of interest. Proteins were tagged with eGfp (enhanced green fluorescent protein; Clontech, Mountain View, CA, USA), or mKate2 (Kat; SHCHERBO *et al.* 2009) for detection. All the plasmids were verified using Sanger sequencing. The homologous integration in *U. maydis* was validated by colony-PCR and Southern blot analysis. Detailed information about the strains, plasmids, and primers is given in Table 1-4. The accession number of *Ustilago maydis* genes used in this study: *khd4* (UMAG_03837), *did2* (UMAG_05607), *rrm4* (UMAG_10836), *arl1* (UMAG_10313), *vma21* (UMAG_11418), *hok1* (UMAG_11790).

The conditions for *U. maydis* cultivation are described elsewhere (BRACHMANN *et al.* 2004). In short, yeast cells were grown in a complete medium (CM) medium supplemented with 1% glucose or 1% arabinose up to an OD_{600} of 0.5 at 28 °C on a rotary shaker at 200 rpm. To induce hyphal growth, yeast cells of 0.5 OD_{600} were shifted to nitrate minimal (NM) medium consisting of 1% glucose or 1% arabinose and grown for 6, 9, 10, and 12 hours (h.p.i.; hours post induction) at 28 °C. In addition to CM medium supplemented with arabinose (1%), the strains expressing arabinose-inducible Khd4 were also grown on CM medium supplemented with glucose (1%) in parallel to repress Khd4 expression, unless otherwise stated.

HyperTRIBE experiment and data processing

HyperTRIBE strains were grown consistently under arabinose-induced promoter-on conditions. Hyphae were induced by shifting 50 ml of exponentially growing cells from CM to NM medium, each supplemented with 1% arabinose. After 6 hours, the hyphal cells were harvested by centrifugation at 7546 *g* for 10 min at 4 °C. Cell pellets were resuspended in 1 ml ice-cold nuclease-free water and transferred to a 2 ml centrifuge tube. Cells were harvested at 7546 *g*, for 10 min at 4 °C, and the supernatant was removed completely. The resulting cell pellets were flash-frozen in liquid nitrogen and stored at -80 °C until further use.

Total RNA was extracted using the RNeasy Plant Mini Kit (74904; Qiagen, Hilden, Germany) following the manufacturer's instructions. Cell pellets were mechanically lysed at 30 Hz for 5 min at 4 °C in Mixer Mill MM400 (Retsch, Haan, Germany), in the presence of glass beads and Buffer RLC (+ß-mercaptoethanol). The resulting cell lysate was transferred to the QIAshredder spin column for further homogenization. The supernatant was transferred to a new centrifuge tube, mixed with 1 volume of 70% ethanol, and added to the RNeasy spin column. The subsequent steps were performed as per the manufacturer's protocol. To eliminate genomic DNA contamination, the on-column DNase digestion was performed using the RNase-Free DNase set (79254; Qiagen, Hilden, Germany). VAHTS® Universal V6 RNA-seq Library Prep Kit for Illumina (NR604-01/02; Vazyme) was used for cDNA library generation. All cDNA libraries expressing hyperTRIBE constructs sequenced using the HiSeq 3000 platform (Illumina), were processed simultaneously to obtain 151 nt single-end reads.

The bioinformatics analyses were based on the *U. maydis* 521 genome sequence (Ustilago_maydis.Umaydi5.621_2.0.dna_rm.chromosome) and the associated gene annotation (Ustilago_maydis.Umaydi5.621_2.0.41.gff3; both downloaded from http://ftp.ensemblgenomes.org/pub/fungi/release-53/fasta/ustilago_maydis/dna/; KÄMPER *et al.* 2006). To incorporate potential 5′ UTR and 3′ UTR regions, which are not currently annotated in the *Ustilago maydis* genome, we manually extended all genes by 300 nucleotides (nt) on each side. This extension was determined based on the transcript read coverage profile (Fig. 5.14E-F; see Differential gene expression analysis). While the majority of UTRs were shorter than 150 nt, we observed a subset of transcripts with UTRs spanning 300 nt in length. To ensure comprehensive coverage of all potential editing sites, we decided to manually extend the genes by 300 nt on both sides of the

open reading frame (ORF). The extended GTF file was converted to refFlat format using the UCSC gtfToGenePred tool.

The A-to-G editing events on transcripts were identified using the wtRNA-RNA approach from the previously established hyperTRIBE pipeline (RAHMAN *et al.* 2018; https://hypertribe.readthedocs.io/en/latest/run.html#b-find-rna-edit-sites-using-wtrna-rna-approaches). In brief, RNA-seq reads were trimmed based on sequencing quality (Phred score) using Trimmomatic (version 0.39; BOLGER *et al.* 2014). Specifically, reads with a Phred score of less than 25 were trimmed and removed when the read length fell below 19 nt. The trimmed reads were then mapped to the *U. maydis* genome sequence and gene annotation using STAR (version 2.5.2b; DOBIN *et al.* 2013), allowing reads that were mapped to exactly one location, had a minimum of 16 matched bases, and contained no more than 7% mismatches per mapped length. Uniquely mapped alignments in SAM format were loaded into a MySQL table with genomic coordinates. The nucleotides at each position in the test mRNA libraries (RBP-Ada-Gfp, control-Ada) were compared with those of the control mRNA library (wtRNA: RBP-Gfp) to identify A-to-G editing sites. Only editing events with a minimum of 20 read coverage and 5% editing were considered for further analysis. Editing sites that are assigned to more than one gene were removed from the analysis. From this, the list of reproducible editing sites that were consistently present in both replicates of either RBP-Ada-Gfp or control-Ada libraries was identified. The resulting reproducible editing events from RBP-Ada-Gfp and control-Ada were compared against each other to determine the editing sites that were unique to RBP-Ada-Gfp (Fig. 5.5A, 5.7A).

Subcellular localization of proteins was defined using DeepLoc-2.0 (THUMULURI *et al.* 2022; https://services.healthtech.dtu.dk/service.php?DeepLoc-2.0) and the cellular compartment ontology. Cellular compartment ontology annotations for *U. maydis* genes were downloaded from QuickGO (BINNS *et al.* 2009,HUNTLEY *et al.* 2015; https://www.ebi.ac.uk/QuickGO/annotations). A gene was assigned to more than one category if they were predicted to localize in more than one subcellular region.

***De novo* motif discovery**

For *de novo* motif discovery, we first extracted sequences by extending 250 nt on both sides of the editing sites using Biostrings (R package; version 2.56.0). We employed XSTREME from the MEME suite for motif discovery and enrichment analysis (GRANT

AND BAILEY 2021). Sequences of length 501 nt were randomly selected from the *U. maydis* genome and used as a background control (random genome background). XSTREME analysis was conducted using default parameters. The relative enrichment ratio (tested sequences vs. random genome background) of the identified motifs was compared against the absolute percentage of tested sequences with enriched motifs. Only motifs that exhibited both high enrichment and overrepresentation were considered potential RBP binding motifs. Motif logos were created using the ggseqlogo package (version 0.1) in R, utilizing the position-specific weight matrix (PWM) of the identified motifs.

Motif analysis

The genomic position of the AUACCC, AGAUCU, GGGUAU, and ACACUC motifs on the *U. maydis* 521 genome sequences (PEDANT database name p3_t237631_Ust_maydi_v2GB) was identified using the Bioconductor package GenomicRanges in R (version 1.40.0; https://bioconductor.org/packages/release/bioc/html/GenomicRanges.html). Sequence information was extracted using Biostrings (R package; version 2.56.0; https://bioconductor.org/packages/release/bioc/html/Biostrings.html). To determine the genomic position of the *de novo* discovered motifs. The matchPWM function from the Biostrings R package was employed to perform the motif-matching process.

To calculate the distance between hyperTRIBE editing sites and the nearest motif, we first obtained the genomic coordinates of editing sites. We then proceeded to determine the distance of each editing site to the nearest motif using the nearest-methods function in the GenomicRanges R package.

To assess motif enrichment across transcript regions (Fig. 2.3F; Fig. 5.11A; Fig. 5.12A), we first determined the relative position of the motifs within the specific transcript regions, namely the 5′ UTR, ORF, and 3′ UTR. This was achieved by calculating the ratio between the distance from the motif start and the start codon to the length of the coding sequence (CDS). A ratio value ranging from 0 to 1 indicates a position within the ORF, a negative value suggests motif occurrence in the 5′ UTR, and a value greater than 1 suggests motif incidence in the 3′ UTR. For regions on the "-" strand, we multiplied the resulting position by -1, to appropriately represent the motif positions on the antisense strand, ensuring that the relative positions remained comparable between the two strands.

Motif enrichment analysis was then carried out by computing the relative proportion of motifs within different transcript regions.

For relative motif position calculation in Appendix, Fig. 5.9D, we first selected a window of 1000 nt with a start or stop codon at the center. We then obtained the genomic coordinates of the AUACCC and AGAUCU motifs within the selected window. The relative position of the motif on target transcripts was calculated by measuring the distance between the motif start position and the start or stop codon.

Differential gene expression analysis

Total RNA from yeast and hyphal (9 h.p.i.) cells was extracted using RNeasy Plant Mini Kit (74904; Qiagen, Hilden, Germany) following the manufacturer's protocol (see HyperTRIBE experiment and data processing). cDNA libraries were prepared using VAHTS® Universal V6 RNA-seq Library Prep Kit for Illumina (NR604-01/02; Vazyme) and sequenced using the HiSeq 3000 platform (Illumina), to obtain 151-nt single-end reads. Approximately, ~10 million raw reads for hyphal and ~20 million raw reads for yeast samples were obtained.

Basic quality control checks on all sequencing datasets were performed using FastQC (https://www.bioinformatics.babraham.ac.uk/projects/fastqc/). RNA-seq data analysis was carried out in Galaxy, an open-source platform (AFGAN *et al.* 2018). The raw sequencing reads were quality filtered based on their quality score and length with Trimmomatic (Version 0.36; BOLGER *et al.* 2014). Specifically, the reads were trimmed 20 nt from the start, trimmed from the end when the Phred score dropped below 30, and discarded if the read length is less than 20 nt. STAR (version 2.7.2b) was used to align the trimmed reads to the *U. maydis* genome (see HyperTRIBE experiment and data processing; DOBIN *et al.* 2013), allowing up to 4% mismatches in the mapped read length while limiting the mapping to one locus. Uniquely mapped reads on each gene were counted using htseq-count (version 0.9.1; ANDERS *et al.* 2014). The resulting raw counts of mRNA libraries were used as input for the subsequent differential gene expression analysis. All differential gene expression analysis was performed using the R/Bioconductor package DESeq2 (LOVE *et al.* 2014). Genes with an absolute fold change>1.5 (after fold change shrinkage) and an adjusted P<0.05 (Benjamini-Hochberg correction) were considered differentially expressed.

To identify differentially expressed genes in hyphae following a morphological switch from yeast, quantitative changes in transcript expression levels were calculated by comparing the hyphal against the yeast mRNA libraries ("hyphae vs. yeast") for wildtype as well as *khd4Δ* strains. As a result, transcripts that were more expressed in the hyphal form obtained a positive log_2-transformed fold change (log_2 fold change), while transcripts that were more expressed in the yeast form obtained a negative log_2 fold change. To identify differentially expressed genes in the hyphal cells after *khd4* deletion, the mRNA libraries from the *khd4Δ* hyphal cells (9 h.p.i.) were compared against the mRNA libraries of wildtype hyphal cells (9 h.p.i.) ("*khd4Δ* hyphae vs. wildtype hyphae").

To identify potential UTR regions, the transcript read coverage profile was generated by analyzing the mapped BAM files (Fig. 5.14A). The coverage function from the IRanges package (R package version 2.32.0) was utilized to calculate the coverage of the mapped BAM file. Subsequently, each coverage value was normalized by dividing it by the total number of reads. To focus on regions surrounding the start or stop codons, we extracted the coverage values within a 501 nt window centered around these codons. These extracted values were then converted to z-scores by subtracting the mean of the respective row from each element in that row and dividing the result by the standard deviation of the row.

Gene ontology (GO) term enrichment analysis

Functional enrichment analysis was performed in R using the R package gprofiler2 (e107_eg54_p17_bf42210; version 0.2.1; https://cran.r-project.org/web/packages/gprofiler2/vignettes/gprofiler2.html; RAUDVERE *et al.* 2019,KOLBERG *et al.* 2020). For the g:Gost analysis, multiple testing correction was performed with the default g:SCS method and a p-value threshold of 0.05. Downloaded Generic EnrichmentMap (GEM) file from g:Profiler was loaded into the Cytoscape (version 3.8.0) plugin, EnrichmentMap (version 1.1.0) to visualize the GO term enrichment analysis (Jaccard coefficient cutoff of >0.25). The clusters were identified and annotated according to the GO-term annotation of the gene sets using the Cytoscape plugins AutoAnnotate (version 1.3.5) and the WorldCloud app (version 3.1.4) (MERICO *et al.* 2010,OESPER *et al.* 2011,KUCERA *et al.* 2016).

Reporter fluorescence measurement

Hyphal growth was induced by shifting 20 ml of exponentially growing yeast cells in CM medium to NM medium, each supplemented with 1% glucose (promoter-off condition) or 1% arabinose (promoter-on condition). After 6 hours 1 ml of culture was harvested at 16000 *g* for 5 min at room temperature. Cell pellets were washed twice in double-distilled water. After harvesting, the supernatant was removed completely. The resulting cell pellets were resuspended using 1 ml of double-distilled water. 200 µl of samples were transferred into black 96-well plates (Greiner 96 Flat Bottom Black Polystyrene: Greiner, Frickenhausen, Germany). Optical density (OD_{600}) and mKate2 fluorescence level (excitation wavelength: 588 nm, emission wavelength: 633 nm) were measured in an Infinite M200 plate reader (Tecan Group Ltd., Männedorf, Switzerland). The fluorescence levels (mKate2) were normalized to the optical density of the cell culture (OD_{600}). The strain constitutively expressing mKate2 (*kat_no motif*) was used for calculating relative mKate2 protein abundance (Table 1-2). Statistical significance was calculated using multiple Student's *t*-test in Prism version 5.04 (GraphPad, La Jolla, CA, USA).

RT-qPCR analysis

Total RNA from hyphal cells (6 h.p.i.) was extracted using the RNeasy Plant Mini Kit (74904; Qiagen, Hilden, Germany) as described earlier (see HyperTRIBE experiment and data processing). 1 µg of total RNA served as a template for first-strand cDNA synthesis with oligo (dT) primers using ProtoScript® II First Strand cDNA Synthesis Kit (NEB). 1 µl of cDNA was used per reaction in qPCR, following the standard Luna® Universal qPCR Master Mix (NEB) protocol in Stratagene Mx3000P (Agilent Technologies). Relative gene expression value was calculated as $\exp(-\Delta C_t)$ (threshold cycles) ratios, with UMAG_04871 (phosphoglycerate kinase; $\log_2$-transformed fold change=0.1, adjusted P=0.55, in "*khd4Δ* hyphae vs. wildtype hyphae" RNA-seq analysis) as a reference gene. The abundance of *mkate2* mRNA was calculated relative to *mkate2* expression in the strain *kat_no motif*. Primers used for RT-qPCR are shown in Table 4. Statistical significance was calculated using multiple Student's *t*-test in Prism version 5.04 (GraphPad, La Jolla, CA, USA).

***Ustilago maydis* cell disruption and immunoblotting analysis**

U. maydis cell disruption was performed as previously reported (DEVAN *et al.* 2022). In short, 50 ml of hyphal cells (6 h.p.i.; see Plasmids, strains, and growth conditions) were

harvested by centrifugation at 7546 *g*, for 10 min. After washing in phosphate-buffered saline of pH 7.0, the samples were flash-frozen in liquid nitrogen and stored at -80 °C until further use. Samples were lysed using a 5 mm stainless-steel bead in Mixer Mill MM400 (Retsch, Haan, Germany) at 30 Hz for 1 min. Cell disruption was repeated 3 times with intermittent liquid cooling steps of 5 min. The resulting homogenized cell powder was resuspended in 1 ml urea buffer (8 M urea; 50 mM Tris/HCl pH 8; containing 1 mM DTT, 0.1 M PMSF, 1 tablet of cOmplete protease inhibitor per 25 ml, Roche, Mannheim, Germany) and centrifuged at 16,000 *g* for 10 min at 4 °C. The supernatant was used for subsequent analysis. Protein concentrations were measured with the Bradford assay (BioRad, Munich, Germany) as per the manufacturer's protocol. Sample volumes were adjusted to equal concentrations, supplemented with Laemmli buffer, and boiled at 95 °C for 10 min. Samples were resolved in 1.5 mm thick 8% SDS-PAGE and transferred to a nitrocellulose membrane (Amersham Protran) for immobilization by semi-dry blotting.

Proteins were detected using the primary antibodies, α-Gfp (Roche, Germany) and α-Actin from mouse (MP Biomedicals, Germany). α-mouse IgG HRP conjugate (Promega, Madison, WI, United States) was used as a secondary antibody. Antibodies bound to nitrocellulose membrane were removed by treating the blot in TBS buffer pH 3.0 (50 mM Tris pH 3.0, 150 mM NaCl) at room temperature, before detecting the constitutively expressed actin control. Detection was carried out using ECL™ Prime (Cytiva RPN2236;). Images were recorded by a luminescence image analyzer, LA5.5000 (GE Healthcare).

Staining techniques

To visualize basal septa and empty sections, 1 ml of cell culture was stained with 1 µl of Calcofluor white staining solution (2 mg/ml; CFW) directly before microscopy with a DAPI filter set (LANGNER *et al.* 2015).

FM4-64 uptake assay was carried out as described previously (HAAG *et al.* 2019). Hyphal growth was induced in NM medium for 10 hours. 1 ml of culture was transferred into a 2 ml centrifuge tube and incubated for 10 min on ice. 4 µM (final concentration) of FM4-64 was added to the cells and incubated for an additional 10 min on ice, protected from light. Cells were washed by centrifugation at 2400 *g* for 3 min at 4 °C. Cell pellets were resuspended in 1 ml of ice-cold NM-glucose medium. Samples were shifted to a

thermoblock set at 1100 rpm and 28 °C for 25 min prior to visualization under fluorescence microscopy.

Vacuolar staining was performed using CMAC (7-amino-4-chloromethylcoumarin; ThermoFisher, Darmstadt, Germany). 1 ml of cell suspension was stained with 10 µM CMAC and incubated for 30 min at 28 °C on a rotating wheel. Cells were washed by centrifugation at 2400 *g* for 3 min. Subsequently, the cell pellets were resuspended in phosphate-buffered saline prior to microscopy with the DAPI filter set.

Microscopy and image processing

For microscopic analysis, 20 ml of yeast cells were grown in CM medium (1% glucose) to an OD_{600} of 0.5. Hyphal cells were induced by shifting 20 ml cell culture from CM medium to NM medium (supplemented either with 1% glucose or 1% arabinose) for 6, 9, 10, and 12 hours. All images and videos were acquired using laser-based epifluorescence-microscopy, Zeiss Axio Observer.Z1 (Oberkochen, Germany) as described previously (BAUMANN *et al.* 2012). The exceptions are the images and videos requiring a filter set for DAPI (4′,6-diamidino-2-phenylindole) which was carried out by Zeiss Axio Imager M1 (Oberkochen, Germany) as indicated before (LANGNER *et al.* 2015). All movies and images were processed using the MetaMorph software package (version 7.7.0.0, Molecular Devices, Seattle, IL, USA).

The hyphal length was determined by measuring the distance between the tip and the basal pole without including the empty sections. Hyphal width was calculated by taking the average thickness measured at three different locations within each hypha. Hyphal cells with empty sections were visualized using Calcofluor White (CFW) and were scored manually. For each experiment, more than 100 cells were counted per strain.

To assess the FM4-64 (ThermoFisher) signal in hyphal cells, movies with an exposure time of 150 ms, and 100 frames were recorded. Kymographs from the movies were generated using the MetaMorph software package. Changes in direction were counted as an individual signal with the following parameters: a signal is processive if particles exhibit a directional travel distance of greater than 5 µm; diffusive if the signal traveled is less than 5 µm but greater than 0 µm. The diffusive particles display random erratic movements without a clear trajectory. More than 25 hyphal cells were analyzed per strain (n=3 independent experiments).

Vacuole distribution was scored by acquiring z-stacks (z-distance- 0.23 µm) and analyzing the maximum projection. The intensity profile of CMAC-stained hyphal cells was performed by line scan. Fluorescent intensity was plotted against their respective position after subtracting the background fluorescence of the micrograph. Vacuole distribution and aberrant cortical localization were scored by visual inspection (Fig. 2.7A-D). For the quantification of vacuole distribution, the line scans (see above; Fig. 2.7A, bottom panel) were used to distinguish normal and disrupted distribution. The cortical localization of vacuoles at the cell edge was quantified by visually counting the cells exhibiting this phenotype. For each strain, more than 25 cells were analyzed.

All quantifications were performed using data obtained from three independent experiments. Data points represent the mean of independent experiments. Prism5 (GraphPad, La Jolla, CA, USA) was used for statistical analysis.

Multiple sequence alignments

Ortholog proteins were identified using BLASTP (https://blast.ncbi.nlm.nih.gov/Blast.cgi?PAGE=Proteins) and FungiDB (https://fungidb.org/fungidb/app). Multiple sequence alignment was carried out using Clustal Omega (MADEIRA *et al.* 2022). Genedoc (version 2.6.002) was used for graphical representation.

5.2.3 Supporting information Figures

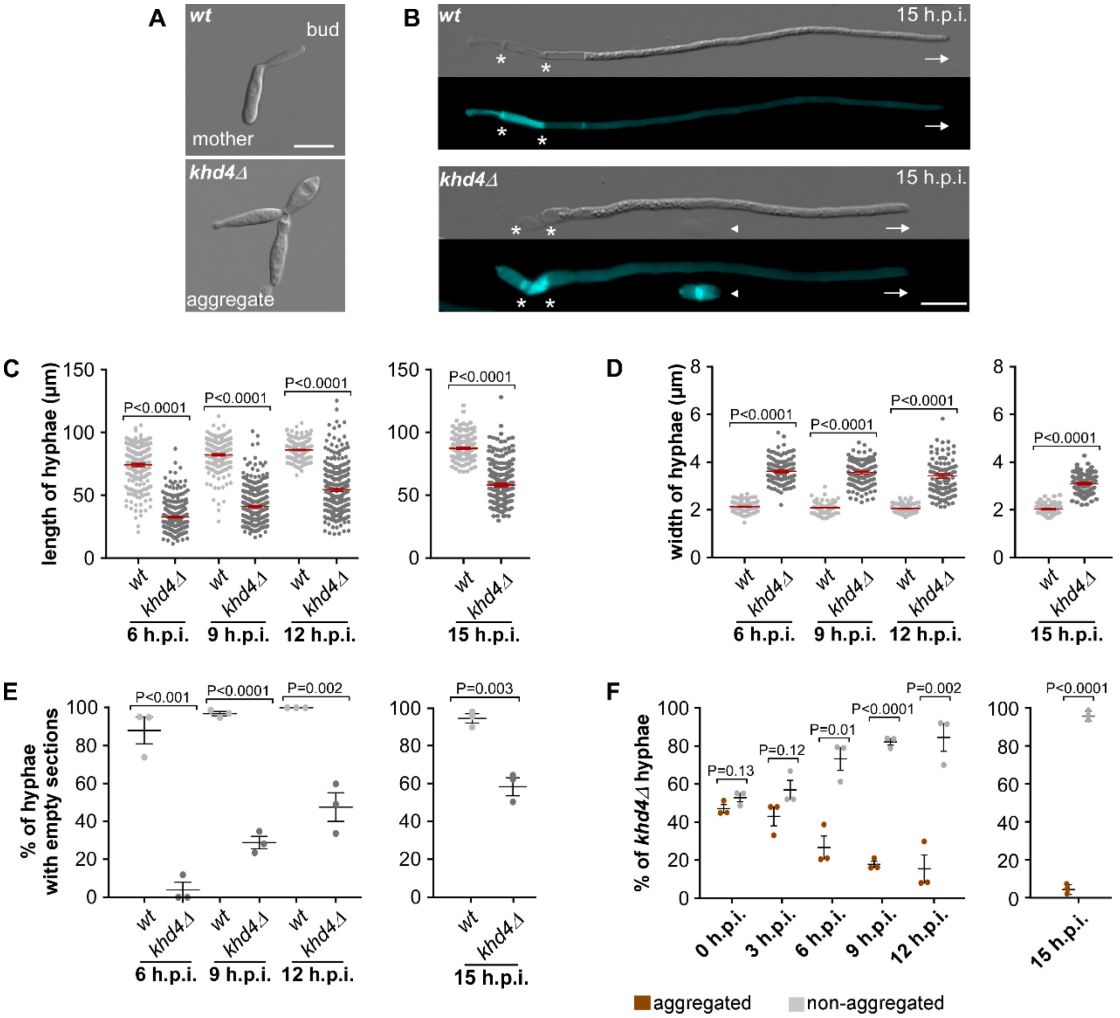

Fig. 5.2. Loss of Khd4 affects the morphology of yeast as well as hyphal cells. **(A)** Differential interference contrast (DIC) images of yeast cells. **(B)** DIC (top panel) and calcofluor white-stained (CFW; bottom panel) images of hyphae grown for 15 h.p.i. (basal septum and growth directions are marked by asterisks and arrows, respectively; triangle indicates a broken empty section; scale bar: 10 µm). **(C)** Hyphal length over time. Data from n=3 independent experiments (>100 hyphae were counted per strain) are overlaid with the mean of means and standard error of the mean (s.e.m., red line). Statistical evaluation was performed using an unpaired two-tailed Student's *t*-test on mean length. **(D)** Hyphal width over time. (Shown are merged data from n=3 independent experiments; >100 hyphae were analyzed; error bars: s.e.m.; unpaired two-tailed Student's *t*-test on mean width). **(E)** Percentage of hyphae with empty sections over time. (Data points represent the average percentage from n=3 independent experiments; >100 hyphae were analyzed per strain; error bars: s.e.m.; unpaired two-tailed Student's *t*-test on the means). **(F)** Percentage of *khd4Δ* hyphae aggregated (brown) or non-aggregated (grey) at different time points. (Data points represent the mean hyphal percentage from n=3 independent experiments; >100 hyphae were counted per strain; error bars: s.e.m.; unpaired two-tailed Student's *t*-test on the means).

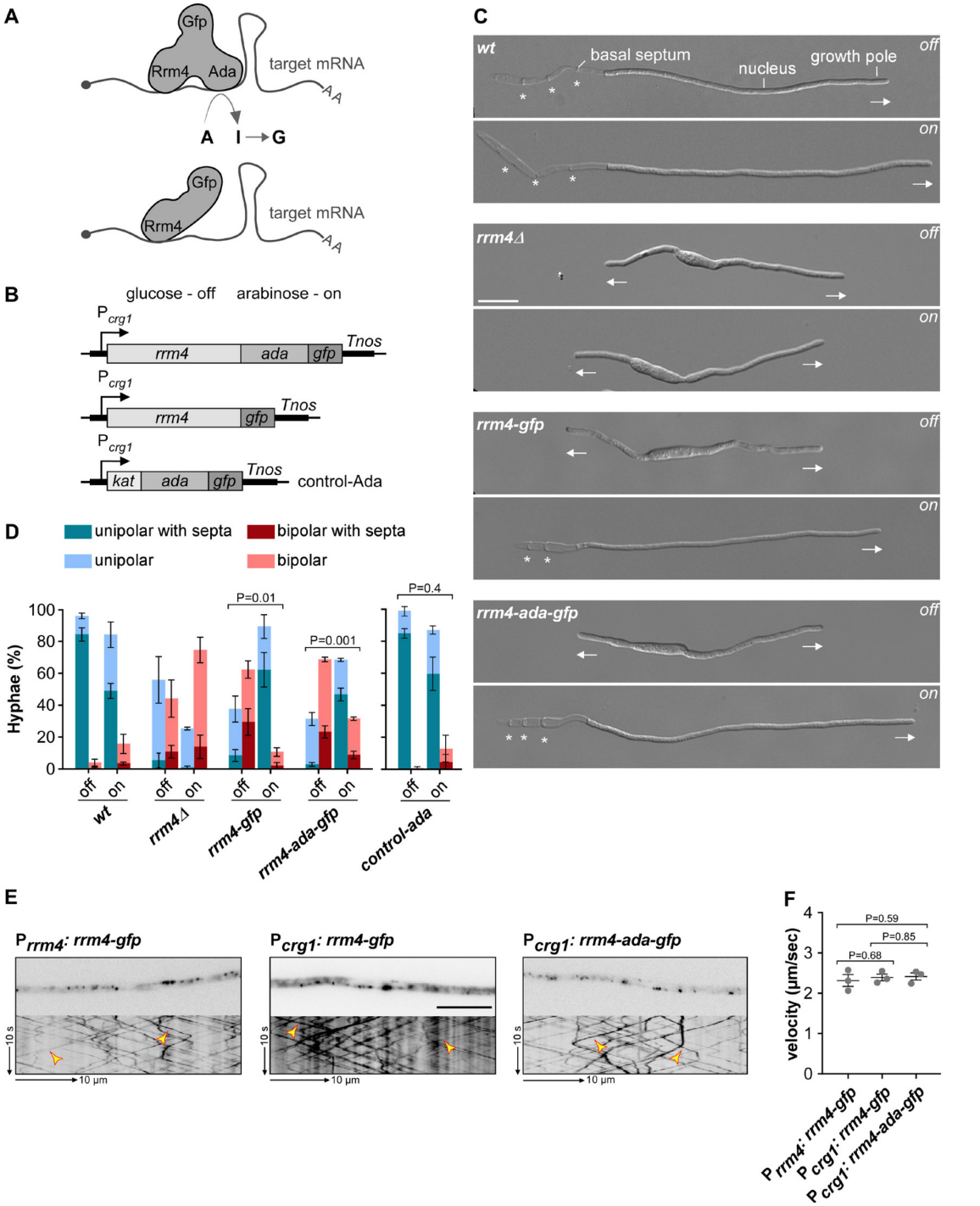

Fig. 5.3. Rrm4-Ada-Gfp fusion protein rescues *rrm4*Δ phenotype. **(A)** Top: Schematic representation of target RNA editing by hyperTRIBE. As the Rrm4-Ada-Gfp fusion protein binds to the target mRNA through Rrm4 (light blue), the fused Ada (dark blue) deaminates the adjacent adenosine (A) to inosine (I) which is converted to guanine (G). Bottom: The binding of control protein Rrm4-Gfp to the target mRNA (Ada- hyperactive version of *Drosophila* ADAR catalytic domain; Gfp- Green fluorescent protein; Filled circle- 5´cap structure; AA- poly(A) tail of target mRNA (grey). **(B)** Schematic representation of hyperTRIBE constructs with arabinose inducible P_{crg1} promoter (on), which is repressed by glucose (off) (*Tnos*- transcription terminator). Fusion proteins of Rrm4, Ada, Gfp, and/or Kat (mKate2- red fluorescent protein; *Tnos*- transcription terminator). The hyperTRIBE constructs are expressed in a strain carrying *rrm4Δ* genetic background. **(C)** DIC images of AB33 hyphal derivatives (6 h.p.i.) under promoter uninduced off (top) and promoter induced on (bottom) conditions. (Arrows and asterisks indicate growth direction and empty sections, respectively; scale bar- 10 µm). **(D)** Quantifying the growth of AB33-derived

hyphal cells shown in B (6 h.p.i.). Unipolarity, bipolarity, and basal septum formations were quantified (error bars: s.e.m.; >100 hyphal cells from n=3 independent experiments were quantified per strain; unpaired two-tailed Student's *t*-test was used for the statistical evaluation of the percentage unipolarity and bipolarity). **(E)** Inverted fluorescent images (top) and their corresponding kymographs (bottom) of AB33-derived hyphal cells (6 h.p.i.) expressing green fluorescent proteins under promoter on condition. P_{rrm4}*: rrm4-gfp* refers to the strain where Rrm4-Gfp is expressed under the endogenous condition. Example processive moving signals are indicated by yellow arrowheads. **(F)** The average velocity of fluorescent signals per 20 µm of hyphal length in AB33 hyphal derivatives is shown in D. For quantification, only processively moving particles (>5 µm) were considered. P_{rrm4}*: rrm4-gfp* refers to the strain where Rrm4-Gfp is expressed under the endogenous condition. Data points represent average velocities from n=3 independent experiments, with mean of means and s.e.m.; >25 hyphal cells were analyzed per strain; unpaired two-tailed Student's *t*-test.

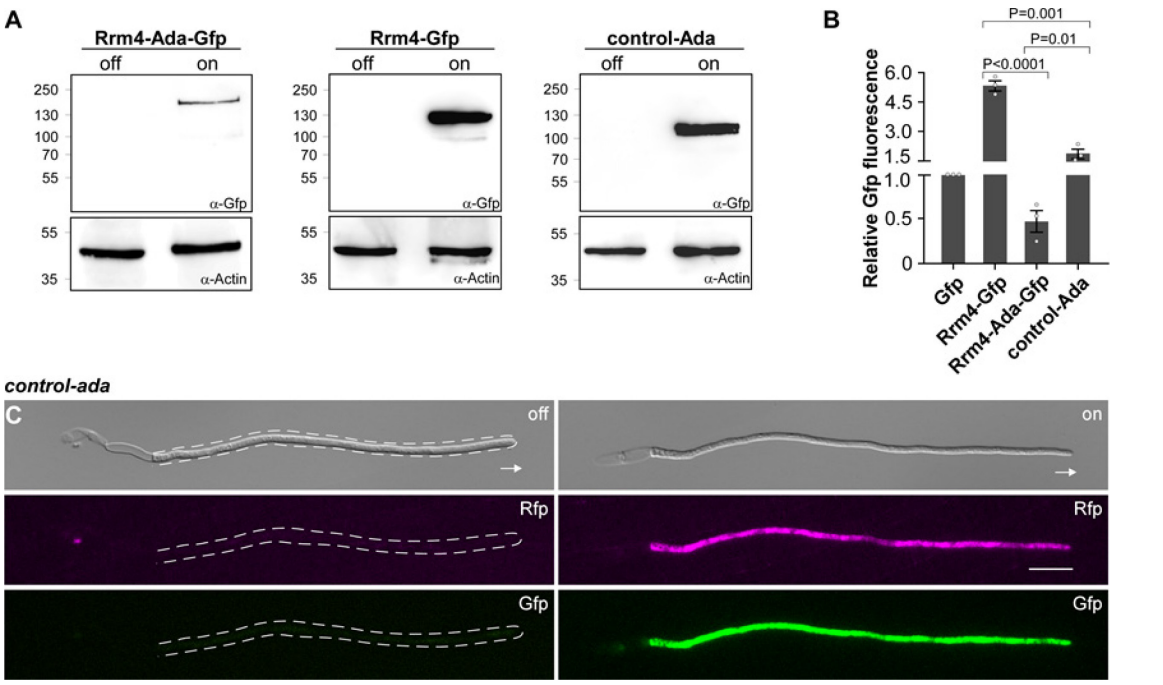

Fig. 5.4. Protein expression analysis of the Rrm4-hyperTRIBE constructs. **(A)** Western blot analysis of the full-length fusion protein expression under promoter uninduced (off) and induced (on) conditions. Immunoblotting was performed using α-Gfp and α-Actin. The size of protein markers (kDa) is shown on the left. (Molecular weight of the full-length fusion proteins: Rrm4-Ada-Gfp- ~158 kDa; Rrm4-Gfp- ~112 kDa; control-Ada- ~99 kDa; Molecular weight of the individual proteins: Rrm4- ~85 kDa, Ada- ~44 kDa, Gfp- ~27 kDa, Kat- ~26 kDa). **(B)** Expression levels of Rrm4-hyperTRIBE constructs. Gfp fluorescence levels were calculated relative to the Gfp control. Statistical analysis was performed using the unpaired two-tailed Student's *t*-test on mean fluorescence level (n=3 independent experiments; error bars: s.e.m.). **(C)** DIC (top panel) and fluorescent images (Rfp- middle panels; Gfp- bottom panels) of hyphae (6 h.p.i.) expressing control-Ada under promoter uninduced off condition (left) and promoter induced on condition (right) (arrows indicate growth direction; scale bar: 10 μm).

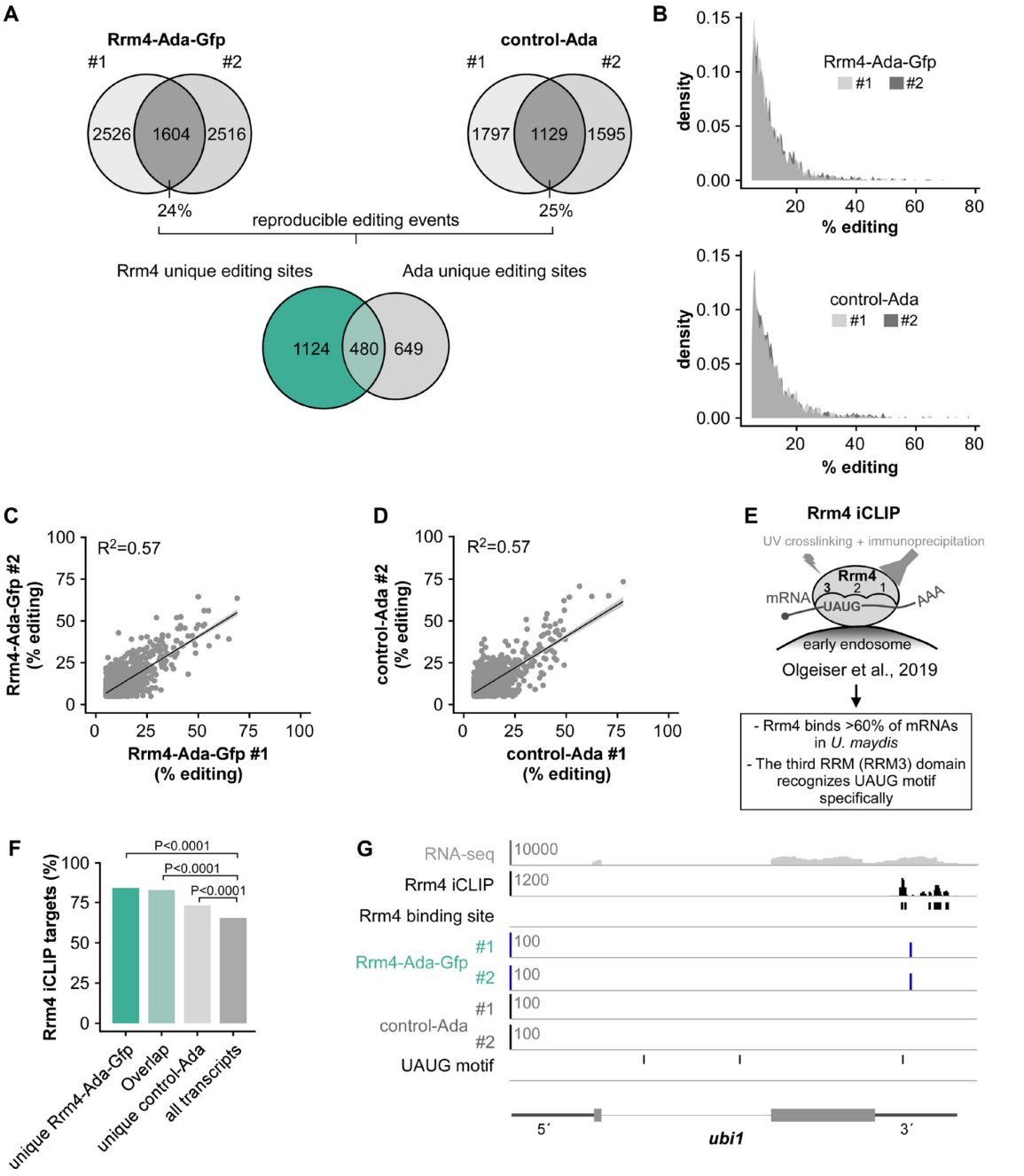

Fig. 5.5. Rrm4-Ada-Gfp identifies bona fide Rrm4 target mRNAs. **(A)** Overview of the hyperTRIBE workflow. Editing events overlapped between the two independent biological replicates of Rrm4-Ada-Gfp (sea green) and control-Ada (grey) data. The indicated values represent the number of editing events in each category. For the analysis, only editing events with ≥5% editing was considered (#1,2- replicates 1 and 2, respectively). Reproducible editing sites overlapped between the two independent biological replicates of the Rrm4-Ada-Gfp (blue) and control-Ada (grey) data were compared with each other. **(B)** Density plot comparing percentage editing in Rrm4-Ada-Gfp (top) and control-Ada (bottom). **(C, D)** Correlation of editing levels between two biological replicates of Rrm4-Ada-Gfp (C) and control-Ada (D) (R^2- coefficient of determination). **(E)** Schematic illustrating the iCLIP results of Rrm4, a key RBP involved in endosomal mRNA transport. The iCLIP method was employed to map the precise binding sites of Rrm4 across transcriptome (OLGEISER *et al.* 2019). Rrm4 is a broadly binding RBP that interacts with more than 60% of mRNAs in *U. maydis*. The RRM3 domain recognizes the UAUG motif on mRNA. **(F)** HyperTRIBE data of Rrm4 on the target transcript *ubi1* (UMAG_02440). Genome viewer tracks displaying RNA-seq read coverage (top panel; grey) followed by Rrm4 iCLIP crosslink signal (black) and

the corresponding Rrm4 binding sites (black) as well as hyperTRIBE signal with editing events from Rrm4-Ada-Gfp (#1-replicate 1, #2-replicate 2; blue) and control-Ada. The position of the UAUG motif is indicated in the bottom track (black). Gene model with exon/intron structures below were extended by 300 nucleotides on either side to include 5´UTR and 3´UTR regions (grey). **(G)** Percentage of Rrm4 iCLIP targets in different transcript sets as indicated in D. Statistical significance was calculated using Fisher's exact test.

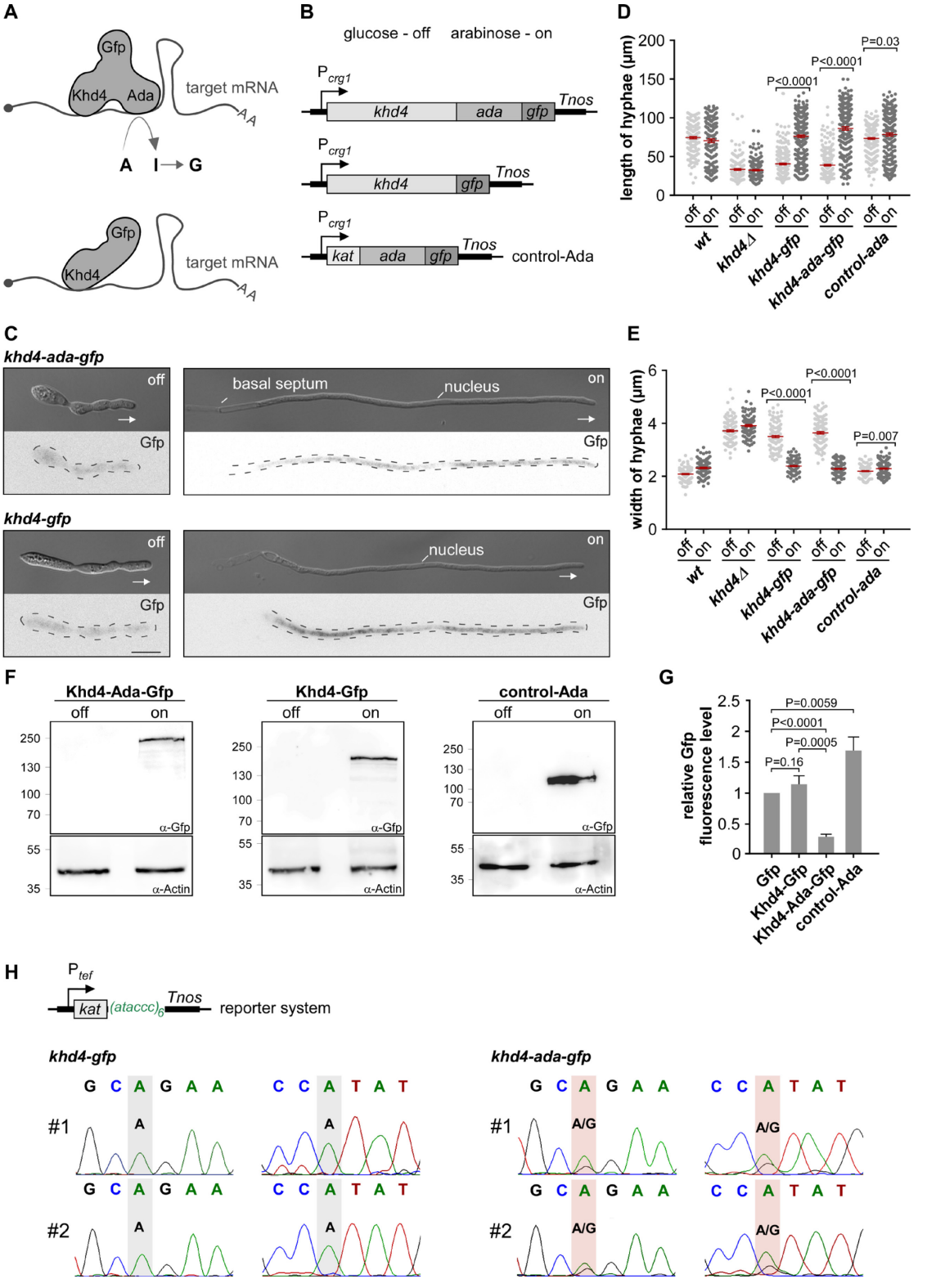

Fig. 5.6. Establishing hyperTRIBE to identify *in vivo* targets of Khd4. **(A)** Schematic illustration of the hyperTRIBE technique. The binding of Khd4-Ada-Gfp fusion protein to target mRNA results in the editing of adjacent adenosine (A) to inosine (I) which is converted to guanine (G; top). The interaction of control protein Khd4-Gfp to the target mRNA is given below (Ada- hyperactive version of *Drosophila* ADAR catalytic domain; Gfp- green fluorescent protein; AA- poly(A) tail, 5′ cap structure is depicted by a grey circle). **(B)** Schematic representation of hyperTRIBE constructs with arabinose inducible P_{crg1} promoter (on), which is repressed by glucose (off). Fusion proteins of Khd4, Ada, Gfp, and/or Kat (mKate2- red

fluorescent protein; *Tnos*- transcription terminator). The hyperTRIBE constructs are expressed in a strain carrying *khd4Δ* genetic background. **(C)** DIC (top panel) and fluorescent images (Gfp; bottom panel) of hyphae (6 h.p.i.) expressing hyperTRIBE constructs in the genetic background of the *khd4Δ* strain under promoter-uninduced off condition (left) and promoter-induced on condition (right) (arrows indicate growth direction; scale bar: 10 µm). **(D)** Length of hyphae: merged data from n=3 independent experiments (error bars: s.e.m. (red line); >100 hyphal cells per strain). Statistical analysis was conducted using the unpaired two-tailed Student's *t*-test on mean length. **(E)** Width of hyphae: merged data from n=3 independent experiments (error bars: s.e.m. (red line); >100 hyphae per strain were measured at three distinct positions within each hypha). Statistical analysis was performed using the unpaired two-tailed Student's *t*-test on mean width. **(F)** Western blot analysis of fusion proteins under uninduced (off) and induced (on) conditions. Results were analyzed with α-Gfp and α-Actin immunoblotting. The size of protein markers (kDa) is shown on the left. (Molecular weight of the full-length fusion proteins: Khd4-Ada-Gfp- ~224 kDa; Khd4-Gfp- ~179 kDa; control-Ada- ~99 kDa; Molecular weight of the individual proteins: Khd4- ~151 kDa, Ada- ~44 kDa, Gfp- ~27 kDa, Kat- ~26 kDa). **(G)** Expression levels of Ada-fusion protein under promoter-induced on condition. The Gfp fluorescence level was calculated relative to the Gfp control. Statistical analysis was performed using the unpaired two-tailed Student's t-test on mean fluorescence level (n=3 independent experiments; error bars: s.e.m.). **(H)** Upper part: reporter constructs expressing synthetic mRNAs containing *kat* coding sequence with the Khd4 binding element AUACCC (*(ataccc)*$_{6;}$ green) in its 3´ UTR, driven by a constitutively active P_{tef} promoter. Lower part: Sanger sequencing of synthetic target mRNA isolated from strains expressing control Khd4-Gfp (left panel) and Khd4-Ada-Gfp (right panel). Data shown here are from two independent experiments (#1 and #2). Edited adenosines are highlighted. Double peaks corresponding to A and G are observed at the edited site.

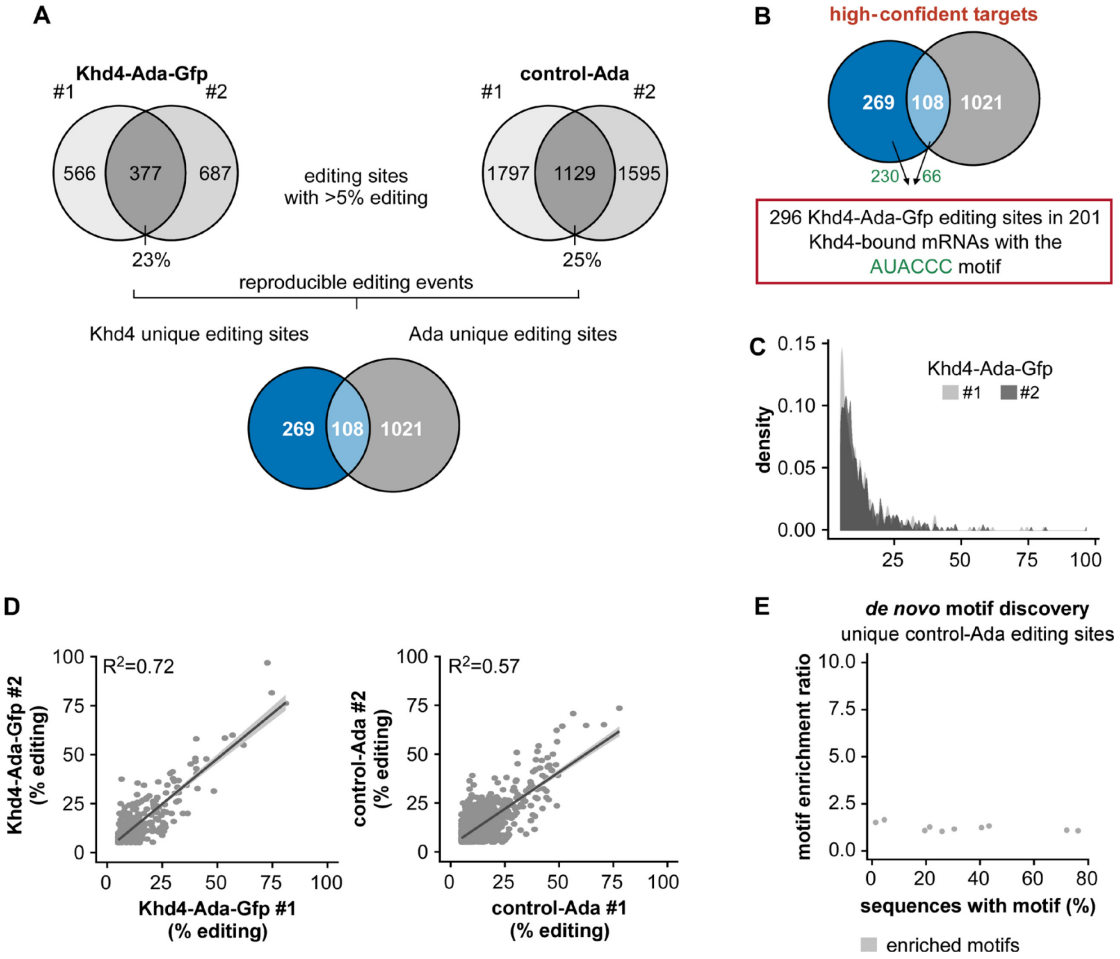

Fig. 5.7. Khd4-Ada-Gfp editing sites are highly reproducible. **(A)** Overview of the hyperTRIBE workflow. Reproducible editing sites overlapped between the two independent biological replicates of the Khd4-Ada-Gfp (blue) and control-Ada (grey) data were compared with each other (#1,2- replicates 1 and 2). Only editing events with 5% editing were used for the analysis. **(B)** The genes corresponding to the Khd4-Ada-Gfp-specific editing sites (blue) were subsequently analyzed for the presence of the AUACCC binding motif and were defined as high-confident Khd4-bound mRNAs (red). High-confident editing sites from each respective category are indicated in green. **(C)** Density plot of percentage editing events in Khd4-Ada-Gfp. **(D)** Scatter plots comparing the correlation of editing levels between two replicates (rep#1,2- replicate 1 and 2) of Khd4-Ada-Gfp and control-Ada. (R^2- coefficient of determination). **(E)** *De novo* motif discovery analysis on sequences carrying unique control-Ada editing sites. Scatter plot comparing the enrichment ratio relative to the background (grey; random genome background) with the percentage of tested sequences containing the enriched motifs.

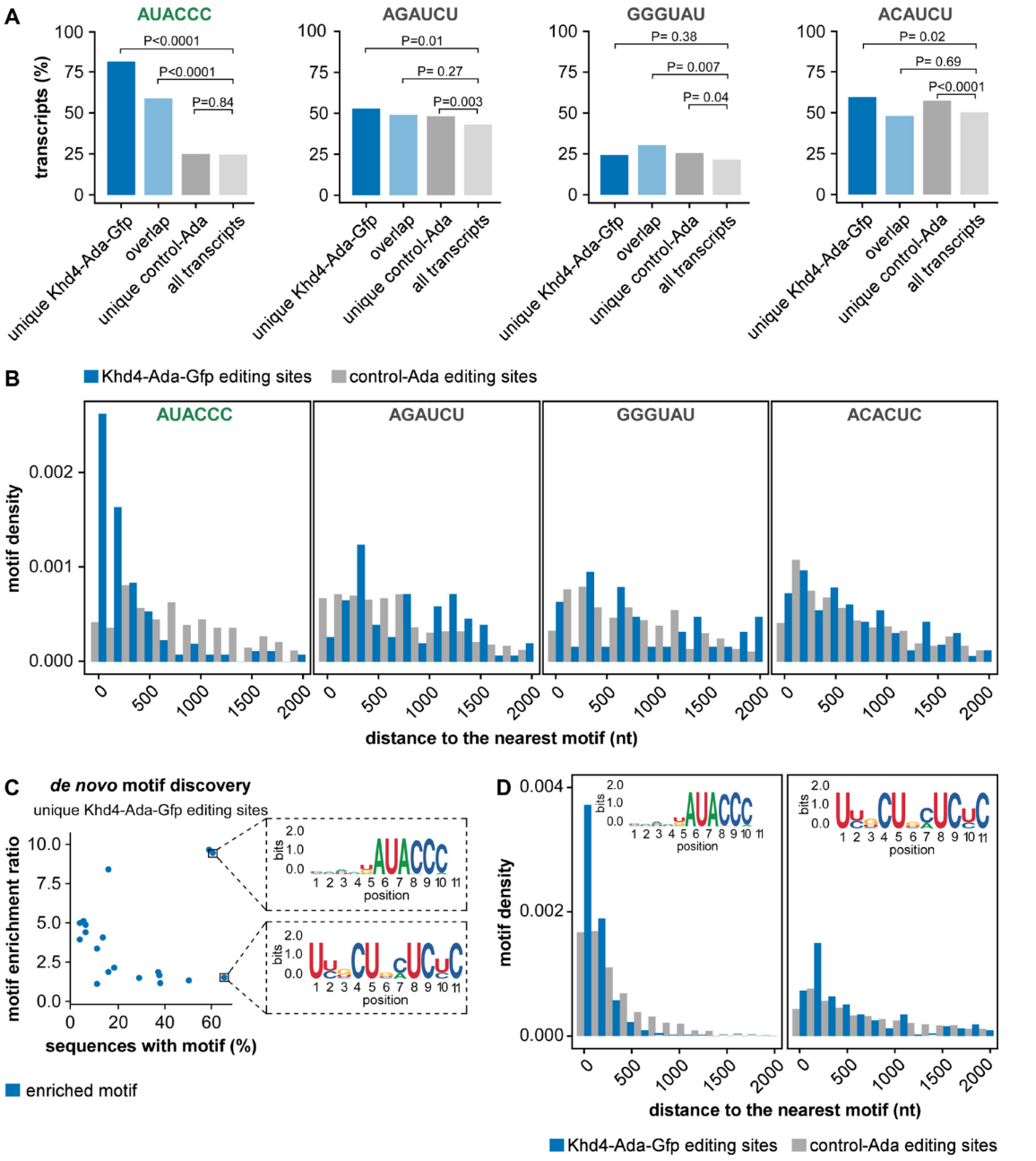

Fig. 5.8. Khd4-Ada-Gfp editing sites are proximal to the AUACCC motif. **(A)** Percentage of transcripts containing the AUACCC, AGAUCU, GGGUAU (antisense motif), and ACAUCU (scrambled sequence) motifs in different transcript sets as indicated in Fig. 2.3B. Statistical significance was determined using Fisher's exact test. **(B)** Histogram illustrating the distribution of editing sites from the nearest AUACCC, AGAUCU, GGGUAU, or ACACUC motifs in transcripts specific to Khd4-Ada-Gfp (blue) compared to control-Ada (grey). **(C)** Scatter plots comparing the relative enrichment ratio (tested sequence vs. random genome background) against the percentage of tested sequences carrying the enriched motifs (blue). Enlarged regions highlight the sequence logo of the selected motifs. Top: motif with a high enrichment ratio and overrepresentation. Bottom: highly overrepresented motif. **(D)** Histogram displaying the distribution of editing sites from the selected *de novo* discovered motifs in transcripts specific to Khd4-Ada-Gfp (blue) and control-Ada (grey). The corresponding sequence logos of the motifs are displayed inside.

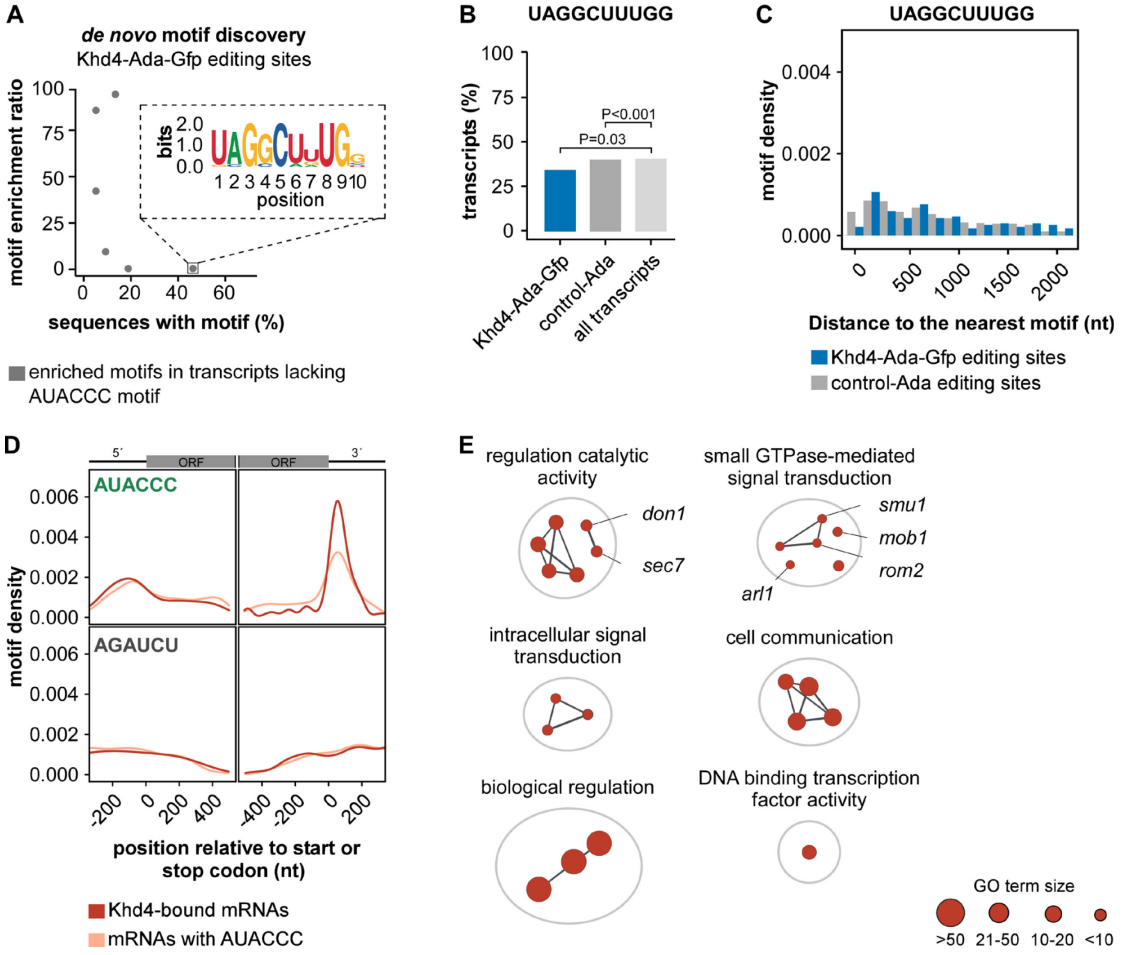

Fig. 5.9. Khd4-Ada-Gfp edited transcripts lacking the AUACCC motif do not show enrichment for other motifs. **(A)** *De novo* motif discovery analysis on transcripts that carried Khd4-Ada-Gfp editing sites but lacked the AUACCC motif. Scatter plot depicts the relative enrichment ratio (tested sequences vs. random genome background) against the percentage of tested sequences carrying the enriched motifs (grey). Enlarged region shows the sequence logo of the most represented motif. **(B)** Percentage of transcripts containing the UAGGCUUUGG motif in different transcript sets of the Venn diagram in Fig. 2.3B. Statistical significance was determined using Fisher's exact test. **(C)** Histogram illustrating the distribution of editing sites from the nearest UAGGCUUUGG motifs in transcripts specific to Khd4-Ada-Gfp (blue) compared to control-Ada (grey). **(D)** Positional maps of the AUACCC (top) and AGAUCU (bottom) motifs relative to the start (left panel) or stop codon (right panel) in Khd4-bound mRNAs (red) compared to all AUACCC-containing mRNAs (salmon). The transcript model on top shows the relative positions of the motifs in the 5′ UTR (5′; black), open reading frame (grey), and 3′ UTR (3′; black). **(E)** GO terms enrichment analysis of Khd4-bound mRNAs (g-SCS, P<0.05). Nodes (red) represent the significantly enriched GO terms, and their size corresponds to the number of genes associated with each term. The edges depict the overlap between genes associated with different GO terms. Highly similar GO terms are clustered and annotated according to the summarizing terms. GO term size is given below. Example genes corresponding to the GO terms GTPase regulator activity (GO:0030695) and small GTPase-mediated signal transduction (GO:0007264) are shown.

A

No.	UMAG_ID [a]	Annotation [b]	AUACCC [c]	GO term_ID [d]	Subcellular localization [e]
1	10152	cytokinesis protein Don1	5´UTR	0030695; 0007264	Cyotplasm
2	12272	Serine/threonine-protein kinase Smu1	5´UTR	0007264	Cyotplasm
3	06062	Rho-GAP domain-containing protein	5´UTR; ORF	0030695	Cyotplasm
4	00149	Adenylate cyclase	5´UTR; ORF	0030695; 0007264	Cyotplasm
5	01834	Uncharacterized protein	5´UTR, ORF	0030695	Cyotplasm
6	10461	SEC7 domain containing protein	ORF	0030695; 0007264	Cyotplasm
7	01378	Uncharacterized protein	ORF	0030695; 0007264	Cyotplasm
8	12185	DH domain-containing protein	ORF	0030695; 0007264	Cyotplasm
9	10305	Rab-GAP TBC domain-containing protein	ORF	0030695	Cyotplasm;Vacuole
10	15070	probable to GDP/GTP exchange factor Rom2p	ORF	0030695; 0007264	Cyotplasm
11	01161	adenylyl cyclase	ORF, 3´UTR	0030695; 0007264	Cyotplasm
12	04323	RING-type domain-containing protein	ORF, 3´UTR	0030695	Cyotplasm
13	10313	**Arl1⋆**	3´UTR	0007264	Cyotplasm;GA
14	02431	Ras-GAP domain containing protein	3´UTR	0030696	Cyotplasm
15	04352	probable MOB1 protein	3´UTR	0007264	Cyotplasm
16	11909	Putative GTP-binding protein	3´UTR	0007264	PM; Vacuole
17	00949	probable RAS GTPase-activating protein sar1	3´UTR	0030695; 0007264	Cyotplasm

GO:0030695 - GTPase regulator activity
GO:0007264- small GTPase mediated signal transduction
GA-Golgi apparatus; PM- Plasma membrane

a UMAG_IDs of target mRNAs
b *U. maydis* annotation according to PEDANT and Uniprot database
c AUACCC motif position
d GO-terms from enrichment analysis
e predicted subcellular location
⋆ Example Khd4-bound mRNA targets from Fig. 3A

B

No.	UMAG_ID [a]	Annotation [b]	AUACCC [c]	Subcellular localization [e]
1	11514	Putative High-affinity glucose transporter	5´UTR	Vacuole
2	00987	Nucleoside diphosphatase	5´UTR	Vacuole; GA
3	10210	Copper transport protein	5´UTR	Vacuole; PM
4	00956	RGS domain-containing protein	5´UTR	Vacuole; PM
5	11352	Neutral ceramidase	5´UTR; ORF; 3´UTR	ER; Vacuole; GA; Secreted
6	04796	C2 domain-containing protein	5´ UTR; ORF	ER
7	12090	Elongation of fatty acids protein	5´UTR; ORF	ER
8	10305	Rab-GAP TBC domain-containing protein	ORF	Cytoplasm; Vacuole
9	01927	1-alkyl-2-acetylglycerophosphocholine esterase	ORF	Cytoplasm; ER
10	12181	Glycosyltransferase family 31 protein	ORF	GA
11	10916	Autophag-related protein 14	ORF	Cytoplasm; endosome; Vacuole
12	00003	golgi apparatus membrane protein	ORF; 3´UTR	PM; Vacuole
13	03569	GH16 domain-containing protein	ORF; 3´UTR	PM; Vacuole
14	02224	Palmitoyltransferase	ORF; 3´UTR	ER; Vacuole; GA
15	15053	DUF3971 domain-containing protein	ORF; 3´UTR	PM; Vacuole
16	11790	**Hok1⋆**	3´UTR	Cytoplasm; EE
17	10284	Putative vacuolar sorting protein HbrA	3´UTR	Cytoplasm; Vacuole
18	04579	PITH domain-containing protein	3´UTR	ER; Cytoplasm
19	02668	SUN domain-containing protein	3´UTR	ER
20	10313	**Arl1⋆**	3´UTR	Cytoplasm; GA
21	05729	PQ loop repeat protein	3´UTR	PM; Vacuole
22	04475	Protein kinase domain-containing protein	3´UTR	PM; Vacuole
23	11406	TLC domain-containing protein	3´UTR	ER
24	11909	Putative GTP-binding protein	3´UTR	PM; Vacuole
25	05167	Secreted protein	3´UTR	Secreted; ER
26	03283	DUF4149 domain-containing protein	3´UTR	ER
27	11418	**Vma21⋆**	3´UTR	ER
28	11017	related to CAP59 (required for capsule formation)	3´UTR	ER; Vacuole; GA

ER- Endoplasmic Reticulum; GA-Golgi apparatus; PM- Plasma membrane; EE- early endosome

Fig. 5.10. Khd4 targets are enriched for membrane trafficking regulators. **(A)** Table depicting Khd4-bound mRNAs enriched for GO terms, small GTPase-mediated signal transduction (GO:0007264), and GTPase regulator activity (GO:0030695). **(B)** Khd4-bound mRNAs are manually curated for subcellular localization to the endomembrane system.

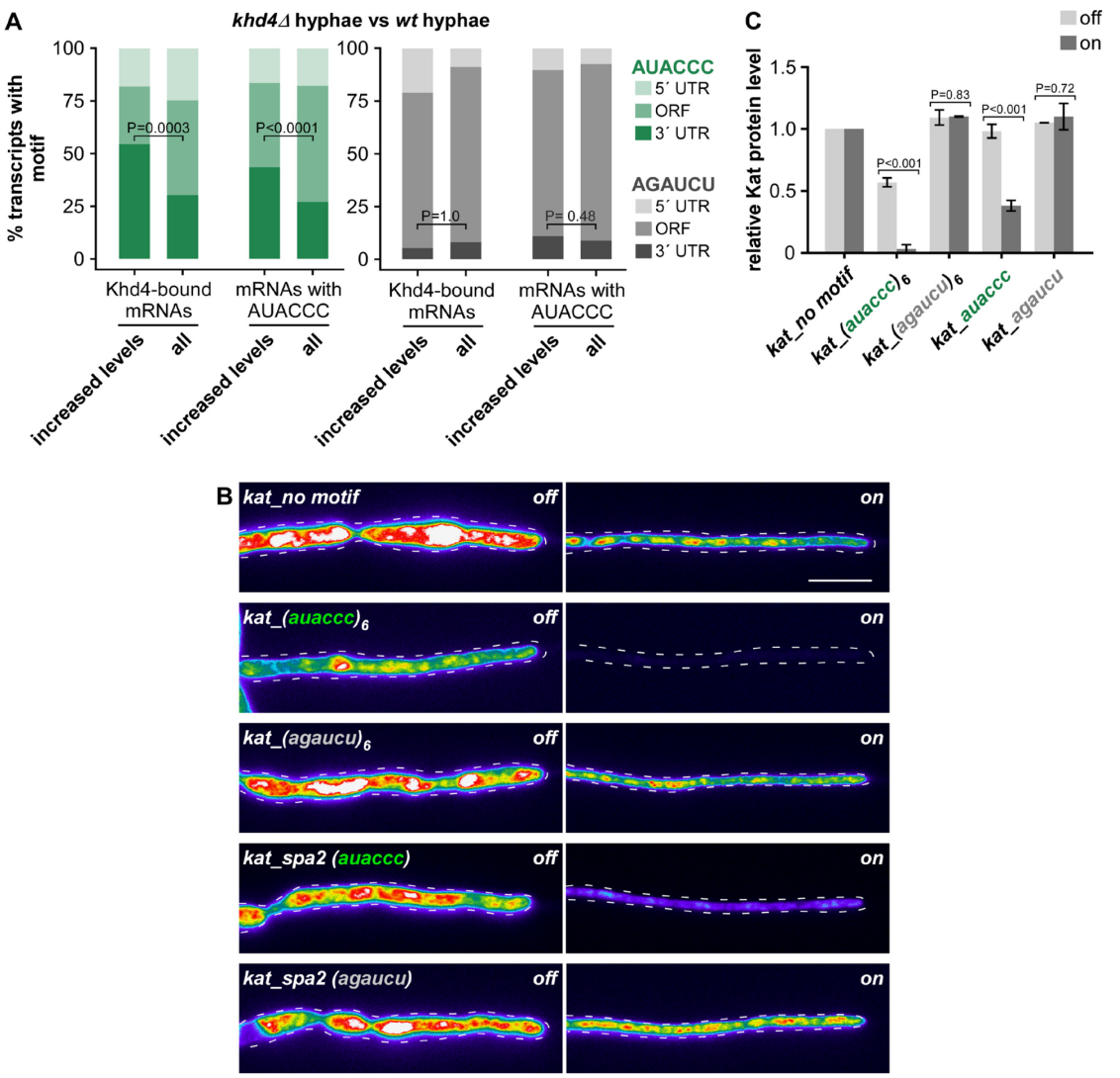

Fig. 5.11. The AUACCC motif in the 3' UTR determines protein levels. **(A)** Percentage of AUACCC (left; green) or AGAUCU (right; grey) motifs per transcript region (5′ UTR, ORF, 3′ UTR) for Khd4-bound mRNAs and mRNAs with AUACCC motifs that show increased expression levels in hyphae upon *khd4* deletion (*khd4Δ* hyphae vs. *wt* hyphae) in comparison to all mRNAs in the respective dataset. Statistical analysis was performed using Fisher's exact test. **(B)** Fluorescent micrographs in false color of hyphae (6 h.p.i.) constitutively expressing *kat* mRNA tethered to different 3′ UTR regions under Khd4-repressed off (left) and Khd4-induced on conditions (right) (*auaccc*$_6$ or *agaucu*$_6$- 3′ UTR consisting of six repeats of the respective motifs; *kat_spa2 (auaccc)*- 36 nt long endogenous 3′ UTR sequence of *spa2* gene that contains a single AUACCC motif; *kat_spa2 (agaucu)*- 36 nt long endogenous 3′ UTR sequence of *spa2* gene that contains the mutated AUACCC motif; Kat- mKate2; scale bar: 10 µm). **(C)** Shown is the modified version of Fig. 2.4E. The Kat fluorescence levels measured in on (dark grey; Khd4-induced) and off conditions (light grey; Khd4-repressed) are shown relative to control Kat levels encoded by *kat_no motif*. Statistical significance between off and on conditions was compared using multiple unpaired Student's *t*-tests. (n=3 independent experiments; error bars: s.e.m.). The presence of six copies of the AUACCC motif in 3′ UTR leads to a stronger reduction in Kat fluorescence levels, even under Khd4-repressed off condition, highlighting the robust regulatory interplay between the tandem AUACCC repeats and basal Khd4 expression.

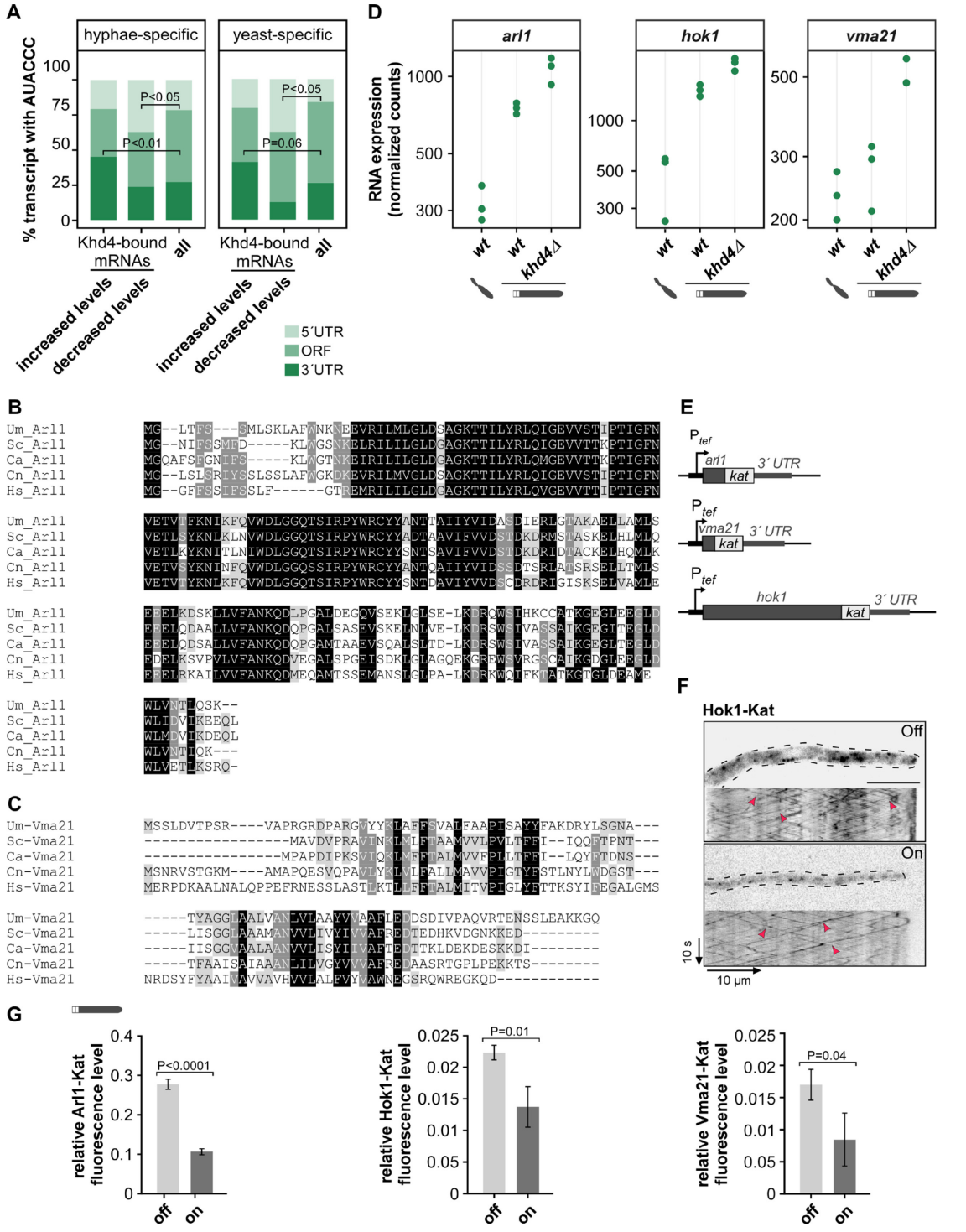

Fig. 5.12. Khd4 binding to the 3′ UTR AUACCC is crucial for determining the precise levels of mRNAs encoding membrane trafficking regulators. **(A)** Percentage of AUACCC motif per transcript region (5′ UTR, ORF, 3′ UTR) in hyphal-specific (left) and yeast-specific (right) Khd4-bound mRNAs that show increased or decreased expression levels in hyphae upon *khd4* deletion (*khd4Δ* hyphae vs. *wt* hyphae) in comparison to all mRNAs in the respective dataset (hyphal-specific or yeast-specific). Statistical analysis was carried out using Fisher's exact test. **(B)** Sequence alignments of Arl1 and **(C)** Vma21. *Um*_Arl1 from *U. maydis* (UMAG_10313), *Sc*_Arl1 from *S. cerevisiae* (NP_009723.3), *Ca*_Arl1 from *C. albicans* (XP_722675.1), *Cn*_Arl1 from *C. neoformans* (XP_012049462.1), *Hs*_Arl1 from *Homo Sapiens* (NP_001168.1). Likewise, *Um*_Vma21 from *U. maydis* (UMAG_11418), *Sc*_ Vma21 from *S. cerevisiae* (NP_011619.3), *Ca*_ Vma21 from *C. albicans* (XP_019330812.1), *Cn*_ Vma21 from *C. neoformans*

(XP_024513701.1), *Hs_* Vma21 from *Homo Sapiens* (NP_001017980.1). **(D)** Plot showing mRNA expression levels (normalized RNA-seq read counts) of target mRNAs namely, *arl1*, *hok1,* and *vma21* in *wt* yeast, *wt* hyphae, and *khd4Δ* hyphae. Green dots represent the values from three biological replicates. **(E)** Ectopic expression constructs of target mRNAs, *arl1*, *vma21*, and *hok1*. ORFs of target mRNAs and the fluorescent tag, *kat* are shown in dark and light grey, respectively. The 3' UTR region (dark grey) was derived from the endogenous 500 bp sequence downstream of the respective target gene stop codon. The constructs were expressed ectopically using the constitutively active P_{tef} promoter. **(F)** Inverted fluorescent images and the corresponding kymographs of hyphal cells constitutively expressing Hok1-Kat in a genetic background of the arabinose inducible Khd4-GFP, under Khd4-repressed off (left) and Khd4-induced on (right) conditions. In the Khd4-repressed off condition, the Hok1-Kat signal was more pronounced on shuttling early endosomes. Red arrowheads indicate the processive signals. Scale bar: 10 µm. **(G)** Expression levels of target proteins in hyphal cells under Khd4-induced on and Khd4-repressed off conditions, measured by Kat fluorescent intensity. The fluorescence level relative to the constitutively expressed Kat control *(kat_no motif)* is given. Statistical evaluation of the relative fluorescent intensity between off and on conditions was performed using unpaired Student's *t*-test (n=3 independent experiments; error bars: s.e.m).

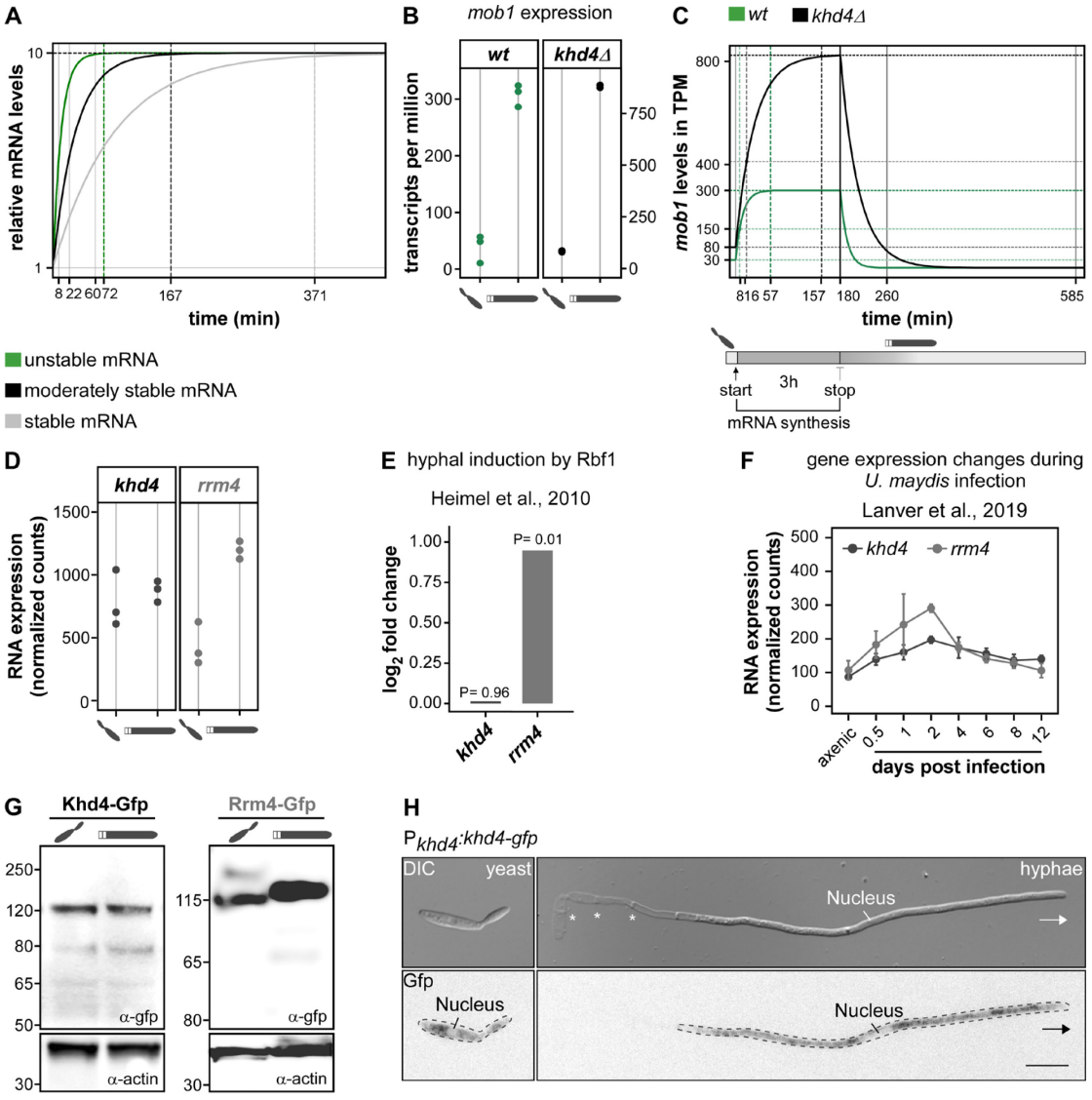

Fig. 5.13. Unstable mRNAs are crucial for rapid gene expression changes. **(A)** Single-compartment model describing induction kinetics of how exemplary mRNAs reach the same steady-state levels with different mRNA half-lives. The unstable mRNA reaches the new steady-state levels (10-fold increase) already after 72 min, compared to 167 min for moderately stable and >300 min for the stable mRNA. Green: Unstable mRNAs with rapid synthesis (0.87 transcripts/min) and short half-life ($t_{1/2}$ = 8 min, similar to *mob1* mRNA). Black: Moderately stable mRNAs with intermediate synthesis rate (0.3 transcripts/min) and half-life ($t_{1/2}$ = 22 min). Grey: Stable mRNA with slow synthesis (0.12 transcripts/min) and long half-life similar to *actin* mRNA ($t_{1/2}$ = 60 min). The half-life data is acquired from *S. cerevisiae* (MILLER *et al.* 2011). The horizontal dashed line indicates the steady-state level (10-fold increase). The vertical dashed lines indicate the mRNA half-lives. **(B)** Steady-state levels of *mob1* in yeast and hyphal stages of wildtype (*wt,* green; left panel) and *khd4*Δ cells (black; right panel). The *mob1* levels are given in transcripts per million (TPM). The hyphal induction in wildtype cells causes a ~10-fold increase in *mob1* level. While the 10-fold increase persisted, the deletion of *khd4* caused elevated *mob1* levels in both yeast and hyphal cells. **(C)** Model-predicted induction kinetics and half-lives for *mob1* mRNA in *wt* and *khd4*Δ cells. Bottom: Schematic of *mob1* induction. The synthesis rate of *mob1* increases during hyphal morphogenesis, resulting in a 10-fold induction measured in our RNA-seq. To visualize the transcriptional shutdown, we arbitrarily assumed that *mob1* transcription ceases after 3 hours, resulting in a return to its original steady-state level. Top: Changes in *mob1* steady-state levels in *wt* (green) and *khd4*Δ (black) cells following the switch from yeast to hyphae. Based on the single-component model, *mob1* mRNA reaches its steady-state level within 57

min of induction in *wt* cells. Moreover, the model predicts that *mob1* mRNA should be stabilized to a half-life of ~22 min in *khd4*Δ cells to account for the measured increase in *mob1* steady-state levels without altering the synthesis rate. The induction kinetics in *khd4*Δ cells are substantially delayed, reaching steady-state levels only after ~157 min. The same is observed after transcriptional shutdown, whereby *mob1* expression reverts to the original steady-state levels within ~80 min in *wt* cells vs. ~400 min in *khd4*Δ cells. The vertical dashed lines indicate the half-life of the corresponding mRNAs. The horizontal dashed lines show the half-maximal levels (light green, light grey for *wt* and *khd4*Δ, respectively) and new steady-state levels (green, black for *wt* and *khd4*Δ, respectively). **(D)** mRNA expression levels (normalized RNA-seq read counts) of *khd4* and *rrm4* in *wt* yeast and hyphal cells. Black and grey dots represent the count values of *khd4* and *rrm4* from n=3 biological replicates. **(E)** Changes in gene expression levels (log_2-transformed fold change; microarray analysis (HEIMEL *et al.* 2010b)) for *khd4* (black) and *rrm4* (grey) after induction of the master regulator Rbf1 required for hyphae formation (HEIMEL *et al.* 2010b). Adjusted P-values from the gene expression analysis are shown on top. **(F)** Changes in gene expression for *khd4* and *rrm4* during pathogenic development of *U. maydis*. The time-course RNA-seq expression data presented here is acquired from (LANVER *et al.* 2018). **(G)** Western blot analysis to examine the expression levels of endogenous Khd4 and Rrm4, which were tagged with Gfp at the C-terminus, in *wt* yeast and hyphal cells. Immunoblotting was performed using α-Gfp and α-Actin. The size of protein markers (kDa) is shown on the left (molecular weight of the proteins: Khd4- ~151 kDa, Rrm4- ~85 kDa, Gfp- ~27 kDa). **(H)** DIC (top) and fluorescence images (bottom) of AB33 yeast (left) and hyphae expressing endogenous Khd4 fused with Gfp at its C terminus (arrows and asterisks indicate growth direction and empty sections, respectively; scale bar: 10 μm).

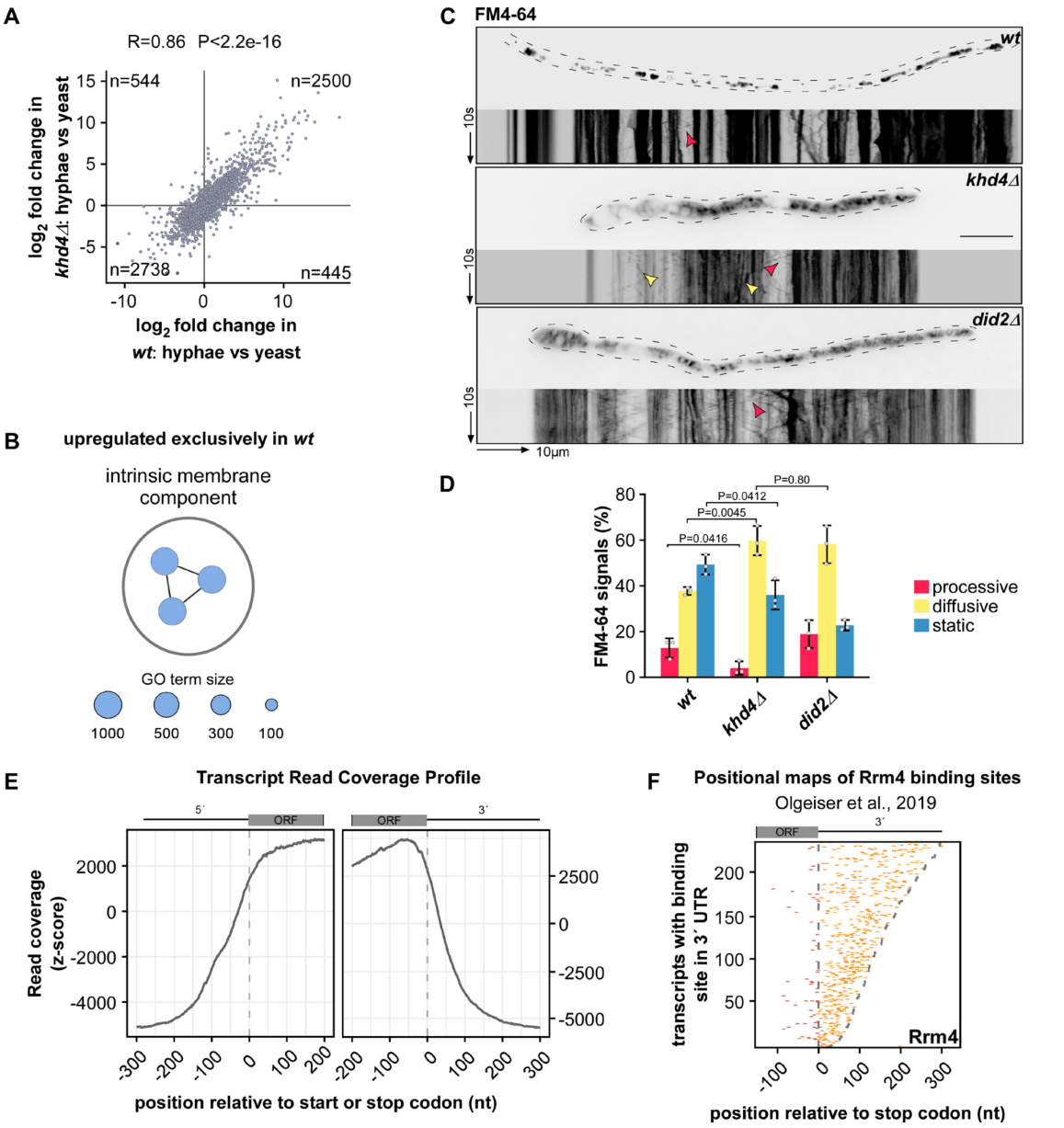

Fig. 5.14. Loss of Khd4 triggers defects in membrane trafficking dynamics. **(A)** Scatter plot comparing the log_2-transformed fold change of genes in *wt* and *khd4*Δ cells upon hyphal induction (*wt*: hyphae vs. yeast and *khd4*Δ: hyphae vs. yeast, respectively). The number of data points in each quadrant is shown inside. (Pearson correlation coefficient R=0.86, P<2.26e-16). **(B)** Gene ontology (GO) terms that are significantly (P<0.05, multiple-testing correction with g: SCS algorithm) overrepresented in upregulated genes that are specific to *wt* cells (light blue) after hyphal induction (orange; >1.5-fold change, P<0.05, Benjamini-Hochberg corrections, >10 average normalized reads). The reference GO term sizes are given below. **(C)** Inverted micrographs (top panel) of AB33 hyphae derivatives (10 h.p.i.) after 25 min of FM4-64 staining. The corresponding kymograph is shown below. (top- wildtype; center- *khd4Δ*; bottom- *did2Δ*; processive and diffusive signals are indicated with red and yellow arrowheads, respectively; scale bar: 10 µm). **(D)** Bar chart depicting the amount of FM4-64 signals (%) in AB33-derived hyphal cells (>25 hyphal cells per strain; error bars: s.e.m.; grey dots represent independent experiments, n=3; signals were scored as processive (red) if the run length is >5 µm, diffusive (yellow) if the run length is <5 µm but >0 µm, static (blue) when the run length is ~0 µm; unpaired Student's *t*-test). **(E)** Normalized read coverage in 5′ and 3′ UTR regions relative to start or stop codon for transcripts expressed in *U. maydis* hyphal cells (9.h.p.i.). The gene model on top shows the relative positions of the ORF and UTRs (5′, 3′- 5′ UTR, and 3′ UTR,

respectively; black). Transcripts are ordered by increasing UTR length. **(F)** Positional maps of Rrm4 iCLIP binding sites relative to stop codon. The 234 randomly selected target transcripts are displayed, highlighting the Rrm4 binding sites (orange) within their 3′ UTR regions. The 3′ UTR region in these transcripts was annotated manually using RNA-seq data obtained from *U. maydis* hyphal cells (2). Grey dotted line depicts the borders of 3′ UTR (this figure is modified and reused from OLGEISER *et al.* 2019). Transcripts are ordered by decreasing UTR length.

5.2.4 Supporting Information Tables

Table 1: Description of *U. maydis* strains used in this study

Strain name with code	locus	Progenitor strain	Short description
AB33 (UMa133)	*b*	FB2	*a2 Pnar: bW2 bE1,* expresses the heteromeric bW/bE transcription factor under the control of inducible P_{nar1} promoter. Hyphal growth is induced by changing the nitrogen source.
AB33 khd4Δ (UMa482)	*khd4*	AB33	Carries *khd4* deletion
AB33 did2Δ (UMa934)	*did2*	AB33	Carries *did2* deletion
AB33 rrm4-gfp (UMa427)	*rrm4*	AB33	Expresses Rrm4 C-terminally fused to eGFP
AB33 khd4-gfp (UMa869)	*khd4*	AB33	Expresses Khd4 C-terminally fused to eGFP
AB33 P_{crg1}: rrm4-ada-gfp / rrm4Δ (UMa2805)	*ip*^{s}	AB33 rrm4Δ	Expresses Rrm4-Ada-Gfp fusion protein under the control of the arabinose-inducible P_{crg1} promoter. The construct is ectopically integrated into the *ip*^{s} locus of the strain carrying *rrm4* deletion.
AB33 P_{crg1}: rrm4 -gfp / rrm4Δ (UMa2805)	*ip*^{s}	AB33 rrm4Δ	Expresses Rrm4- Gfp fusion protein under the control of the arabinose-inducible P_{crg1} promoter. The construct is ectopically integrated into the *ip*^{s} locus of the strain carrying *rrm4* deletion.
AB33 P_{crg1}: khd4-ada-gfp / khd4Δ (UMa2988)	*ip*^{s}	AB33 khd4Δ	Expresses Khd4-Ada-Gfp fusion protein under the control of the arabinose-inducible P_{crg1} promoter. The construct is ectopically integrated into the *ip*^{s} locus of the strain carrying *khd4* deletion.
AB33 P_{crg1}: khd4-gfp / khd4Δ (UMa2989)	*ip*^{s}	AB33 khd4Δ	Expresses Khd4-Gfp fusion protein under the control of the arabinose-inducible P_{crg1} promoter. The construct is ectopically integrated into the *ip*^{s} locus of the strain carrying *khd4* deletion.
AB33 P_{crg1}: kat-ada-gfp (UMa3083)	*ip*^{s}	AB33	Expresses Kat-Ada-Gfp fusion protein under the control of the arabinose-inducible P_{crg1} promoter. The construct is ectopically integrated into the *ip*^{s} locus.
AB33 P_{crg1}: khd4-gfp / khd4Δ / upp3Δ (UMa3138)	*upp3*	AB33 P_{crg1}: khd4-gfp / khd4Δ	*upp3* deletion in the strain that carries *khd4* deletion and ectopically expresses *khd4-gfp* under the control of the arabinose-inducible P_{crg1} promoter

AB33 P_{crg1}: khd4-ada-gfp / khd4Δ / upp3Δ (UMa3290)	*upp3*	AB33 P_{crg1}: khd4-ada-gfp / khd4Δ	*upp3* deletion in the strain that carries *khd4* deletion and ectopically expresses *khd4-ada-gfp* under the control of arabinose inducible P_{crg1} promoter.
AB33 P_{tef}: kat_$(auaccc)_6$ / P_{crg1}: khd4-ada-gfp / khd4Δ / upp3Δ (UMa3293)	*upp3*	AB33 P_{crg1}: khd4-ada-gfp / khd4Δ / upp3Δ	Expression of *mkate2 (kat)* ORF containing six tandem repeats of the *auaccc* motif in its 3′ UTR using the constitutively active P_{tef} promoter. The construct is integrated into the *upp3Δ* locus of the strain ectopically expressing *khd4-ada-gfp* under the control of the P_{crg1} promoter and carrying *khd4* deletion.
AB33 P_{tef}: kat_$(auaccc)_6$ / P_{crg1}: khd4-gfp / khd4Δ / upp3Δ (UMa3140)	*upp3*	AB33 P_{crg1}: khd4-gfp / khd4Δ / upp3Δ	Expression of *kat* ORF containing six tandem repeats of the *auaccc* motif in its 3′ UTR using the constitutively active P_{tef} promoter. The construct is integrated into the *upp3Δ* locus of the strain expressing *khd4-gfp* ectopically under the control of the P_{crg1} promoter and carrying the *khd4* deletion.
AB33 P_{tef}: kat_no motif / P_{crg1}: khd4-gfp / khd4Δ / upp3Δ (UMa3139)	*upp3*	AB33 P_{crg1}: khd4-gfp / khd4Δ / upp3Δ	Expression of *kat* ORF containing no motif in its 3′ UTR using the constitutively active P_{tef} promoter. The construct is integrated into the *upp3Δ* locus of the strain expressing *khd4-gfp* ectopically under the control of the P_{crg1} promoter and carrying the *khd4* deletion.
AB33 P_{tef}: kat_$(agaucu)_6$ / P_{crg1}: khd4-gfp / khd4Δ / upp3Δ (UMa3141)	*upp3*	AB33 P_{crg1}: khd4-gfp / khd4Δ / upp3Δ	Constitutively expresses the *kat* ORF containing six tandem repeats of the *agaucu* motif in its 3′ UTR under the control of the P_{tef} promoter. The construct is integrated into the *upp3Δ* locus of the strain expressing *khd4-gfp* ectopically under *hd4* deletion. the control of the P_{crg1} promoter and carrying the *k*
AB33 P_{tef}: kat_(auaccc) / P_{crg1}: khd4-gfp /khd4Δ/upp3Δ (UMa3238)	*upp3*	AB33 P_{crg1}: khd4-gfp / khd4Δ / upp3Δ	Expression of the *kat* ORF carrying 36 nt 3′ UTR sequences from *spa2* gene which contains one *auaccc* motif. Constitutive expression was carried out using the P_{tef} promoter. The construct is integrated into the *upp3Δ* locus of the strain expressing *khd4-gfp* ectopically under the control of the P_{crg1} promoter and carrying the *khd4* deletion.
AB33 P_{tef}: kat_(agaucu) / P_{crg1}: khd4-gfp /khd4Δ/upp3Δ (UMa3239)	*upp3*	AB33 P_{crg1}: khd4-gfp / khd4Δ / upp3Δ	Expression of the *kat* ORF carrying 36 nt 3′ UTR sequences from *spa2* gene where *auaccc* sequence is mutated to *agaucu*. Constitutively active P_{tef} promoter was used for expression. The construct is integrated into the

			upp3Δ locus of the strain expressing *khd4-gfp* ectopically under the control of the P_{crg1} promoter and carrying the *khd4* deletion.
AB33 P_{tef}: arl1-kat_ arl1 3′ UTR / P_{crg1}: khd4-gfp /khd4Δ/upp3Δ (UL0008)	*upp3*	AB33 P_{crg1}: khd4-gfp / khd4Δ / upp3Δ	Constitutive expression of target mRNA *arl1* fused with *kat* using P_{tef} promoter. 500 nt long endogenous sequence downstream of the *arl1* stop codon was used as the 3′ UTR region The construct is integrated into the *upp3Δ* locus of the strain expressing *khd4-gfp* ectopically under the control of the P_{crg1} promoter and carrying the *khd4* deletion.
AB33 P_{tef}: hok1-kat_ hok1 3′ UTR / P_{crg1}: khd4-gfp /khd4Δ/upp3Δ (UL0012)	*upp3*	AB33 P_{crg1}: khd4-gfp / khd4Δ / upp3Δ	Constitutive expression of target mRNA *hok1* fused with *kat* using P_{tef} promoter. 500 nt long endogenous sequence downstream of the *hok1* stop codon was used as the 3′ UTR region. The construct is integrated into the *upp3Δ* locus of the strain expressing *khd4-gfp* ectopically under the control of the P_{crg1} promoter and carrying the *khd4* deletion.
AB33 P_{tef}: vma21-kat_ vma21 3′ UTR / P_{crg1}: khd4-gfp /khd4Δ/upp3 (UL0009)	*upp3*	AB33 P_{crg1}: khd4-gfp / khd4Δ / upp3Δ	Constitutive expression of target mRNA *vma21* fused with *kat* using P_{tef} promoter. 500 nt long endogenous sequence downstream of the *vma21* stop codon was used as the 3′ UTR region. The construct is integrated into the *upp3Δ* locus of the strain expressing *khd4-gfp* ectopically under the control of the P_{crg1} promoter and carrying the *khd4* deletion.

UMa & UL: internal strain reference number; Kat: mKate2, a monomeric form of the red fluorescent protein; eGFP- enhanced GFP.

Table 2: Generation of *U. maydis* strains used in this study

Strain name	Relevant genotypes	Strain code	Progenitor strain	Transformed plasmid	Locus	References
AB33	*a2 Pnar:bW2 bE1*	UMa133	FB2	pAB33	*b*	BRACHMANN *et al.* 2004
AB33 khd4Δ	*khd4*	UMa482	AB33	pUMa1142	*khd4*	VOLLMEISTER *et al.* 2009
AB33 did2Δ	*did2*	UMa934	AB33	pUMa1699	*did2*	HAAG *et al.* 2017
AB33 rrm4-gfp	*rrm4*	UMaxxx	AB33	pUMa496	*rrm4*	BECHT *et al.* 2006

AB33 khd4-gfp	*khd4*	UMa869	AB33	pUMa1484	*khd4*	VOLLMEISTER *et al.* 2009
AB33 P_{crg1}: rrm4-ada-gfp / rrm4Δ	*rrm4Δ / rrm4-ada-gfp*	UMa2805	AB33 rrm4Δ	pUMa3975	*ip^s*	This study
AB33 P_{crg1}: rrm4- gfp / rrm4Δ	*rrm4Δ / rrm4-gfp*	UMa2807	AB33 rrm4Δ	pUMa3981	*ip^s*	This study
AB33 P_{crg1}: khd4-ada-gfp / khd4Δ	*khd4Δ / khd4-ada-gfp*	UMa2988	AB33 khd4Δ	pUMa4057	*ip^s*	This study
AB33 P_{crg1}: khd4-gfp / khd4Δ	*khd4Δ / khd4-ada-gfp*	UMa2989	AB33 khd4Δ	pUMa4080	*ip^s*	This study
AB33 P_{crg1}: kat-ada-gfp	*kat-ada-gfp*	UMa3083	AB33	pUMa4290	*ip^s*	This study
AB33 P_{crg1}: khd4-gfp / khd4Δ / upp3Δ	*khd4Δ / khd4-gfp / upp3Δ*	UMa3138	AB33 P_{crg1}: khd4-gfp / khd4Δ	pUMa4378	*upp3*	This study
AB33 P_{crg1}: khd4- ada-gfp / khd4Δ / upp3Δ	*khd4Δ / khd4-ada-gfp / upp3Δ*	UMa3290	AB33 P_{crg1}: khd4-ada-gfp / khd4Δ	pUMa4378	*upp3*	This study
AB33 P_{tef}: kat_$(auaccc)_6$ / P_{crg1}: khd4-ada-gfp / khd4Δ / upp3Δ	*khd4Δ / khd4-ada-gfp / upp3Δ*	UMa3293	AB33 P_{crg1}: khd4-ada-gfp / khd4Δ / upp3Δ	pUMa4385	*upp3*	This study
AB33 P_{tef}: kat_$(auaccc)_6$ / P_{crg1}: khd4-gfp / khd4Δ / upp3Δ	*khd4Δ / khd4-gfp / upp3Δ*	UMa3140	AB33 P_{crg1}: khd4-gfp /	pUMa4385	*upp3*	This study

			khd4Δ / upp3Δ			
AB33 P_{tef}: kat_no motif / P_{crg1}: khd4-gfp / khd4Δ / upp3Δ	*khd4Δ / khd4-gfp / upp3Δ*	UMa3139	AB33 P_{crg1}: khd4-gfp / khd4Δ / upp3Δ	pUMa4383	*upp3*	This study
AB33 P_{tef}: kat_$(agaucu)_6$ / P_{crg1}: khd4-gfp / khd4Δ / upp3Δ	*khd4Δ / khd4-gfp / upp3Δ*	UMa3141	AB33 P_{crg1}: khd4-gfp / khd4Δ / upp3Δ	pUMa4384	*upp3*	This study
AB33 P_{tef}: kat_(auaccc) / P_{crg1}: khd4-gfp / khd4Δ / upp3Δ	*khd4Δ / khd4-gfp / upp3Δ*	UMa3238	AB33 P_{crg1}: khd4-gfp / khd4Δ / upp3Δ	pUMa4531	*upp3*	This study
AB33 P_{tef}: kat_(agaucu) / P_{crg1}: khd4-gfp / khd4Δ / upp3Δ	*khd4Δ / khd4-gfp / upp3Δ*	UMa3239	AB33 P_{crg1}: khd4-gfp / khd4Δ / upp3Δ	pUMa4532	*upp3*	This study
AB33 P_{tef}: arl1-kat_ arl1 3′ UTR / P_{crg1}: khd4-gfp / khd4Δ / upp3Δ	*khd4Δ / khd4-gfp / upp3Δ / arl1-kat*	UL0008	AB33 P_{crg1}: khd4-gfp / khd4Δ / upp3Δ	pUL0007	*upp3*	This study
AB33 P_{tef}: hok1-kat_ hok1 3′ UTR / P_{crg1}: khd4-gfp / khd4Δ / upp3Δ	*khd4Δ / khd4-gfp / upp3Δ / hok1-kat*	UL0012	AB33 P_{crg1}: khd4-gfp / khd4Δ / upp3Δ	pUL0011	*upp3*	This study

AB33 P_{tef}: vma21-kat_ vma21 3´ UT / P_{crg1}: khd4-gfp / khd4Δ / upp3Δ	*khd4Δ / khd4-gfp / upp3Δ / vma21 -kat*	UL0009	AB33 P_{crg1}: khd4-gfp / khd4Δ / upp3Δ	pUL0008	*upp3*	This study

UMa & UL: internal strain reference number; pUMa & pUL: internal plasmid reference number.

Table 3: Description of plasmids used for strain generation in this study

Plasmid name	Plasmid code	Resistance cassette	Short description
p P_{crg1}: Rrm4-Ada-Gfp (CbxR)	pUMa3975	CbxR (for integration into *ip* locus)	Plasmid for ectopic integration and expression of Rrm4-Ada-Gfp. The 2379 bp *rrm4*-ORF is fused C-terminally to the 1200 bp *adar* catalytic domain (Ada) with three repeats of GGGGS linker in between, followed by eGFP fusion. The construct is under the control of arabinose inducible P_{crg1} promoter and flanked by the T_{nos}-terminator.
p P_{crg1}: Rrm4-Gfp (CbxR)	pUMa3981	CbxR (for integration into *ip* locus)	Plasmid for ectopic integration and expression of Rrm4-Gfp. The 2379 bp *khd4*-ORF is fused C-terminally with eGFP. The construct is flanked upstream and downstream by the arabinose inducible P_{crg1} promoter and the T_{nos}-terminator, respectively.
p P_{crg1}: Khd4-Ada-Gfp (CbxR)	pUMa4057	CbxR (for integration into *ip* locus)	Plasmid for ectopic integration and expression of Khd4-Ada-Gfp. The 4282 bp *khd4*-ORF is fused C-terminally to the 1200 bp *adar* catalytic domain (Ada) with three repeats of GGGGS linker in between, followed by eGFP fusion. The construct is under the control of arabinose inducible P_{crg1} promoter and flanked by the T_{nos}-terminator.
p P_{crg1}: Khd4-Gfp (CbxR)	pUMa4080	CbxR (for integration into *ip* locus)	Plasmid for ectopic integration and expression of Khd4-Gfp. The 4282 bp *khd4*-ORF is fused C-terminally with eGFP. The construct is flanked upstream and downstream by the arabinose inducible P_{crg1} promoter and the T_{nos}-terminator, respectively.

p P_{crg1}: Kat-Ada-Gfp (CbxR)	pUMa4290	CbxR (for integration into *ip* locus)	Plasmid for ectopic integration and expression of Kat-Ada-Gfp. Like p P_{crg1}: Khd4-Ada-Gfp (CbxR) but *khd4*-ORF was replaced with *kat*-ORF.
p Upp3Δ (G418R)	pUMa4378	G418R (Sfi1-insert of pMF1-g)	Plasmid used for *upp3* deletion. The G418R cassette is flanked upstream by 1.5 kb and downstream by 1.9kb of the immediate genomic region flanking *upp3.* The resistance cassette is derived from pMF1-g. (SARKARI *et al.* 2014, BAUMANN *et al.* 2012)
p P_{tef}: Kat_$(AUACCC)_6$ (NatR)	pUMa4385	NatR (Sfi1-insert of pMF-1n)	Plasmid for the ectopic expression of Kat reporter at *upp3Δ* locus. Six tandem repeats of the *auaccc* motif were placed at the 3′ UTR region of *kat*-ORF and expressed under the control of constitutively active P_{tef} promoter. The construct contains a T_{nos} terminator, and a nourseothricin-resistance cassette and is flanked by upstream and downstream regions of the *upp3Δ* locus for homologous recombination.
p P_{tef}: Kat (NatR)	pUMa4383	NatR (Sfi1-insert of pMF-1n)	Plasmid for the ectopic expression of Kat reporter at *upp3Δ* locus. Like p P_{tef}: Kat_$(AUACCC)_6$ (NatR) but contains no specific motif in the 3′ UTR region The *kat*-ORF is immediately followed by a T_{nos} terminator. Reporter expression is carried out by the constitutively active P_{tef} promoter. The construct contains a nourseothricin-resistance cassette and is flanked by upstream and downstream regions of the *upp3Δ* locus for homologous recombination.
p P_{tef}: Kat_$(AGAUCU)_6$ (NatR)	pUMa4384	NatR (Sfi1-insert of pMF-1n)	Plasmid for the ectopic expression of Kat reporter at *upp3Δ* locus. Like p P_{tef}: Kat_$(AUACCC)_6$ (NatR) but contains six tandem repeats of *agaucu* motif in the 3′ UTR region Reporter expression is carried out by the constitutively active P_{tef} promoter. The construct contains a T_{nos} terminator and a nourseothricin-resistance cassette and is flanked by upstream and downstream regions of the *upp3Δ* locus for homologous recombination.

p P_{tef}: Kat_Spa2 short (AUACCC) (NatR)	pUMa4531	NatR (Sfi1-insert of pMF-1n)	Plasmid for the ectopic expression of Kat reporter at *upp3Δ* locus. Like p P_{tef}: Kat_$(AUACCC)_6$ (NatR) but consists of 36 nt 3′ UTR sequence from *spa2* gene, containing one *auaccc* motif, in its 3′ UTR region. Reporter expression is carried out by the constitutively active P_{tef} promoter. The construct contains a T_{nos} terminator and a nourseothricin-resistance cassette and is flanked by upstream and downstream regions of the *upp3Δ* locus for homologous recombination.
p P_{tef}: Kat_Spa2 short (AGAUCU) (NatR)	pUMa4532	NatR (Sfi1-insert of pMF-1n)	Plasmid for the ectopic expression of Kat reporter at *upp3Δ* locus. Like p P_{tef}: Kat_Spa2 short (AUACCC) (NatR) but the *auaccc* motif is mutated to *agaucu*. Reporter expression is carried out by the constitutively active P_{tef} promoter. The construct contains a T_{nos} terminator and a nourseothricin-resistance cassette and is flanked by upstream and downstream regions of the *upp3Δ* locus for homologous recombination.
p P_{tef}: Arl1-Kat_3′ UTR arl1 (NatR)	pUL0007	NatR (Sfi1-insert of pMF-1n)	Plasmid expressing target mRNA *arl1* ectopically at *upp3Δ* locus. The 739 bp long *arl1*-ORF is fused C-terminally to Kat and expressed under the control of the constitutive P_{tef} promoter. ~ 500 bp long endogenous sequence downstream of the *arl1* stop codon was used as the 3′ UTR region. The construct contains a T_{nos}-terminator and a nourseothricin-resistance cassette and is flanked by upstream and downstream regions of the *upp3Δ* locus for homologous recombination.
p P_{tef}: Hok1-Kat_3′ UTR hok1 (NatR)	pUL0011	NatR (Sfi1-insert of pMF-1n)	Plasmid expressing target mRNA *hok1* ectopically at *upp3Δ* locus. The 2814 bp long *hok1*-ORF is fused C-terminally to Kat and expressed under the control of the constitutive P_{tef} promoter. ~ 500 bp long endogenous sequence downstream of *hok1* stop codon was used as the 3′ UTR region. The construct contains a T_{nos}-terminator and a nourseothricin-resistance cassette

			and is flanked by upstream and downstream regions of the *upp3Δ* locus for homologous recombination.
p P_{tef}: Vma21-Kat_3′ UTR vma21 (NatR)	pUL0008	NatR (Sfi1-insert of pMF-1n)	Plasmid expressing target mRNA *arl1* ectopically at *upp3Δ* locus. The 385 bp long *vma21*-ORF is fused C-terminally to Kat and expressed under the control of the constitutive P_{tef} promoter. A 500 bp long endogenous sequence downstream of the *vma21* stop codon was used as the 3′ UTR region. The construct contains a T_{nos}-terminator and a nourseothricin-resistance cassette and is flanked by upstream and downstream regions of the *upp3Δ* locus for homologous recombination.

pUMa & pUL: internal plasmid reference number

Table 4: Oligos used in this study

Designation	Nucleotide sequence (5' → 3')	Remarks
oUM27	AATAGGCCTGAGTGGCCATGGCCGAATCGATTTACG	*rrm4-fwd*
oUM573	CGCGGCCTGAGTGGCCATGGATTTCTACTCGACGTCCTTC	*khd4- fwd*
oUM574	GTAATAGGCCGCGTTGGCCGCCCGGTCAAAAGCGAGTTGAG	*khd4- rev*
oUM420	CATATAGGGATTCTGCCAGTCCGAACTC	*ada- rev*
oAB292	CGGAGGCGGTGGTTCCGGTGGCGGAGGATCGG-GAGGTGGCGGTTCGTC	*GGGGS linker- fwd*
oAB293	CATGGACGAACCGCCACCTCCCGATCCTCCGCCACCGGAAC-CACCGCCTCCGGTAC	*GGGGS linker- rev*
oRL1385	CACCATATGGTGAGCAAGGGCGAGGAGC	*gfp- fwd*
oAB1	GCAAGGCCTGAGTGGCCATGGTGTCGGAGCTCATC	*kat- fwd*
oAB2	GTCTGGCCGCGTTGGCCCTCATATGGCGGTGACCG	*kat- rev*
oMB611	GATGCTCTTCCGTGCCATGGTGTCGGAGCTCATC	*kat reporter-fwd*

oAB222	GGCGCGCCTATAGTTAACGCTATCAGGCGTAGTCGGGCAC-GTCGTAAG	*kat reporter-rev*
oAB232	AACATACCCATACCCATACCCATACCCATACCCATACCCGG	*(auaccc)$_6$- fwd*
oAB233	CGCGCCGGGTATGGGTATGGGTATGGGTATGGGTATGGG-TATGTT	*(auaccc)$_6$- rev*
oAB234	AACAGATCTAGATCTAGATCTAGATCTAGATCTAGATCTGG	*(agaucu)$_6$- fwd*
oAB235	CGCGCCAGATCTAGATCTAGATCTAGATCTAGATCTA-GATCTGTT	*(agaucu)$_6$- rev*
oAB531	AACCGTCAATCACGAATGATACCCACCTTGTCACCCGAGGG	*spa2 short (auaccc)- fwd*
oAB532	CGCGCCCTCGGGTGACAAGGTGGGTATCATTCGTGATTGAC-GGTT	*spa2 short (auaccc)- rev*
oAB533	AACCGTCAATCACGAATGAGATCTACCTTGTCACCCGAGGG	*spa2 short (agaucu)-fwd*
oAB534	CGCGCCCTCGGGTGACAAGGTAGATCTCATTCGTGATTGAC-GGTT	*spa2 short (agaucu)-rev*
oCD81	GCTGGCAATTGATGGGTCTCACATTCTCGTC	*arl1- fwd*
oCD82	GCGCCGACTAGTCTTGCTTTGCAATGTGTTG	*arl1- rev*
oCD192	GCGGCTATGTTAACTCCATTCGAGACCTCCGATAC	*3′ UTR (arl1) - fwd*
oCD193	AGTCATGGCGCGCCTGCATTGTCTACCTGTGCTGAAG	*3′ UTR (arl1) - rev*
oCD208	GCCGATCAATTGATGTCGGACACGCATGACCC	*hok1- fwd*
oCD209	ATCGTAACTAGTCCTGCGACTAGCGAGCTGC	*hok1- rev*
oCD210	GGGCGGCGGTTAACTGTCGGAACCCTTTTTTATATACC	*3′ UTR (hok1) - fwd*
oCD211	GATCTAGGCGCGCCCACCTTTACCACCAACTAC	*3′ UTR (hok1) - rev*
oCD83	GAGCGCAATTGATGTCAAGCCTGGATGTG	*vma21- fwd*
oCD84	GCGGTCACTAGTTTGACCTTTCTTCGCCTCAAGACTG	*vma21- rev*

oCD194	GCTACGGTTAACGTAAGGAACATGACGAAGCAGG	*3′ UTR (vma21) - fwd*
oCD195	ACTATAGGCGCGCCTGTGGGAAGTGACACTGGTG	*3′ UTR (vma21) - rev*
oCD483	GACAAGGAAACCTACGTCGAG	*kat-RT-qPCR-fwd*
oCD484	TAGAGCGGACCCTGCATA	*kat-RT-qPCR-rev*
oCD485	GTTCCGCGAGACCATTCTTA	*pgk1-RT-qPCR- fwd*
oCD486	CCGGCAAAGTTGTCAAACTC	*pgk1-RT-qPCR- rev*

Fwd-forward; Rev-reverse

Table 5: Pathways with an overrepresentation of AUACCC-containing virulence transcripts.

KEGG pathway	AUACCC		all genes		Enrichment (AUACCC-containing transcripts over all genes)
	no. of genes in the pathway	all	no. of genes in the pathway	all	
Amino sugar and nucleotide sugar metabolism	8	1043	22	4190	1.460821058
Autophagy - other	5	1043	18	4190	1.115904975
Base excision repair	6	1043	21	4190	1.147787974
Cell cycle - yeast	24	1043	56	4190	1.721681961
DNA replication	7	1043	24	4190	1.171700224
Endocytosis	11	1043	36	4190	1.227495472
Galactose metabolism	5	1043	13	4190	1.545099196
Homologous recombination	5	1043	15	4190	1.33908597
Inositol phosphate metabolism	7	1043	18	4190	1.562266965
MAPK signaling pathway - yeast	15	1043	35	4190	1.721681961

Meiosis - yeast	17	1043	38	4190	1.797194328
Mismatch repair	5	1043	19	4190	1.057173134
Mitophagy - yeast	5	1043	17	4190	1.181546444
Motor proteins	9	1043	27	4190	1.33908597
mRNA surveillance pathway	10	1043	29	4190	1.385261348
N-Glycan biosynthesis	8	1043	27	4190	1.19029864
Nucleocytoplasmic transport	12	1043	44	4190	1.095615794
Nucleotide metabolism	6	1043	23	4190	1.047980324
Phosphatidylinositol signaling system	6	1043	18	4190	1.33908597
Pyrimidine metabolism	5	1043	17	4190	1.181546444
RNA degradation	6	1043	24	4190	1.004314477
Spliceosome	14	1043	45	4190	1.249813572
Steroid biosynthesis	5	1043	10	4190	2.008628955
Sulfur metabolism	5	1043	13	4190	1.545099196
Terpenoid backbone biosynthesis	6	1043	15	4190	1.606903164
Various types of N-glycan biosynthesis	5	1043	19	4190	1.057173134

§ Enrichment score:1 = no enrichment; >1 = AUACCC-containing transcripts are overrepresented in comparison to reference; <1 = AUACCC-containing transcripts are underrepresented in comparison to reference. The enrichment score is computed as the ratio of the percentage of AUACCC-containing transcripts within a pathway to the percentage of all transcripts present in that pathway.

5.3 Appendix 3

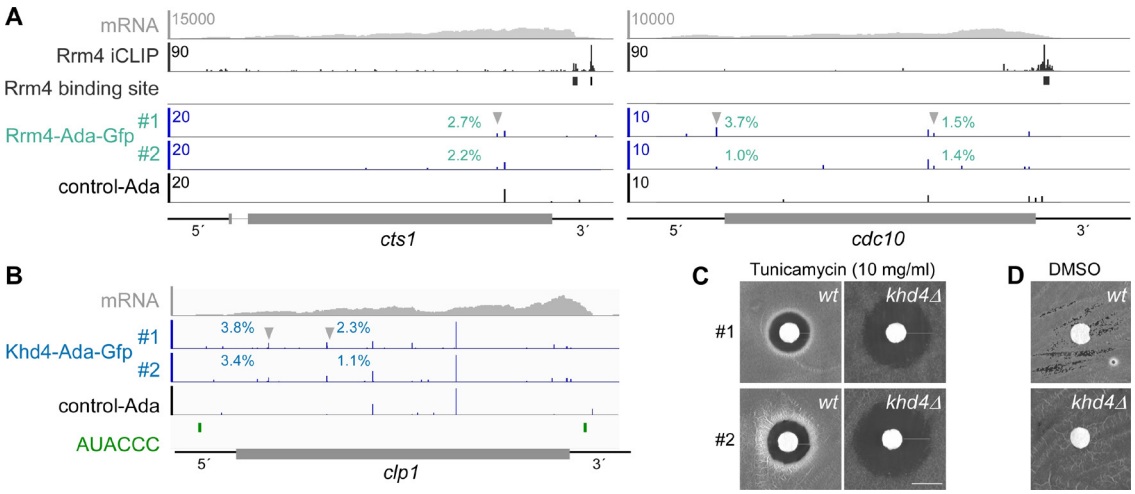

Fig. 5.15. Low editing efficiency of *Drosophila* Ada and high tunicamycin sensitivity of *khd4Δ*cells **(A)** HyperTRIBE data of Rrm4-Ada-Gfp on *cts1* and *cdc10* mRNAs with an editing threshold of >1%. Tracks showing mRNA read coverage (grey) followed by iCLIP data (crosslink events- dark grey; Rrm4 binding site-dark grey) and hyperTRIBE editing events of Rrm4-Ada-Gfp (#1,2 indicates biological replicate; blue) and control-Ada (black). Reproducible editing sites and their corresponding editing levels are indicated by arrow heads and numbers (green), respectively. The gene model with the exon/intron structure below was extended by 300 nt on either side to include 5′ and 3′ UTRs (5′ and 3′, respectively). **(B)** HyperTRIBE data of Khd4-Ada-Gfp on *clp1* mRNA with an editing threshold of >1%. Tracks showing mRNA read coverage (grey) followed by hyperTRIBE editing events of Khd4-Ada-Gfp (#1,2 indicates biological replicate; blue) and control-Ada (blue). Reproducible editing sites and their corresponding editing levels are indicated by arrow heads and numbers (blue), respectively. The gene model with the exon/intron structure below was extended by 300 nt on either side to include 5′ and 3′ UTRs (5′ and 3′, respectively). **(C)** Tunicamycin or **(D)** DMSO sensitivity of *khd4Δ* yeast cells in comparison to wildtype (wt) yeast cells, conducted using an agar diffusion assay. This assay involved the placement of a filter saturated with the respective inhibitor (Tunicamycin-10 mg/ml) onto agar plate hosting either *wt* or *khd4Δ* yeast cells. White line (C) indicates the radius of the restriction zone.

6 References

Abruzzi, K. C., Ratner, C. and Rosbash, M., (2023) Comparison of TRIBE and STAMP for identifying targets of RNA binding proteins in human and Drosophila cells. *Rna* 29**:** 1230-1242.

Abudayyeh, O. O., Gootenberg, J. S., Franklin, B., Koob, J., Kellner, M. J., Ladha, A., Joung, J., Kirchgatterer, P., Cox, D. B. T. and Zhang, F., (2019) A cytosine deaminase for programmable single-base RNA editing. *Science* 365**:** 382-386.

Afgan, E., Baker, D., Batut, B., van den Beek, M., Bouvier, D., Čech, M., Chilton, J., Clements, D., Coraor, N., Grüning, B. A., Guerler, A., Hillman-Jackson, J., Hiltemann, S., Jalili, V., Rasche, H., Soranzo, N., Goecks, J., Taylor, J., Nekrutenko, A. and Blankenberg, D., (2018) The Galaxy platform for accessible, reproducible and collaborative biomedical analyses: 2018 update. *Nucleic Acids Res* 46**:** W537-W544.

Ahearn, I. M., Haigis, K., Bar-Sagi, D. and Philips, M. R., (2011) Regulating the regulator: post-translational modification of RAS. *Nat Rev Mol Cell Biol* 13**:** 39-51.

Anders, S., Pyl, P. T. and Huber, W., (2014) HTSeq—a Python framework to work with high-throughput sequencing data. *Bioinformatics* 31**:** 166-169.

Anderson, P., (2010) Post-transcriptional regulons coordinate the initiation and resolution of inflammation. *Nat.Rev.Immunol* 10**:** 24-35.

Anonymous, (2017) Stop neglecting fungi. *Nat Microbiol* 2**:** 17120.

Apirion, D., (1973) Degradation of RNA in Escherichia coli: a hypothesis. *Molecular and General Genetics MGG* 122**:** 313-322.

Arkowitz, R. A., and Bassilana, M., (2015) Regulation of hyphal morphogenesis by Ras and Rho small GTPases. *Fungal Biology Reviews* 29**:** 7-19.

Arribas-Hernández, L., Rennie, S., Köster, T., Porcelli, C., Lewinski, M., Staiger, D., Andersson, R. and Brodersen, P., (2021) Principles of mRNA targeting via the *Arabidopsis* m(6)A-binding protein ECT2. *Elife* 10.

Barreau, C., Paillard, L. and Osborne, H. B., (2005) AU-rich elements and associated factors: are there unifying principles? *Nucleic Acids Res* 33**:** 7138-7150.

Baumann, S., Komissarov, A., Gili, M., Ruprecht, V., Wieser, S. and Maurer, S. P., (2020) A reconstituted mammalian APC-kinesin complex selectively transports defined packages of axonal mRNAs. *Science Advances* 6**:** eaaz1588.

Baumann, S., König, J., Koepke, J. and Feldbrügge, M., (2014) Endosomal transport of septin mRNA and protein indicates local translation on endosomes and is required for correct septin filamentation. *EMBO Rep* 15**:** 94-102.

Baumann, S., Pohlmann, T., Jungbluth, M., Brachmann, A. and Feldbrügge, M., (2012) Kinesin-3 and dynein mediate microtubule-dependent co-transport of mRNPs and endosomes. *J Cell Sci* 125**:** 2740-2752.

Bayne, R. A., Jayachandran, U., Kasprowicz, A., Bresson, S., Tollervey, D., Wallace, E. W. J. and Cook, A. G., (2022) Yeast Ssd1 is a non-enzymatic member of the RNase II family with an alternative RNA recognition site. *Nucleic Acids Res* 50**:** 2923-2937.

Becht, P., König, J. and Feldbrügge, M., (2006) The RNA-binding protein Rrm4 is essential for polarity in *Ustilago maydis* and shuttles along microtubules. *J Cell Sci* 119**:** 4964-4973.

Becht, P., Vollmeister, E. and Feldbrügge, M., (2005) Role for RNA-binding proteins implicated in pathogenic development of *Ustilago maydis*. *Eukaryot Cell* 4**:** 121-133.

Beckmann, K., Grskovic, M., Gebauer, F. and Hentze, M. W., (2005) A dual inhibitory mechanism restricts msl-2 mRNA translation for dosage compensation in Drosophila. *Cell* 122**:** 529-540.

Berepiki, A., Lichius, A. and Read, N. D., (2011) Actin organization and dynamics in filamentous fungi. *Nat Rev Microbiol* 9**:** 876-887.

Bernstein, P. L., Herrick, D. J., Prokipcak, R. D. and Ross, J., (1992) Control of c-myc mRNA half-life in vitro by a protein capable of binding to a coding region stability determinant. *Genes & development* 6**:** 642-654.

Béthune, J., Jansen, R. P., Feldbrügge, M. and Zarnack, K., (2019) Membrane-associated RNA-binding proteins orchestrate organelle-coupled translation *Trends Cell Biol.* 29**:** 178-188.

Bielska, E., Schuster, M., Roger, Y., Berepiki, A., Soanes, D. M., Talbot, N. J. and Steinberg, G., (2014) Hook is an adapter that coordinates kinesin-3 and dynein cargo attachment on early endosomes. *J Cell Biol* 204**:** 989-1007.

Binns, D., Dimmer, E., Huntley, R., Barrell, D., O'Donovan, C. and Apweiler, R., (2009) QuickGO: a web-based tool for Gene Ontology searching. *Bioinformatics* 25**:** 3045-3046.

Birgisdottir, Å. B., and Johansen, T., (2020) Autophagy and endocytosis – interconnections and interdependencies. *Journal of Cell Science* 133.

Bisnett, B. J., Condon, B. M., Lamb, C. H., Georgiou, G. R. and Boyce, M., (2021) Export Control: Post-transcriptional Regulation of the COPII Trafficking Pathway. *Frontiers in Cell and Developmental Biology* 8.

Biswas, J., Rosbash, M., Singer, R. H. and Rahman, R., (2021) Protocol for using TRIBE to study RNA-protein interactions and nuclear organization in mammalian cells. *STAR Protoc* 2**:** 100634.

Bittner, E., Stehlik, T. and Freitag, J., (2022) Sharing the wealth: The versatility of proteins targeted to peroxisomes and other organelles. *Front Cell Dev Biol* 10**:** 934331.

Bloom, A. L. M., Jin, R. M., Leipheimer, J., Bard, J. E., Yergeau, D., Wohlfert, E. A. and Panepinto, J. C., (2019) Thermotolerance in the pathogen *Cryptococcus neoformans* is linked to antigen masking via mRNA decay-dependent reprogramming. *Nat Commun* 10**:** 4950.

Blue, R. E., Curry, E. G., Engels, N. M., Lee, E. Y. and Giudice, J., (2018) How alternative splicing affects membrane-trafficking dynamics. *J Cell Sci* 131.

Bolger, A. M., Lohse, M. and Usadel, B., (2014) Trimmomatic: a flexible trimmer for Illumina sequence data. *Bioinformatics* 30**:** 2114-2120.

Bölker, M., Genin, S., Lehmler, C. and Kahmann, R., (1995) Genetic regulation of mating and dimorphism in *Ustilago maydis*. *Canadian Journal of Botany* 73**:** 320-325.

Bos, J. L., Rehmann, H. and Wittinghofer, A., (2007) GEFs and GAPs: critical elements in the control of small G proteins. *Cell* 129**:** 865-877.

Bottin, A., Kämper, J. and Kahmann, R., (1996) Isolation of a carbon source-regulated gene from *Ustilago maydis*. *Mol Gen Genet* 253**:** 342-352.

Bourke, A. M., Schwarz, A. and Schuman, E. M., (2023) De-centralizing the Central Dogma: mRNA translation in space and time. *Molecular Cell* 83**:** 452-468.

Brachmann, A., König, J., Julius, C. and Feldbrügge, M., (2004) A reverse genetic approach for generating gene replacement mutants in *Ustilago maydis*. *Mol Genet Genomics* 272**:** 216-226.

Brachmann, A., Weinzierl, G., Kämper, J. and Kahmann, R., (2001) Identification of genes in the bW/bE regulatory cascade in *Ustilago maydis*. *Mol Microbiol* 42**:** 1047-1063.

Brand, A., (2012) Hyphal Growth in Human Fungal Pathogens and Its Role in Virulence. *International Journal of Microbiology* 2012**:** 517529.

Brand, A., and Gow, N. A., (2009) Mechanisms of hypha orientation of fungi. *Curr Opin Microbiol* 12**:** 350-357.

Brannan, K. W., Chaim, I. A., Marina, R. J., Yee, B. A., Kofman, E. R., Lorenz, D. A., Jagannatha, P., Dong, K. D., Madrigal, A. A., Underwood, J. G. and Yeo, G. W., (2021) Robust single-cell discovery of RNA targets of RNA-binding proteins and ribosomes. *Nat Methods* 18**:** 507-519.

Briata, P., Forcales, S. V., Ponassi, M., Corte, G., Chen, C. Y., Karin, M., Puri, P. L. and Gherzi, R., (2005) p38-dependent phosphorylation of the mRNA decay-promoting factor KSRP controls the stability of select myogenic transcripts. *Mol Cell* 20**:** 891-903.

Brown, G. D., Denning, D. W., Gow, N. A., Levitz, S. M., Netea, M. G. and White, T. C., (2012a) Hidden killers: human fungal infections. *Sci Transl Med* 4**:** 165rv113.

Brown, G. D., Denning, D. W. and Levitz, S. M., (2012b) Tackling human fungal infections. *Science* 336**:** 647.

Bruce, S. R., and Wilkinson, M. F., (2006) Messenger RNA Stability, pp. 1065-1065 in *Encyclopedic Reference of Genomics and Proteomics in Molecular Medicine*. *Springer Berlin Heidelberg*, Berlin, Heidelberg.

Burgess, D. J., (2019) Expanding options for RNA based editors. *Nature Reviews Genetics* 20**:** 563-563.

Busch, A., Brüggemann, M., Ebersberger, S. and Zarnack, K., (2020) iCLIP data analysis: A complete pipeline from sequencing reads to RBP binding sites. *Methods* 178**:** 49-62.

Carbó, N., and Pérez-Martín, J., (2008) Spa2 is required for morphogenesis but it is dispensable for pathogenicity in the phytopathogenic fungus *Ustilago maydis*. *Fungal Genet Biol* 45**:** 1315-1327.

Chávez, S., García-Martínez, J., Delgado-Ramos, L. and Pérez-Ortín, J. E., (2016) The importance of controlling mRNA turnover during cell proliferation. *Curr Genet* 62**:** 701-710.

Chen, W., and Moore, M. J., (2015) Spliceosomes. *Curr Biol* 25**:** R181-183.

Cheng, A. P., Kwon, S., Adheshara, T., Göhre, V., Feldbrügge, M. and Weiberg, A., (2023) Extracellular RNAs of plant-colonizing fungi: from molecular mechanisms to crop solutions. *Appl. Microbiol. Biotechnol.* accepted for publication.

Cheng, Y.-L., Hsieh, H.-Y. and Tu, S.-L., (2021) A new method to identify global targets of RNA-binding proteins in plants. *bioRxiv***:** 2021.2006.2011.448000.

Chicoine, J., Benoit, P., Gamberi, C., Paliouras, M., Simonelig, M. and Lasko, P., (2007) Bicaudal-C recruits CCR4-NOT deadenylase to target mRNAs and regulates oogenesis, cytoskeletal organization, and its own expression. *Dev Cell* 13**:** 691-704.

Cioni, J. M., Lin, J. Q., Holtermann, A. V., Koppers, M., Jakobs, M. A. H., Azizi, A., Turner-Bridger, B., Shigeoka, T., Franze, K., Harris, W. A. and Holt, C. E., (2019) Late Endosomes Act as mRNA Translation Platforms and Sustain Mitochondria in Axons. *Cell* 176**:** 56-72.e15.

Cléry, A., and Allain, F., (2012) From structure to function of RNA binding domains. *RNA binding proteins***:** 137-158.

Collart, M. A., Panasenko, O. O. and Nikolaev, S. I., (2013) The Not3/5 subunit of the Ccr4-Not complex: A central regulator of gene expression that integrates signals between the cytoplasm and the nucleus in eukaryotic cells. *Cellular Signalling* 25**:** 743-751.

Commer, B., and Shaw, B. D., (2020) Current views on endocytosis in filamentous fungi. *Mycology* 12**:** 1-9.

Corley, M., Burns, M. C. and Yeo, G. W., (2020) How RNA-Binding Proteins Interact with RNA: Molecules and Mechanisms. *Mol Cell* 78**:** 9-29.

Cremer, T., Jongsma, M. L. M., Trulsson, F., Vertegaal, A. C. O., Neefjes, J. and Berlin, I., (2021) The ER-embedded UBE2J1/RNF26 ubiquitylation complex exerts spatiotemporal control over the endolysosomal pathway. *Cell Rep* 34**:** 108659.

Das, S., Vera, M., Gandin, V., Singer, R. H. and Tutucci, E., (2021) Intracellular mRNA transport and localized translation. *Nature Reviews Molecular Cell Biology* 22**:** 483-504.

Dautt-Castro, M., Rosendo-Vargas, M. and Casas-Flores, S., (2021) The Small GTPases in Fungal Signaling Conservation and Function. *Cells* 10.

Dave, P., Roth, G., Griesbach, E., Mateju, D., Hochstoeger, T. and Chao, J. A., (2023) Single-molecule imaging reveals translation-dependent destabilization of mRNAs. *Mol Cell* 83**:** 589-606.e586.

de Lange, E. S., Balmer, D., Mauch-Mani, B. and Turlings, T. C., (2014) Insect and pathogen attack and resistance in maize and its wild ancestors, the teosintes, pp. *Wiley Online Library*.

Decker, C. J., and Parker, R., (2012) P-bodies and stress granules: possible roles in the control of translation and mRNA degradation. *Cold Spring Harb Perspect Biol* 4**:** a012286.

Devan, S.-K., Schott-Verdugo, S., Müntjes, K., Bismar, L., Reiners, J., Hachani, E., Schmitt, L., Höppner, A., Smits, S. H. J., Gohlke, H. and Feldbrügge, M., (2022) A MademoiseLLE domain binding platform links the key RNA transporter to endosomes. *PLOS Genet* 18**:** e1010269.

Diaz-Muñoz, M. D., and Osma-Garcia, I. C., (2022) The RNA regulatory programs that govern lymphocyte development and function. *WIREs RNA* 13**:** e1683.

Dobin, A., Davis, C. A., Schlesinger, F., Drenkow, J., Zaleski, C., Jha, S., Batut, P., Chaisson, M. and Gingeras, T. R., (2013) STAR: ultrafast universal RNA-seq aligner. *Bioinformatics* 29**:** 15-21.

Doehlemann, G., Okmen, B., Zhu, W. and Sharon, A., (2017) Plant Pathogenic Fungi. *Microbiol Spectr* 5.

Doehlemann, G., Van Der Linde, K., Aßmann, D., Schwammbach, D., Hof, A., Mohanty, A., Jackson, D. and Kahmann, R., (2009) Pep1, a secreted effector protein of *Ustilago maydis*, is required for successful invasion of plant cells. *PLoS pathogens* 5**:** e1000290.

Doherty, E. E., Wilcox, X. E., van Sint Fiet, L., Kemmel, C., Turunen, J. J., Klein, B., Tantillo, D. J., Fisher, A. J. and Beal, P. A., (2021) Rational Design of RNA Editing Guide Strands: Cytidine Analogs at the Orphan Position. *Journal of the American Chemical Society* 143**:** 6865-6876.

Du, Z., Lee, J. K., Fenn, S., Tjhen, R., Stroud, R. M. and James, T. L., (2007) X-ray crystallographic and NMR studies of protein-protein and protein-nucleic acid interactions involving the KH domains from human poly(C)-binding protein-2. *Rna* 13**:** 1043-1051.

Efstathiou, S., Ottens, F., Schütter, L.-S., Ravanelli, S., Charmpilas, N., Gutschmidt, A., Le Pen, J., Gehring, N. H., Miska, E. A., Bouças, J. and Hoppe, T., (2022) ER-associated RNA silencing promotes ER quality control. *Nature Cell Biology* 24**:** 1714-1725.

Eifler, T., Pokharel, S. and Beal, P. A., (2013) RNA-Seq analysis identifies a novel set of editing substrates for human ADAR2 present in *Saccharomyces cerevisiae*. *Biochemistry* 52**:** 7857-7869.

Elson, S. L., Noble, S. M., Solis, N. V., Filler, S. G. and Johnson, A. D., (2009a) An RNA transport system in *Candida albicans* regulates hyphal morphology and invasive growth. *PLoS Genet.* 5**:** e1000664.

Elson, S. L., Noble, S. M., Solis, N. V., Filler, S. G. and Johnson, A. D., (2009b) An RNA transport system in *Candida albicans* regulates hyphal morphology and invasive growth. *PLoS Genet* 5**:** e1000664.

Erwig, L. P., and Gow, N. A. R., (2016) Interactions of fungal pathogens with phagocytes. *Nat.Rev.Microbiol* 14**:** 163-176.

Essig, K., Kronbeck, N., Guimaraes, J. C., Lohs, C., Schlundt, A., Hoffmann, A., Behrens, G., Brenner, S., Kowalska, J., Lopez-Rodriguez, C., Jemielity, J., Holtmann, H., Reiche, K., Hackermüller, J., Sattler, M., Zavolan, M. and Heissmeyer, V., (2018) Roquin targets mRNAs in a 3′-UTR-specific manner by different modes of regulation. *Nature Communications* 9**:** 3810.

Fabian, M. R., Frank, F., Rouya, C., Siddiqui, N., Lai, W. S., Karetnikov, A., Blackshear, P. J., Nagar, B. and Sonenberg, N., (2013) Structural basis for the recruitment of the human CCR4-NOT deadenylase complex by tristetraprolin. *Nat Struct Mol Biol* 20**:** 735-739.

Fernandes, K. E., and Carter, D. A., (2020) Cellular plasticity of pathogenic fungi during infection. *PLoS Pathog* 16**:** e1008571.

Ferro-Novick, S., Reggiori, F. and Brodsky, J. L., (2021) ER-Phagy, ER Homeostasis, and ER Quality Control: Implications for Disease. *Trends Biochem Sci* 46**:** 630-639.

Finnigan, G. C., Ryan, M. and Stevens, T. H., (2011) A genome-wide enhancer screen implicates sphingolipid composition in vacuolar ATPase function in *Saccharomyces cerevisiae*. *Genetics* 187**:** 771-783.

Fischer, N., and Weis, K., (2002) The DEAD box protein Dhh1 stimulates the decapping enzyme Dcp1. *Embo j* 21**:** 2788-2797.

Fisher, M. C., Gow, N. A. and Gurr, S. J., (2016) Tackling emerging fungal threats to animal health, food security and ecosystem resilience. *Philos Trans R Soc Lond B Biol Sci* 371.

Fisher, M. C., Gurr, S. J., Cuomo, C. A., Blehert, D. S., Jin, H., Stukenbrock, E. H., Stajich, J. E., Kahmann, R., Boone, C., Denning, D. W., Gow, N. A. R., Klein, B. S., Kronstad, J. W., Sheppard, D. C., Taylor, J. W., Wright, G. D., Heitman, J., Casadevall, A. and Cowen, L. E., (2020) Threats Posed by the Fungal Kingdom to Humans, Wildlife, and Agriculture. *mBio* 11.

Fisher, M. C., Henk, D. A., Briggs, C. J., Brownstein, J. S., Madoff, L. C., McCraw, S. L. and Gurr, S. J., (2012) Emerging fungal threats to animal, plant and ecosystem health. *Nature* 484**:** 186-194.

Fones, H. N., Fisher, M. C. and Gurr, S. J., (2017) Emerging Fungal Threats to Plants and Animals Challenge Agriculture and Ecosystem Resilience. *Microbiol Spectr* 5.

Freitag, J., Ast, J. and Bolker, M., (2012) Cryptic peroxisomal targeting via alternative splicing and stop codon read-through in fungi. *Nature* 485**:** 522-525.

Freitag, J., Lanver, D., Böhmer, C., Schink, K. O., Bölker, M. and Sandrock, B., (2011) Septation of infectious hyphae is critical for appressoria formation and virulence in the smut fungus *Ustilago maydis*. *PLoS Pathog* 7**:** e1002044.

Frick, W. F., Pollock, J. F., Hicks, A. C., Langwig, K. E., Reynolds, D. S., Turner, G. G., Butchkoski, C. M. and Kunz, T. H., (2010) An emerging disease causes regional population collapse of a common North American bat species. *Science* 329**:** 679-682.

Fromme, J. C., Orci, L. and Schekman, R., (2008) Coordination of COPII vesicle trafficking by Sec23. *Trends in Cell Biology* 18**:** 330-336.

Galez, H. A., Roelants, F. M., Palm, S. M., Reynaud, K. K., Ingolia, N. T. and Thorner, J., (2021) Phosphorylation of mRNA-Binding Proteins Puf1 and Puf2 by TORC2-Activated Protein Kinase Ypk1 Alleviates Their Repressive Effects. *Membranes* 11**:** 500.

Gank, K. D., Yeaman, M. R., Kojima, S., Yount, N. Y., Park, H., Edwards, J. E., Jr., Filler, S. G. and Fu, Y., (2008) SSD1 is integral to host defense peptide resistance in *Candida albicans*. *Eukaryot Cell* 7**:** 1318-1327.

Gann, A., (2010) Jacob and Monod: From Operons to EvoDevo. *Current Biology* 20**:** R718-R723.

García-Mauriño, S. M., Rivero-Rodríguez, F., Velázquez-Cruz, A., Hernández-Vellisca, M., Díaz-Quintana, A., De la Rosa, M. A. and Díaz-Moreno, I., (2017) RNA binding protein regulation and cross-talk in the control of AU-rich mRNA fate. *Frontiers in molecular biosciences* 4**:** 71.

Garcia-Solache, M. A., and Casadevall, A., (2010) Global warming will bring new fungal diseases for mammals. *mBio* 1.

Gebauer, F., Schwarzl, T., Valcárcel, J. and Hentze, M. W., (2021) RNA-binding proteins in human genetic disease. *Nature Reviews Genetics* 22**:** 185-198.

Gerstberger, S., Hafner, M. and Tuschl, T., (2014) A census of human RNA-binding proteins. *Nat Rev Genet* 15**:** 829-845.

Gherzi, R., Lee, K. Y., Briata, P., Wegmüller, D., Moroni, C., Karin, M. and Chen, C. Y., (2004) A KH domain RNA binding protein, KSRP, promotes ARE-directed mRNA turnover by recruiting the degradation machinery. *Mol Cell* 14**:** 571-583.

Glazier, V. E., Kaur, J. N., Brown, N. T., Rivera, A. A. and Panepinto, J. C., (2015) Puf4 regulates both splicing and decay of HXL1 mRNA encoding the unfolded protein response transcription factor in *Cryptococcus neoformans*. *Eukaryot Cell* 14**:** 385-395.

Göhre, V., Vollmeister, E., Bölker, M. and Feldbrügge, M., (2012) Microtubule-dependent membrane dynamics in *Ustilago maydis*: Trafficking and function of Rab5a-positive endosomes. *Commun Integr Biol* 5**:** 485-490.

Gow, N. A., Brown, A. J. and Odds, F. C., (2002) Fungal morphogenesis and host invasion. *Curr Opin Microbiol* 5**:** 366-371.

Gow, N. A. R., van de Veerdonk, F. L., Brown, A. J. P. and Netea, M. G., (2012) *Candida albicans* morphogenesis and host defence: discriminating invasion from colonization. *Nature Reviews Microbiology* 10**:** 112-122.

Grant, C. E., and Bailey, T. L., (2021) XSTREME: Comprehensive motif analysis of biological sequence datasets. *bioRxiv***:** 2021.2009.2002.458722.

Griffing, L. R., Lin, C., Perico, C., White, R. R. and Sparkes, I., (2017) Plant ER geometry and dynamics: biophysical and cytoskeletal control during growth and biotic response. *Protoplasma* 254**:** 43-56.

Grzybowska, E. A., and Wakula, M., (2021) Protein Binding to Cis-Motifs in mRNAs Coding Sequence Is Common and Regulates Transcript Stability and the Rate of Translation. *Cells* 10.

Haag, C., Klein, T. and Feldbrügge, M., (2019) ESCRT Mutant Analysis and Imaging of ESCRT Components in the Model Fungus *Ustilago maydis*. *Methods Mol Biol* 1998**:** 251-271.

Haag, C., Pohlmann, T. and Feldbrügge, M., (2017) The ESCRT regulator Did2 maintains the balance between long-distance endosomal transport and endocytic trafficking. *PLoS Genet* 13**:** e1006734.

Hafner, M., Katsantoni, M., Köster, T., Marks, J., Mukherjee, J., Staiger, D., Ule, J. and Zavolan, M., (2021) CLIP and complementary methods. *Nature Reviews Methods Primers* 1**:** 20.

Hall, R. A., and Wallace, E. W. J., (2022) Post-transcriptional control of fungal cell wall synthesis. *Cell Surf* 8**:** 100074.

Hampel, M., Jakobi, M., Schmitz, L., Meyer, U., Finkernagel, F., Doehlemann, G. and Heimel, K., (2016) Unfolded Protein Response (UPR) Regulator Cib1 Controls Expression of Genes Encoding Secreted Virulence Factors in *Ustilago maydis*. *PLoS One* 11**:** e0153861.

Hargrove, J. L., and Schmidt, F. H., (1989) The role of mRNA and protein stability in gene expression. *Faseb j* 3**:** 2360-2370.

Harting, R., and Heimel, K., (2020) Genetics of the Unfolded Protein Response in Fungi, pp. 49-76 in *Genetics and Biotechnology*, edited by J. P. Benz and K. Schipper. *Springer International Publishing*, Cham.

Haugland, R. P., (1995) Detecting Enzymatic Activity in Cells Using Fluorogenic Substrates. *Biotechnic & Histochemistry* 70**:** 243-251.

He, B., Cai, Q., Qiao, L., Huang, C. Y., Wang, S., Miao, W., Ha, T., Wang, Y. and Jin, H., (2021) RNA-binding proteins contribute to small RNA loading in plant extracellular vesicles. *Nat. Plants* 7**:** 342-352.

Hebert, D. N., Garman, S. C. and Molinari, M., (2005) The glycan code of the endoplasmic reticulum: asparagine-linked carbohydrates as protein maturation and quality-control tags. *Trends Cell Biol* 15**:** 364-370.

Heck, A. M., and Wilusz, J., (2018) The Interplay between the RNA Decay and Translation Machinery in Eukaryotes. *Cold Spring Harb Perspect Biol* 10.

Heimel, K., (2015) Unfolded protein response in filamentous fungi-implications in biotechnology. *Appl Microbiol Biotechnol* 99**:** 121-132.

Heimel, K., Freitag, J., Hampel, M., Ast, J., Bölker, M. and Kämper, J., (2013) Crosstalk between the unfolded protein response and pathways that regulate pathogenic development in Ustilago maydis. *Plant Cell* 25**:** 4262-4277.

Heimel, K., Scherer, M., Schuler, D. and Kämper, J., (2010a) The *Ustilago maydis* Clp1 Protein Orchestrates Pheromone and b-Dependent Signaling Pathways to Coordinate the Cell Cycle and Pathogenic Development. *Plant Cell* 22**:** 2908-2922.

Heimel, K., Scherer, M., Vranes, M., Wahl, R., Pothiratana, C., Schuler, D., Vincon, V., Finkernagel, F., Flor-Parra, I. and Kämper, J., (2010b) The transcription factor Rbf1 is the master regulator for b-mating type controlled pathogenic development in *Ustilago maydis*. *PLoS Pathog* 6**:** e1001035.

Hentze, M. W., Castello, A., Schwarzl, T. and Preiss, T., (2018) A brave new world of RNA-binding proteins. *Nat Rev Mol Cell Biol* 19**:** 327-341.

Herzog, V. A., Reichholf, B., Neumann, T., Rescheneder, P., Bhat, P., Burkard, T. R., Wlotzka, W., von Haeseler, A., Zuber, J. and Ameres, S. L., (2017) Thiol-linked alkylation of RNA to assess expression dynamics. *Nature Methods* 14**:** 1198-1204.

Hinnebusch, A. G., Ivanov, I. P. and Sonenberg, N., (2016) Translational control by 5'-untranslated regions of eukaryotic mRNAs. *Science* 352**:** 1413-1416.

Hoenigl, M., Seidel, D., Sprute, R., Cunha, C., Oliverio, M., Goldman, G. H., Ibrahim, A. S. and Carvalho, A., (2022) COVID-19-associated fungal infections. *Nature Microbiology* 7**:** 1127-1140.

Hollien, J., and Weissman, J. S., (2006) Decay of endoplasmic reticulum-localized mRNAs during the unfolded protein response. *Science* 313**:** 104-107.

Hollingworth, D., Candel, A. M., Nicastro, G., Martin, S. R., Briata, P., Gherzi, R. and Ramos, A., (2012) KH domains with impaired nucleic acid binding as a tool for functional analysis. *Nucleic Acids Res* 40**:** 6873-6886.

Hu, G., Bakkeren, E., Caza, M., Horianopoulos, L., Sánchez-León, E., Sorensen, M., Jung, W. and Kronstad, J. W., (2021) Vam6/Vps39/TRAP1-domain proteins influence vacuolar morphology, iron acquisition and virulence in *Cryptococcus neoformans*. *Cell Microbiol* 23**:** e13400.

Humphreys, C. P., Franks, P. J., Rees, M., Bidartondo, M. I., Leake, J. R. and Beerling, D. J., (2010) Mutualistic mycorrhiza-like symbiosis in the most ancient group of land plants. *Nature Communications* 1**:** 103.

Huntley, R. P., Sawford, T., Mutowo-Meullenet, P., Shypitsyna, A., Bonilla, C., Martin, M. J. and O'Donovan, C., (2015) The GOA database: gene Ontology annotation updates for 2015. *Nucleic Acids Res* 43**:** D1057-1063.

Ingole, K. D., Nagarajan, N., Uhse, S., Giannini, C. and Djamei, A., (2022) Tetracycline-controlled (TetON) gene expression system for the smut fungus Ustilago maydis. *Frontiers in Fungal Biology* 3.

Jankowski, S., Pohlmann, T., Baumann, S., Müntjes, K. M., Devan, S. K., Zander, S. and Feldbrügge, M., (2019) The multi PAM2 protein Upa2 functions as novel core component of endosomal mRNA transport. *EMBO Rep.* 24**:** e47381.

Jia, L., Mao, Y., Ji, Q., Dersh, D., Yewdell, J. W. and Qian, S. B., (2020) Decoding mRNA translatability and stability from the 5' UTR. *Nat Struct Mol Biol* 27**:** 814-821.

Jin, H., Xu, W., Rahman, R., Na, D., Fieldsend, A., Song, W., Liu, S., Li, C. and Rosbash, M., (2020) TRIBE editing reveals specific mRNA targets of eIF4E-BP in *Drosophila* and in mammals. *Sci Adv* 6**:** eabb8771.

Jin, Y., Zhang, W. and Li, Q., (2009) Origins and evolution of ADAR-mediated RNA editing. *IUBMB Life* 61**:** 572-578.

Just, W. W., and Peränen, J., (2016) Small GTPases in peroxisome dynamics. *Biochim Biophys Acta* 1863**:** 1006-1013.

Kalem, M. C., Subbiah, H., Leipheimer, J., Glazier, V. E. and Panepinto, J. C., (2021) Puf4 Mediates Post-transcriptional Regulation of Cell Wall Biosynthesis and Caspofungin Resistance in *Cryptococcus neoformans*. *mBio* 12.

Kämper, J., Kahmann, R., Bölker, M., Ma, L.-J., Brefort, T., Saville, B. J., Banuett, F., Kronstad, J. W., Gold, S. E., Müller, O., Perlin, M. H., Wösten, H. A. B., de Vries, R., Ruiz-Herrera, J., Reynaga-Peña, C. G., Snetselaar, K., McCann, M., Pérez-Martín, J., Feldbrügge, M., Basse, C. W., Steinberg, G., Ibeas, J. I., Holloman, W., Guzman, P., Farman, M., Stajich, J. E., Sentandreu, R., González-Prieto, J. M., Kennell, J. C., Molina, L., Schirawski, J., Mendoza-Mendoza, A., Greilinger, D., Münch, K., Rössel, N., Scherer, M., Vraneš, M., Ladendorf, O., Vincon, V., Fuchs, U., Sandrock, B., Meng, S., Ho, E. C. H., Cahill, M. J., Boyce, K. J., Klose, J., Klosterman, S. J., Deelstra, H. J., Ortiz-Castellanos, L., Li, W., Sanchez-Alonso, P., Schreier, P. H., Häuser-Hahn, I., Vaupel, M., Koopmann, E., Friedrich, G., Voss, H., Schlüter, T., Margolis, J., Platt, D., Swimmer, C., Gnirke, A., Chen, F., Vysotskaia, V., Mannhaupt, G., Güldener, U., Münsterkötter, M., Haase, D., Oesterheld, M., Mewes, H.-W., Mauceli, E. W., DeCaprio, D., Wade, C. M., Butler, J., Young, S., Jaffe, D. B., Calvo, S., Nusbaum, C., Galagan, J. and Birren, B. W., (2006) Insights from the genome of the biotrophic fungal plant pathogen *Ustilago maydis*. *Nature* 444**:** 97-101.

Kanehisa, M., and Sato, Y., (2020) KEGG Mapper for inferring cellular functions from protein sequences. *Protein Sci* 29**:** 28-35.

Kanehisa, M., Sato, Y. and Kawashima, M., (2022) KEGG mapping tools for uncovering hidden features in biological data. *Protein Sci* 31**:** 47-53.

Kaygun, H., and Marzluff, W. F., (2005) Regulated degradation of replication-dependent histone mRNAs requires both ATR and Upf1. *Nature Structural & Molecular Biology* 12**:** 794-800.

Kearse, M. G., and Wilusz, J. E., (2017) Non-AUG translation: a new start for protein synthesis in eukaryotes. *Genes Dev* 31**:** 1717-1731.

Keene, J. D., (2007) RNA regulons: coordination of post-transcriptional events. *Nat Rev Genet* 8**:** 533-543.

Keene, J. D., and Tenenbaum, S. A., (2002) Eukaryotic mRNPs may represent posttranscriptional operons. *Mol Cell* 9**:** 1161-1167.

Kivioja, T., Vähärautio, A., Karlsson, K., Bonke, M., Enge, M., Linnarsson, S. and Taipale, J., (2011) Counting absolute numbers of molecules using unique molecular identifiers. *Nat Methods* 9**:** 72-74.

Koepke, J., Kaffarnik, F., Haag, C., Zarnack, K., Luscombe, N. M., König, J., Ule, J., Kellner, R., Begerow, D. and Feldbrügge, M., (2011) The RNA-binding protein Rrm4 is essential for efficient secretion of endochitinase Cts1. *Mol Cell Proteomics* 10**:** M111.011213.

Kolberg, L., Raudvere, U., Kuzmin, I., Vilo, J. and Peterson, H., (2020) gprofiler2 -- an R package for gene list functional enrichment analysis and namespace conversion toolset g:Profiler. *F1000Res* 9.

König, J., Baumann, S., Koepke, J., Pohlmann, T., Zarnack, K. and Feldbrügge, M., (2009) The fungal RNA-binding protein Rrm4 mediates long-distance transport of *ubi1* and *rho3* mRNAs. *Embo j* 28**:** 1855-1866.

König, J., Julius, C., Baumann, S., Homann, M., Göringer, H. U. and Feldbrügge, M., (2007) Combining SELEX and the yeast three-hybrid system for *in vivo* selection and classification of RNA aptamers. *Rna* 13**:** 614-622.

Kremp, M., Bittner, E., Martorana, D., Klingenberger, A., Stehlik, T., Bölker, M. and Freitag, J., (2020) Non-AUG translation initiation generates peroxisomal isoforms of 6-phosphogluconate dehydrogenase in fungi. *Front Cell Dev Biol* 8**:** 251.

Kucera, M., Isserlin, R., Arkhangorodsky, A. and Bader, G. D., (2016) AutoAnnotate: A Cytoscape app for summarizing networks with semantic annotations. *F1000Res* 5**:** 1717.

Kumamoto, C. A., and Vinces, M. D., (2005) Contributions of hyphae and hypha-co-regulated genes to *Candida albicans* virulence. *Cell Microbiol* 7**:** 1546-1554.

Kuttan, A., and Bass, B. L., (2012) Mechanistic insights into editing-site specificity of ADARs. *Proc Natl Acad Sci USA* 109**:** E3295-3304.

Kwon, S., Rupp, O., Brachmann, A., Blum, C. F., Kraege, A., Goesmann, A. and Feldbrügge, M., (2021) mRNA Inventory of Extracellular Vesicles from *Ustilago maydis*. *J. Fungi* 7.

Labbaoui, H., Bogliolo, S., Ghugtyal, V., Solis, N. V., Filler, S. G., Arkowitz, R. A. and Bassilana, M., (2017) Role of Arf GTPases in fungal morphogenesis and virulence. *PLoS Pathog* 13**:** e1006205.

Langner, T., Öztürk, M., Hartmann, S., Cord-Landwehr, S., Moerschbacher, B., Walton, J. D. and Göhre, V., (2015) Chitinases Are Essential for Cell Separation in *Ustilago maydis*. *Eukaryot Cell* 14**:** 846-857.

Lanver, D., Berndt, P., Tollot, M., Naik, V., Vranes, M., Warmann, T., Münch, K., Rössel, N. and Kahmann, R., (2014) Plant surface cues prime *Ustilago maydis* for biotrophic development. *PLoS Pathog* 10**:** e1004272.

Lanver, D., Mendoza-Mendoza, A., Brachmann, A. and Kahmann, R., (2010) Sho1 and Msb2-Related Proteins Regulate Appressorium Development in the Smut Fungus *Ustilago maydis* *The Plant Cell* 22**:** 2085-2101.

Lanver, D., Müller, A. N., Happel, P., Schweizer, G., Haas, F. B., Franitza, M., Pellegrin, C., Reissmann, S., Altmüller, J., Rensing, S. A. and Kahmann, R., (2018) The Biotrophic Development of *Ustilago maydis* Studied by RNA-Seq Analysis. *Plant Cell* 30**:** 300-323.

Lanver, D., Tollot, M., Schweizer, G., Lo Presti, L., Reissmann, S., Ma, L. S., Schuster, M., Tanaka, S., Liang, L., Ludwig, N. and Kahmann, R., (2017) *Ustilago maydis* effectors and their impact on virulence. *Nat Rev Microbiol* 15**:** 409-421.

Lewis, H. A., Musunuru, K., Jensen, K. B., Edo, C., Chen, H., Darnell, R. B. and Burley, S. K., (2000) Sequence-specific RNA binding by a Nova KH domain: implications for paraneoplastic disease and the fragile X syndrome. *Cell* 100**:** 323-332.

Li, B., Liu, L., Li, Y., Dong, X., Zhang, H., Chen, H., Zheng, X. and Zhang, Z., (2017) The FgVps39-FgVam7-FgSso1 Complex Mediates Vesicle Trafficking and Is Important for the Development and Virulence of *Fusarium graminearum*. *Mol Plant Microbe Interact* 30**:** 410-422.

Li, G., Dulal, N., Gong, Z. and Wilson, R. A., (2023) Unconventional secretion of *Magnaporthe oryzae* effectors in rice cells is regulated by tRNA modification and codon usage control. *Nat. Microbiol.*

Liao, Y. C., Fernandopulle, M. S., Wang, G., Choi, H., Hao, L., Drerup, C. M., Patel, R., Qamar, S., Nixon-Abell, J., Shen, Y., Meadows, W., Vendruscolo, M., Knowles, T. P. J., Nelson, M., Czekalska, M. A., Musteikyte, G., Gachechiladze, M. A., Stephens, C. A., Pasolli, H. A., Forrest, L. R., St George-Hyslop, P., Lippincott-Schwartz, J. and Ward, M. E., (2019) RNA Granules Hitchhike on Lysosomes for Long-Distance Transport, Using Annexin A11 as a Molecular Tether. *Cell* 179**:** 147-164.e120.

Liu, H., Li, Y., Chen, D., Qi, Z., Wang, Q., Wang, J., Jiang, C. and Xu, J.-R., (2017) A-to-I RNA editing is developmentally regulated and generally adaptive for sexual reproduction in *Neurospora crassa*. *Proc Natl Acad Sci USA* 114**:** E7756-E7765.

Liu, M., Lu, B., Fan, Y., He, X., Shen, S., Jiang, C. and Zhang, Q., (2019) TRIBE Uncovers the Role of Dis3 in Shaping the Dynamic Transcriptome in Malaria Parasites. *Front Cell Dev Biol* 7**:** 264.

Liu, X., Hu, G., Panepinto, J. and Williamson, P. R., (2006) Role of a VPS41 homologue in starvation response, intracellular survival and virulence of *Cryptococcus neoformans*. *Mol Microbiol* 61**:** 1132-1146.

Lo Presti, L., Lanver, D., Schweizer, G., Tanaka, S., Liang, L., Tollot, M., Zuccaro, A., Reissmann, S. and Kahmann, R., (2015) Fungal effectors and plant susceptibility. *Annu Rev Plant Biol* 66**:** 513-545.

Loubradou, G., Brachmann, A., Feldbrügge, M. and Kahmann, R., (2001) A homologue of the transcriptional repressor Ssn6p antagonizes cAMP signalling in *Ustilago maydis*. *Mol Microbiol* 40**:** 719-730.

Love, M. I., Huber, W. and Anders, S., (2014) Moderated estimation of fold change and dispersion for RNA-seq data with DESeq2. *Genome Biol* 15**:** 550.

Lunde, B. M., Moore, C. and Varani, G., (2007) RNA-binding proteins: modular design for efficient function. *Nature Reviews Molecular Cell Biology* 8**:** 479-490.

Ma, W., and Mayr, C., (2018) A Membraneless Organelle Associated with the Endoplasmic Reticulum Enables 3'UTR-Mediated Protein-Protein Interactions. *Cell* 175**:** 1492-1506.e1419.

Macbeth, M. R., Schubert, H. L., VanDemark, A. P., Lingam, A. T., Hill, C. P. and Bass, B. L., (2005) Inositol Hexakisphosphate Is Bound in the ADAR2 Core and Required for RNA Editing. *Science* 309**:** 1534-1539.

Mackereth, C. D., and Sattler, M., (2012) Dynamics in multi-domain protein recognition of RNA. *Curr Opin Struct Biol* 22**:** 287-296.

Madeira, F., Pearce, M., Tivey, A. R. N., Basutkar, P., Lee, J., Edbali, O., Madhusoodanan, N., Kolesnikov, A. and Lopez, R., (2022) Search and sequence analysis tools services from EMBL-EBI in 2022. *Nucleic Acids Res***:** gkac240.

Mahlert, M., Leveleki, L., Hlubek, A., Sandrock, B. and Bölker, M., (2006) Rac1 and Cdc42 regulate hyphal growth and cytokinesis in the dimorphic fungus *Ustilago maydis*. *Mol Microbiol* 59**:** 567-578.

Malkus, P., Graham, L. A., Stevens, T. H. and Schekman, R., (2004) Role of Vma21p in assembly and transport of the yeast vacuolar ATPase. *Mol Biol Cell* 15**:** 5075-5091.

Manning, B. D., Padmanabha, R. and Snyder, M., (1997) The Rho-GEF Rom2p localizes to sites of polarized cell growth and participates in cytoskeletal functions in *Saccharomyces cerevisiae*. *Mol Biol Cell* 8**:** 1829-1844.

Marcelo, A., Koppenol, R., de Almeida, L. P., Matos, C. A. and Nóbrega, C., (2021) Stress granules, RNA-binding proteins and polyglutamine diseases: too much aggregation? *Cell Death Dis* 12**:** 592.

Martínez-Espinoza, A. D., García-Pedrajas, M. a. D. and Gold, S. E., (2002) The Ustilaginales as plant pests and model systems. *Fungal genetics and biology* 35**:** 1-20.

Matthews, M. M., Thomas, J. M., Zheng, Y., Tran, K., Phelps, K. J., Scott, A. I., Havel, J., Fisher, A. J. and Beal, P. A., (2016) Structures of human ADAR2 bound to dsRNA reveal base-flipping mechanism and basis for site selectivity. *Nat Struct Mol Biol* 23**:** 426-433.

McMahon, A. C., Rahman, R., Jin, H., Shen, J. L., Fieldsend, A., Luo, W. and Rosbash, M., (2016) TRIBE: Hijacking an RNA-Editing Enzyme to Identify Cell-Specific Targets of RNA-Binding Proteins. *Cell* 165**:** 742-753.

Medina-Munoz, H. C., Lapointe, C. P., Porter, D. F. and Wickens, M., (2020) Records of RNA locations in living yeast revealed through covalent marks. *Proc Natl Acad Sci USA* 117**:** 23539-23547.

Mendonsa, S., von Kügelgen, N., Dantsuji, S., Ron, M., Breimann, L., Baranovskii, A., Lödige, I., Kirchner, M., Fischer, M., Zerna, N., Bujanic, L., Mertins, P., Ulitsky, I. and Chekulaeva, M., (2023) Massively parallel identification of mRNA localization elements in primary cortical neurons. *Nature Neuroscience* 26**:** 394-405.

Merico, D., Isserlin, R., Stueker, O., Emili, A. and Bader, G. D., (2010) Enrichment map: a network-based method for gene-set enrichment visualization and interpretation. *PLoS One* 5**:** e13984.

Meyer, K. D., Patil, D. P., Zhou, J., Zinoviev, A., Skabkin, M. A., Elemento, O., Pestova, T. V., Qian, S. B. and Jaffrey, S. R., (2015) 5' UTR m(6)A Promotes Cap-Independent Translation. *Cell* 163**:** 999-1010.

Miao, P., Mao, X., Chen, S., Abubakar, Y. S., Li, Y., Zheng, W., Zhou, J., Wang, Z. and Zheng, H., (2023) The mitotic exit mediated by small GTPase Tem1 is essential for the pathogenicity of Fusarium graminearum. *PLoS Pathog* 19**:** e1011255.

Miller, C., Schwalb, B., Maier, K., Schulz, D., Dümcke, S., Zacher, B., Mayer, A., Sydow, J., Marcinowski, L., Dölken, L., Martin, D. E., Tresch, A. and Cramer, P., (2011) Dynamic transcriptome analysis measures rates of mRNA synthesis and decay in yeast. *Mol Syst Biol* 7**:** 458.

Miller, J. E., and Reese, J. C., (2012) Ccr4-Not complex: the control freak of eukaryotic cells. *Critical Reviews in Biochemistry and Molecular Biology* 47**:** 315-333.

Min, H., Turck, C. W., Nikolic, J. M. and Black, D. L., (1997) A new regulatory protein, KSRP, mediates exon inclusion through an intronic splicing enhancer. *Genes Dev* 11**:** 1023-1036.

Min, K., Neiman, A. M. and Konopka, J. B., (2020) Fungal Pathogens: Shape-Shifting Invaders. *Trends Microbiol* 28**:** 922-933.

Minegishi, K., Rothé, B., Komatsu, K. R., Ono, H., Ikawa, Y., Nishimura, H., Katoh, T. A., Kajikawa, E., Sai, X., Miyashita, E., Takaoka, K., Bando, K., Kiyonari, H., Yamamoto, T., Saito, H., Constam, D. B. and Hamada, H., (2021) Fluid flow-induced

left-right asymmetric decay of *Dand5* mRNA in the mouse embryo requires a Bicc1-Ccr4 RNA degradation complex. *Nat Commun* 12**:** 4071.

Monzón-Casanova, E., Matheson, L. S., Tabbada, K., Zarnack, K., Smith, C. W. J. and Turner, M., (2020) Polypyrimidine tract-binding proteins are essential for B cell development. *eLife* 9**:** e53557.

Moore, A. E., Chenette, D. M., Larkin, L. C. and Schneider, R. J., (2014) Physiological networks and disease functions of RNA-binding protein AUF1. *Wiley Interdiscip Rev RNA* 5**:** 549-564.

Moskowitz, H. S., Yokoyama, C. T. and Ryan, T. A., (2005) Highly cooperative control of endocytosis by clathrin. *Mol Biol Cell* 16**:** 1769-1776.

Mueller, A. N., Ziemann, S., Treitschke, S., Aßmann, D. and Doehlemann, G., (2013) Compatibility in the *Ustilago maydis*–maize interaction requires inhibition of host cysteine proteases by the fungal effector Pit2. *PLoS pathogens* 9**:** e1003177.

Müntjes, K., Devan, S. K., Reichert, A. S. and Feldbrügge, M., (2021) Linking transport and translation of mRNAs with endosomes and mitochondria. *EMBO Rep* 22**:** e52445.

Müntjes, K., Philipp, M., Hüsemann, L., Heucken, N., Weidtkamp-Peters, S., Schipper, K., Zurbriggen, M. D. and Feldbrügge, M., (2020) Establishing Polycistronic Expression in the Model Microorganism *Ustilago maydis*. *Front Microbiol* 11**:** 1384.

Naranjo-Ortiz, M. A., and Gabaldón, T., (2019) Fungal evolution: major ecological adaptations and evolutionary transitions. *Biol Rev Camb Philos Soc* 94**:** 1443-1476.

Neve, J., Patel, R., Wang, Z., Louey, A. and Furger, A. M., (2017) Cleavage and polyadenylation: Ending the message expands gene regulation. *RNA Biol* 14**:** 865-890.

Nguyen, D. T. T., Lu, Y., Chu, K. L., Yang, X., Park, S. M., Choo, Z. N., Chin, C. R., Prieto, C., Schurer, A., Barin, E., Savino, A. M., Gourkanti, S., Patel, P., Vu, L. P., Leslie, C. S. and Kharas, M. G., (2020) HyperTRIBE uncovers increased MUSASHI-2 RNA binding activity and differential regulation in leukemic stem cells. *Nat Commun* 11**:** 2026.

Nicastro, G., Taylor, I. A. and Ramos, A., (2015) KH–RNA interactions: back in the groove. *Current Opinion in Structural Biology* 30**:** 63-70.

Niessing, D., Jansen, R. P., Pohlmann, T. and Feldbrügge, M., (2018) mRNA transport in fungal top models. *Wiley Interdiscip Rev RNA* 9.

Oesper, L., Merico, D., Isserlin, R. and Bader, G. D., (2011) WordCloud: a Cytoscape plugin to create a visual semantic summary of networks. *Source Code Biol Med* 6**:** 7.

Olayioye, M. A., Noll, B. and Hausser, A., (2019) Spatiotemporal Control of Intracellular Membrane Trafficking by Rho GTPases. *Cells* 8.

Olgeiser, L., Haag, C., Boerner, S., Ule, J., Busch, A., Koepke, J., König, J., Feldbrügge, M. and Zarnack, K., (2019) The key protein of endosomal mRNP transport Rrm4 binds translational landmark sites of cargo mRNAs. *EMBO Rep* 20.

Palmer, G. E., Kelly, M. N. and Sturtevant, J. E., (2005) The *Candida albicans* vacuole is required for differentiation and efficient macrophage killing. *Eukaryot Cell* 4**:** 1677-1686.

Palumbo, M. C., Farina, L. and Paci, P., (2015) Kinetics effects and modeling of mRNA turnover. *Wiley Interdiscip Rev RNA* 6**:** 327-336.

Parker, R., (2012) RNA degradation in *Saccharomyces cerevisae*. *Genetics* 191**:** 671-702.

Pasquier, G., (2023) COVID-19-associated mucormycosis in India: Why such an outbreak? *J Mycol Med* 33**:** 101393.

Patiño-Medina, J. A., Valle-Maldonado, M. I., Maldonado-Herrera, G., Pérez-Arques, C., Jácome-Galarza, I. E., Díaz-Pérez, C., Díaz-Pérez, A. L., Araiza-Cervantes, C. A., Villagomez-Castro, J. C., Campos-García, J., Ramírez-Díaz, M. I., Garre, V. and Meza-Carmen, V., (2019) Role of Arf-like proteins (Arl1 and Arl2) of *Mucor circinelloides* in virulence and antifungal susceptibility. *Fungal Genet Biol* 129**:** 40-51.

Pennisi, E., (2010) Armed and dangerous, pp. *Science*.

Pereira, J., and Lupas, A. N., (2018) The ancestral KH peptide at the root of a domain family with three different folds. *Bioinformatics* 34**:** 3961-3965.

Pérez-Ortín, J. E., Alepuz, P., Chávez, S. and Choder, M., (2013) Eukaryotic mRNA decay: methodologies, pathways, and links to other stages of gene expression. *J Mol Biol* 425**:** 3750-3775.

Piao, W., Li, C., Sun, P., Yang, M., Ding, Y., Song, W., Jia, Y., Yu, L., Lu, Y. and Jin, H., (2023) Identification of RNA-Binding Protein Targets with HyperTRIBE in *Saccharomyces cerevisiae*. *International Journal of Molecular Sciences* 24**:** 9033.

Pinter, N., Hach, C. A., Hampel, M., Rekhter, D., Zienkiewicz, K., Feussner, I., Poehlein, A., Daniel, R., Finkernagel, F. and Heimel, K., (2019) Signal peptide peptidase activity connects the unfolded protein response to plant defense suppression by *Ustilago maydis*. *PLoS Pathog* 15**:** e1007734.

Pirozynski, K., and Malloch, D., (1975) The origin of land plants: a matter of mycotrophism. *Biosystems* 6**:** 153-164.

Popovic, D., Nijenhuis, W., Kapitein, L. C. and Pelkmans, L., (2020) Co-translational targeting of transcripts to endosomes. *bioRxiv***:** 2020.2007.2017.208652.

Protter, D. S. W., and Parker, R., (2016) Principles and Properties of Stress Granules. *Trends Cell Biol* 26**:** 668-679.

Puerner, C., Serrano, A., Wakade, R. S., Bassilana, M. and Arkowitz, R. A., (2021) A Myosin Light Chain Is Critical for Fungal Growth Robustness in *Candida albicans*. *mBio* 12**:** e0252821.

Puig, S., Askeland, E. and Thiele, D. J., (2005) Coordinated remodeling of cellular metabolism during iron deficiency through targeted mRNA degradation. *Cell* 120**:** 99-110.

Rahman, R., Xu, W., Jin, H. and Rosbash, M., (2018) Identification of RNA-binding protein targets with HyperTRIBE. *Nat Protoc* 13**:** 1829-1849.

Ramanathan, A., Robb, G. B. and Chan, S. H., (2016) mRNA capping: biological functions and applications. *Nucleic Acids Res* 44**:** 7511-7526.

Ramanathan, M., Porter, D. F. and Khavari, P. A., (2019) Methods to study RNA-protein interactions. *Nat Methods* 16**:** 225-234.

Raudvere, U., Kolberg, L., Kuzmin, I., Arak, T., Adler, P., Peterson, H. and Vilo, J., (2019) g:Profiler: a web server for functional enrichment analysis and conversions of gene lists (2019 update). *Nucleic Acids Res* 47**:** W191-w198.

Reid, D. W., and Nicchitta, C. V., (2015) Diversity and selectivity in mRNA translation on the endoplasmic reticulum. *Nature Reviews Molecular Cell Biology* 16**:** 221-231.

Riquelme, M., Aguirre, J., Bartnicki-García, S., Braus, G. H., Feldbrügge, M., Fleig, U., Hansberg, W., Herrera-Estrella, A., Kämper, J., Kück, U., Mouriño-Pérez, R. R., Takeshita, N. and Fischer, R., (2018) Fungal Morphogenesis, from the Polarized Growth of Hyphae to Complex Reproduction and Infection Structures. *Microbiol Mol Biol Rev* 82.

Rojas, A. M., Fuentes, G., Rausell, A. and Valencia, A., (2012) The Ras protein superfamily: evolutionary tree and role of conserved amino acids. *J Cell Biol* 196**:** 189-201.

Roy, B., and Jacobson, A., (2013) The intimate relationships of mRNA decay and translation. *Trends Genet* 29**:** 691-699.

Ruan, X., Hu, K. and Zhang, X., (2023) PIE-seq: identifying RNA-binding protein targets by dual RNA-deaminase editing and sequencing. *Nature Communications* 14**:** 3275.

Sankaranarayanan, S., Haag, C., Petzsch, P., Köhrer, K., Matuszyńska, A., Zarnack, K. and Feldbrügge, M., (2023a) The mRNA stability factor Khd4 defines a specific mRNA regulon for membrane trafficking in the pathogen *Ustilago maydis*. *Proc Natl Acad Sci USA* 120**:** e2301731120.

Sankaranarayanan, S., Kwon, S., Heimel, K. and Feldbrügge, M., (2023b) The RNA world of fungal pathogens. *PLoS Pathog*.

Sarkari, P., Reindl, M., Stock, J., Müller, O., Kahmann, R., Feldbrügge, M. and Schipper, K., (2014) Improved expression of single-chain antibodies in *Ustilago maydis*. *J Biotechnol* 191**:** 165-175.

Scherer, M., Heimel, K., Starke, V. and Kämper, J., (2006) The Clp1 protein is required for clamp formation and pathogenic development of *Ustilago maydis*. *Plant Cell* 18**:** 2388-2401.

Schirawski, J., Böhnert, H. U., Steinberg, G., Snetselaar, K., Adamikowa, L. and Kahmann, R., (2005) Endoplasmic reticulum glucosidase II is required for pathogenicity of *Ustilago maydis*. *Plant Cell* 17**:** 3532-3543.

Schmitz, L., Kronstad, J. W. and Heimel, K., (2020) Conditional gene expression reveals stage-specific functions of the unfolded protein response in the *Ustilago maydis*-maize pathosystem. *Mol Plant Pathol* 21**:** 258-271.

Schmitz, L., McCotter, S., Kretschmer, M., Kronstad, J. W. and Heimel, K., (2018) Transcripts and tumors: regulatory and metabolic programming during biotrophic phytopathogenesis. *F1000Res* 7.

Schuchardt, I., Assmann, D., Thines, E., Schuberth, C. and Steinberg, G., (2005) Myosin-V, Kinesin-1, and Kinesin-3 cooperate in hyphal growth of the fungus Ustilago maydis. *Mol Biol Cell* 16**:** 5191-5201.

Schueren, F., Lingner, T., George, R., Hofhuis, J., Dickel, C., Gartner, J. and Thoms, S., (2014) Peroxisomal lactate dehydrogenase is generated by translational readthrough in mammals. *Elife* 3**:** e03640.

Schuhmacher, J. S., Tom Dieck, S., Christoforidis, S., Landerer, C., Davila Gallesio, J., Hersemann, L., Seifert, S., Schäfer, R., Giner, A., Toth-Petroczy, A., Kalaidzidis, Y., Bohnsack, K. E., Bohnsack, M. T., Schuman, E. M. and Zerial, M., (2023) The Rab5 effector FERRY links early endosomes with mRNA localization. *Mol Cell* 83**:** 1839-1855.e1813.

Shcherbo, D., Murphy, C. S., Ermakova, G. V., Solovieva, E. A., Chepurnykh, T. V., Shcheglov, A. S., Verkhusha, V. V., Pletnev, V. Z., Hazelwood, K. L., Roche, P. M., Lukyanov, S., Zaraisky, A. G., Davidson, M. W. and Chudakov, D. M., (2009) Far-red fluorescent tags for protein imaging in living tissues. *Biochem J* 418**:** 567-574.

Shi, W., Stolze, S. C., Nakagami, H., Misas Villamil, J. C., Saur, I. M. L. and Doehlemann, G., (2023) Combination of *in vivo* proximity labeling and co-immunoprecipitation identifies the host target network of a tumor-inducing effector in the fungal maize pathogen Ustilago maydis. *J Exp Bot* 74**:** 4736-4750.

Snead, W. T., and Gladfelter, A. S., (2019) The Control Centers of Biomolecular Phase Separation: How Membrane Surfaces, PTMs, and Active Processes Regulate Condensation. *Molecular Cell* 76**:** 295-305.

Stauffer, B., and Powers, T., (2015) Target of rapamycin signaling mediates vacuolar fission caused by endoplasmic reticulum stress in *Saccharomyces cerevisiae*. *Mol Biol Cell* 26**:** 4618-4630.

Steinberg, G., (2014) Endocytosis and early endosome motility in filamentous fungi. *Curr Opin Microbiol* 20**:** 10-18.

Steinberg, G., Peñalva, M. A., Riquelme, M., Wösten, H. A. and Harris, S. D., (2017) Cell Biology of Hyphal Growth. *Microbiol Spectr* 5.

Steinberg, G., and Perez-Martin, J., (2008) *Ustilago maydis*, a new fungal model system for cell biology. *Trends Cell Biol* 18**:** 61-67.

Sternburg, E. L., Gruijs da Silva, L. A. and Dormann, D., (2022) Post-translational modifications on RNA-binding proteins: accelerators, brakes, or passengers in neurodegeneration? *Trends Biochem Sci* 47**:** 6-22.

Stiebler, A. C., Freitag, J., Schink, K. O., Stehlik, T., Tillmann, B. A., Ast, J. and Bölker, M., (2014) Ribosomal readthrough at a short UGA stop codon context triggers dual localization of metabolic enzymes in fungi and animals. *PLoS Genet* 10**:** e1004685.

Sudbery, P. E., (2011) Growth of *Candida albicans* hyphae. *Nat Rev Microbiol* 9**:** 737-748.

Sugui, J. A., Kwon-Chung, K. J., Juvvadi, P. R., Latge, J. P. and Steinbach, W. J., (2014) *Aspergillus fumigatus* and related species. *Cold Spring Harb Perspect Med* 5**:** a019786.

Sun, M., Schwalb, B., Pirkl, N., Maier, K. C., Schenk, A., Failmezger, H., Tresch, A. and Cramer, P., (2013) Global analysis of eukaryotic mRNA degradation reveals Xrn1-dependent buffering of transcript levels. *Mol Cell* 52**:** 52-62.

Tafech, A., Bennett, W. R., Mills, F. and Lee, C. H., (2007) Identification of c-myc coding region determinant RNA sequences and structures cleaved by an RNase1-like endoribonuclease. *Biochimica et Biophysica Acta (BBA)-Gene Structure and Expression* 1769**:** 49-60.

Taheri-Talesh, N., Xiong, Y. and Oakley, B. R., (2012) The functions of myosin II and myosin V homologs in tip growth and septation in Aspergillus nidulans. *PLoS One* 7**:** e31218.

Terfrüchte, M., Joehnk, B., Fajardo-Somera, R., Braus, G. H., Riquelme, M., Schipper, K. and Feldbrügge, M., (2014) Establishing a versatile Golden Gate cloning system for genetic engineering in fungi. *Fungal Genet Biol* 62**:** 1-10.

Terfrüchte, M., Reindl, M., Jankowski, S., Sarkari, P., Feldbrügge, M. and Schipper, K., (2017) Applying Unconventional Secretion in *Ustilago maydis* for the Export of Functional Nanobodies. *Int J Mol Sci* 18**:** 937.

Thammahong, A., Dhingra, S., Bultman, K. M., Kerkaert, J. D. and Cramer, R. A., (2019) An Ssd1 Homolog Impacts Trehalose and Chitin Biosynthesis and Contributes to Virulence in *Aspergillus fumigatus*. *mSphere* 4.

Theil, K., Herzog, M. and Rajewsky, N., (2018) Post-transcriptional Regulation by 3' UTRs Can Be Masked by Regulatory Elements in 5' UTRs. *Cell Rep* 22**:** 3217-3226.

Thompson, M. K., Ceccarelli, A., Ish-Horowicz, D. and Davis, I., (2023) Dynamically regulated transcription factors are encoded by highly unstable mRNAs in the Drosophila larval brain. *Rna*.

Thumuluri, V., Almagro Armenteros, J. J., Johansen, A. R., Nielsen, H. and Winther, O., (2022) DeepLoc 2.0: multi-label subcellular localization prediction using protein language models. *Nucleic Acids Res* 50**:** W228-234.

Tian, L., Doroshenk, K. A., Zhang, L., Fukuda, M., Washida, H., Kumamaru, T. and Okita, T., (2020) Zipcode RNA-Binding Proteins and Membrane Trafficking Proteins Cooperate to Transport Glutelin mRNAs in Rice Endosperm. *Plant Cell* 32**:** 2566-2581.

Tuck, A. C., Rankova, A., Arpat, A. B., Liechti, L. A., Hess, D., Iesmantavicius, V., Castelo-Szekely, V., Gatfield, D. and Bühler, M., (2020) Mammalian RNA Decay Pathways Are Highly Specialized and Widely Linked to Translation. *Mol Cell* 77**:** 1222-1236.e1213.

Ueno, T., Taga, Y., Yoshimoto, R., Mayeda, A., Hattori, S. and Ogawa-Goto, K., (2019) Component of splicing factor SF3b plays a key role in translational control of polyribosomes on the endoplasmic reticulum. *Proc Natl Acad Sci USA* 116**:** 9340-9349.

Valverde, R., Edwards, L. and Regan, L., (2008) Structure and function of KH domains. *Febs j* 275**:** 2712-2726.

Van Nostrand, E. L., Freese, P., Pratt, G. A., Wang, X., Wei, X., Xiao, R., Blue, S. M., Chen, J.-Y., Cody, N. A. L., Dominguez, D., Olson, S., Sundararaman, B., Zhan, L., Bazile, C., Bouvrette, L. P. B., Bergalet, J., Duff, M. O., Garcia, K. E., Gelboin-Burkhart, C., Hochman, M., Lambert, N. J., Li, H., McGurk, M. P., Nguyen, T. B., Palden, T., Rabano, I., Sathe, S., Stanton, R., Su, A., Wang, R., Yee, B. A., Zhou, B., Louie, A. L., Aigner, S., Fu, X.-D., Lécuyer, E., Burge, C. B., Graveley, B. R. and Yeo, G. W., (2020) A large-scale binding and functional map of human RNA-binding proteins. *Nature* 583**:** 711-719.

Van Treeck, B., and Parker, R., (2018) Emerging Roles for Intermolecular RNA-RNA Interactions in RNP Assemblies. *Cell* 174**:** 791-802.

Vijjamarri, A. K., Niu, X., Vandermeulen, M. D., Onu, C., Zhang, F., Qiu, H., Gupta, N., Gaikwad, S., Greenberg, M. L., Cullen, P. J., Lin, Z. and Hinnebusch, A. G., (2023) Decapping factor Dcp2 controls mRNA abundance and translation to adjust metabolism and filamentation to nutrient availability. *eLife* 12**:** e85545.

Vlasova-St Louis, I., and Bohjanen, P. R., (2011) Coordinate regulation of mRNA decay networks by GU-rich elements and CELF1. *Curr Opin Genet Dev* 21**:** 444-451.

Vollmeister, E., (2009) *Das AUACCC-bindende Protein Khd4 kontrolliert Morphogenese und Pathogenität in Ustilago maydis*. *Philipps-Universität Marburg*.

Vollmeister, E., Haag, C., Zarnack, K., Baumann, S., König, J., Mannhaupt, G. and Feldbrügge, M., (2009) Tandem KH domains of Khd4 recognize AUACCC and are essential for regulation of morphology as well as pathogenicity in *Ustilago maydis*. *Rna* 15**:** 2206-2218.

Vollmeister, E., Schipper, K., Baumann, S., Haag, C., Pohlmann, T., Stock, J. and Feldbrügge, M., (2012) Fungal development of the plant pathogen *Ustilago maydis*. *FEMS Microbiology Reviews* 36**:** 59-77.

Walters, R., and Parker, R., (2014) Quality control: Is there quality control of localized mRNAs? *J Cell Biol* 204**:** 863-868.

Wang, J., Choi, J. M., Holehouse, A. S., Lee, H. O., Zhang, X., Jahnel, M., Maharana, S., Lemaitre, R., Pozniakovsky, A., Drechsel, D., Poser, I., Pappu, R. V., Alberti, S. and Hyman, A. A., (2018) A Molecular Grammar Governing the Driving Forces for Phase Separation of Prion-like RNA Binding Proteins. *Cell* 174**:** 688-699.e616.

Wedlich-Söldner, R., Bölker, M., Kahmann, R. and Steinberg, G., (2000) A putative endosomal t-SNARE links exo- and endocytosis in the phytopathogenic fungus *Ustilago maydis*. *Embo j* 19**:** 1974-1986.

Wedlich-Söldner, R., Schulz, I., Straube, A. and Steinberg, G., (2002) Dynein supports motility of endoplasmic reticulum in the fungus Ustilago maydis. *Mol Biol Cell* 13**:** 965-977.

Weiberg, A., Wang, M., Lin, F. M., Zhao, H., Zhang, Z., Kaloshian, I., Huang, H. D. and Jin, H., (2013) Fungal small RNAs suppress plant immunity by hijacking host RNA interference pathways. *Science* 342**:** 118-123.

Wenzel, E. M., Elfmark, L. A., Stenmark, H. and Raiborg, C., (2022) ER as master regulator of membrane trafficking and organelle function. *J Cell Biol* 221.

White, E. J., Brewer, G. and Wilson, G. M., (2013) Post-transcriptional control of gene expression by AUF1: mechanisms, physiological targets, and regulation. *Biochim Biophys Acta* 1829**:** 680-688.

Wiedner, H. J., and Giudice, J., (2021) It's not just a phase: function and characteristics of RNA-binding proteins in phase separation. *Nature Structural & Molecular Biology* 28**:** 465-473.

Wolozin, B., and Ivanov, P., (2019) Stress granules and neurodegeneration. *Nat Rev Neurosci* 20**:** 649-666.

Xu, W., Rahman, R. and Rosbash, M., (2018) Mechanistic implications of enhanced editing by a HyperTRIBE RNA-binding protein. *Rna* 24**:** 173-182.

Yu, C. J., and Lee, F. J., (2017) Multiple activities of Arl1 GTPase in the trans-Golgi network. *J Cell Sci* 130**:** 1691-1699.

Zander, S., Baumann, S., Weidtkamp-Peters, S. and Feldbrügge, M., (2016) Endosomal assembly and transport of heteromeric septin complexes promote septin cytoskeleton formation. *J Cell Sci* 129**:** 2778-2792.

Zheng, P., Nguyen, T. A., Wong, J. Y., Lee, M., Nguyen, T. A., Fan, J. S., Yang, D. and Jedd, G., (2020) Spitzenkörper assembly mechanisms reveal conserved features of fungal and metazoan polarity scaffolds. *Nat Commun* 11**:** 2830.

Zhou, G., Niu, R., Zhou, Y., Luo, M., Peng, Y., Wang, H., Wang, Z. and Xu, G., (2021) Proximity editing to identify RNAs in phase-separated RNA binding protein condensates. *Cell Discov* 7**:** 72.

Zhou, Y., Manghwar, H., Hu, W. and Liu, F., (2022) Degradation Mechanism of Autophagy-Related Proteins and Research Progress. *International Journal of Molecular Sciences* 23**:** 7301.

Zhu, X.-M., Li, L., Wu, M., Liang, S., Shi, H.-B., Liu, X.-H. and Lin, F.-C., (2019) Current opinions on autophagy in pathogenicity of fungi. *Virulence* 10**:** 481-489.

7 Authors contribution

Parts of this dissertation (Chapter 3.1; Chapter 5, Appendix 1-2) have been previously published (SANKARANARAYANAN *et al.* 2023a,SANKARANARAYANAN *et al.* 2023b), and are reproduced under the terms of the Creative Commons Attribution 4.0 International License (CC BY). No modifications were made to the published materials, except for minor adjustments in figure placement or text and table formatting. The results and data interpretation remain unaltered in any way. The contributions of co-authors in these studies are described below:

Chapter 2.1:

- Prof. Dr. Michael Feldbrügge supervised all the wet lab experiments in the study.
- Dr. Kathi Zarnack supervised all the bioinformatics analyses in the study.
- Prof. Dr. Anna Matuszynska from the RWTH Aachen derived the mathematical model to study mRNA kinetics during hyphal morphogenesis. This derivation is presented in the subsection “Mathematical modeling to study dynamic mRNA concentration changes” in Chapter 5, Appendix 2 (Refer to the table below for figure references).
- All aspects of NGS library preparation, RNA sequencing, as well as the initial processing and quality control of the sequencing data, were carried out by the team led by Prof. Dr. Karl Köhrer, with significant contributions from the key member Dr. Patrick Petzsch and Thorsten Wachtmeister from the Biologisch-Medizinisches Forschungszentrum (BMFZ) at Heinrich Heine University Düsseldorf.
- Dr. Carl Haag co-supervised the wet lab experiments initially.
- M. Sc Nina Kim Stoffel performed the Western blot experiment in Fig. 5.13G, analyzing the levels of Khd4-Gfp and Rrm4-Gfp levels in yeast and hyphal cells (Refer to the table below for figure references).
- All the remaining wet lab and bioinformatics analyses were carried out by M. Tech Srimeenakshi Sankaranaraynan.
- M. Tech Srimeenakshi Sankaranarayanan, Prof. Dr. Michael Feldbrügge, and Dr. Kathi Zarnack wrote the manuscript.

Chapter 2.2:

Superresolution Structured Illumination Microscopy images were acquired by Dr. Sebastian Hänsch from the Center for Advanced Imaging (CAI) at Heinrich Heine University Düsseldorf (Refer to the table below for figure references).

Chapter 5.1:

- Prof. Dr. Michael Feldbrügge authored the section "Endosomal mRNA transport generates and prevents intracellular gradients in infectious hyphae" and contributed to the introduction, conclusions future directions, and the design of Fig 5.1.
- Dr. Seomun Kwon wrote the part on "Extracellular vesicle-mediated transport of RNAs determines host communication" part and contributed to the design and development of Fig 5.1.
- Prof. Dr. Kai Heimel authored the section "Cytoplasmic mRNA splicing coordinates UPR and ER trafficking during infection".
- M. Tech Srimeenakshi Sankaranarayanan authored the sections "Regulation of mRNA stability determines membrane trafficking dynamics", and "Diverse RNA regulation determines peroxisomal protein entry", designed and created Fig. 5.1, and contributed to the introduction, conclusions and future directions.

The source references and co-authors for the figures used or reused in this thesis are listed below.

Figure No. in this dissertation	Source/Co-author	License
1.1	GEBAUER *et al.* 2021	Springer Nature license No. 5625890803643
1.4	LANVER *et al.* 2017	Springer Nature license No. 5617680925598
1.5E	M.Sc. Lea Geißl	
2.1-2.7; 5.2-5.14	SANKARANARAYANAN *et al.* 2023a	CC BY
5.1	SANKARANARAYANAN *et al.* 2023b	CC BY
5.13A, C	Prof. Dr. Anna Matuszynska	
5.13G	M.Sc. Nina Kim Stoffel	
5.14F	OLGEISER *et al.* 2019	CC BY
2.9A-B	Dr. Sebastian Hänsch	
All figures, except those listed in bold above.	Srimeenakshi Sankaranaraynan	

Acknowledgements

First and foremost, I would like to express my immense gratitude to my PhD supervisor, Prof. Dr. Michael Feldbrügge, for his great support in completing my PhD thesis. This achievement is a direct outcome of the platform you provided that helped me to grow both intellectually and personally. I deeply appreciate the freedom you gave me to engage in scientific research, fostering my independence, and equipping me with valuable skills and knowledge vital for success in research and academia. The milestones I have achieved thus far have exceeded the expectations of my 24-year-old self during our initial meeting. Thank you for recognizing the spark of motivation and interest in science within me back in 2017, and for believing in me even when I had doubts. Thank you so much.

I would like to thank Prof. Dr. Heiner Schaal for agreeing to be my second supervisor and for his invaluable guidance and feedback. Thanks to the graduate school Molecules of Infection (MOI III) for their generous funding. Special appreciation to Dr. Stephanie Spelberg and Dr. Sabrina Zander for their help in MOI III. I also extend my sincere thanks to Dr. Sigrun Wegener–Feldbrügge and her coworkers from JUNO for their support with organizational matters, making my life in Germany easier.

A special thanks to Dr. Kathi Zarnack for her great guidance in computational biology, motivation, and mentorship. My heartfelt thanks go to Dr. Carl Haag, not only for teaching me essential wet lab techniques patiently but also for all cheerful scientific discussions and ideas, a great motivation.

I am grateful to all our collaborators for their contributions to this study: Dr. Andreas Brachmann, for his intellectual support, particularly in NGS sequencing and the experimental design of the hyperTRIBE technique; Prof. Dr. Anna Matuszynska for helping us with mathematical modeling studies; Prof. Dr. Karl Köhrer, Dr. Patrick Petzsch and Thorsen Wachtmeister from BMFZ, HHU, Düsseldorf for NGS support; Special recognition goes to Ute Gengenbacher and Simone Krüger for their technical assistance in strain generation, especially with spontaneous inoculation and shifting. I appreciate Dr. Lilli Bismar, Dr. Kira Müntjes, Nina Kim Stoffel, Taniya Binny, Sanchi Dali, Dr. Imran Khan for proofreading and correcting this thesis.

This journey would have only been half as joyful without the support of my wonderful colleagues from AG Feldbrügge. I extend special thanks to Senthil, Silke, Jessica, Lilli, Marcus, and Ute for helping me settle in Düsseldorf during my early days. My Sincere appreciation also goes to both past and current Rab Lab members, including Thomas, Carl, Senthil, Jessica, Woogie, Minerva, Melanie, Nina, Sai, Jungho, Lilli, Marcus, Lea, and Kira for their constructive discussions and research collaborations. I would also like to thank all the other colleagues of the Institute of Microbiology for their support. From a small pipette to my computer, nothing would have worked if it was not for Uli. Thank you Uli. I feel so fortunate to have done my PhD at AG Feldi during your time there.

I would like to extend my special appreciation to my fellow lab colleagues, Senthil, Woogie, Jessica, Minerva, Summiya, and Sanchi, for their support, enjoyable moments, and the time they've devoted to both me and my research. Your encouragement and camaraderie have been invaluable throughout this journey. Specifically, to Senthil and Woogie for all the late-night scientific, political, and philosophical discussions. I am grateful to our HHU Indian community, including Senthil, Bala, Rizwan, Sarnava, Taniya, Sai, Feby, Dibin, Rajesh, Ruchika, and Arun for all the memories and the great times we have had. To my dear friend, Karthika, heartfelt thanks. Our lively conversations and shared meals have made my time in Düsseldorf special and supportive. I would like to express my gratitude to Harsha and Gayatri, who have become like a second home in Düsseldorf. Without them, my life here would have been much dimmer. Thank you both for always being there for me.

My heartfelt thanks to my partner, Imran, for all his love and support throughout my PhD journey. Thank you for being the guiding light during the darkest times and for adding laughter to our shared moments.

Above all, I would not be here if it were not for my Amma Mrs. Ananthavalli, and my Appa Mr. Sankaranarayanan, whose unwavering love and trust in me have been a constant source of support, even in the face of numerous obstacles. I am indebted to my great sisters, Vaishnavi and Bhuvana, for their constant care and protective support. A special thanks to my niece, Diya, whose love is truly heartwarming. Finally, I would like to thank all the fellow scientists, I have read about, encountered in the lab, crossed paths with, and met in meetings, and conferences, whose work and dedication have been a continuous source of inspiration for my scientific pursuits.